A BETA SPECTROMETER USING A GE(HP) DETECTOR IN A HIGH MAGNETIC FIELD

by

Ali Khalil Al-Alousi

A thesis submitted to the
Faculty of Graduate Studies and Research
in partial fulfillment of the requirements
for the degree of Master of Science

Foster Radiation Laboratory
McGill University, Montreal
Quebec, Canada

 December, 1984

ABSTRACT

The role of beta spectroscopy in nuclear physics and fundamental interaction studies has been thoroughly reviewed. The various methods and techniques of beta spectroscopy have been comprehensively studied.

A new, high precision, beta spectrometer suitable for the study of nuclei far from stability has been constructed. The spectrometer consists of a superconducting transport solenoid and a semiconductor beta detector. The superconducting solenoid has a maximum magnetic field of 4.4 tesla, and a room temperature bore with a diameter of 7.3 cm. The beta detector is a windowless high purity germanium diode with dimensions of 15 mm x 500 mm^2 .

The cryogenic performance of the magnet's liquid helium cryostat has been thoroughly tested and analyzed.

The trajectories of the beta particles in the magnetic field of the solenoid were studied using a computer simulation.

The performance of the spectrometer was tested under different experimental conditions and measurements of the beta spectra of standard sources were used to evaluate its overall effectiveness.

A rapid source introduction mechanism has been used in conjunction with the spectrometer and isotopes with half lives as short as 10 sec have been studied.

The performance parameters of the spectrometer: 25% transmission, 0.45% resolution at 1 MeV, 1.8×10^{-2} cm^2 luminosity, 6 MeV maximum beta ray energy, and a gamma ray suppression ratio of 250, compare quite favourably to those achieved with previous spectrometer designs.

A beta-gamma coincidence system has also been tested for use with the superconducting transport solenoid.

RESUME

Le rôle de la spectroscopie bêta en physique nucléaire et lors d'études d'interactions fondamentales a été entièrement revu. Les différentes méthodes et techniques propres à la spectroscopie bêta ont été étudiées avec soin.

Un nouveau spectromètre bêta de haute précision, spécialement adapté à l'étude des noyaux loin de la stabilité, a été construit. Ce spectromètre consiste en un solénoïde de transport supraconducteur et d'un détecteur bêta semi-conducteur. Le solénoïde supraconducteur développe un champ magnétique maximum de 4.4 tesla et est doté d'une ouverture de 7.3 cm de diamètre qui demeure à la température de la pièce. Le détecteur bêta consiste en une diode au germanium de haute pureté, sans fenêtre. Ses dimensions sont de 15 mm x 500 mm^2.

Les performances cryogéniques du cryostat d'Hélium liquide, destiné à refroidir l'aimant, ont été éprouvées et analysées en profondeur.

Les trajectoires des particules bêta soumises au champ magnétique ont été étudiées par simulation sur ordinateur.

Les performances du spectromètre ont été étudiées sous différentes conditions expérimentales et son efficacité globale a été évaluée à l'aide de mesure de spectres bêta de sources standards.

Un mécanisme rapide, pour l'introduction des sources, a été utilisé avec le spectromètre; ceci a permis d'étudier des isotopes de demie-vies aussi courtes que 10 sec.

Les paramètres de performance du spectromètre se comparent favorablement à ceux déjà obtenus pour d'autres types de spectromètres: transmission de 25%, résolution de 0.45% à 1 MeV, luminosité de 1.8×10^{-2} cm , énergie bêta maximum de 6 MeV et rapport de supression de raie gamma de 250.

Un système de coincidence bêta-gamma, faisant usage du solénoïde de transport supraconducteur, a aussi été mis à l'essai.

ACKNOWLEDGEMENTS

I would like to begin by thanking my research supervisor, Professor R.B. Moore for his guidance and support throughout the various stages of this work. The design of the spectrometer on which this thesis reports was largely due to him. His technical skill and mastery was of crucial importance in the development of the spectrometer.

My greatest thanks go to Dr. D.W. Hetherington. A large part of the work reported in this thesis was performed in collaboration with him during his doctoral research. His determination of the response function of the spectrometer, and the analysis programs and procedures he developed are indispensible prerequisites for the use of the spectrometer.

The contributions of the technical and research staff of the Foster Radiation Laboratory to the development of the spectrometer are gratefully acknowedged. Special thanks go to Messers Steve Kecani and John Egyed for their efforts during its construction.

I would like to thank Ms. Paula Siepniewicz for the long hours she spent typing and editing the major part of this thesis. I would also like to express my grateful appreciation to Mr. Ian Bonnell for the many hours he volunteered to spend preparing the diagrams for this thesis.

I should like to thank Mr. Richard Turcotte for translating the abstract of this thesis to French.

My colleagues E., N., and D., Freds are thanked for their moral support and comraderie.

Financial support from the Department of Physics in the form of a Carl Reinhardt scholarship has been greatly appreciated.

Finally, I would like to end by thanking my family for their unfailing support and unwavering faith without which this work would not have been possible. With everlasting gratitude I dedicate this thesis to them as a token of my eternal indebtedness.

TABLE OF CONTENTS

LIST OF FIGURES

LIST OF TABLES

CHAPTER 1

INTRODUCTION

Since it was first discovered by H. Becquerel in 1896 (Becquerel 1896), radioactivity has been both an object of intense study and a tool for investigating other phenomena in nature. Radioactivity can be defined as the emission of particles or electromagnetic radiation from the atomic nucleus. Through this emission, the nucleus rids itself of excess energy. The investigation of the the radioactive properties of nuclei forms a prominent part of discipline of nuclear spectroscopy (the study of how nuclei absorb and emit energy). It has served as a rich source of information on the properties of the nucleus and the interactions among its constituent particles (nuclear structure and nuclear forces).

There are three main types of radioactivity, commonly known as α, β, and γ radiation. Although Becquerel was unaware of it, the bulk of the radiation he had observed consisted of β particles or electrons (Pais 1977). Ever since then, the study of β decay has played an important role in the development of nuclear science providing invaluable data on the structure of the nucleus and one of the basic forces in nature, the weak interaction.

Some of the most fruitful contributions of nuclear physics to the understanding of elementary particle interactions have been in the area of the weak interaction. In this context, the phenomenon of nuclear β decay holds the distinction of being the most fully investigated manifestation of this fundamental interaction (Blin-Stoyle 1973 pp. 17-20). In particular, experiments on nuclear β decays (or, in the nomenclature of elementary particle physics, low-energy semileptonic strangeness-conserving transitions) are traditionally the most accurate type of weak interaction experiments (Boothroyd et al. 1984).

No attempt will be made in this thesis to rehash the theory of β decay. A set of excellent reviews of the thoery is available in the literature (Lipkin 1962; Wu & Moszkowski 1966; Schopper 1966; Konopinski 1966; Strachan 1969; Blin-stoyle 1973; Morita 1973; Lee & Cheng 1981; Behrens & Burhing 1982; and references therein).

1.1 The role of β spectroscopy in nuclear physics

The term nuclear β decay describes the process of direct decay of a parent nucleus into a different (daughter) nucleus by the simultaneous emission of an electron (positron) and an electron antineutrino (neutrino) (Kofoed-Hansen & Christensen 1962).

A nuclear β decay can be symbolically represented as follows:

$$^{A}Z \longrightarrow {}^{A}(Z+1) + \beta^{-} + \bar{\nu} \quad \text{For electron emission}$$

and

$$^{A}Z \longrightarrow {}^{A}(Z-1) + \beta^{+} + \nu \quad \text{For positron emission}$$

Where

^{A}Z is the parent nucleus with atomic number Z and mass number A.

$^{A}(Z+1)$ is the daughter nucleus in the decay of a neutron rich parent nucleus.

$^{A}(Z-1)$ is the daughter nucleus in the decay of a neutron deficient parent nucleus.

β^{-}, β^{+} are an electron (negatron) or a positron respectively.

ν, $\bar{\nu}$ are an electon neutrino or an electron antineutrino respectively.

Because of the fact that an electon neutrino (antineutrino) carries no electric charge, little or no rest mass, and interacts with matter almost exclusively through the weak interaction, its detection is very difficult and quite impractical. Therefore, in most cases in β spectroscopy only the electrons (positrons) are detected and their energy analysed.

The energy released in a nuclear β decay is shared unequally and in a statistical manner between the two particles emitted in the decay, the electron (positron) and the antineutrino (neutrino). (Only a very small fraction of the energy is carried off by the recoiling daughter nucleus). Because of this energy sharing, the β particles are emitted in a continuous distribution of energies (a spectrum).

Throughout this thesis the term "β spectrum" will be used to refer to this continuous (energy or momentum) spectrum of electrons or positrons emitted in the nuclear β' decay. Similarly, the terms "β rays" and "β particles" will be used to refer to the electrons or positrons emitted in

the decay (Hamilton 1966).

By studying the shape of the energy spectrum of the electrons (positrons) emitted in a β decay, much can be learned about certain fundamental aspects of the weak interaction. Also a great deal of data can be obtained about the nuclei involved in the decay (Daniel 1968).

An important piece of information that can be obtained is the endpoint of the β spectrum (the maximum energy with which the β particles are emitted from the nucleus). Coupled with knowledge of the level structure of the daughter nucleus it can be used to calculate the energy difference (Q_β) (and therefore the mass difference) between the ground states of the parent and daughter nuclei.

Careful measurements of the β particle energy spectrum can also be used to determine the probability of β decay to the different excited states and the ground state of the daughter nucleus (β braching ratios). This can be very useful in establishing and clarifying the level scheme of the daughter nucleus. The use of beta spectroscopy in the determination of the β branching ratios has gained more importance recently since the validity of the usual technique of γ ray intensity balance for their measurement has been questioned, especially in cases where the decay schemes are complex (Hardy et al. 1977; Munnich 1980).

The endpoint energies of the different branches and the β feeding to each branch can be combined with the half life of the decaying nucleus to calculate the so called ft values. (The ft value is a measure of the strength of the decay or the rate of the transition). For more accurate ft value determinations, such as those required for nuclear matrix elements calculations in forbidden decays, careful measurements of the shapes of the beta specta are required (Schopper 1966 p. 278).

Nuclear beta transitions are usually classified according to the spin and parity changes during the decay, into allowed and several types of forbidden transitions (Wu & Moszkowski 1966 p. 59). The ft values of the superallowed (allowed transitions between members of the same isospin multiplet, i.e. between analogue states), allowed, and the various forbidden transitions are different enough that knowledge of the ft value for a certain transition can be used to assign the transition to one of these categories. Hence, measurements of the ft values can be used to infer the spin and parity changes during the transition and therefore help

in the determination of the spins and parities of the nuclear states involved in the beta decay.

Among the forbidden β transitions there are certain types that are referred to as "unique transitions" because of the particular shapes of their β spectra. Therefore, the detection of such a β spectrum shape can distinguish a transition as being "unique" and can be used to determine the specific spin and parity changes during the transition, as dictated by the appropriate selection rules that apply to unique transitions.

On a more fundamental level, the methods of beta spectroscopy have been quite useful in determining the type of interactions involved in nuclear β decay and in checking the validity of the standard vector minus axial-vector (V-A) model of the weak interaction. An upper limit on the value of the Fierz interference term (and therefore on the possible existence of a scalar or a tensor interaction in nuclear β decay) can be derived from careful spectral shape measurements of allowed β decays and from the ft values of $0^+ \longrightarrow 0^+$ superallowed pure Fermi transitions (Daniel 1968; Blin-Stoyle 1973 pp. 111-113; Morita 1973 p. 21, pp. 35-36; Hardy & Towner 1975; Thies et al. 1978; Boothroyd et al. 1984).

Measurements of the ft values of $0^+ \longrightarrow 0^+$ superallowed Fermi transitions can also serve as a test for an important aspect of β decay theory, namely, the conserved vector current hypothesis (CVC). One of the predictions of the CVC theory is that the ft values for superallowed transitions, after certain calculated corrections are made, should be identical (Hardy & Towner 1975; Thies et al. 1978; Davids et al. 1979; Behrens & Buhring 1982 pp. 486-499; Kruger et al. 1983). In fact, a role of major significance in nuclear science is played by this ft value. It is required for the calculation of the vector coupling constant of nuclear beta decay; a quantity of fundamental importance in physics (Hardy & Towner 1975; Raman et al. 1975; Wilkinson 1975; Szybisz 1979).

The CVC hypothesis also predicts statistical shapes for the beta spectra of superallowed pure Fermi transitions (after certain theoretical corrections are applied) with no energy dependent shape factors. Precise spectral shape determinations for these transitions can therefore serve as a test for CVC. More importantly they serve as a check on the accuracy of the corrections that are applied to the spectrum and in particular the radiative corrections. The radiative corrections enter in the evaluation

of the vector coupling constant of the weak interaction and therefore their values must be known as reliably as possible (Thies et al. 1978; Davids et al. 1979; Kruger et al. 1983).

An important test of the CVC hypothesis is furnished by measurements of the deviations of the shapes of β spectra of certain allowed decays (mirror Gamow-Teller transitions e.g. ^{12}N, ^{12}B, ^{20}F, ^{20}Na) from the statistical shape. These deviations (or shape factors) are used to evaluate the weak magnetism term in beta decay, the magnitude of which is predicted by CVC (Wu 1977; Genz et al. 1976a; Kaina et al. 1977; Calprice & Alburger 1978; Van Elmbt 1981; Kruger et al. 1983; Hetherington et al. 1983).

Another contribution of beta spectroscopy to the understanding of the mechanism of the weak interaction has been in the search for second class currents in nuclear β becay (hadronic currents that are irregular under G-parity operation i.e. G-parity non-conserving currents). Spectral shape and ft value measurements for superallowed Fermi transitons can be used to look for the effects of second class polar-vector currents and to set an upper limit on the possible presence of the induced scalar interaction (these studies are closely linked to tests of the CVC) (Szybisz 1979; Szybisz & Silbergleit 1981a,b; Holstien 1984). On the other hand, the asymmetry in the ft values of some mirror β decays (e.g. ^{12}B, ^{12}N β decays) has been used to test the occurance of second class axial currents (induced tensor interactions) (Blin-Stoyle 1973 pp. 107-111; Morita 1973 pp. 153-155, p. 298; Wilkinson 1975; Wu 1977).

Measurements of the shapes of the β spectra of some first forbidden transitions ($0^{\pm} \longrightarrow 0^{\pm}$ or unique first forbidden) have been used to test the partially conserved axial current hypothesis of beta decay (PCAC). These tests consist mainly of extracting a value for the pseudoscalar coupling constant from the shape of the β spectrum and comparing it to the predictions of PCAC. In addition, precise shape measurements of these first forbidden β spectra have been used to look for other contributions to nuclear β decay induced by the strong interaction, especially the induced tensor term (sometimes also referred to as the induced pseudotensor) (Schopper 1966 pp. 222-224, pp. 236-238; Blin-stoyle 1973 pp. 87-89; Bosch et al. 1973; Holstein 1974; Behrens et al. 1975). Most of these investigations have pointed to the need for more precise shape

factor measurements in order to obtain more conclusive estimates for the values of the pseudoscalar and pseudotensor coupling constants (Krmpotic & Tadic 1969; Abecasis & Krmpotic 1970).

Since the Hamiltonian of the weak interaction is considered to be quite well known and understood, measurements of the beta decay observables can be used to study the nuclear structure of the decay participants. The accurate determination of the shapes and ft values of forbidden beta spectra allows one to evaluate the matrix elements between the nuclear states involved in the beta transition (sometimes knowledge of other β decay observables is required too). These nuclear matrix elements (β moments) represent the overlap between the wavefunctions describing the parent nucleus and those of the daughter nucleus. Therefore they contain the properties of the initial and final states and are quite useful in nuclear structure studies (Schopper 1966 pp. 245-348; Daniel 1968; Booij 1970; Morita 1973 pp. 222-225, pp. 229-233; Hughes 1980; Behrens & Buhring 1982 pp. 537-607). Moreover, the CVC theory predicts the ratios of certain matrix elements in forbidden β decays (especially first forbidden nuclear matrix elements) and therefore the evaluation of such matrix elements provides an indirect test of this theory (Smith & Simms 1970; Blin-Stoyle 1973 pp. 64-68).

The ft values of the superallowed β decays of $T_z = -1/2$ mirror nuclei (or other superallowed $J^\pi \longrightarrow J^\pi$, $J \neq 0$, $\Delta T = 0$ decays) can be used to calculate the Gamow-Teller (GT) matrix elements which provide a sensitive test for theoretical nuclear structure calculations (Aysto et al. 1984; Arai et al. 1984). Similarly, ft values of allowed GT transitions can be used to deduce the GT matrix elements between the states involved in these transitions (Behrens & Buhring 1982 pp. 534-536). On the other hand, for the superallowed decays where accurate shell model calculations of the GT matrix elements are possible, or where reliable estimates of the GT matrix elements are available from magnetic moment data, the ft values of the transitions can be used to examine a more fundamental problem, the renormalization of the axial-vector coupling constant of the weak interaction in nuclei (Wilkinson 1975; Azuelos & Kitching 1977; Raman et al. 1978; Behrens & Buhring 1982 pp. 499-506).

Another example of an area where β spectroscopy has contributed to both nuclear structure and fundamental interaction studies is the

investigation of isospin mixing in nuclear states. The isospin impurities of nuclear states are usually obtained from the ft values of isospin forbidden Fermi transitions (pure or mixed). These are transitions between members of two different isospin multiplets ($\Delta T \neq 0$), with spin and parity changes of either $0^+ \longrightarrow 0^+$ (pure), or $J^\pi \longrightarrow J^\pi, \Delta J=0, J \neq 0$ (mixed). From the ft values of isospin forbidden pure Fermi transitions, the magnitudes of the isospin mixing and the effective Coulomb matrix elements (charge-dependent matrix elements) between nuclear states can be calculated. For mixed transitions other β decay observables are also required. Consequently, the amount of analogue symmetry breaking in the states due to both the long range Coulomb force and the charge dependence of the nucleon-nucleon potential can be assessed (Bloom 1966; Blin-Stoyle 1973 pp. 68-79; Raman et al. 1975; Behrens & Buhring 1982 pp. 527-536). Furthermore, careful measurements of the shapes of the energy spectra of the β particles emitted in these decays help in clarifying the relative strength of the second forbidden contributions to the decays and therefore in obtaining more accurate estimates of the isospin admixtures in nuclear states (Van Neste et al. 1966; Sastry 1969). Finally, these studies of isospin mixing in nuclear β decays can also serve as a measure of the validity of the CVC theory (Blin-Stoyle 1973 p. 68, p. 77).

As illustrated by the examples above, the nucleus offers many advantages for use as a microscopic "laboratory" to study the effect of the various fundamental interactions in the diverse environments offered by the different nuclei (Blin-Stoyle 1973 p. 17). The importance of β spectroscopy in observing these effects is quite apparent. In this context, the possible occurance of very small anomalous shape factors in the beta spectra of some hindered β decays has been used to explore the possible presence of some exotic processes in nuclear beta decay (Morita 1973 pp. 227-229).

One more application for beta spectrum shape measurements can be found in studies involving internal conversion electrons. One of the most straightforward and accurate methods of measuring the internal conversion coefficients is the peak-to-beta-spectrum (PBS) method. The use of this method requires a precise evaluation of the total beta spectrum intensity and therefore explicit knowledge of the shape factors describing the β spectrum over the full energy range (Van Nooijen 1966).

Finally, attention has centered in the past few years on the β investigation of the shape of the β spectrum of tritium near the endpoint. This method is being used to measure the rest mass of the electron antineutrino (Lyubimov et al. 1980; Simpson 1981).

1.2 Nuclei far from stability

Nuclei can be defined in terms of two quantities, their atomic number (or number of protons Z) and the number of neutrons (N) they contain. The diverse properties of nuclei are a consequence of the different combinations of the N and Z numbers. Certain combinations produce nuclei that are stable against β decay. These nuclei are said to fall on the line of β stability. Nuclei with N and Z numbers that are very different from those of the β stable ones are said to be far off the stability line. They are also referred to as exotic nuclei implying that they are attractively strange or unusual objects. These nuclei are characterized by short half lives and large decay energies which give rise to unusual decay modes such as β delayed particle emission.

On the basis of sheer numbers, the importance of nuclei far from stability is obvious. It is conservatively estimated that there are 10000 nuclei that could exist for a sufficiently long time to observe or study, if the means could be found to produce them artificially. This is to be compared with approximately 300 isotopes that occur in nature and about 2000 nuclides whose existence has been experimentally determined but for many of which additional information is scanty (Hardy 1982). (See figure 1.1)

This large number of nuclear species with widely varying neutron to proton ratios provides an excellent opportunity for observing the variation of nuclear properties as a function of extreme changes in the numbers of proton and neutron in the nucleus. Thus, nuclei far from β stability are a good testing ground for many nuclear structure and nuclear mass theories that have been mostly formulated on the basis of data obtained from stable or long lived nuclides. The availability of exotic nuclei therefore enhances the concept of the nucleus as a laboratory. The increase in the number of available nuclei allows one to have a more versatile choice of a specific nuclear property or transiton type to reflect an important feature of one of the fundamental interactions. One

Figure 1.1

The chart of nuclides. Stable isotopes are represented by black squares. The region of known nuclides unstable against beta decay is enclosed by the broken contour. The diagonal smooth lines indicate the approximate locations of the neutron and proton drip lines. The circular lines are isodeformation curves showing the domains where nuclear deformation occurs. The straight vertical and horizontal lines indicate the locations of the neutron and proton shell closures respectively.

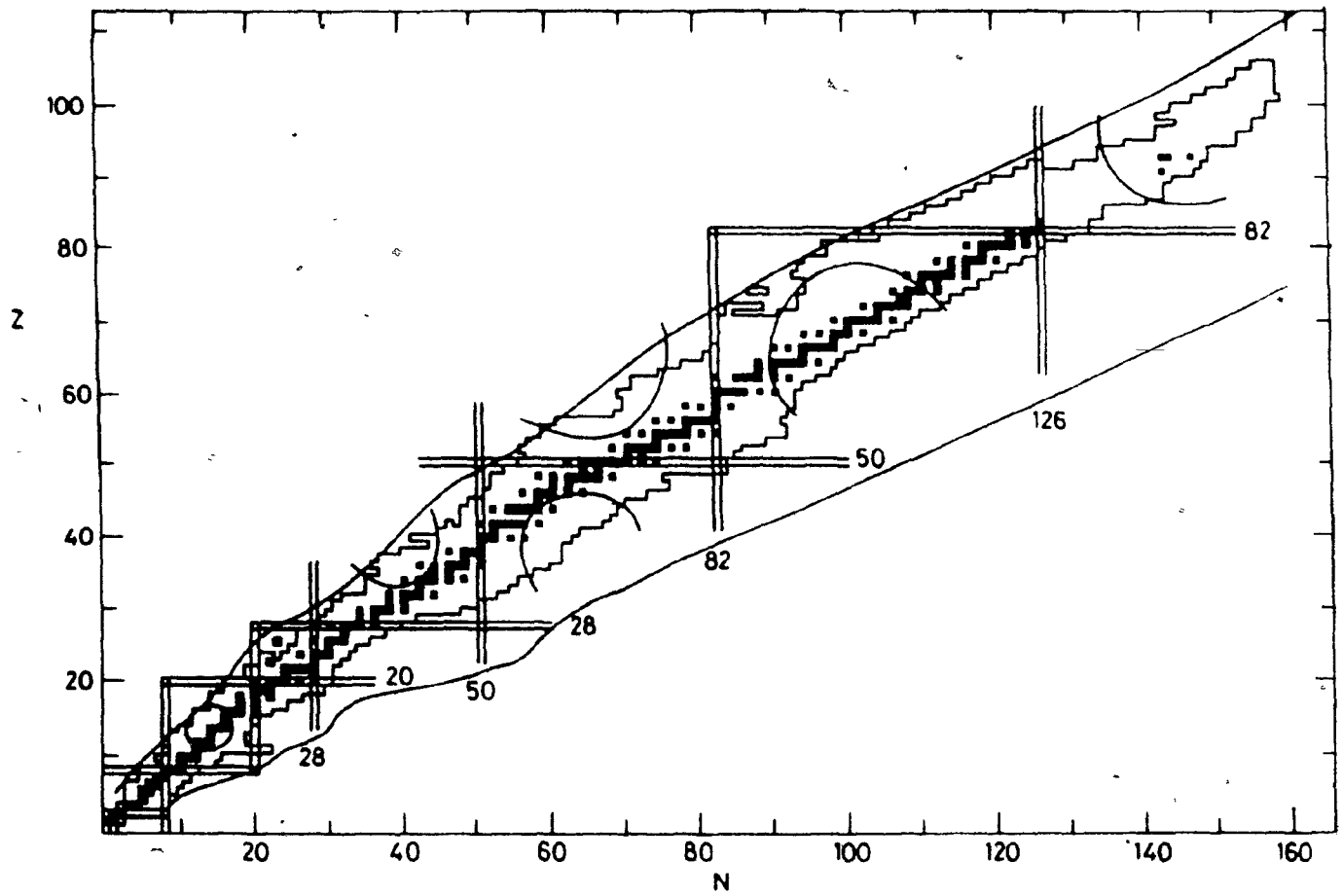
Z
N
20
40
60
80
100
120
140
160
20
40
60
80
100
28
20
50
28
50
82
126
82

'can therefore select a particular process which is sensitive to a certain aspect of the interaction under study or a process where an undesired effect is strictly forbidden. Because of all of this and more (Berlovich 1970), the study of nuclei far from the line of β stability has become a center of attention and activity in nuclear science in recent years (Bergstrom 1966a,b; Forsling et al. 1966; CERN-1970; CERN-1976; Chrien 1977; Ravn 1979; Hansen 1979; Hamilton et al. 1979; Gelletly 1980; von Eigdy 1980; Jonson 1981a,b; Lee 1981; CERN-1981; Hamilton 1982; and references therein).

1.3 Beta Spectroscopy of Nuclei Far from Stability

Measurement of the energy spectra of β particles emitted in the decay of nuclei in the far off stability region is a topic of interest for several reasons. For example, the well known mass parabola (for fixed mass number A) shows a dramatic increase in the β decay energy with increasing distance away from stability. This increase in the decay energy affords a new view on the weak interaction process. It also leads to the population of states above the threshold for particle emission which in turn gives rise to β delayed emission of protons, neutrons, or alpha particles in these nuclei, a phenomenon that for the most part is unknown near stability.

As mentioned before, measurement of the β endpoint enegy can be used to determine the mass difference between the ground states of nuclei. Thus following a β decay chain and measuring the Q_β for each decay, until a stable nucleus where a direct mass measurement has been made is reached, enables one to infer the masses of the unstable nuclei in the isobaric chain. This method of mass determination is the most commonly used method for nuclei far from stability since off-line direct mass measurement methods are not applicable because of the short half lives of the nuclei involved. In comparison to on-line direct mass measurement methods, Q_β measurements are considerably simpler and require less sophisticated equipment and techniques (Epherre et al. 1980 and references 1-9 therein). They are particularly advantageous for nuclei of elements which are not easily ionizable or for nuclei with long lived isomeric states (Wollnik et al. 1980; Wollnik 1980; Hardy 1980).

The mass of the ground state of the nucleus is one of its most

important properties. The precise determination of masses of an extensive set of nuclei would help in mapping the mass surface far from stability. It would also facilitate extrapolations to even more exotic regions and aid in locating the positions of the neutron and proton drip lines and the limits for stability against alpha emission and spontaneous fission. Such a set of mass measurements would also provide a scoreboard for testing existing nuclear mass theories. These tests become increasingly more stringent as the nuclei are farther removed from stability. Such mass measurements would therfore also permit a better determination of the parameters of existing mass formulae.

From nuclear mass data one can calculate nuclear binding energies. A systematic study of these values provides information about the shapes of nuclei and their shell structure. They can show the effects of pairing, shell closures, the onset of nuclear deformations and perhaps reveal unexpected structures in new regions (Hansen 1979; Hardy 1980; Munnich 1980; Detraz et al. 1983).

Knowledge of the Q_β values can also be used to guide searches for β delayed particle emitters (precursors) in decays where Q_β exceeds the binding energy of the particle in the nucleus.

Extending the investigation of superallowed beta decays to heavier nuclei is quite an interesting prospect. However, the nuclei in which these decays take place fall farther away from stability as their mass number A increases. (^{74}Rb is the heaviest Z=N nucleus known with a superallowed Fermi transition while ^{71}Kr is the heaviest T_z= -1/2 nucleus with a superallowed decay). Since these nuclei are so far removed from stability, using simple nuclear reactions to measure the energy difference between the parent and daughter states is not feasible and therefore exotic heavy reactions have been proposed (Davids et al. 1979). On the other hand, Q_β measurements provide an attractive alternative and allow for the expansion of superallowed β decay studies to heavier regions of the chart of nuclides with important implications for nuclear structure work, nuclear mass formulae, and fundamental physics (the nature of the weak interactions and the structure of the nucleon) (Wilkinson 1975; Arai et al. 1981; Hardy 1983; Aysto et al. 1984; Arai et al. 1984).

An important concept in nuclear physics which gains even more significance in regions far from stability is that of the beta strength

function. It expresses the effect of nuclear stucture on β decay, and represents a valuable tool for studying the nuclear matrix elements of the states involved in the decay. Careful measurements of the β ray energy spectrum down to and including the low energy portion, presents a straightforward method of obtaining the beta strength function (Iafigliola et al. 1983a). It is quite advantageous in regions far from stability where complete decay schemes are unavailable and where other methods of beta strength measurement are complicated and inefficient (Hansen 1973).

Beta spectroscopy of nuclei far from stability has some applications in other fields of science and technology too. For example, knowledge of the β decay energies, beta strength functions, and decay rates is quite important for certain astrophysical calculations such as those of the r-process in nucleosynthesis (Arnould 1980; Klapdor et al. 1981).

Three other important applications involve the β spectroscopy of short lived fission products. The first concerns the use of reactor antineutrinos in experiments (Vogel 1979). For the interpretation of the results of these experiments, it is important to know the energy spectrum of the antineutrinos emitted during the β decay of the fission products. The energy spectrum of the antineutrinos is simply the complement of the energy spectrum of the β particles emitted during the decays of the fission products and which can be measured using β spectroscopy methods. Decays with high Q_β values are especially significant since they are responsible for the important high energy portion of the antineutrino spectrum (Avignone & Greenwood 1980).

The second application concerns the calculation of the power developed in the fuel of a nuclear reactor by the decaying fission products. This power is estimated to be about 7% of the total reactor power at equilibrium (Rudstam et al. 1981). It would have an even more important role in the case of an emergency shutdown since it is possible to stop the fission process in a reactor rapidly but it is impossible to stop the decay of the fission products. Knowledge of the average energy of the emitted β particles in the decay and the feeding to different states in the daughter nucleus is crucial for such calculations.

The third application involves the use of β spectroscopy methods in searches for fission products with very high β decay energies (>15 MeV).

These searches provide information on the yield of light nuclei (A=8~15) in fission and on the probable production of "abnormal" nuclei in the fission process. Two examples of such abnormal nuclei are: nuclei very close to the nucleon drip lines, and density isomers resulting from pion condensation in the nucleus (Borovoy et al. 1979 and references therein).

The importance of determining the properties of different nuclei increases with their distance from the line of stability. This is mainly because little is known about these nuclei and also because extrapolations from the region of stability tend to show large discrepencies. However, the experimental difficulties involved in studying these nuclei increase in the same fashion.

Measurements of the β spectra of exotic nuclei is complicated by their short half lives and by the large amount of energy available for the decay. This high Q_β means that the electrons (or positrons) to be measured have high energies (typically between 5 and 10 MeV). It also implies that the daughter nucleus is going to be produced in a variety of excited states, which de-excite by high energy multiple γ ray emission.

The experimental program on which this thesis reports revolves around the design, construction and development of a spectrometer for measurements of the β ray spectra of nuclei far from stability. The aim of the design is to produce a spectrometer suitable for use in the determination of β decay endpoint energies and the relative intensities of the different β transitons in multi-branch decays in these nuclei. The spectrometer should also have the high degree of precision and sensitivity required for accurate spectral shape determinations (measurements of the shape factors of the β spectrum).

As will be seen in the next chapter, most previous spectrometer designs are plagued with problems that render them either unsuitable for the study of β spectra of short lived nuclei or unfit for accurate spectral shape determinations (or sometimes both). Indeed large discrepencies between measurements done with different spectrometers are still plentiful in the published litreature (Paul 1965; Daniel 1968; Behrens & Szybsiz 1976). The inconsistency in the data on beta spectra shape measurements has been frustrating to such an extent that the suggestion was made to accept the theoretical predictions for the shapes of the spectra and use these predictions to test the accuracy of the

experimental methods for shape determination (Nichols et al. 1966). It has also been suggested that in cases where the shapes of β spectra are needed for other applications (such as the PBS method for conversion coefficient measurements), that the spectra be reconstructed from knowledge of other observables in the β decay rather than rely on the experimental shape measurement (Van Lieshout 1966).

1.4 The Present Beta Spectrometer

The β spectrometer described here is a radically improved version of a previous design which was developed at this lab (Moore et al. 1976; Rehfield 1977). The basic idea behind both spectrometers remains the same, but the capabilities and attractive features of the present one far exceed the former.

The principle on which both spectrometers are based is the use of a high purity germanium crystal (Ge(HP)) as an electron detector and spectrometer. The excellent resolution of the Ge(HP) detector and its capability of measuring the energies of incident particles over a wide range simaltaneously (a multichannel device) are fully exploited by using it in a high transmission arrangement (see appendix A for glossary). At the same time, by greatly enhancing the ratio of β particles to γ rays incident on the detector, the high sensitivity of the Ge(HP) detector to γ rays is not allowed to result in any significant contamination of the β spectrum with γ ray counts.

The two conditions above can be fulfilled by placing both the radioactive source and the detector along the axis of a strong cylindrically symmetric magnetic field, separated from each other by as great a distance as is feasible. In this specific spectrometer, a superconducting solenoid furnishes the strong magnetic field which deflects the β particles emitted from the source and channels them to the detector. In this role the solenoidal field acts simply as an electron guide with no energy or momentum selection. As for the γ rays, the solid angle into which they should emitted from the source so as to strike the detector is simply the geometric solid angle subtended by the detector at the source. This solid angle could be made very small by increasing the source-detector separation. The acceptance solid angle for the β rays is determined by several factors including the position of the radioactive

source in the magnetic field, the magnetic field strength and geometry, the surface area of the detector, and the β ray energies. It can reach up to 50% of 4π for reasonably high electron energies in the present spectrometer. At 25% electon transmission the enhancement ratio of electrons to γ rays incident on the detector is larger than 250. This coupled to an electron energy resolution of about 4.5 keV (0.45% at 1 MeV electon energy and better for higher energies) and the broad band nature of the instrument make the capabilities of this spectrometer truly unique.

1.5 Organization of the Thesis

Since this thesis deals mainly with the design and construction of a new beta spectrometer, it was felt that a review of the literature on the subject of beta spectroscopy methods and techniques would be quite helpful. Hence, Chapter 2 of this thesis is a comprehensive review of the different types of beta spectrometers in existence, concentrating primarily on the distortions that they inevitably introduce to the measured beta spectra and the possibiltiy of overcoming such distortions through the use of new techniques.

Chapter 3 of the thesis deals with the design and construction of the superconducting solenoid which forms a major component of the present beta spectrometer. A complete analysis of the thermal properties and performance of the liquid helium cryostat of the superconducting magnet is also included.

Chapter 4 concentrates on the different source-detector combinations used with the spectrometer. It contains detailed descriptions of the two detector systems that have been tested with the spectrometer. The different source introduction mechanisms (and the associated vacuum system) that are in use with the spectrometer are also treated at length. A discussion of the principles of operation of the semiconductor detectors is included in this chapter as well.

In Chapter 5, the problems of calculating the magnetic field of the solenoid and the trajectories of the beta particles in the magnetic field are dealt with. Several examples of the performance of the spectrometer are also given in this chapter.

Finally, the general conclusions drawn from this work are discussed in Chapter 6.

CHAPTER 2

A CRITICAL REVIEW OF BETA SPECTROSCOPY METHODS AND TECHNIQUES

It is clear from the discussion in the previous chapter that accurate measurements of β spectra (determinations of the exact shape of the spectrum and the energy of the endpoint) are quite important. In order to effect these measurements various ideas have been exploited in the design of β spectrometers throughout the evolution of nuclear physics.

There are two fundamental principles upon which β spectroscopic methods are based. The first is the measurement of the momentum (energy) of the electrons by deflecting them in a magnetic (electric) field. The second is the determination of the total energy deposited by the β particles in an absorbing medium when they are stopped in it. In general, spectrometers based on the latter principle act as detectors and energy resolving devices simultaneously. The relative merits and drawbacks of the different types of β spectrometers will be discussed at some length in what follows.

2.1 Deflection Spectrometers

2.1.1 Electrostatic Spectrometers

Because of the very high electric fields needed for analyzing high energy β particles, and the fact that the focusing properties of electrostatic fields are not relativistically invariant, electrostatic spectrometers are only suited for studies of low energy β transitions. Therefore, they have not received much attention in nuclear spectroscopy but have been extensively developed for atomic physics and surface analysis studies (Siegbahn 1965, p.172; Gerholm 1961).

2.1.2 Magnetic Spectrometers

A great deal of effort and ingenuity was put in the development of magnetic spectrometers for electron spectroscopy, especially in the improvement of their resolution. The concentration on the achievement of high resolution in these spectrometers was motivated by the fact that they

were the primary tool in high resolution investigations of electromagnetic transitions in nuclei. In addition to being used to measure continuous β spectra, these spectrometers were used in the determination of the energies of internal conversion electrons and γ rays. The gamma rays were detected and measured through the secondary electrons (photoelectric, Compton, and pairs) that they produced in external radiators placed in the source position of the magnetic spectrometer (Hedgran 1952; Deutsch & Kofoed-Hansen 1959; Mladjenovic 1961; Backstrom et al. 1962; Gerholm 1965; Murray et al. 1965; Hollander 1966; Browne 1972; Mladjenovic 1976, p.20; Bartholomew & Lee-Whiting 1979).

Thus magnetic spectrometers played a role similar to the one played today by high resolution semiconductor germanium detectors in the determination of the different quantum levels of excited nuclei through γ ray spectroscopy.

Although magnetic spectrometers still provide the best resolution achievable in electron spectroscopy ($\sim 0.01\%$ momentum resolution, Siegbahn 1965, p.86), they are not well suited to studies involving nuclei far from stability (Bergstrom 1966b). Several factors that are inherent in the design and operation of these spectrometers are responsible for limiting their usefulness in the field of β spectroscopy of short-lived nuclei.

The intrinsic dependence of good resolution of magnetic spectrometers on poor transmission is one such factor (Wu & Geoffrion 1960). The small acceptance solid angles (a few percent of the 4π at a few percent resolution, Siegbahn 1965) and the fact that the measurements are performed in small steps covering a narrow momentum band in each step (single channel instruments) result in the long counting periods that are characteristic of such spectrometers.

The long counting periods represent a clear disadvantage in short-lived nuclei. The large number of background counts accumulated during the long counting periods reduces the significance of the information that can be obtained from the β spectra. Moreover, any time variations in the background over the long counting periods can introduce serious distortions to the shape of β spectra that are difficult to correct (Graham et al. 1960).

Another problem associated with magnetic spectrometers is their unsuitability for coincidence measurements (Siegbahn 1965, p.161; Graham

et al. 1960). The small acceptance solid angle (usually less than 10% of 4π) of these spectrometers reduces the probability that an electron will enter and be detected in the spectrometer in coincidence with a photon or another particle emitted in a different direction and detected by another detector. Increasing the source strength to counter the low efficiency would increase the coincidence rate, however it would also reduce the ratio of true to chance coincidences thus reducing the usefulness of the accumulated data (Spejewski 1966).

Finally, there is the problem of β spectrum shape distortions caused by the finite resolution of the spectrometer. Because of the inherent interdependence between the resolution and transmission of magnetic spectrometers, operating them in a high transmission mode results inevitably in a deterioration in the resolution. The finite resolution of the spectrometer manifests itself in a broadening of the width of monoenergetic electron lines as measured by the spectrometer. The spectrum generated by a monoenergetic electron line measured with a β spectrometer is often referred to as the response function of the spectrometer. If the response function of the spectrometer is a symmetric guassian in shape, then the deterioration of resolution results in distortions to the shapes of the continuous β spectra at the low and high energy ends of the spectrum. Special correction techniques have to be applied to the measured spectrum to remove the effects of such distortions, especially near the endpoint. However, if the response function of the spectrometer is not symmetric (as in the case of semicircular spectrometers for example), then the distortions extend over the whole spectrum and have to be effectively corrected for over the full energy range. (Owen & Primakoff 1948, 1950; Paul 1964, 1965; Nagarajan et al. 1969; Lizurej 1980).

Excellent reviews of the various aspects of magnetic β spectrometry have been published prior to 1965. The most definitive being the work of K. Siegbahn (1965). This work also includes a comprehensive listing of the previous surveys of the field of β spectrometer theory and design. Since 1965 until the present, the reviews of the field that have appeared in the literature are largely due to the work of M. Mladjenovic (1971, 1972, 1976, 1979).

The problems associated with the different components of the

spectrometer and the distortions they cause are discussed below.

2.1.2a The Radioactive Source

1) Normalization

Since magnetic spectrometers are single channel instruments, careful corrections have to be made to account for the decay of the source during the time needed to record a spectrum. The application of such corrections require: an accurate determination of the half-life of the decaying nucleus under study, knowledge of the concentrations and the half-lives of any radioactive contaminants in the source, and ensuring that none of the source activity escapes through evaporation, diffusion out of the source, or any other mechanism during the long counting periods (Bergstrom et al. 1963).

In the case of short-lived nuclei, several sources have to be used during the spectrum accumulation and therefore the measurements have to be normalized to the same source activity. Achieving this normalization with the high degree of accuracy required for careful spectral shape determinations is quite a complicated task (Armini et al. 1967; Halbig et al. 1974; Genz et al. 1976a; Calprice & Alburger 1978). An excellent discusssion of some of the problems involved in the normalization of the spectrum is given by Van Elmbt (1981).

2) Source Shape and Size

Magnetic spectrometers place some demands on the geometry of the radioactive source. Flat spectrometers ($\pi\sqrt{2}$ or semicircular magnets for example) require rectangular sources, while lens type spectrometers (Siegbahn-Slatis intermediate image spectrometer for example) require circular sources (Mladjenovic 1976, p.32). Source sizes that are as small as possible are usually used since the resolution of the spectrometer is dependent on the size of the radioactive source (Wu & Geoffrion 1960; Deutsch & Kofoed-Hansen 1959). The typical source dimensions are a few millimeters (diameter for lens type spectrometers and width in flat spectrometers) and can sometimes be as small as a fraction of a millimeter (Alburger 1956; Fujioka 1970). Any variation in the geometry of the source (size or shape) can lead to differences in the resolving power and

therefore in the transmission of the spectrometer (Lewin 1966).

When several sources are used to accumulate a single spectrum, as is the case in studies of nuclei far from stability, reproducibility of the size and shape of the source has to be ensured for all of them. This is especially important if a spectrometer with low luminosity is used since variations in the shape of the source have serious effects on the resolution of such spectrometers (Halbig et al. 1974). The use of magnetic spectrometers on-line and in conjunction with an isotope separator (as is frequently required in short lived nuclei), aggravates these problems further since neither the size nor the position of the sources produced on-line will be constant (Avignone et al. 1973; Halbig et al. 1974). Positioning the source in the spectrometer also has to be done very carefully (a maximum tolerance of 0.1 mm along certain axes is required even in spectrometers with modest resolution (Wegstedt 1956)) (see magnetic field section).

3) Source Thickness and Uniformity

Because of the low efficiency of magnetic spectrometers, sources of high activity are needed in order to achieve an acceptable count rate above the background. The source activities required in these spectrometers are typically several MBq (several tens of μCi) (Van Atta et al. 1950; Graham et al. 1960; Van Klinken et al. 1968; Christmas & Cross 1978; Van Elmbt 1981). However, sometimes activities as high as 750 MBq (∿20 mCi) are required to obtain good statistics (Wortman & Langer 1963). The requirement for strong sources coupled to the restrictions imposed on the source size results in the use of sources of increased thickness (Hughes 1980, p.107).

It has long been known that the use of thick sources (>10 μg/cm) in β spectroscopy causes a deterioration in resolution as a result of the energy loss and straggling (variation of energy loss of monoenergetic particles) of electrons in the source material (Mladjenovic 1976, p.19). Since the energy loss and the straggling in a thick source are dependent on the energy of the electrons, it will be different for different parts of the spectrum and will result in spectral shape distortions and a general shift in the spectrum to the low energy side (Feldman & Wu 1949; Knop & Paul 1965).

The increased source thickness also causes an increase in the number of β particles backscattered from the source material itself. Since this effect is also dependent on the energy of the β particles it will result in distortions to the shape of the measured β spectrum (Bergstrom et al. 1963).

The most important effect of source thickness is the distortion to the shapes of β spectra caused by multiple forward scattering in the source material (Daniel 1968). Since electrons passing through the source material at large angles with respect to the normal to the source surface traverse more source material, they will be scattered more than those moving close to the normal direction. This scattering causes the source to have more particles emitted in directions close to the normal than at large angles to the normal (Paul 1965); there is electron anisotropy. Moreover, the anisotropy will be energy dependent with larger values at lower energies (Spalek 1982). It will therefore cause the spectrometer to have an energy dependent effective acceptance solid angle resulting in deviations of the measured spectrum from its true shape (Paul 1965; Hoffmann & Baier 1965; Parker & Slatis 1965).

The self-absorption of low energy β particles in thick sources can also result in distortions to the shapes of β spectra. This effect, however, is negligible for source thickness smaller than a few hundred $\mu g/cm^2$ (Booij 1970).

Attempting to ease the limitation on source size by constructing larger spectrometers (which have higher luminosity and can therefore accommodate larger sources without a deterioration in resolution) creates other complications. As the source size increases with the increase in the spectrometer size, so does the sensitive counter area required to detect the β particles. Therefore the advantage gained from the larger source area may be nullified by an increase in the background count rate due to the larger detector volume (Graham et al. 1960). The increase in the dimensions of the spectrometer also implies that the magnetic field required to focus electrons of a given energy will be lower and in fact can be quite small for low β particle energies and large spectrometers. The effects of magnetic interference from magnetic sources outside the spectrometer will be more severe (Siegbahn & Edvardson 1956; Graham et al. 1960). The increase in the cost of the spectrometer as its dimensions are

enlarged is another limiting factor.

Clearly, with increased source thickness, it is difficult to attempt to make sources of high degree of uniformity (Langer et al. 1949). Non-uniformity in the source thickness contributes to the distortions in the shape of a continuous β spectrum due to β particle scattering in the thickest regions of the source (Hughes 1980, p.107).

4) Source Backing

Beta sources are usually deposited on thin foils made from organic materials with low atomic number (Z) (e.g. mylar) to minimize the probability of electrons backscattering from the source backing. Most of these organic materials are also very good insulators, and since strong radioactive sources are needed for magnetic spectrometers, these sources may charge by several kilovolts relative to ground as a result of the build-up of electric charge caused by the β particles leaving the source and the small electrical capacity of the source. Beta particles emitted from such a source experience an energy shift due to their Coulomb interaction with the electric field of the charged source (Hayward 1953; Parker & Slatis 1965; Mitchell 1965, p.486). This effect is obviously time dependent due to the build up of charge with time (Braden et al. 1948) and would therefore cause serious distortions to the β spectrum collected by a single channel instrument such as a magnetic spectrometer (Douglas 1949). Preventing charge build-up on the source when the use of metallic foils is to be avoided is not an easy task (Langer 1948; Nichols et al. 1961).

5) Background Associated with the Radioactive Source

The requirement for strong sources introduces yet another problem in magnetic spectrometers. In many cases, the β decay is accompanied by intense γ ray emission (especially in nuclei far from stability), the γ rays can end up striking the detector after one or more collisions with the different components inside the spectrometer (Schwarzchild et al. 1956; Wortman & Langer 1963; Nagarajan et al. 1969). The γ rays can also cause the production of secondary electrons (electron-positron pairs, Compton and photoelectric) inside the spectrometer including the source itself and the source backing (Wortman & Langer 1963; Fujioka 1970).

These electrons are deflected in the magnetic field of the spectrometer and quite often are detected by the detector thus adding to the background and distorting the β spectrum (Deutsch & Kofoed-Hansen 1959; Backstrom et al. 1962; Booij 1970 pp. 49-51; Mladjenovic 1976 p.19; Hughes 1980, p.119; Van Elmbt 1981, p.64).

2.1.2b The Spectrometer's Chamber and Baffles

The determination of the momentum of the electrons in the magnetic field of the spectrometer is accomplished by a system of slits and baffles that limit the possible trajectories for electrons emitted from the source so that only those electrons in a small, chosen momentum interval corresponding to a specific trajectory are focused and can reach the detector and be counted. Electrons tracing other trajectories are stopped in the baffles.

1) Scattering of β Particles from Solid Objects in the Spectrometer Chamber

Beta particles with momentum values outside the desired band can reach the detector after one or more collisions with the baffles, the walls of the spectrometer or the source mounting (Schwarzchild et al. 1956; Burgov et al. 1961; Kofoed-Hanssen & Christensen 1962 p.39; Beekhuis & de Waard 1965; Paul 1965; Booij 1970; Nagarajan & Venkata Reddy 1970; Mladjenovic 1976, p.32; Christmas & Cross 1978).

The probability of an electron being scattered in a given direction after such a collision depends on the energy of the incident electron (Knop & Paul 1965). In addition, scattering from these thick objects occurs at depths that are comparable to the electron ranges. Hence the electrons will not only change direction but also suffer a significant energy loss in most cases (Paul 1965; Booij 1970). Some of these scattered electrons will therefore be counted at a momentum setting which is higher or lower than their initial momenta. The contributions of such events to the detector count rate are dependent on the energy of the primary electrons, the magnetic field strength and the resolution of the spectrometer (Gerholm & Lindskog 1963). Scattered electrons will therefore distort the shape of the β spectrum over the entire energy range (Genz et al. 1976; Hughes 1980, p.128).

The scattering of β particles from various objects inside the spectrometer can even cause counts at energies higher than the endpoint of the spectrum. This effect is quite serious in beta spectra with an intense low energy branch and a high energy weak branch (Schwarzchild et al. 1956; Bartlett et al. 1962; Wortman & Langer 1963; Paul 1965; Hsue et al. 1966a,b).

The scattering and stopping of β particles in solid objects in the spectrometer can also be accompanied by the ejection of secondary electrons which can end up in the detector causing background counts and spectral shape distortions. This effect will be different for positrons and negatrons spectra due to the different directions of charged particle paths (Kofoed-Hansen & Christensen 1962, p.40).

2) Scattering from Baffle Edges

If a spectrum with a high endpoint is being investigated, then fairly thick baffles are needed to completely stop electrons with momenta outside the desired band. The probability of β particle scattering from such thick edges is appreciable. Since the high energy β particles will suffer less scattering than ones with lower energy, the transmission of the baffles could become energy dependent causing serious distortions to the β spectrum and shifts in the observed endpoint of the spectrum (Porter et al. 1957; Kofoed-Hansen & Christensen 1962, p.39; Camp & Langer 1963; Van Klinken et al. 1968; Howe 1969; Booij 1970 p. 48; Zeeman et al. 1971; Hughes 1980, p.130).

3) Photon Production

The stopping of β particles with undesired momenta in the spectrometer's baffles and the scattering of β particles from the different solid objects inside the spectrometer can also be accompanied by bremsstrahlung radiation emission (Langer et al. 1964; Behrens et al. 1972; Calprice & Alburger 1978), and in the case of positrons by annihilation photons (Bartlett et al. 1962; Camp & Langer 1963; Booij 1970).

Photons thus produced might strike the detector directly or they might scatter from one of the spectrometer's components producing secondary electrons. Since the trajectories of the primary and secondary

electrons, and the locations of the sites of such photon producing collisions are dependent on the magnetic field strength (i.e. momentum setting of the spectrometer) (Bartlett et al. 1962; Gerholm & Lindskog 1963), their contribution to the detector count rate will vary at different parts of the spectrum and therefore cause the collected spectrum to deviate from its true shape.

4) Trochoidal Orbits

Another phenomenon which can cause counts beyond the endpoint and considerable distortions to the shapes of β spectra is that of low energy electrons reaching the detector after executing several turns in the spectrometer (trochoidal orbits) (Freedman et al. 1960; Bourgov et al. 1961; Booij 1970; Christmas & Cross 1978). The number of additional counts that these electrons cause in the detector increases with the increase in the strength of the magnetic field (Booij 1970). Therefore they represent an energy dependent contribution to the accumulated spectrum and introduce spectra shape distortions.

Because of all the phenomena mentioned in this section, a great deal of effort has to be invested in designing, testing, positioning and adjusting the baffles (Lee et al. 1963; Paul 1965). Special attention has to be paid to the shapes of the baffles, their thickness, the material from which they are made and the inclination of their edges. In addition, extra baffles have to be installed to reduce the intensity of scattered electrons (Langer & Cook 1948; Porter et al. 1957; Graham et al. 1960; Bartlett et al. 1962; Kofoed-Hansen & Christensen 1962, p.39; Camp & Langer 1963; Siegbahn et al. 1964; Van Klinken et al. 1968; Daniel et al. 1970; Antman et al. 1970; Booij 1970). All these baffles have to be electrically grounded to avoid the build-up of electrostatic charges on them. The accumulation of such charges on the baffles will cause electric potentials that alter the focusing properties of magnetic spectrometers (Owen & Cook 1949; Langer et al. 1950; Van Atta et al. 1950; Nichols et al. 1961; Christmas & Cross 1978). In fact, the shapes and endpoints of β spectra measured with magnetic spectrometers are found to be dependent on the number of the baffles used and their settings (Nichols et al. 1961; Van Klinken et al. 1968; Nagarajan 1969).

2.1.2c The Magnetic Field

Since the deflection experienced by β particles in the magnetic field of the spectrometer is used to determine their momenta, the generation of a magnetic field of a precise shape and magnitude inside the spectrometer is a crucial requirement for accurate measurements of the shapes of β spectra. Indeed some of the major tasks in constructing magnetic spectrometers are the design and fabrication of the magnet and the verification that the desired field magnitude and geometry have been achieved.

After achieving the desired field, the processes of alignment of the source, the detector and the different baffles in their proper positions in the magnetic field have to be performed with extreme care and diligence (Lee et al. 1963; Alburger 1956; Nagarajan et al. 1969; Van Elmbt 1981). Smaller spectrometers with low luminosity and low dispersion are more sensitive to the effects of misalignment than larger spectrometers.

Failure to maintain perfect alignment results in deviations in the properties of the spectrometer and therefore distortions to the β spectrum (Deutsch & Kofoed-Hansen 1959). In studies of short-lived nuclei, many sources are needed during the accumulation of a single spectrum. It is vital that the introduction of these sources be done rapidly while at the same time maintaining the accuracy and the reproducibility of the source position. Variations in the position of the source in the magnetic field cause variations in the resolution, transmission and calibration of the spectrometer (Wegstedt 1957).

There are three commonly used methods for generating the magnetic field of a β spectrometer.

1) Permanent Magnets

Permanent magnets are suitable only for the constant field, variable trajectory type spectrographs. The resolution of such spectrometers varies inversely with the momentum of the β particles. Furthermore, the transmission decreases as the momentum increases in a more complicated manner (Wu & Geoffrion 1960). This aggravates the problems of analyzing continuous β spectra and accurately determining their shape.

If permanent magnets are used, a set of spectrographs of different magnetic field strengths is needed to cover a wide range of energies (Mladjenovic 1971).

Another shortcoming from which these spectrometers suffer is that of stability. In order to keep the magnetic field strength stable and constant, the magnet has to be kept at a constant temperature at all times and not only during the measurements (Mladjenovic 1976, p.31). Achieving the desired magnetic field with permanent magnets can be a complex and tedious process involving the use of coils incorporated into the spectrometer to initially magnetize the permanent magnets (Slatis 1958).

For all these reasons, the use of permanent magnets does not present an attractive option in comparison with alternative methods of achieving the desired magnetic field. These alternative methods involve the generation of the magnetic field through the use of electromagnetic coils either with or without a ferromagnetic core.

2) Iron-Free Magnets

Iron-free spectrometers at first sight seem to offer a reasonable solution to the problems of creating the required magnetic field because of the linear relationship between the current in the coils and the magnetic field and the constancy of the shape of the magnetic field with varying magnetic field strength. However, these magnets suffer from several drawbacks some of which will be discussed here.

a) Non-Linearity

Deviations from the strict proportionality between the spectrometer's current and the focused electron's momentum may arise from several sources. Such deviations from linearity are quite difficult to detect at high field strengths due to the lack of suitable monoenergetic electron calibration sources with energies above $\sim$ 1 Mev (Siegbahn 1965, p.198-202).

One source of non-linearity is the hysteresis effect caused by ferromagnetic materials in the vicinity of the spectrometer as the field of the spectrometer is varied (Christmas & Cross 1973, 1978).

A second source of deviation from linearity are the eddy currents

that are set up in any conducting part of the magnet or the spectrometer when the current in the coil is being changed. Rapid variations of the magnetic field are sometimes required in studies of short-lived nuclei. The change in the magnetic flux passing through the conducting components of the spectrometer induces eddy currents in these components. The eddy currents in turn create a magnetic field of their own which opposes the change in the magnetic field of the coils. As a result of this, the variation in the magnetic field inside the volume of spectrometer will lag behind the current in the coils. The functional dependence of the magnetic field on the current will be multivalued, exhibiting effects similar to those of hysteresis in ferromagnetic materials.

Because the eddy currents do not have the same spatial distribution as the current in the coils, the magnetic field they produce does not have the same geometry as the field generated by the coils. Therefore, the rapidly varying field in the spectrometer has a geometry quite different from that of the static field. Predicting the geometry of the time varying field is quite difficult.

The phenomenon of eddy currents in iron-free spectrometers results in calibration shifts and variations in the transmission of the spectrometer (a detailed discussion of such effects is given by Van Elmbt (1981)).

b) Temperature Sensitivity

The magnetic field magnitude and geometry remain constant (at a given current) only if the temperature of the coils is kept constant. The temperature of the spectrometer's vacuum chamber has to be held constant as well in order to avoid misalignments of the various components. At high fields (i.e. high currents passing through the coils) the rise in temperature caused by Joule heating can produce dimensional changes which can alter the focusing magnetic field in strength and geometry (Siegbahn et al. 1964). The same effect can also be produced by variations in ambient temperature (Christmas & Cross 1973).

In order to counteract these problems, an effective temperature stabilization scheme is needed. To achieve such a stabilization it is necessary to have sophisticated systems both for cooling the coils and air conditioning the room where the spectrometer is located. Temperature

stability usually has to be maintained at better than ±1° C. Special attention has to be paid to avoiding current leakage through the cooling system or surface leakage at high humidity (∿70% relative humidity) (Graham et al. 1960; Siegbahn et al. 1964; Daniel et al. 1970; Hughes 1980).

c) Deguassing

Iron-free spectrometers have the disadvantage of high sensitivity to stray magnetic fields. These stray fields can be produced by ferromagnetic materials in the proximity of the spectrometer location, including structural iron in the building housing it or ferrous ores in the surrounding area (Graham et al. 1960). The stray magnetic fields can also be generated by such objects as motor vehicles or electric motors.

Therefore, the sites in which iron-free magnetic spectrometers can be placed are quite limited. Moreover, the design of the vacuum system of the spectrometer and the choice of its components is made quite complicated since pumps have to be located far away from the spectrometer (Freedman et al. 1960; Graham et al. 1960; Christmas & Cross 1973).

The limitation of the site location of iron-free magnetic spectrometers places severe restrictions on the usefulness of these spectrometers in studies of nuclei far from stability. Such studies are typically carried out at sites near reactors, accelerators or isotope separators where machines, other magnets and ferrous materials are in abundance (Daniel et al. 1970; Mladjenovic 1976, p.29; Jeuch & Mampe 1977; Kane 1979).

The high degree of sensitivity of iron-free spectrometers to the presence of any ferromagnetic materials limits the choice of materials that can be used in their construction (Christmas & Cross 1973) and in the mechanical and electronic support equipment associated with the spectrometers (Nilsson et al. 1967; Hughes 1980, p.90).

An important source of magnetic field perturbation is the earth's magnetic field. Certain counter-measures have to be taken to correct for the influence of the earth's magnetic field on the field of iron-free β spectrometers. The counter-measures include the alignment of the spectrometer with the earth's magnetic field (or one of its components) and the cancellation of the this field with a pair of Helmholtz coils (Van

Atta et al. 1950; Schmidt 1952), or the use of a complex system made up of several sets of compensating coils to cancel the effects of the earth's magnetic field (Graham et al. 1960; Siegbahn et al. 1964; Daniel et al. 1970). Obviously this compensation is valid only for a specific location and has to be altered if the spectrometer is moved.

Some iron-free spectrometers have been equipped with automatic deguassing systems to correct for changes in the ambient magnetic field such as those caused by magnetic storms, which would otherwise render measurements performed with the spectrometer (during the magnetic transients) useless (Graham & Gieger 1961).

The problems of eliminating the effects of the external magnetic fields are complicated by the large volumes of iron-free spectrometers. The large volume is a consequence of the low magnetic field strengths that are usually obtainable with iron-free coils. All of the problems associated with the effects of external magnetic fields on the operation of iron-free spectrometers clearly make these spectrometers rather inflexible and increase the problems of using them in investigations of nuclei far from stability.

d) Problems Caused by the High Electrical Currents of Iron-Free Magnetic β Spectrometers

Accurate measurements of the electric current in iron-free spectrometers are quite complicted due to the wide range of current values that have to be measured (Graham et al. 1960; Burgov et al. 1961; Siegbahn et al. 1964; Daniel et al. 1970; Fujioka 1970; Van Elmbt 1981). The maximum values of the currents that have to be measured are typically several tens of amperes or even up to several hundreds of amperes in some cases (Alburger 1956).

An important disadvantage of iron-free spectrometers is their high power requirements. Typical values are tens of kilowatts needed to focus electrons of energies of a few MeV (Alburger 1956; Freedman et al. 1960; Graham et al. 1960; Siegbahn et al. 1964; Daniel et al. 1970; Fujioka 1970).

3) Iron-Core Spectrometers

For spectrometers incorporating iron-core electromagnets,

especially those with fully enclosing iron yokes, the problems of neutralizing external magnetic fields are relieved because of the shunting effect of the iron (Hayward 1953; Wegstedt 1957; Gerholm & Lindskog 1963; Halbig et al. 1974). These magnets also have the advantage of low power consumption (more than a factor of 50 lower than comparable iron-free spectrometers, see for example Hedgran (1952) and Siegbahn et al. (1964)) and easier field shaping through the machining of the iron poles to the appropriate profile (Bartlett et al. 1962; Mladjenovic 1976, p.31).

The problem with iron-core spectrometers is that one is dependent on the magnetic properties of iron which are a function of the field strength. Therefore, a major difficulty with iron-core spectrometers is the non proportional relationship between the magnetic field (B) experienced by the β particles and the exciting current in the coils (Paul 1965; Booij 1970). This is the result of the non linearity of the magnetization curve of the ferromagnetic materials that make up the magnet poles, even when the best quality pure iron is used (Wegstedt 1957; Mampe et al. 1978). In addition to being non-linear, the relationship between the magnetic field and the exciting current is multivalued and dependent on the history of the magnetization of the ferromagnetic material. This results from the dependence of the shape of the hysteresis loop on the maximum field intensity (H) to which the material has been subjected (Reitz & Milford 1967, p.197).

Because of the non-proportional relationship between the current and the magnetic field and its multivalued nature, it is necessary to measure the magnetic field directly and control the current accordingly (Siegbahn & Edvarson 1956). Relying on measurements of the current alone can result in non-linearities in the calibration of the spectrometer which in turn can cause serious distortions to the shapes of beta spectra. In fact even if the relationship between the magnetic field and the exciting current is assumed to be linear, any change in the calibration constant (which can result from changes in the magnetic state of the iron core) causes considerable deviations in the shape of the beta spectrum (Nagarajan and Venkata Reddy 1970). However, measuring the field directly introduces the problems of the stability and accuracy of the field measuring system and especially its calibration and temperature sensitivity (Backstrom et al. 1962; Booij 1970; Antman et al. 1970; Halbig

et al. 1974).

The magnetic field measurement is usually performed at one location in the spectrometer's magnetic field. The validity of such a measurement relies on the assumption that the magnetic field will maintain the same spatial distribution independent of the magnitude of the field (i.e. that the relationship between the current in the coils and the value of the magnetic field is identical for every point in the spectrometer for the full range of magnetic field values over which the spectrometer operates). These assumptions cannot hold true for a wide range of magnetic field values since the field form and geometry are to some extent dependent on the magnetization state of the iron (Siegbahn & Edvarson 1956; Backstrom et al. 1962; Lyutyi et al. 1970). At high excitation currents (i.e. high magnetic fields) saturations will affect the field shape (Mladjenovic 1976, p.30). On the other hand, because of the dependence of the magnetic permeability of iron on the magnetic field at low field strengths, the geometry of the magnetic field will change at low excitation currents thus limiting the low energy range of the β spectra which can be measured with these spectrometers (Booij et al. 1969; Booij 1970 pp. 52-61).

The remnant magnetization of the core material does not have the same distribution in space as the induced field (Langer & Cook 1948). This is due to several factors: the non-linear dependence of the remnant field on the maximum magnetic flux to which it has been subjected (a problem for non-uniform field magnets), inhomogeneities of the magnetic material, and remnant magnetization induced by eddy currents (Jeuch & Mampe 1977; Kane 1979).

Changes in the geometry of the magnetic field cause energy dependent variations in the transmission and resolution of the spectrometer (Booij et al. 1969; Booij 1970; Nagarajan & Venketa Reddy 1970; Jeuch & Mampe 1977). Such changes are suspected of causing considerable distortions to the β spectra (Howe 1968). Changes in the magnetic field geometry can also cause calibration shifts especially at high magnetic fields.

All of this necessitates a very careful and elaborate demagnetization procedure in order to be able to obtain reproducible results (Booij et al. 1969; Booij 1970 pp. 57, 61; Sattler et al. 1975; Jeuch & Mampe 1977).

Finally, one of the problems experienced by iron-core magnetic spectrometers, which is detrimental in studies of decays with short half-lives, is that of eddy currents excited in the iron core of the magnet during changes in the spectrometer's magnetic field. Such currents can persist for as long as several minutes, distorting the geometry of the magnetic field and impeding data acquisition (Kane 1979).

2.1.2d The Power Supply

Magnetic spectrometers employing electromagnets for the generation of the magnetic field require highly stabilized current supplies (typically 1 part in 10^4 stabilization (Nagarajan & Venketa Reddy 1970; Mladjenovic 1976)) in order to avoid changes in the field values during data accumulation at a single magnetic field setting. The power supplies must also be stabilized against fluctuations in the ambient temperature (Sattler et al. 1975). Furthermore, the demand for high stability is combined with the requirement for high output power in the case of iron-free spectrometers.

Measurements of continuous β spectra with magnetic spectrometers require frequent changes in the magnetic field in order to scan the whole spectrum. For studies of short-lived nuclei, the time lost while the magnetic field is being changed has to be kept to a minimum. It is important therefore to have a field control and stabilization system with a rapid response if investigations of nuclei far from stability are attempted with magnetic spectrometers (Halbig et al. 1974; Sattler et al. 1975).

2.1.2e The Detector

To detect and count the β particles focused by the magnetic spectrometer, scintillators, semiconductor detectors and gas filled chambers have been used. The gas filled chambers are operated either as proportional or Gieger-Muller counters.

A problem that is common to the various counting systems used is that of the dependence of counting losses in the pulse processing circuitry (pile-up and dead time losses) on the counting rate. These count rate dependent losses combined with the large variations in the count rates over the β spectrum and the single channel nature of magnetic

spectrometers result in a dependence of the counting losses on the energy of the β particles. Such a phenomenon is therefore a potentially serious source of spectral shape distortions (Nichols et al. 1961; Christmas & Cross 1978).

1) Gas Filled Counters

There are several problems associated with the use of these counters. Some of these problems are:

a) Window Thicknesses

Gas filled detectors require sufficiently thick entrance windows (of the order of mg/cm^2) to withstand the pressure difference between the counter gas on one side and the vacuum in the spectrometer chamber on the other. As a consequence of this thickness, the window has an energy dependent transmission for β particles, especially in the low energy region (Kofoed-Hansen & Christensen 1962, p.39; Booij 1970; Christmas & Cross 1978; Mampe et al. 1978).

In position sensitive proportional counters, multiple scattering in the entrance window or in the detector gas can also result in variations in the resolution with energy for electron energies below 1 MeV (Yoshida et al. 1978).

b) Efficiency

Another problem of gas filled chambers is caused by the energy dependence of the detector efficiency as a result of the dependence of the counting rate on the voltage across the chamber and the variation of this dependence with the incident β particle energy (Mampe et al. 1978; Christmas & Cross 1978; Knoll 1979, p.208).

c) Slow Pulse Rise Time

The pulse rise times of gas filled counters are usually quite long (of the order of microseconds) (Knoll 1979 p.204). Moreover, G.M. tubes have dead times that are of the order of 50-200 μsec. These long dead times limit the counting rates that can be handled with the detectors and increase the importance of the corrections that have to be applied to account for counting losses (Fujioka 1970; Booij 1970 p.37; Knoll 1979).

d) High Background

The large volume of gas chambers results in high background counting rates caused mainly by γ rays (Graham et al. 1960; Wortman & Langer 1963).

e) Cumbersome Design and Operation

The problems of breakage of the entrance windows, bulky gas flow systems required for counter gas filling, counter gas composition and purity all add to the complications associated with magnetic spectrometers.

2) Scintillators

Organic scintillators (anthracene or plastic) coupled to photomultiplier tubes are quite commonly used as β detectors in conjunction with magnetic spectrometers. The pulse height information available from such detectors helps in discriminating against counts caused by background radiation and scattered electrons (Lee et al. 1963; Beekhuis & de Waard 1965; Van Klinken et al. 1968; Nagarajan et al. 1969). The excellent timing characteristics of scintillators are quite useful in coincidence work.

However scintillators also suffer from several drawbacks some of which are listed below:

a) Sensitivity to γ Rays

Due to the higher density of scintillators compared to gas filled chambers, scintillators are more sensitive to γ rays incident on them. Gamma rays scattered in the spectrometer or emanating from sources outside the spectrometer can therefore add to the background (Camp & Langer 1963; Van Elmbt 1981).

b) Magnetic Field Effects

The sensitivity of photomultiplier tubes to magnetic fields is also a cause for concern. The trajectories of electrons travelling from one stage to another within the photomultiplier are particularly sensitive to the existence of magnetic fields because of their low average energy (of the order of 100eV) (Knoll 1979, p.298). The magnetic field of the

spectrometer can therefore cause gain shifts in the photomultiplier tube. These shifts will change with changes in the spectrometer's field as it scans the β spectrum, resulting in energy dependent shape distortions (Van Elmbt 1981, p.92).

Any magnetic shielding scheme used for the photomultiplier tube will interfere with the magnetic field of the spectrometer and disturb its focusing properties (Graham et al. 1960; Antman et al. 1970). Using a long light guide between the scintillator and the photomultiplier to reduce such magnetic disturbances will add considerably to the detector's noise (Paul & Hofmann 1963; Van Elmbt 1981).

c) Backscattering

Beta particles incident on the scintillator can backscatter without depositing enough energy in the detector to exceed the discriminator level of the counting circuit. Such events will not be registered as counts in the β spectrum. The fraction of monoenergetic electrons incident on the detector which will not contribute to the count rate is a function of both the energy of the incident electrons and the discriminator level. The high noise level in scintillation detectors necessitates the setting of the discriminator at a high level and therefore the fraction of lost counts to the total number can be of the order of a few percent (Paul 1965; Nagarajan et al. 1969). The loss of counts through backscattering from the detector can cause serious β spectrum shape deviations. Corrections for this effect require an extrapolation of the tail of response function to zero energy in order to account for the number of lost counts. Reasonably accurate knowledge of the shape of the detector's response function to β particles is needed in order to effect such corrections (Paul & Hofmann 1963).

d) In-Flight Annihilation

In measurements of β^+ spectra, the in-flight annihilation of some of the positrons incident in the scintillator and the subsequent escape of the annihilation photons can also cause problems (Deutsch et al. 1977). The problems are caused by positrons that annihilate before losing enough energy in the detector to pass the detection threshold. Since the probability of in-flight annihilation is dependent on the energy of the

incident positrons (Azuelos & Kitching 1976) this effect will be energy dependent as well. Furthermore, because the phenomenon of in-flight annihilation is peculiar to positrons, it could lead to discrepancies when positrons are measured with spectrometers that have been tested using negative β particles (negatrons) only.

e) The Volatility of Anthracene in Vacuum

Beta spectra measured with magnetic spectrometers incorporating anthracene crystals as detectors can show shape distortions which are caused by the reduction in the transmission of the spectrometer as the anthracene sublimes resulting in a reduction in the active area for β particle detection. Using large crystals results in an increase in the background count rate caused by scattered electrons and γ radiation. Defining the sensitive detection area with a baffle placed in front of the detector results in a significant increase in electron scattering (Nichols et al. 1961).

f) Dependence of the Gain of PMT's on Count Rate

The instabilities and variations of gain of photomultiplier tubes with count rates are also serious problems which have to be tackled (Knoll 1979, pp.28-93).

3) Silicon Detectors

Silicon detectors are also used as electron counters in combination with magnetic spectrometers. The simplicity of operation of these detectors, their small size, low γ ray sensitivity and excellent resolution are their main attractive features when considered for use in magnetic spectrometers (Wortman & Langer 1963; Langer et al. 1964; Booij et al. 1969; Booij 1970; Antman et al. 1970).

Multidetector arrays can be conveniently built from silicon, and these detectors can be used as position sensitive counters in magnetic spectrometers with extended focal planes (e.g. $\pi\sqrt{2}$ spectrometers). Such an arrangement greatly reduces the time required for the accumulation of a spectrum (Nilsson et al. 1967; Armini et al. 1967; Bertolini & Rota 1968; Graham & Geiger 1972). However, this type of detector deployment suffers

from an important difficulty; variations in momentum resolution and transmission at the detectors' locations along the focal plane. These variations in transmission and resolution result in variations in the detection efficiency among the detectors and can therefore cause spectral shape distortions if not corrected for. Determining the corrections that have to be applied to the spectrum is a complicated procedure with a high degree of uncertainty (Armini et al. 1967).

The superior energy resolution of solid state detectors is exploited in discriminating against electrons scattered in the spectrometer and background radiation reaching the detector. Most often, solid state detectors employed in conjunction with magnetic β spectrometers are used simply as counters. They are either coupled to a discriminator and a scalar or used with an energy gate set on the detector pulses by means of a single channel analyzer but without accumulating any pulse height information (Graham et al. 1960; Wortman & Langer 1963; Langer et al. 1964; Antman et al. 1970; Fujioka 1970; Genz et al. 1976; Hughes et al. 1980, p.88). However, by performing pulse height analysis on the detector output pulses at each momentum setting of the magnetic and retaining only the counts whose energy falls within the momentum setting of the spectrometer, more effective discrimination against unwanted counts can be achieved (Hsue et al. 1966a; Robert et al. 1970).

The main drawback of using silicon detectors is that their response functions for β particles and their efficiencies at different β particle energies have to be fairly well-known. In particular, the ratio of electrons backscattered from the detector for different incident electron energies has to be well-known in order to be able to correct for the part of the low energy tail in the response function which falls below the discriminator level (Booij 1970; Hsue et al. 1966b). If the backscattering of β particles from the detector is not taken into account, spectral shape deviation will appear, especially in the low energy part of the spectrum (Langer et al. 1964; Hughes 1980, p.138).

The limited thickness in which silicon detectors are available restricts the maximum energy of the β particles that can be studied. For β particles whose range in silicon exceeds the thickness of the detector, the efficiency of detection decreases rather rapidly with energy and an accurate knowledge of the response function is crucial (Nilsson et al.

1967; Antman et al. 1970; Hughes 1980). Moreover, since the detector's efficiency for counting β particles and the variation of this efficiency with electron energy are dependent on the discriminator level, the setting of this level and ensuring its stability during the long measurement time is of great importance (Nilsson et al. 1967; Hughes 1980, p.138).

The determination of the detection efficiency, its dependence on β particle energy and the corrections that have to be applied to the accumulated spectrum as a result, is a complicated task which can introduce serious errors to the shape of the β spectrum (Hsue et al. 1966a,b; Nilsson et al. 1967; Booij 1970 p.38; Hughes 1980, p.138).

In all of the cases described above, the momentum of the β particles is determined by the magnetic field and the energy resolution of the semiconductor detector is used only to distinguish counts resulting from the focused electrons in the desired momentum range from scattered electrons and background counts.

2.2 Hybrid Spectrometers

The use of silicon detectors in association with magnetic β spectrometers was developed further in hybrid spectrometers. Instead of relying on the dispersion of β particles in the magnetic field to determine their momenta, the energy resolution of the silicon detector is used to measure the energy of the β particles. In effect, the silicon detectors in this case are acting as multichannel electron spectrometers while the magnet is used to transport the electrons from the source to the detector, select a fairly wide range of electron momenta and suppress the γ ray flux incident on the detector. The magnetic spectrometer can therefore be operated in a high transmission mode without compromising the overall resolution of the system. Thus in the same counting period it is possible to accumulate a much broader portion of the spectrum with a hybrid spectrometer than with a magnetic spectrometer of comparable resolution. This is a clear advantage in measurements involving a short-lived activity (Catura 1965).

To collect a continuous β spectrum with a hybrid spectrometer, the magnetic field is swept over the range of electron momenta of interest. The pulse height information obtained from the silicon detector together with the corresponding magnetic field values are stored and from this data

the spectrum is reconstructed (Kantele et al. 1975).

Some of the electrons incident on the silicon detector are backscattered from the detector without depositing their full energy in the detector. Furthermore, if the range of the incident electrons in silicon exceeds the thickness of the detector, a certain fraction of the incident electrons penetrate through the detector depositing only a fraction of their energy there. These two effects give rise to a low energy tail in the recorded spectra of monoenergetic electron lines and result in a reduction of the full energy peak efficiency of the spectrometer. In order to eliminate these two effects, counts in the silicon detector are accepted only if the energy deposited within the detector corresponds to a momentum value which falls within the momentum window set by the magnetic field of the spectrometer. This momentum window is moved synchronously with the magnetic field as it is swept to cover the full spectrum (Westerberg et al. 1975; Kantele et al. 1975; Draper et al. 1978).

In addition to the problems that are particular to their type, hybrid spectrometers suffer from many of the problems of both magnetic spectrometers and semiconductor silicon β spectrometers. In common with magnetic spectrometers they have the disadvantages of small transmission (a few percent or less only) and the need to correct for source decay during the accumulation time so as to normalize to the same source strength. Furthermore, the magnetic field value has to be determined fairly accurately during its sweep across the spectrum. The need for these accurate magnetic field measurements comes about because some of the corrections that have to be applied to the spectrum are dependent on the momentum of the focused electrons. One such correction results from a basic property of magnetic spectrometers, namely their constant (or near constant) relative momentum resolution ($\Delta p/p$ = constant). Because of this, the absolute momentum resolution and therefore the absolute width of the transmitted momentum range (i.e. the momentum window Δp) is a linear function of the momentum of the transmitted electrons (Catura 1965; Westerberg et al. 1975; Kantele et al. 1975; Draper et al. 1978). Another correction which requires knowledge of the magnetic field of the spectrometer is the forementioned momentum gating of the energy spectrum collected by the semiconductor detector.

The problem which hybrid spectrometers share with semiconductor spectrometers is that of incomplete energy deposition of the β particles in the detector medium as a result of backscattering and bremsstrahlung radiation production. The ratio of electrons depositing their full energy to the total number of incident electrons is dependent on the energy of the incident electrons (Berger et al. 1969). Thus if the energy spectrum registered by the semiconductor detector is collected in a singles mode, then these incomplete energy absorption events will cause a shift in the spectrum from higher to lower energies and result in considerable distortion to the spectrum. Correcting the spectrum for this effect involves an accurate knowledge of the response of the semiconductor to monoenergetic electrons over the full range of energies under study, which is certainly not easily obtainable. If, on the other hand, the energy spectrum is gated with a momentum window (as described above) the efficiency of the spectrometer system will be dependent on the energy of the transmitted electrons. The variation in efficiency with energy has to be precisely determined and corrected for (Kantele et al. 1975).

The use of silicon detectors in hybrid spectrometers limits the maximum energy of the β transitions that can be studied with these spectrometers since silicon spectrometers are available up to a sensitive thickness of 5 mm only. This thickness corresponds to the range of electrons of 2 MeV in silicon (Berger et al. 1969). Above this energy, the full energy peak efficiency of the detector drops sharply and the detector's response to monoenergetic electrons becomes even more complicated (Nilsson et al. 1967; Berger et al. 1969 and references therein). Because of this phenomena and because of the uncertainties in the corrections that have to be applied to the spectrum, hybrid spectrometers have only been rarely used to measure the continuous beta spectra of decaying nuclei (Kantele et al. 1975). Their use has been largely confined to internal conversion electron studies, especially on-line or in-beam (Westerberg et al. 1975; Draper et al. 1978; Lountama et al. 1979; Mladjenovic 1979 and references therein).

2.3 Energy Deposition Spectrometers

These spectrometers operate on the principle of measurement of the energy deposited by the incoming radiation in the detector material. One

method of measuring the deposited energy is to count the number of photons that are produced in a scintillating medium due to the interaction of radiation with the medium (scintillation spectrometers). Alternatively, the deposited energy can be measured by counting the number of charge carriers (amount of ionization) produced by the incident particle during its interaction with an absorbing medium (proportional counters and solid state detectors).

Both of these methods of detection and energy measurement lend themselves to the construction of multichannel devices where a wide range of energies can be measured simultaneously. This is an attractive feature of energy deposition spectrometers (energy sensitive detectors) which considerably shortens the amount of time required to measure a β spectrum to a given statistical accuracy. As a result of the shorter measurement times, multichannel instruments are quite useful in studies of short-lived nuclei. They also suffer less than single channel instruments from time dependent background counting rates and from the effects of contaminant build up in the radioactive source (Cambi et al. 1972).

Furthermore, since the full β spectrum is recorded during a single measurement, there is no need for normalizing the spectrum to the source strength.

Because of the multichannel nature of energy deposition spectrometers and the possibility of using them in geometries where the solid angle of detection is large, the source strengths that are required are usually less than those needed for magnetic spectrometers. Therefore, problems with source thickness and uniformity are not as severe as in the case of magnetic spectrometers. Finally, source shape, size, and positioning is not as critical as in the case of magnetic spectrometers.

All of these desirable features of energy sensitive detectors make them quite attractive for use as β spectrometers in studies of nuclei far from stability.

In order for an energy deposition spectrometer to make a good β ray spectrometer it must have the following characteristics:

1) Linearity

The output pulse generated by the spectrometer must be proportional to the energy deposited in it or at least the relationship between the

deposited energy and the generated pulse has to be well-known. It is also preferable if height of the pulse generated per unit energy deposited in the detector is independent of the type of radiation that deposited the energy in the detector since this will greatly simplify the task of calibrating the β spectrometer.

2) Size

The spectrometer should have dimensions large enough to completely stop β rays of different energies within the range of interest.

3) High Efficiency

The spectrometer should be employed in a high transmission arrangement and have as high an efficiency as possible for the detection of the full energy of the β particles incident on it.

4) γ Ray Suppression

The spectrometer should be able to suppress the detection of other types of interfering radiation, especially γ rays.

2.3.1 Spectra Distortions Associated with Energy Deposition Spectrometers

2.3.1a Distortions Caused by the Response Function of the Detector

The pulse height spectrum generated by an energy sensitive detector when monoenergetic particles are incident on it is commonly known as the response function of the detector. An ideal response function would be a delta function at an energy equal to that of the incident particles. However, the response function of energy deposition spectrometers to β particles is far from having such an ideal shape. It is this departure from the ideal response function shape that is responsible for some of the distortions to the shapes of β spectra measured with energy sensitive detectors. These distortions are serious enough that β spectrum measurements made with energy sensitive detectors are practically useless without the application of correction techniques to account for the particular shape of the response function of the spectrometer in use.

Contributions to the shape of the response function come mainly from:

1) Resolution

When an energy sensitive detector is irradiated with monoenergetic β particles, the amplitudes of the pulses generated by the spectrometer will not all be the same. Part of this variation in pulse amplitude is due to the finite resolution of the spectrometer which is caused by the statistical fluctuations arising from the discrete nature of the energy conversion and detection method, and by the random noise within the detector and the electronic instrumentation associated with it.

2) Incomplete Energy Deposition

Another cause for the pulse amplitude variation is the incomplete deposition of the full energy of the β particles in the detector material since only a fraction of the impinging monoenergetic β particles deposit all of their energy in the detector. This fraction depends on the dimensions of the detector, the material from which it is made, the energy of the incident β particles and the geometry of the detector with respect to the incoming electrons. The incomplete energy deposition is caused mainly by:

(a) Backscattering of the β particles from the detector. The low mass of the electrons causes them to be easily deflected from their original direction during their interaction with matter. Thus an electron entering the detector might undergo sufficient deflection (usually after several scatterings in the detector) to emerge from the same surface through which it entered, before it had deposited all of its energy in the detector. This phenomenon is termed backscattering.

The ratio of the number of backscattered β particles to the number of incident β particles is called the backscattering coefficient. As the thickness of the stopping material increases so does the backscattering coefficient until it reaches a saturation value. For normally incident β particles, the saturation is reached when the thickness of the stopping material is about half the range of the incident β particles in the material (Knop & Paul 1965 Fig. 7, p.9).

The saturation backscattering coefficient depends on the atomic number (Z) of the absorber and the energy of the β particles. It is highest for high Z materials, low energy incident β particles and large

angles of incidence (angles measured with respect to the detector's surface) (Morozov 1973; Seltzer & Berger 1974; Knoll 1979, p.61-62). Tabata et al. (1971) and Kuzminikh & Vorobiev (1975) give empirical and calculated expressions for the variation of the backscattering coefficient with the Z of the stopping material, the energy of the incident β particles and the angles of incidence.

(b) The escape of bremsstrahlung photons out of the detector. Bremsstrahlung is the electromagnetic radiation emitted by charged particles (β particles in this case) as they decelerate during their interaction with the detector material. Due to the statistical nature of the photon interaction with matter, some of this bremsstrahlung escapes from the detector resulting in incomplete energy deposition for the incident β particles. The fraction of electron energy converted into bremsstrahlung in an absorber increases with an increase in the energy of the incident electron and with an increase in the Z of the stopping material (Knoll 1979, p.20-21, 57).

(c) Transmission through, or sidescattering out of the detector. In the case of detectors with dimensions smaller than the range of the incident β particles in the detector material, only a fraction of the particles will be stopped in the detector. The rest of the β particles are scattered out of the sides of the detector or pass through it before losing all their energy. The fraction of β particles stopped in the detector decreases as the energy of the β particles is increased, if the dimensions of the detector are held constant (Berger et al. 1969; Antman & Svahn 1970; Morozov 1973; Lund & Rudstam 1976; Noma et al. 1983; Bom 1984).

Shape of the Response Function

Due to the effects mentioned above, the shape of the response function of energy sensitive detectors to electrons is different from that of the ideal delta function. The electron response function of these detectors is usually made up of a full energy peak which represents counts from detector pulses generated by electrons that deposit all their energy in the detector, and a low energy tail which extends from the full energy peak to zero energy. The low energy tail results from pulses generated by electrons that have not deposited all of their energy in the detector (Energy lost through bremsstrahlung, backsctter, sidescatter and

transmission). The width of the full energy peak depends on the resolution of the spectrometer. Therefore for low resolution spectrometers (such as scintillators) some of the counts in the "full energy peak" may result from events in which some of the electron's energy was lost through bremsstrahlung, but which are not resolved from events where the total energy of the electron was deposited in the detector (Titus 1970).

In the case of positrons incident on energy sensitive detectors, all of the phenomenon described previously for electrons are present although their relative contributions may be different from those in the case of electrons (Knop & Paul 1965 p.9; Sen & Patro 1966; Antman & Svahn 1970; Knoll 1979 p.62). In addition, the effects of the production of annihilation radiation, and the subsequent absorption of some or all of the annihilation energy are present as well. After the positrons are stopped in the detector, they annihilate with electrons from the detector material producing two photons of 511 keV energy each, travelling in opposite directions. There is a finite probability that some or all of the energy of one or both of these photons will be deposited in the detector. Since the deposition of this annihilation radiation is coincident with the deposition of the positron's kinetic energy, they will add up and appear as one signal with a pulse height proportional to the sum of the energies. This summing can also take place when the positron is stopped in the detector but some of its kinetic energy is lost through the escape of bremsstrahlung radiation from the detector medium. Another possibility is that of in-flight annihilation of the positron in the detector material, after it has deposited only a fraction of its kinetic energy in the detector. Again some or all of the annihilation energy can sum up with the deposited kinetic energy.

Therefore, the response function of energy sensitive detectors to positrons is more complicated than that for electrons. In addition to the full energy peak and the low energy tail (the shape and height of which are different from those in the electron case), the response function to positrons has a high energy portion which extends from the full energy peak to an energy of 1022 keV above the peak as a result of the summing of the annihilation radiation energy (Cramer et al. 1962; Beck 1969; Kaina 1977; Rehfield 1977; Johnston et al 1981; Clifford 1981; Avignone et al. 1983; Bom 1984).

2.3.1b Distortions Resulting from the Multichannel Nature of the Spectrometers

1) Coincident Summing

The β decay of a parent nucleus quite often is followed by the emission of coincident γ rays from the daughter nucleus. Because of the sensitivity of energy deposition spectrometers to γ rays, the summing of some or all of the energy of a γ ray coincident with the β ray results in serious distortions to the β spectrum (O'Kelley 1961 p. 426, 430). The importance of this effect depends on the solid angle of detection and the γ ray efficiency of the detector.

2) Random Pile-Up

This is another summing effect which results from the accidental addition of two separate pulses originating from two non-coincident radiations that happen to be detected within a time interval shorter than the resolving time of the spectrometer and the associated electronics (O'Kelley 1961 p.431). The pulse height generated by the addition will depend on the heights of the inividual pulses and their time separation. The importance of this effect increases as the count rate is increased (Knoll 1979).

2.3.1c Distortions Caused by β Particle Scattering

The combination of the energy analysis and the detection functions in one component in energy deposition spectrometers results in other problems as well.

The passage of the β particles in any material intervening between the radioactivity and the detector (such as detector dead layers, electrical contacts, windows, reflectors, finite thickness of the radioactive source, etc.) results in energy losses and degradation. The energy loss of the β particles depends (among other things) on their initial energy and the angles of incidence (Knop & Paul 1965). Such an energy loss will therefore result in distortions to the shapes of β spectra (Gardner & Meinke 1958; Crameret al 1962; Dakubu & Gilboy 1978; Clifford 1981).

At low β particle energies (below 100 keV), the absorption of β particles in the intervening materials also becomes a source of distortions (Persson 1964, Jacobs et al 1967). Another distorting effect arises from the detection of β particles reaching the detector after their energy has been degraded by scattering from objects in the vicinity of the source or detector (such as collimators, source holders, chamber walls, etc.) (Bertolini et al 1969; Cramer et al 1962; Persson 1964; McMillan 1970; Ishii 1975; Kaina et al. 1977; Dakubu & Gilboy 1978; Borovoy et al. 1979; Clifford 1981; Bom 1983). Even elastically scattered β particles reaching the detector will result in distortions to the shape of the β spectrum since the probability of such scattering is energy dependent and therefore the efficiency of the spectrometer system will be dependent on the energy of the incident β particles.

Similarly, if the source-detector combination is placed in air (or any other gas) rather than vacuum (as is the case in many scintillation spectrometer arrangements), then energy losses experienced by the β particles, the absorption of some of the β particles in the gas, and changes in the efficiency of the spectrometer due to scattering in the gas will all result in β spectrum deviations, especially at low energies (Bisi et al. 1956; Gardner & Meinke 1958; Bosch & Urstein 1963; Kennett & Keech 1963; Nicler & Bell 1965; Persson 1964; McMillan 1970).

In the case of positrons, annihilation photons can be produced during the scattering and stopping of positrons in any material in the vicinity of the source or detector (Hoyle et al. 1983). These photons represent a potential source of γ ray background that have to be taken into account.

2.3.2 Types of Energy Deposition β Spectrometers:

2.3.2a Proportional Counters

High pressure proportional counters have been used to study β decays with endpoints below 1.5 MeV (Fulbright 1955). However, their poor energy resolution (12% for a well designed counter Wu & Geoffrion 1960), the large detector dimensions needed to stop high energy β rays (due to the low density of gases and therefore the long range of energetic β particles in them (Knoll 1979 p.359)), make them unsuitable for precise β

spectrometry.

The cumbersome problems involved in the design and operation of proportional counters render them unviable options as β spectrometers, especially for accurate spectroscopy in regions far from stability. These difficulties include: γ ray background in the counters due to their large volume, poor linearity, dependence of pulse height on count rate, slow pulse rise time, and the necessity of introducing the sources internally into the high pressure chambers since thick walls are needed in order to withstand the pressure differential (Fulbright 1955; Wu & Geoffrion 1960; Wortman & Langer 1963; Curran & Wilson 1965; Knoll 1979).

2.3.2b Scintillators

Solid scintillators, both plastic (organic) and crystalline (organic and inorganic), coupled to photomultiplier tubes (PMT's) have been often used in β spectrometry.

In comparison with proportional counters, the higher density of the solid scintillators makes them suitable for the manufacture of β spectrometers of reasonable dimensions even for high energy β particles. The excellent timing characteristics of scintillators (especially organic plastics) are quite advantageous in β spectroscopy applications especially in coincidence experiments (O'Kelley 1961; Bosch & Urstein 1963; Birks 1964 pp. 370-375; Neiler & Bell 1965).

However, solid scintillation β spectrometers suffer from several drawbacks which lessen their usefulness as tools for precise β spectrometry. Some of these drawbacks are: their modest resolution, the non-linearities that are inherent in the operation of PMT's (Cramer et al. 1962; Knoll 1979 p.290), the dependence of the gain of the PMT on the count rate in the spectrometer, instabilities and long term drift in the gain of the PMT, and the non-linear energy response of scintillators.

1) Resolution

Among these drawbacks, the major shortcoming of scintillators is perhaps their poor resolution caused mainly by the statistical spread in the height of the pulses generated by the spectrometer. The chain of events which must take place in converting the incident radiation

to light and the subsequent generation of an electrical signal involves many inefficient steps. The most important of these steps is the conversion of scintillation light to photoelectrons by the photocathode of the PMT. At this point the number of information carriers (photoelectrons) is at a minimum and therefore the statistical fluctuations in this number are most significant (Knoll 1979 pp. 334-338, p.359). As a result of this, the typical resolution of a plastic scintillator is about 8% to 10% at 1 MeV electron energy (Tsoulfanidis 1983 p.407, see also; Ketelle 1950; Cramer et al. 1962; Rhode & Johnson 1962;Bosch & Urstein 1963; Snyder & Beard 1964; Sen & Patro 1966; DiCola et al. 1967; Munnich 1980; DeBeer et al. 1970; Clifford 1981). The resolution of anthracene, stilbene and NaI(Tl) crystals is a few percent better than that of plastics as a result of the higher scintillation efficiency of crystalline scintillators in comparison with plastics (Bisi et al. 1956; Bosch & Urstein 1963; Persson 1964; Sen & Patro 1966; Borovoy et al. 1979; see also Knoll 1979 table 8-1, pp. 246-247).

In general, and unlike magnetic spectrometers, the resolution of scintillation spectrometers is dependent on the energy of the incident β particles (Bosch & Urstein 1963). The resolution ($\Delta E/E$) is usually proportional to $E^{-1/2}$ (E= energy absorbed in the scintillator) (Gardner 1960; O'Kelley 1961 p.428; Cramer et al. 1962; Birks 1964 p. 370; Sen and Patro 1966; Beck 1969; Wohn et al. 1972; Otto et al. 1979; Tsoulfanidis 1983 p. 407). The $E^{-1/2}$ energy dependence is a direct consequence of the fact that the major contribution to the resolution comes from the statistical fluctuations in the number of photoelectrons. Departures from the $E^{-1/2}$ dependence of resolution on energy have been observed (Ricci 1957; Persson 1964). This is usually the result of the contribution of light collection efficiency to the resolution.

The poor resolution of scintillation spectrometers results in distortions to the shape of the β spectrum, particularly at the low and high energy ends of the spectrum (Gardner & Meinke 1958; Cramer et al. 1962; Wenninger et al. 1968). The distortions of the high energy portion the β spectrum have adverse effects on the accuracy with which the endpoint of the β spectrum can be determined (Bisi et al. 1956; Garder 1960; Persson 1964; Slavinsakas et al. 1965; Sen & Patro 1966; Wohn et al. 1972; Girard & Avignone 1978; Bom 1983). Deconvolution techniques are

required to correct for these resolution caused distortions (Kettelle 1950; Freedman et al. 1956; Gardner & Meinke 1958; Gardner 1960; Bertolini et al. 1960; Cramer et al. 1962; Rhode & Johnson 1962; Bosch & Urstein 1963; Persson 1964; Snyder & Beard 1964; Worman & Cramer 1964; Slavinskas et al.1965; Rogers & Gordon 1965; Jacobs et al. 1967; DiCola et al.1967; Klyuchnikov et al. 1968; Beck 1969; Wohn et al. 1972; D'Auria et al. 1976; Stippler et al. 1978; Otto et al. 1979; Clifford 1981; Wouters et al. 1983). For the application of these deconvolution techniques, the variation in the resolution as a function of energy has to be known or measured (DiCola et al. 1967 and references therein; Tsoulfanidis et al. 1969). Moreover, these corection methods tend to fail at low energies (below 100 to 200 keV) due to the deterioration in resolution at low energies, thus limiting the range of energies over which the spectrometer can be useful (O'Kelley 1961; Bertolini et al. 1964; Nieler & Bell 1965, DiCola et al. 1967).

2) Non-linearities and Calibration Problems

The non-linearity of scintillation β spectrometers is another important shortcoming. The non-linearity results mainly from variations in the scintillation efficiency with the energy of incident electrons (especially in inorganic crystals; Birks 1964 pp. 431-437; Knoll 1979 p.259 p.338), or from variations in light collection efficiency with β ray energy (especially in large plastic scintillators; Gardner & Meinke 1958; Cramer et al. 1962; Wohn et al. 1972).

The non-linearities, gain drifts and instabilities in scintillation spectrometers are all potential sources of considerable distortions in measurements of β spectra. These effects are quite hard to detect because of the continuous nature of the β spectrum. Determining the non-linearities of scintillation spectrometers and correcting for them or in fact even obtaining a simple energy calibration of these spectrometers(especially organic scintillators) is quite a difficult task. At energies below 1 MeV where conversion electron sources are available for calibration, the resolution of the spectrometers is usually poor enough that the K and L conversion lines overlap resulting in a doublet peak. In order to use these doublet peaks for calibration, one has to know not only the energies of the K and L conversion lines but also their

relative intensities in order to reconstruct the doublet peak (Rhode & Johnson 1962; Wohn et al. 1972; Borovoy et al. 1979). Alternatively, X ray coincidence techniques have to be used in order to distinguish the K and L conversion lines (Persson 1964; Snyder & Beard 1964; De Beer et al. 1970).

Another problem of calibrating with conversion electrons is that calibrations obtained with electrons are not valid if the spectrometer is to be used to study positron spectra. The differences between positrons and electrons in the energy loss per unit path length in the scintillation material result in differences in the scintillation response (or efficiency) of the spectrometer for the two different types of β particles. This in turn results in different output pulse heights for the same deposited energy depending on whether the energy was delivered by electrons or positrons. Furthermore, the difference between the two calibrations is a function of the deposited energy (Rhode & Johnson 1962).

At energies higher than 1 MeV the calibration problem is complicated by the lack of convenient high energy conversion electron sources. At these energies, both Compton edges of high energy γ rays and endpoints of β spectra have been used for calibration (Bisi et al. 1956; Gardner & Meinke 1958; Cramer et al. 1962; Beck 1969; Wohn et al. 1972; Bosch et al. 1973; Stippler et al. 1978; Wouters et al. 1983; Hoyle et al. 1983). One problem that is experienced when the Compton edges of γ rays are used for calibration is the difficulty in defining the location of the Compton edge due to the poor resolution of the scintillation spectrometers and the high intensity of the Compton continuum (below the Compton edge) due to multiple γ ray scatterings in the scintillator (Ricci 1957; Cramer et al. 1962; Beck 1969; Wohn et al. 1972). Another problem originates from the fact that γ rays illuminate the whole volume of the scintillator while the β particles are confined to certain regions of the scintillator (especially when collimators are used). In addition, the β particles penetrate only to a well defined depth in the scintillator which is determined by their range in the scintillating medium while the γ rays interact essentially with the whole scintillator. Therefore, the existence of any differences in the different regions of the scintillator as to the efficiency of their optical coupling to the photocathode will result in differences between the γ ray calibration and

the appropriate calibration for β rays (Cramer et al. 1962).

The use of β endpoint measurements for calibration is hampered by the lack of an adequate set of previous accurate endpoint measurements for decays that are convenient to use in calibrating the spectrometer (Ricci 1957). Another difficulty results from the need to use an iterative procedure to obtain the energy calibration. This is because the calibration β spectra have to be corrected for the spectrometer's response function and such correction techniques in turn require knowledge of the calibration (Wohn et al. 1972; Wohn & Talbert 1978; Clifford 1981 p.41).

Monoenergetic electron or positron beams from accelerators or magnetic spectrometers have also been used in calibrating scintillation β spectrometer (Kaina et al. 1977; Stippler et al. 1978; Otto et al. 1979; Pahlmann et al. 1982). This method suffers from the problems of reproducing the same experimental condition during calibration as those prevelant at the time of β spectra accumulation (angles of incidence of particles on detector, stray magnetic fields from the accelerator or the magnetic spectrometer, electronic settings, etc.).

The high efficiency for γ ray detection of inorganic scintillation β spectrometers (especially NaI(Tl) crystals) is often exploited in calibrating these detectors using the full energy peak that results from the absorption of all the energy of the γ ray in the detector (Der Mateosian and Smith 1952: Lewis 1952; Leutz & Ziegler 1962; Wenninger et al. 1968). The drawback of this technique is the uncertainty in the calibration which results from differences in the scintillation efficiency of the detector for γ rays and electrons of the same energy (Birks 1964 pp. 431-437; Knoll 1979 p.259,338). Differences in the scintillator volumes illuminated by the γ rays and β rays that were mentioned before can result in differences between β ray & γ ray calibrations as well.

3) Reflector Thickness

In most scintillation spectrometers, the β particles have to traverse the thickness of a light reflector that surrounds the scintillator before depositing their energy in the spectrometer. Such a reflector is necessary for the efficient collection of the scintillation light. However, its presence represents a dead layer which will result in distortions to the shape of the spectrum due to the energy loss and

absorption of low energy β particles. Special care and attention are paid to minimizing its thickness (Persson 1964; Jacobs et al. 1967; Beck 1969; Titus 1970; Clifford 1981).

Inorganic Scintillators

Thallium activated alkali halide crystals (eg. NaI(Tl), RbI(Tl), CsI(Tl)) have been sometimes used as β spectrometers (Lewis 1952, Der Mateosian & Smith 1952; Egelkrat & Leutz 1960, 1961; Leutz 1961; Leutz & Ziegler 1962; Nieler & Bell 1965; Sen & Patro 1966; Wenninger et al. 1968; Kaina et al. 1977). Among these, NaI(Tl) crystals are probably the most popular.

The high atomic number of the Iodine (Z=53) in these crystals and the high density of NaI (3.67 g/cm^3) (Knoll 1979 p.257) causes them to have a high efficiency for the detection of γ rays (O'Kelley 1961). This high γ ray efficiency enables one to monitor the calibration and control the stability of the spectrometer by monitoring the position of a γ peak from a radioactive source (Kaina et al. 1977).

On the other hand, the high effective Z of these crystals has some detrimental effects as well.

1) γ Ray Background

The high γ ray efficiency results in a large γ ray background that is superimposed on the γ spectrum, problems with large β-γ summing (random & coincident) and large summing probability for the annihilation radiation energy in the case of positrons. In fact, because of the high γ ray efficiency of these crystals they are ineffective for use as β spectrometers except in cases where the β decys are not accompanied by γ ray emission or where very effective γ ray suppression methods are used. In the case of positron emission, special techniques to eliminate the effects of 511 pile-up are used (Wenninger et al.1968).

2) Increased Production and Escape of Bremsstrahlung Radiation

The higher Z of inorganic scintillators results in a larger cross section for the production of bremsstrahlung radiation during the stopping of β particles in the crystal. The high Z also results in a higher cross section for reabsorption of this radiation. Nevertheless, the net

fraction of the incident electron energy that escapes from the stopping medium in the form of bremsstrahlung radiation increases with Z almost linearly (Berger & Seltzer 1965, 1968). This causes the response function of NaI(Tl) to electrons to depart considerably from the ideal form.

3) Increased Backscattering

Since the fraction of backscattered electrons increases with an increase in the Z of the stopping material (Knoll 1979 p.62), a large fraction (about 50% or more) of the incident electrons will scatter out of the detector before losing their full energy (Bosch & Urstein 1963; Neiler & Bell 1965: Sen & Patro 1966; Titus 1970). This renders inorganic scintillation crystals useless as β spectrometers unless the adverse effects of backscattering are overcome. To achieve this, several different approaches have been tried:

a) Internal Sources

The use of internal sources in inorganic scintillators has been accomplished by incorporating radioactive atoms into the crystal structure of the scintillator during the crystal growing process (Lewis 1952; DerMateosian and Smith 1952; Egelkraut & Leutz 1960, 1961; Leutz 1961; Leutz & Ziegler 1962; Nieler & Bell 1965; Wenninger et al. 1968). This technique eliminates the spectral distortions that are usually caused by the radioactive source and by the scattering of β particles in windows and dead layers and allows for the extension of the spectral measurements to very low energies. It also provides for high efficiency counting of the radioactivity (essentially 4π efficiency).

There are several shortcomings that are inherent to this technique. Among these is the obvious difficulty of estimating the influence of the background counts due to sources of radiation external to the detector on the β spectrum. Another problem is the escape of β particles through the surfaces of the crystal before they have deposited their full energy in the scintillator (DerMateosian & Smith 1952). To reduce the effects of this phenomenon on the shape of the β spectrum, the volume of the scintillation crystal has to be made as large as possible in order to reduce the surface to volume ratio and therefore the probability of β particle escape (Wenninger et al.1968). The use of a larger crystal also results in less bremsstrahlung escape but it would complicate the problems

of γ ray background and β-γ summing.

An important drawback of the use of internal sources is the high probability of coincident summing of γ rays, annihilation photons and conversion electrons with β particles. This high probability stems from the large solid angle (practically 4π) in which the activity is counted (O'Kelley 1961; Nieler & Bell 1965).

The difficulty of measuring the response function of internal source spectrometers to β particles is also a cause of trouble. The contributions to the response function of these spectrometers come mainly from the poor resolution and bremsstrahlung radiation losses. Simulating the effects caused by the distribution of the β activity throughout the crystal is nearly impossible.

The main failure of the technique of internal sources is its non-versatility since it is applicable only to a few elements and of these only fairly long-lived isotopes (several days at least) can be studied.

b) 4π Geometry

This method is somewhat similar to the previous one. Here the radioactive source is completely sandwiched between two NaI(Tl) crystals such that electrons backscattered from one detector will enter the second one and deposit their energy there (Bannerman et al. 1951; Ketelle et al. 1956). The two crystals are viewed either by one or two photomultiplier tubes and the coincident signals from the two halves are summed.

A more detailed discussion of 4π β spectroscopic techniques will be given in the sections dealing with organic scintillators and silicon detectors. Suffice to mention here that the use of NaI(Tl) crystals in a 4π geometry results in the same type of problems that are experienced by the two other types. The problems are further complicated by the high γ ray efficiency of NaI(Tl) crystals and therefore the higher probability for summing of coincident γ and X rays. The high Z of NaI crystals also aggravates the problems associated with bremstrahlung production and escape and backscatter losses due to the imperfect attainment of the 4π geometry.

The technique of $\underline{4\pi}$ counting in NaI crystals has not found many applications in $\underline{\beta}$ spectroscopy. It has been used mainly to increase the efficiency for coincident summing and thus to help in establishing the

relationships between different radiations emitted from the same isotope which in turn help to clarify the decay scheme. The technique has been applied mainly to internal conversion electron studies.

c) Antibackscattering Veto Detectors

To reject electrons backscattered out of a scintillation crystal, special detectors surrounding the crystal and operated in an anticoincidence mode with the scintillation spectrometer have been used (Kaina 1977).

In addition to the obvious complexity of such an arrangement, it also suffers from low efficiency as a result of the small solid angle left available after the installation of the veto detectors, if effective rejection of backscattered electrons is to be achieved. The high backscattering coefficent of NaI also implies that the majority of counts are rejected as a result of backscattering.

Since the ratio of backscattered to incident electrons depends on the energy of the incident electrons (Titus 1970), the efficiency of a system with antibackscattering veto detectors will be energy dependent and has to be accurately determined.

d) The Triple Coincidence Method

This method is applicable only to positrons. It attempts to eliminate the effects of backscattering by demanding a coincidence between pulses generated by the positrons in the β scintillator and the pulses generated by the two annihilation photons in two γ ray detectors placed close to the β scintillator (Sen & Patro 1966). Thus counts are registered only if they result from positrons that have annihilated inside the β spectrometer. A detailed discussion of the problems of this technique is given in Appendix B.

Finally, a problem that is particular to NaI(Tl) crystals is caused by their hygroscopic nature. As a result, they have to be kept in a dry atmosphere or in vacuum at all times and are therefore usually encapsulated in a protective enclosure with fairly thick entrance windows (0.3 mm Al in the work of Kaina 1977). The passage of β particles through such a window results in considerable distortions to the β spectrum (Bosch & Urstein 1963).

Organic Scintillators

Organic scintillators, including pure crystals and liquid or solid (plastic) solutions, are perhaps the most popular type of β spectrometers in use. Their fast flourescence decay time (in the nanosecond range) is very useful for fast timing applications (O'Kelley 1961 p.241). It also allows one to operate organic scintillation spectrometers at high counting rates without the adverse effects of random pulse pile-up (Iafigliola et al. 1983a).

The low effective atomic number of organic scintillators (see Tsoulfanidis 1983, Table 6.2 p.202) results in a considerable reduction in the ratio of backscattered to incident electrons in comparison to inorganic scintillators and semiconductor detectors (O'Kelley 1961 p. 421, 425; DiCola et al. 1967; Titus 1970; Knoll 1979 pp. 61-62). Since the cross section for bremsstrahlung production also decreases with a decrease in Z (Knoll 1979 p. 57) less energy is lost from the detector through this mechanism as well (Berger & Seltzer 1965, 1968). Furthermore, because of the low effective Z of organic scintillators and their low density (Anthracene 1.25 g/cm ^{3}, plastics $\sim$1g/cm^3 see Knoll 1979 table 8-1 pp. 246-247), the probability of γ ray interaction per unit thickness of the detector is smaller in organic scintillators than in semiconductor or inorganic scintillation spectrometers.

Anthracene (a crystalline organic scintillator) was an early favourite for use in β spectroscopy. However, it has been largely replaced by organic plastics because of the problems associated with its usage. The main problems which are encountered with anthracene are its volatility in vacuum (Nieler & Bell 1965 p.251), its fragility, and the dependence of its scintillation efficiency on the orientation of the directions of the incident electrons with respect to the crystal axis (Knoll 1979 p.243).

Organic plastic scintillators are widely used as β spectrometers in studies of nuclei far from stability and especially for Q_β measurements in these nuclei (see for example Cramer et al. 1962; Beck 1969; Wohn et al. 1972; Westgaard et al. 1972; D'Aura et al. 1976; Stippler et al. 1978;Davids et al. 1979; Otto et al. 1979; Munnich 1980;Pahlman et al. 1980; Clifford 1981; Johnston et al. 1981; Della Negra et al. 1982; Detraz et al. 1983; Wouters et al 1983; see also CERN 1970, 1976, 1981; AMCO 5;

AMCO 6). The low cost of plastic scintillators, their ruggedness, availability in practically any size and machinability to any desired shape have made them quite popular (Gardner & Meinke 1958; O'Kelley 1961 p.420, 425; Cramer et al. 1962).

However, these organic scintillators suffer from several drawbacks that limit their usefulness as precise β spectrometers. One of these drawbacks is the problem of γ sensitivity. As mentioned before, organic scintillators have a low γ ray interaction probability per unit thickness of the detector. Nevertheless, because of the low density of plastic scintillators, detectors manufactured from this material have to have large dimensions in order to be able to stop high energy β particles within the detector volume. The larger volumes result in high γ ray sensitivities as will be illustrated below (see also Gardner & Mienke 1958).

For 10 MeV electrons incident on a typical plastic scintillation β spectrometer (made from NE 102 plastic for example), the detector thickness required to stop the electrons is about 5 cm. At this thickness, the detection efficiency for a 1 MeV γ ray is about 30% (Data taken from Nuclear Enterprises 1980). The same 10 MeV electrons have a range of about 1 cm in germanium (Haller & Goulding 1981). A germanium detector of this thickness interacts with about 25% of a beam of 1 MeV photons incident on it (Haller 1982). Thus the γ sensitiviy of large plastic scintillators is just as important as that of germanium detectors (Padro et al. 1977). In fact, because of the lower effective atomic number of organic scintillators in comparison with Ge detectors, the full energy peak-to-Compton ratio for γ rays is smaller in plastic scintillators. This, combined with the poor resolution of scintillators, causes the effects of γ ray contamination of the continuous β spectrum to be more difficult to detect and correct in organic scintillators than in Ge detectors (Padro et al. 1977 and figure 4 therein). For these reasons, an effective γ ray suppression technique has to be used in conjunction with the use of organic scintillators as β spectrometers.

In addition to the problem of γ sensitivity and the problems mentioned in the beginning of this section such as difficulties with calibration and linearity, and poor resolution, organic scintillators (like all energy deposition β spectrometers) suffer from distortions of

the β spectra caused by electron backscattering.

Because of the dependence of the ratio of backscattered to incident electrons on the energy of the incident electrons and the angles of incidence (Titus 1970), estimates for this ratio in different β scintillation spectrometers tend to vary depending on the source detector geometry and the energy range of interest. Values given in the literature range all the way from 4% to 35% for energies below 1.5 MeV and angles of incidence ranging from normal to the surface of the detector to 70° to the normal (Freedman et al. 1956; Gardner & Meinke 1958; Bertolini et al. 1960; Cramer et al.1962; Bosch & Urstein 1963; Persson 1964; Slavinskas et al. 1965; Neiler & Bell 1965; Sen & Patro 1966; DiCola et al. 1967; Tsoulfanidis et al. 1969; Titus 1970; Bosch et al. 1973).

The backscattering of β particles from organic scintillators results in excess counts at low energies and deviations of Fermi-Kurie plots from linearity. It can also affect the accuracy with which the end point can be determined (Bisi et al. 1956; Gardner & Meinke 1958; Bertolini et al. 1960; Cramer et al. 1962; Bosch & Urstein 1963; Kennett & Keech 1963; Slavinskas et al. 1965; Sen & Patro 1966). To reduce the distorting effects of backscattering on the shapes of β spectra accumulated with organic scintillation spectrometers several solutions have been attempted.

1) Collimation

By limiting the angles of incidence through collimation, such that the β particles enter the surface of the detector perpendicular (or near perpendicular) to it, the percentage of backscattered electrons can be reduced. Beta rays entering the detector at near normal incidence angles have a greater chance of penetrating deep into the detector before scattering (O'Kelley 1961; Bosch & Urstein 1963).

The main problems resulting from collimation are the reduction in the efficiency of the spectrometer as a result of the reduction in solid angle for β particle detection (0.5% of 4π in the work of Persson 1964) and the problems caused by β particle scattering from the collimator (Persson 1964; Clifford 1981). Careful attention has to be paid to the design of the collimator and the material from which it is built (De Beer et al. 1970). A low Z material (e.g. Prespex) will result in less

electron scattering but it will also result in the enhancement of the solid angle for γ ray detection over that for β particles since it will have little collimating effect if any on the γ rays emitted from the source (Gardner & Meinke 1958). Such a collimator will also have little attenuation effect on the annihilation photons produced by positrons that are stopped in the collimator. On the other hand, a high Z material (e.g. lead) will result in a high probability for electron scattering from the collimator and a high cross section for bremsstrahlung production by β particles during their interaction with the collimator material (Cramer et al. 1962).

2) Well-Type Scintillators

By using a hollow scintillator with a hole in the shape of a truncated cone machined into it, and by placing the radioactive source at the top of the cone, the fraction of backscattered electrons escaping the detector can be significantly reduced (up to an order of magnitude lower than in flat scintillators) (Bisi et al. 1956; Gardner & Meinke 1958; O'Kelley 1961; Bosch & Urstein 1963; Neiler & Bell 1965; Wohn et al. 1972). In this arrangement, the β particles emitted from the radioactive source are effectively being collimated and directed into the bottom of the well that is machined in the scintillator so that most of the backscattered β particles will strike another part of the scintillator and deposit their energy there.

The main problems affecting this arrangement are the reduction in the solid angle (0.7% of 4π in the work of Wohn et al. 1972), and the difficulties in light collection resulting from the shape of the scintillator especially in the large volume detectors that are needed for the study β spectra with high endpoint energies (Freedman et al. 1956; Gardner & Meinke 1958). The poor light collection from the conical section can introduce a non-linearity in the calibration of the spectrometer (Kennett & Keech 1963; Wohn et al. 1972).

3) Antibackscattering Veto Detectors

In this technique, veto detectors surround the scintillation spectrometer and detect any β particles scattered out of it. Employed in an anticoincidence mode, the detectors are used to reject events in which

the β particles are backscattered from the scintillation spectrometer before losing all of their energy there. These detectors can also act as active collimators to define the angles of incidence of the β particles on the scintillator. And if they are made to enclose the β scintillation spectrometer from all sides, they can serve to reject events in which the β particles are sidescattered out of, or transmitted through, the spectrometer (Kennett & Keech 1963). Depending on the γ ray detection efficiency of the veto detectors, they can also be helpful in eliminating some of the events in which a fraction of the energy of the β particles is lost from the spectrometer in the form of bremsstrahlung radiation.

One of the principle drawbacks of such a system is its low efficiency as mentioned before in the discussion of similar systems used in conjunction with inorganic β scintillator. The solid angle for β ray detection in spectrometers with antibackscattering detectors is usually smaller than that in well-type spectrometers (Kennett & Keech 1963). Another problem is the dependence of efficiency on the β particle energy and the difficulty in determining this dependence (Kennett & Keech 1963).

4) The Triple Coincidence Method

This method is similar to the one described for inorganic scintillators. The positrons are detected in coincidence with the two annihilation photons to ensure that none of the backscattered electrons contribute to the accumulated spectrum (D'Auria & Preiss 1966; Sen & Patro 1966; Beck 1969; De Beer et al. 1970). This technique suffers from the same problems as in the case of inorganic scintillators except that the effects of bremsstrahlung production and escape, and the effects resulting from γ ray interactions with the β scintillator are less important than in the case of inorganic spectrometers due to the low Z of plastics. (See Appendix B for a full discussion of the triple coincidence method).

5) Correcting the β Spectrum for the Effects of Backscattering

When flat organic β scintillation spectrometers are used, the distortions to the shapes of β spectra, which result from the backscattering of β particles, can be corrected for using one of several deconvolution technique. Usually these techniques are used to correct for the effects of resolution, bremsstrahlung escape, and backscattering

simultaneously. Therefore they show the same deficiencies at the low energy end of the spectrum as the resolution correction techniques. Sometimes the backscattering and resolution corrections are applied separately (Persson 1964; Slavinskas et al. 1965).

The application of the β spectrum correction procedures requires a precise determination of the shape of the response function of the scintillation spectrometer to β particles (Freedman et al. 1956; Gardner & Meinke 1958; Gardner 1960; Bertolini et al. 1960; Persson 1964; Slavinskas et al. 1965; Sen & Patro 1966; Jacobs et al. 1967; DiCola et al. 1967; Beck 1969; Bosch et al. 1973; D'Auria et al. 1976; Otto et al. 1979; Clifford 1981). Knowledge of the relative contributions of the different parts of the response function (e.g. total counts in the full energy peak compared to the backscatter tail) is usually not good enough, especially when measurements of the β spectrum shape factors are attempted (DiCola et al. 1967).

As mentioned before, the response function of β spectrometers to electrons and positrons are considerably different so that response function measurements for one type of β particles are generally not applicable to the other. The differences in the shapes of the electron and positron response functions are a consequence of the differences in the backscattering coefficients for positive and negative β particles and the effects of annihilation radiation pile-up (Cramer et al. 1962; Sen & Patro 1966; Beck 1969; De Beer et al. 1970; Johnston et al. 1981; Clifford 1981).

An important aspect in the determination of the response function of a spectrometer is that the experimental conditions prevalent during the accumulation of the β spectrum should be duplicated when the response function is measured (Freedman et al. 1956; Bertolini et al. 1960; Cramer et al. 1962; Persson 1964; DiCola et al. 1967). The source-detector geometry is a parameter that should be reproduced during measurements of the response function (D'Auria et al. 1976; Otto et al. 1979). This is because of the strong dependence of the backscattering coefficient on the angles of incidence of the β particles (Titus 1970).

Other methods for analyzing β spectra and accounting for the detector distortions without the direct use of the response function have also been applied (Westgaard et al. 1972; Davids et al. 1974; Pardo et al.

1977; Parks et al. 1977; Stippler et al. 1978; Davids et al. 1979; Detraz et al. 1983). These techniques are usually too crude to be applicable in precise shape factor measurements. Their main use has been in the determination of endpoint energies with modest accuracy.

Several methods have been used for the determination of the response function:

a) Measurements of the Spectrometers Response Function Using Internal Conversion Electrons

The use of internal conversion sources for the determination of the response function of the spectrometer is limited to energies below 1 MeV due to the lack of convenient conversion electron sources above this energy. In addition, the response function measured with conversion electrons is not valid for positrons.

X ray and γ ray coincidence techniques are required to separate the K and L conversion lines from each other and to reduce the background caused by the noncoincident β and γ rays emitted from the source. Even then, the Compton background caused by γ rays that cannot be eliminated with coincidence techniques is quite important and has to be carefully subtracted from the spectrum (Freedman et al. 1956; Gardner 1960; Bertolini et al. 1960; Bosch & Urstein 1963; Persson 1964; Sen & Patro 1966; Jacobs et al. 1967; Tsoulfanidis et al. 1969; De Beer et al. 1970).

b) The Use of Accelerators or Magnetic Spectrometers

Monoenergetic electron and positron beams from accelerators and/or magnetic spectrometers have been frequently used for measurements of the response function. The main difficulties experienced with this method are the reproduction of the angles of incidence of β particles on the surface of the detector (Titus 1970: D'Auria et al. 1976; Otto et al. 1979; Clifford 1981), determining the accelerator dependent background and correcting for it (Cramer et al. 1962; Titus 1970), determining the resolution of the magnetic spectrometer or the energy spread of the accelerator beam and correcting for it (Beck 1969; Titus 1970; Wohn et al. 1972) and finally shielding the scintillation β spectrometer against the magnetic fields of accelerators and spectrometers (Titus 1970; Clifford 1981).

c) Monte Carlo Methods

The suggestion has been made to use Monte Carlo methods to simulate the response of the scintillation spectrometer to β particles (Sen & Patro 1966). Such a simulation should take into account not only the interaction of the β particles with the scintillation medium but also the dependence of light collection efficiency on the location of the interaction.

6) The Use of Internal Sources

Two different techniques for incorporating the radioactivity to be studied within the scintillator material have been used. In the first, the radioactive source material is added to the plastic scintillator during manufacture thus becoming an integral part of the spectrometer. This approach eliminates many of the problems associated with the use of external sources such as low efficiency and backscattering. However it is difficult to find a chemical form in which to introduce the radioactivity which will not quench the flourescence of the scintillator (O'Kelley 1962 p.427). The technique is also limited by the time needed to perform the chemical and physical processes required to incorporate the radioactive isotope into the scintillator. This time limitation severly restricts the half-lives of the isotopes that can be studied using such a technique. Other problems mentioned in the section on the use of internal sources in inorganic scintillators such as electron escape through the scintillator surfaces, difficulties with response function measurements, background evaluation, and $\beta - \gamma$ summing all apply to plastic scintillators as well. For all of these reasons this technique has not been widely applied to β spectroscopy studies but rather to absolute counting of weak, low energy β activities (Birks 1964 p. 358 pp. 361-370).

In the second technique, the carbon in the scintillation medium is activated using nuclear reactions induced by neutrons or protons (Birks 1964 p.371). The carbon isotopes thus produced act as internal sources and can be studied with the scintillation spectrometer. Such a technique, however, is obviously so limited in the number of isotopes to which it can be applied that it does not merit further discussion.

7) 4π Detection

In order to eliminate the effects of backscattering, 4π counting techniques have also been used in conjunction with organic scintillators. In such a set-up, the source is almost completely surrounded by the scintillation medium such that β particles backscattered from any portion of the scintillator will impinge on another part of it. Therefore few, if any, β particles can escape the spectrometer. Two different approaches to achieving the 4π geometry have been attempted. In the first approach, the radioactive source is sandwiched between two scintillators, each viewed by a different photomultiplier tube. The output pulses from the PMT's are summed in coincidence with each other (Rhode & Johnson 1962 and references 1-6 therein, Klyuchnikov et al. 1968). In the second approach, either the scintillator (plastic or anthracene) is divided into two halves between which the radioactive source is sandwiched, or a slot is machined into a plastic scintillator and the radioactive source is inserted in the slot. In both cases, the scintillation medium is viewed by one PMT only (Ketelle 1950; Shline 1957; Snyder & Beard 1964; Rogers & Gordon 1965; Westgaard et al. 1972).

Problems of 4π Scintillation Spectrometers

Although the 4π detection method does eliminate most of the effects of β particle backscattering from the scintillator, it nevertheless suffers from some important deficiencies:

a) Deterioration in Resolution

When two PMT's are used in a sum-coincidence mode, the resolution of the 4π spectrometer is worse than the resolution of either of the two halves separately. This is usually the case when signals from two detectors are summed since the resolutions of the two detectors are added in quadratures.

b) Gain Matching

When two PMT's are used, the output gains from the two PMT's have to be perfectly matched so that the output pulses generated by the spectrometer are not dependent on the particular path that the β particles follow in the two scintillators (Rhode & Johnson 1962). Similarly, when only one PMT views the scintillation medium it is important to verify that the scintillation efficiency and the light collection efficiency of the

two halves of the spectrometer are the same (Kettelle 1950).

Failure to attain such matching of the two halves of the spectrometer results in a worsening of the resolution of the spectrometer and distortions in the shapes of monoenergetic electron lines measured with the sepctrometer. This in turn causes changes in the shape of the response function of the spectrometer and distortions to the shapes of continuous β spectra. Verifying that the gain match is achieved over the full energy range of interest is quite important since any non-linearities in the system would result in a gain mismatch of the two halves of the spectrometer. Checking for these mismatches is subject to the same type of difficulties as calibrating these 4π scintillation spectrometers.

c) Calibration

In addition to the calibration problems suffered by all scintillation β spectrometers and which were discussed previously, 4π systems suffer from additional problems that are peculiar to this technique.

Depending on the thickness of the scintillators used, X ray coincidence techniques used to separate the K conversion line from the L and M lines may not be applicable to 4π systems. The large thickness needed to stop β particles from decays with high endpoint energies result in severe attenuation of the low energy X rays and a drastic reduction in efficiency if a coincidence technique is used.

The internal conversion electrons that are used to calibrate 4π scintillation spectrometers are always followed by the coincident emission of X rays and/or Auger electrons. The large solid angle of detection offered by 4π spectrometers results in a high probability for detecting these coincident radiations. Because of the coincidence sum mode of operation of 4π spectrometers, the output pulse generated by the spectrometer will be proportional to the sum of the energy of the conversion electron plus the energy of the particular Auger electron or X ray that accompanies it. Since each internal conversion transition can be accompanied by one or several different Auger transition and/or X rays, and since some of the X rays can escape undetected or deposit only a fraction of their energy in the detector, the resulting conversion electron spectrum will not be a single line but rather a distribution made up of a continuum and several discrete lines at the different sum

energies. However, the poor resolution of the scintillation spectrometer spreads these lines into one continuous distribution with an approximately guassian shape. Determining the shape of this distribution and the energy of its peak requires a complicated calculation involving the different X ray intensities, flourescent yields, K to L conversion ratios and the response function of the scintillator to X rays. Such a sophisticated calculation with all the associated uncertainties is needed in order to obtain a simple energy calibration for the 4π scintillation spectrometer. The uncertainties in the calibration are further augmented if the spectrometer systems suffers from the non-linearities and energy detection thresholds (at low energies) that are often observed in organic scintillators (Persson 1964; Sen & Patro 1966). A full description of all complications involved in calibrating 4π plastic scintillation β spectrometers is given in the work of Rhode & Johnson (1962).

d) Losses in Dead Layers

In a 4π arrangement, in order for electrons backscattered from one detector to be detected in the second scintillator, they have to pass through the source material, source backing and covering, and any dead layers (such as reflectors) on the front face of the scintillators. The energy loss of β particles in these layers is quite important since it is dependent on the energy of β particles and is highest at low energies where the probability of backscattering is at its highest as well. Moreover, the high backscattering probability for low energy β particles implies that the β particles can undergo several backscatterings in the 4π spectrometer each time passing through all the inactive layers and losing energy in a non-linear fashion. The distorting effects of the energy loss and absorption of low energy β particles in the dead layers on the shape of the β spectrum are quite serious, especially in the low energy portion of the spectrum (Snyder & Beard 1964; Klyuchnikov et al. 1968). The existence of these adverse effects restricts the thickness of the source backing to extremely thin films and therefore limits the method and the speed with which sources can be introduced in the spectrometer (Rhode & Johnson 1968).

e) Imperfect 4π Geometry

Any separation between the two detectors in a 4π spectrometer results in the escape of some of the backscattered electrons through the

gap between the two halves of the spectrometer before having deposited their full energy in the scintillator. Since the backscattering probability is dependent on the energy of the incident β particles, the fraction of β particles escaping from the spectrometer will likewise be a function of the β particle energy, resulting in distortion to the shape of the β spectrum.

Although this effect in plastic 4π scintillation spectrometers is not as serious as in the case of 4π inorganic scintillators or semiconductor spectrometers, nevertheless Rhode & Johnson (1962) place an upper limit of about 0.6 mm (0.025 in) on the separation between the two detectors. This separation must also be reproducible to avoid discrepancies between measurements made at differnt times.

f) Coupling the Two Halves of the Spectrometer.

It follows from the discussion of the two preceeding points that the two halves of the spectrometer enclosing the radiactive source have to be as close together as possible and the dead layers between them have to be as thin as possible. Therefore, in most cases the two halves are directly coupled to each other optically with no reflectors separating them from the source. Such an arrangement requires a light-tight enclosure to surround the spectrometer and imposes restrictions on the source introduction mechanism and therefore on the half lives of the isotopes that can be studied with this technique (Rhode & Johnson 1962; Snyder & Beard 1964).

g) Non-coincident γ Ray Background

Due to the small separation between the two halves of the spectrometer, the background resulting from the detection of non-coincident γ rays emitted from the radiactive source can not be easily estimated using the conventional technique of covering the source with a β absorber and recording the γ background alone (Gardner & Meinke 1958; O'Kelley 1962).

h) Summing of Coincident Radiation

The large solid angle for radiation detection in 4π spectrometers results in a high probability that any radiation emitted in coincidence with the β particles will be detected and some or all of its energy summed with that of the β particles. This is an important effect in cases where the β decay is accompanied by coincident γ ray emission, especially if the

γ transition happens to be highly converted.

Since the γ rays do not always deposit their full energy in the spectrometer, their detection adds a Compton continuum in summation with the β spectrum. Moreover, if positron spectra are being measured, then some or all of the energy of the two 511 KeV annihilation photons can sum up with the kinetic energy deposited by the positrons and with any coincident γ rays resulting in further complications of the measured β spectra (Sheline 1957). All of these coincident summation effects cause severe distortions to the β spectra measured with 4 π scintillation spectrometers in a manner which is difficult to interpret. They can also result in counts above the end point of the β spectrum (Gardner & Meinke 1958; O'Kelley 1961, Neiler & Bell 1965).

In order to reduce the summing effects of γ rays and coincident radiation, a γ detector is placed outside the β spectrometer and operated in coincidence with it. The β particles counts are retained only if they are detected in coincidence with the detection of the full energy of a γ ray in the external β detector. (O'Kelley 1961; Rhode & Johnson 1962 and references 4, 5 therein; Snyder & Beard 1964; Neiler & Bell 1965; Westgaard et al. 1972; see also the section on the β-γ coincidence method for γ ray suppression).

To eliminate the effects of annihilation radiation summing, the triple coincidence method is usually used in conjunction with 4π scintillation spectrometers. In some cases a third γ ray detector is operated in coincidence with the other detector (four fold coincidence) and used to suppress the detection of coincident γ rays (see Appendix B).

i) Measurement of the Response Function of a 4π Spectrometer

Deconvoluting the β ray spectra measured with 4π scintillation spectrometers in order to correct for the distortions caused by the response function of the spectrometer requires knowledge of the shape of the response function and changes in the shape over a wide range of energies (DiCola et al, 1967). The response function of these spectrometers cannot be assumed guassian in shape. The effects of energy loss and absorption of low energy β particles in the source, dead layers and windows, imperfect 4π geometry and bremsstrahlung escape result in the addition of a low energy tail to the guassian response function. Knowledge of the shape of this response function is crucial when β

spectrum shape factors are investigated (Snyder & Berard 1964; DiCola et al. 1967).

Direct measurements of the response function of a 4π spectrometer to electrons above 1 MeV are not possible. This is due to the lack of convenient conversion electron sources at these energies and the impossibility of introducing monoenergetic electron beams from accelerators or magnetic spectrometers into the 4π spectrometer. As for positrons, since there are no monoenergetic positron emitters, direct measurements of the response function are not possible.

Magnetic Transport

An alternative method to that of having the scintillation medium surround the source is to separate the two halves of the scintillation spectrometer (between which the source is located) from each other and rely on a homogeneous magnetic field to transport the β particles from the source to the detectors. The magnetic field also guides the β particles backscattered from one half of the scintillation spectrometer to the second half (Christensen et al. 1967).

The problems of this method are essentially the same as those of other 4π scintillation spectrometers except that the magnetic transport method suffers less from the adverse effect of the γ ray background and X ray summing. This is a result of the separation between the source and the detectors and therefore the lower solid angle for γ ray detection. The strong magnetic field used to transport the β particles requires the use of long light guides in order to be able to position the PMT far away from the scintillator so as to lessen the magnetic field effects on the PMT. The use of long light guides increases the noise in the system and results in a deterioration in resolution of the spectometer.

The magnetic transport method has been used more frequently with 4π silicon spectrometer arrangements and therefore a more detailed discussion of its merits and limitations appears in the section on silicon spectrometers. Most of the arguments appearing there are applicable to 4π scintillation spectrometery using magnetic tranport especially those concerning increased energy loss in dead layers and long transient times.

2.3.2c Seiconductor Spectrometers

Semiconductor detectors, manufactured from silicon or germanium, have been successfully used as β spectrometers. Although their energy resolution (usually a few keV), is not as good as the best quality magnetic spectrometers at low energies, they can usually surpass the resolution of most magnetic spectrometers at high energies (Reynolds & Persson 1965; Hollander 1966; Spejewski 1966; Bertolini & Rota 1968; Trischuk & Kankeleit 1968). Furthermore, the multichannel nature of semiconductor spectrometers and the possibility of using them in high luminosity configurations have made these spectrometers quite popular as tools in electron spectroscopy (Gibson et al. 1965).

Compared to other multichannel electron spectrometers (organic scintillators and proportional chambers), semiconductor detectors have the advantages of far superior resolution, smaller dimensions (as a result of their higher density), minimal circuitry, strict proportionality between the output pulse and the energy deposited in the detector (i.e. linearity and independence of the pulse height from the type of particle depositing the energy), freedom from drift, insensitivity of pulse height to count rate, and thin entrance windows (Gibson et al. 1965 p.363; Bertolini & Rota; Knoll 1979 p. 402).

However, due to the higher Z of semiconductor β spectrometers in comparison with plastic scintillators, the distortions to the shapes of β spectra caused by the backscattering of β particles and the escape of bremsstrahlung radiation from the detector will be more severe.

Silicon Spectrometers

Silicon detectors of all types: surface barrier, diffused junction, and lithium drifted, were the first semiconductor detectors to be used extensively in β spectrometry as a result of their earlier development in comparison with germanium detectors (see McKenzie 1979).

As β spectrometers, silicon detectors have some important advantages over germanium detetors. These advantages include the possibility of using silicon detectors at room temperature (although for best resolution they have to be cooled to cryogenic temperatures) and the lower atomic number of silicon (Z=14 for silicon, Z=32 for germanium).

The lower atomic number of silicon detectors and their lower density in comparison to germanium render them less sensitive to γ rays above 40 keV (Haller 1982). The lower Z results in lower backscattering coefficients (the saturation backscattering for normally incident 1 MeV electrons is about 9% and 24% for silicon and germanium respectively, values calculated from the expresssion given by Kuzminik & Vorobiev 1975). Likewise, as a result of the low Z of silicon, less energy is lost through bremsstrahlung production and escape from silicon detectors than in the case of germanium spectrometers (Berger & Seltzer 1965, 1968; Grosswendt 1974).

Among silicon β detectors, the Si(Li) type is the most commonly used type since better resolution (in comparison to diffused junction detectors) can be achieved with this type.

Several silicon β spectrometer arrangements have been reported in the literature (see for example the compilation of Behrens & Szybisz 1976 and references in Bertolini & Rota 1968).

These silicon β spectrometers can be divided into two types: ones with low source-detector geometry (solid angle of detection < 2π) and 4π detection systems.

Low Geometry Silicon β Spectrometers

Many such spectrometer configurations have been used in β spectroscopy (Bosch et al. 1963; Bertolini et al. 1964; Charoenkwan 1965; Marlow & Waggoner 1967; Bertolini & Rota 1968; McMillan 1970; Bosch et al 1974; Lund & Rudstam 1976; Dakubu & Gilboy 1978).

The main problem encountered with low geometry silicon β spectrometers is the spectral shape distortion caused by β particle backscattering from the detector. This distortion manifests itself as an excess of counts in the low energy region of the β spectrum. It can also result in errors in the determination of endpoint energy (Charoenkwan 1965).

As in the case of organic scintillators, the estimates for the ratio of backscattered to incident β particles vary depending on the energy and the angles of incidence of β particles on the surface of the detector in the particular spectrometer set-up. These estimates vary from 8% to 45% (Bertolini et al. 1964; Charoenkwan 1965; Bertolini & Rota 1968 and references therein; Berger et al. 1969 and references therein; Booij

1970; Antman & Svahn 1970; Bosch et al. 1974; Lund & Rudstam 1976; Dakubu & Gilboy 1978).

Correction procedures that account for the effects of backscattering (and sometimes resolution) on the β spectra measured with silicon detectors have been reported (Bertolini et al. 1964; Charoenkwan 1965; DiCola et al. 1967; Dakubu & Gilboy 1978). These correction procedures usually require knowledge of the response function of the silicon detectors to β particles. Alternative methods which do not require direct knowledge of the response function but require comparisons with standard spectrum measurements have also been used (Charoenkwan 1965; McMillan 1970).

The techniques for determining the response function of silicon detectors to β particles are similar to those used for plastic scintillators: conversion electrons detected in coincidence with electromagnetic radiation (Bosch et al. 1963; Bertolini et al. 1964; Charoenkwan 1965; Dakubu & Gilboy 1978), mono-energetic beams from magnetic spectrometers or accelerators, and Monte Carlo methods (Brundit & Sen 1965 and reference 2 therein; Nilsson et al. 1967; Berger et al 1969 and references 1-9 therein; Antman & Svahn 1970; Booij 1970; Hughes 1980).

In general, measurements of the response functions of silicon detectors suffer from the same difficulties as in the case of scintillators. Again, the same experimental conditions prevelant during measurements of the β spectra should be duplicated when the response function is measured. In this context, the effects of β particle scattering in the source and backscattering from the source backing have an important influence on the response function of the spectometers (Bertolini et al. 1964; Charoenkwan 1965; Dakubu & Gilboy 1978). Other problems experienced in the measurements of the response function of silicon detectors are: differences in the response function for electrons and positrons, background related to the magnetic spectrometer or accelerator, and difficulties in determining the resolution of the magnetic spectrometer and ensuring that it does not influence the response function measurement (Berger et al. 1969 and references therein; Antman & Svahn 1970). As an alternative to correcting the measured β spectrum for the effects of backscattering, the use of antibackscattering veto detectors has been proposed and used in an experimental arrangement (Lund

& Rudstam 1976). The determination of the efficiency of the β spectrometer and especially the variation of efficiency with energy becomes of paramount importance in this case (Lund & Rudstam 1976).

A 4π anticoincidence arrangement with two silicon detectors sandwiching the radioactive source has also been attempted (Schmitz et al. 1972). In this configuration, one detector is chosen as the β spectrometer and operated in anticoincidence with the second detector (Flothmann et al. 1969; Schmitz et al. 1972). This technique has the added advantage of reducing the contribution to the background orginating from Compton scattering of γ rays emitted from the source since Compton events in which the veto detector is triggered by the scattered photons are rejected.

The same antibackscattering technique has been tried in a 4π spectrometer which uses a magnetic field to transport the electrons from the source to one of the detectors, and backscattered electrons from one detector to the other. Again, one of the two silicon detectors is operated as veto detector to reject backscattered electrons. An estmiate of the backscattering coefficient of silicon for 0.5 and 1 MeV incident electrons was obtained (~29%) but no detailed investigation of the suitability of the technique for β spectroscopy was carried out (Andersen & Christensen 1968).

There are two serious drawbacks associated with the use of 4π anti-backscattering arrangments. The first is the dependence of the backscattering coefficient on energy which results in an energy dependent efficiency for the whole spectrometer system. The second problem is caused by the fact that the energy spectrum of the backscattered β particles extends to very low energies. The low energy portion of the backscattered spectrum results from events in which the β particles deposit most (but not all) of their energy in the spectrometer and are then backscattered with only a small fraction of their incident energy remaining. Because of the existence of a low energy threshold in the anticoincidence unit (of about 10 keV), such events will not trigger the anticoincidence circuit and the counts generated by the β particles in the spectrometer before being backscattered will therefore be retained. This results in a lwo energy "shoulder" in the spectrum of a monoenergetic electron line and serious distortions in the case of continous β spectra

(Schmitz et al. 1972).

4π Silicon Spectrometer Systems

4π silicon spectrometers have been used quite extensively for β spectroscopy studies. There are two approaches to achieving the 4π geometry: close proximity of the detectors to the radioactive source and magnetic transport of the β particles from the source to the detectors.

4π Spectroscopy Using Two Silicon Detectors in Close Proximity to the source

This type of spectrometer arrangement is probably the most widely used among silicon β spectrometers. In this configuration the radioactive source is sandwiched between two silicon detectors which are placed close to each other (separation between detectors <<1 mm). The source is therefore almost completely surrounded from all directions by the detectors and β particles emitted in approximately 4π solid angles are detected. Moreover, electrons backscattered from one detector will end up being detected in the second detector and thus the effects of backscattering are almost completely eliminated. To achieve this, the total energy of the backscattered electron is accounted for by summing the coincident pulses from the two detectors (Reynolds & Persson 1965; Spejewski 1966; Persson et al. 1971; Gils et al. 1972; Schmitz et al. 1972, Schuperferling & Hoffmann 1974).

In general, 4π silicon spectrometer systems suffer from the same type of problems discussed in the section on 4π organic scintillation β spectrometers.

a) Deterioration in Resolution

As a result of summing the signals from the two silicon detectors, the resolution of the 4π spectrometer will be worse than the resolution of either of the two detectors separately. This reflects the sum of the resolution of the two detectors (in quadratures) and any imperfections in the sum circuitry (Schmitz et al. 1972; Flothmann et al. 1972). The resolution of 4π silicon spectrometers is usually of the order of 10 keV (Reynolds & Persson 1965; Spejewski 1966; Trischuk & Kankeleit 1968; Persson et al. 1971; Flothman et al. 1972). If the two detectors are connected, in parallel with each other, to the input of the same

preamplifier, the increase in the input capacitance to the preamplifier (as a result of the summing of the capacitances of the two detectors) causes a deterioration in resolution as well (Tsoulfandis 1983, p. 317).

b) Gain Matching

In most cases in 4π silicon spectrometers, the output pulses from the two detectors are amplified separately and then added to each other electronically in a sum amplifier. Since the output pulses are summed, the gains of the two halves of the 4π spectrometer (the detectors and the associated ciruitry: preamplifier, amplifier, etc.) have to be perfectly matched. Provisions for keeping the gains stable have to be made as well (Reynolds & Persson 1965; Trischuk & Kankeleit 1968; Persson et al. 1971; Gils et al. 1972).

In certain cases the two detectors are similar enough that the pulses from the two detectors can be added by simply connecting the two detectors in parallel to each other and feeding the pulses into the same preamplifier (Spejewski 1966, Trischuk & Kankeleit 1967). In this case it is crucial that the number of charge carriers generated and collected by each detector, per unit deposited energy, should be the same. In other words, one has to ensure that the two detectors are nearly identical and no significant differences in the Fano factor or in charge trapping exist between the two detectors, otherwise the charges collected by the two detectors can not be summed directly (Trischuk & Kankeleit 1967, 1968).

c) Calibration

The improved resolution of silicon spectrometers simplifies the problems involved in calibrating 4π silicon β spectrometers in comparison to plastic scintillation spectrometers. Nevertheless, the uncertainties in the determination of the conversion electron energies caused by the summing of coincident radiation (X rays and Auger electrons) are still a source of problems in 4π silicon spectrometers. Such summing causes shifts in the energies of the conversion lines used for calibration and distortions to the shapes of their peaks. (Spejewski 1966; Schmitz et al. 1972).

d) Losses in Dead Layers

In analogy to 4π scintillation spectrometers, β particles suffer energy losses during their passage through the source material, the thin film covering it, the backing (for backscattered electrons) and the thin

insensitive regions on the front surfaces of the detectors (this region is made up of the front face electrical contact and usually a thin dead layer of silicon) (Persson et al. 1971; Schuperferling 1975). The energy loss of the β particles in these layers is dependent on their initial energy (Haller & Goulding 1981), and can therefore result in serious distortions to the shapes of β spectra. Furthermore, the low energy β particles which have the highest rate of energy loss in these dead layers also have a higher backscattering probability than high energy β particles. Therefore the low energy β particles have a higher probability of traversing more dead layers and of losing more energy in doing so (Trischuk & Kankeleit 1968; Gils et al. 1972; Schmitz et al. 1972).

Because of the 4π geometry of the detectors, β particles emitted at practically any angle (including very shallow angles) are accepted by the detectors. Beta particles emitted at shallow angles follow longer paths through the dead layers and therefore lose more energy than particles emitted at angles close to the perpendicular to the surface of the detectors. As a result of these differences in path length, the energy loss of β particles will be a function of their angle of emission. Even β particles of the same energy will experience considerably different energy losses depending on the angles of emission (Flothmann et al. 1972). Since the angles of emission of β particles that are accepted by the detectors depend on the distance between the two detectors, the adverse effects of energy losses in the dead layers will be critically dependent on the separation between the two detectors (Flothmann et al. 1972; Schmitz et al. 1972).

These energy losses can cause small downward shifts in the energies of monoenergetic electron lines (Trischuk & Kankeleit 1968, Flothman et al. 1972), deterioration in the resolution of the 4π spectrometer as a result of the spread in energy losses caused by the differences in the number of passages through the dead layers (Persson et al. 1971; Schmitz et al. 1972), asymmetries in the shapes of monoenergetic electron peaks (Flothmann et al. 1972) and can even result in a small satellite peak at an energy lower than that of the full energy peak (Schuperferling 1974). All of these effects will obviously cause a considerable deformation of the shape of the response function of the spectrometer and therefore result in important distortions of the true shapes of β spectra.

e.) Imperfect 4π Geometry

The near impossibility of attaining a perfect 4π source-detectors geometry with silicon detectors results in serious distortions to the shapes of β spectra. The difficulty in realizing a 4π geometry stems from several factors (Gils et al. 1972). The finite (however small) thickness of the front contacts of the detectors effectively separates the two detectors and leaves a small gap in the active detector material surrounding the source (Schmitz et al. 1972). Another factor is the requirement that the radioactive sources be deposited on, and covered with, thin films in order to avoid contaminating the detectors by depositing the radioactivity directly on their surfaces (Trischuk & Kankeleit 1968). The delicate nature of the front surfaces of the two detectors requires that they should not come into direct contact with each other or with other surfaces (source covering or backing) (Gils et al. 1972). Finally, the need sometimes to avoid electrical breakdown between the two detectors places a restriction on how close to each other they can be positioned (Reynolds & Persson 1965).

The finite separation between the two detectors (imperfect 4π geometry) brought about by the factors mentioned above result in quite remarkable distortions to the shapes of β spectra measured with 4π silicon spectrometers. In fact, the measured shape factors of the β spectrum have values that are function of the separation between the two detectors (Reynolds & Persson 1965, Trischuk & Kankeleit 1968).

The β spectrum shape distortions are caused by β particles escaping through the gap between the two detectors after they have been backscattered from one of the detectors and lost some of their energy there (Reynolds & Persson 1965). The escape of some of the backscattered β particles manifests itself as an excess of low energy counts in the β spectrum (up to several percent) (Reynolds & Persson 1965; Spejewski 1966). In the spectrum of a monoenergetic line, the distortion appears as a low energy continuum extending from the full energy peak to zero energy (Flothman et al. 1972; Schuperferling 1975). In the work of Gils et al. (1972), an upper permissible limit of 0.05 mm was set on the separation between the two detectors of (for detectors of 2 cm^2 surface area each) was set.

f) Source Introduction Mechanism

All of the 4π silicon β spectrometer systems mentioned above are operated at about liquid nitrogen temperature in order to improve the resolution of the detectors For example, an improvement in resolution of a single Si(Li) detector from 60-75 keV at 25°C to 5.0 keV at 77K was observed in the work of Spejewski 1966 . The requirement that the radioactive sources, which are mounted on extremely thin films to minimize dead layer losses, be introduced from outside the spectrometer (where they are at atmospheric pressure and room temperature conditions) into the tiny gap between the two detectors (which are under vacuum and at cryogenic temperatures) and be accurately positioned there, obviously complicates the design and engineering problems quite considerably. This is especially true in the case of short lived nuclei where the whole process of source introduction has to be accomplished as rapidly as possible (Gils et al. 1972). As a matter of fact, most of the 4π silicon spectrometer systems are not equipped to handle short lived activities since the detectors have to be warmed up to room temperature and atmospheric pressure and moved away from each other before a new source can be introduced (Reynolds & Persson 1965; Spejewski 1966; Trischuk & Kankeleit 1967; Schmitz et al, 1972).

g) Non-Coincident γ Ray Background

As in the case of organic scintillators, Compton scattering of non-coincident γ rays adds to the background experienced by 4π silicon spectrometers (Spejewski 1966; Schmitz et al. 1975).

h) Summing of Coincident Radiation

As mentioned in the section on 4π scintillation spectrometers, the large solid angle for radiation detection results in a high probability for the summing of the energy of the β particles with some or all of the energy of any coincident radiation. Such summing results in serious spectra shape distortions. (Spejewski 1966; Gils et al. 1972; Schmitz et al. 1972; Flothmann et al, 1972; Schuperferling 1975.

To suppress the effects of coincident γ ray summing, β-γ coincidence techniques using one or two large NaI(Tl) γ detectors surrounding the 4π spectrometer have been utilized. (Spejewski 1966, Gils et al. 1972, Schuperferling & Hoffmann 1974).

Beta decays are always accompanied by the coincident emission of a

continuous spectrum of γ rays. This phenomenon is called internal bremsstrahlung emission and originates from the electromagnetic interaction of the nucleus with emitted β particles (Petterson 1965). In 4π silicon β spectrometry some of the internal bremsstrahlung photons will interact with the β detectors and deposit some or all of their energy there in coincidence with the deposition of the energy of the β particles. The summation of energies that ensues causes distortions in the shape of the β spectrum that have to be corrected for (Trischuk & Kankeleit 1967).

i) External Bremsstrahlung Emission

Because of the high Z of silicon in comparison with organic scintillators, the phenomenon of bremsstrahlung production and escape from the β spectrometer is more important in 4π silicon spectrometers. This effect increases in importance with the increase in the endpoint energy of the β spectrum (Flothmann et al. 1972; Gils et al. 1972). In a monoenergetic electron line spectrum bremsstrahlung losses manifest themselves in asymmetries in the shape of the electron line and a low energy continuum and even a broad satellite peak below the full energy peak (Flothmann et al. 1972).

The distortions to the shape of β spectra resulting from bremsstrahlung escape are dependent on the exact geometry and sizes of the source and the detectors. An accurate evaluation of the magnitude of the effect of bremsstrahlung on the shape of the β spectrum requires an extensive Monte Carlo simulation. Using such an evalution, special corrections have to be applied to the β spectrum to rectify the distortions caused by bremsstrahlung losses (Trischuk & Kankeleit 1976; Gils et al. 1972; Weißner et al. 1973). The failure to apply these corrections can result in considerable deviations from the true shape of the β spectrum, especially near the endpoint.

j) Deconvoluting the β Spectrum and Measurement of the Response Function of the Spectrometer.

Beta spectra measured with 4π silicon spectrometers usually have to be corrected for the finite resolution of the spectrometer system, especially near the endpoint (Reynolds & Persson 1965; Willett & Spejewski 1967; Trischuk & Kankeleit 1967; Schmitz et al. 1972). The distorting effects of energy loss in dead layers, bremsstrahlung losses and the escape of some of the backscattered electrons due to imperfections in the

4π geometry combine to produce asymmetries in the shape of the response function of 4π silicon spectrometers (Persson et al. 1971; Flothmann et al. 1972; Schuperferling 1975).

The shape of the response function can no longer be approximated by a symmetric guassian and the exact shape of the response of a particular spectrometer has to be determined accuarately in order to be able to deconvolute the measured β spectra from its distorting effects (Schuperferling 1975).

Internal conversion electrons, in coincidence with the appropriate X rays, have been used to measure the response function of 4π silicon spectrometers. The X ray coincidence condition is used to remove the β and γ ray background that accompany the conversion electrons (Persson et al. 1971; Flothmann et al. 1972; Schuperferling 1975). The problems encountered in using this method for response function measurement are discussed in detail in the work of Flothmann et al. (1972). Briefly, the major difficulties are: attentuation of the X rays in the silicon detectors to such an extent that in order to obtain acceptable coincidence counting rates the separation between the two detectors has to be increased to expose the radioactive source to the X ray detector, thus altering the response function of the spectrometer in the process; problems of variation in the coincidence counting efficiency with the deposited β particle energy; choice of the appropriate internal conversion transition with long lived isomeric states in order for the coincidence method to be effective in suppressing the β and γ rays (Schuperferling 1975); and finally the problem of γ rays causing coincidence counts in the X rays detectors after being Comptom scattered from the β detectors (Schupeferling 1975).

A Monte Carlo simulation of the response function has also been attempted with limited success. (It failed to reproduce the shape of experimentally measured monoenergetic electron lines (Schuperferling 1975)).

2) 4π β Spectroscopy Using the Magnetic Transport Technique

In this approach, a strong cylindrically symmetric magnetic field, supplied by a superconducting solenoid serves as an electron guide transporting the β particles from the source to the detectors and the backscattered β particles from one detector to the other. The source is

placed at the center of the solenoid, and the detectors are placed along the axis of the solenoid on either side of the source separated from each other by a considerable distance (>10 cm). Beta particles emitted from the source (in a 4π solid angle) follow helical trajectories in the magnetic field and are transported to either one of the detectors depending on the original direction in which they were emitted. Beta particles that are backscattered from one detector travel in the opposite direction and are detected by the second detector. The two detectors are operated in a summation mode and therefore the energy deposited by a β particle in both detectors is added up in the same manner as in more conventional 4π β spectrometers. The strong magnetic field confines the particles to orbits of small radii so that they are intercepted and analyzed by one of the silicon detectors. The purpose that the magnetic field serves is to allow the two silicon detectors to be physically separated from the source and from each other while at the same time maintaining the 4π solid angle for β ray detection.

The separation between the source and the detectors results in a small geometrical solid angle subtended by the detectors at the source and therefore in a reduction in the probability for γ ray detection. As a consequence of this, the ratio of the solid angle for the detection of β rays to that for γ rays is greatly enhanced (a factor of 100 or more) and quite an effective suppression of the Compton background (caused by the interaction of γ rays with the silicon detectors) is achieved (Shera et al. 1967; Andersen & Christensen 1968; McMillan 1970; Hamilton 1975).

In addition to the technical problems of contructing a superconducting magnet system with the required cryostat and associated support equipment (vacuum, power supply, etc.), the 4π detection method using a magnetic guide suffers from the same difficulties experienced by the usual 4π silicon detector arrangemetns (except for problems that are caused by γ ray detection).

The deterioration in resolution caused by signal summing is still a problem (Shera et al. 1967; Hamilton 1975). Moreover, the space limitations inside the bore of the solenoid require that the preamplifiers be placed outside the solenoid and at a considerable distance form the detectors. This results in the use of long cables between the detectors and the preamplifiers and therefore in a large input capacitance for the

preamplifier which in turn causes a degredation in the resolution of the spectrometer system (Shera et al. 1967; Andersen & Christensen 1968; Anderson 1968). The resolution of these 4π spectrometers is typically in the 10-20 keV range (Christensen & Andersen 1968; McMillan 1970).

The summing of electrons (internal conversion and Auger electronss) emitted from the source in coincidence with the β particles is a problem in these spectrometers as well (Shera et al. 1967; Hamilton 1975). In fact, the conversion electron spectrum of ^{207}Bi measured with 4π silicon spectrometers employing a magnetic field always contains KK, KL & LL sum peaks resulting from the addition of the various components of two coincident internal conversion transitions in the decay of this isotope (Anderson & Christensen 1968).

A problem which is peculiar to this type of spectrometer is caused by the long transit time taken by backscattered electrons to travel from one detector to the other. Depending on the distance between the two detectors, the energy of the β particles under study, and the integration time of the amplifier, up to a few percent of the counts generated by backscattered β particles may fall outside the intergration time of amplifier and therefore not be counted. This effect increases in importance if multiple backscatterings are considered (Shera et al. 1967).

The helical paths that the β particles follow in the solenoidal field result in an increase in the energy loss suffered by the β particles when they traverse any dead layers intervening between the source and the detectors. This is a consequence of the increase in the mean path length in the dead layers caused by the spiral trajectories that the β particles are forced to follow by their interaction with the magnetic field (Hamilton 1975).

The treatment of the problem of β particle trajectories in the magnetic field of the solenoids has been quite rudimentary. The simplifying assumption of a uniform magnetic field has always been used instead of using the actual magnetic field geometry generated by the solenoid (Shera et al. 1967; Andersen & Christensen 1968; McMillan 1970; Andersen 1974). As a result of this simplification, there has probably been an underestimation of the significance of backscattered β particles that are not detected in the second detector. These β particles that miss detection are usually backscattered β particles that remerge from the

surface of the detector far away from the solenoid axis and at large angles with respect to this axis and therefore follow trajectories with radii large enough that they collide with the magnet's bore or miss the second detector altogether (Andersen & Christensen 1968).

The problems of source detector alignment and source introduction mechanisms are still complicated in spite of the considerable separation between the two detectors. The space limitations imposed by the diameter of the magnet's bore is the cause of these complications.

Finally, because of the particular source-detector geometry in these spectrometers and the fact that the source and detectors are contained within the solenoid and its cryostart, these spectrometers are not suitable for $\beta - \gamma$ coincidence studies (McMillan 1970).

The Limitations of Silicon β Spectrometers

The major drawback of silicon spectrometers is their limited sensitive thickness and and therefore the limited range of β decay energies that can be studies using them. In the case of Si(Li) detectors, the restriction on active detector thickness is the result of the low mobility of lithium in silicon and therefore the limited thickness of the compensated region which may be obtained with lithium drifting (Coche & Siffert 1968). In the case of diffused junction and surface barrier detectors, the limit on the sensitive detector thickness is set by the resistivity of the starting silicon material available and by the voltage that the detector's contacts can withstand before breakdown (Coche & Siffert 1968 p 133).

Although Coche & Siffert (1968 p 161) seem to indicate that the thickness of the compensated region, obtained by lithium drift, can be as high as 10 or 15 mm, nevertheless silicon detectors (lithium drifted or otherwise) are available commercially with sensitive thicknesses of up to 5 mm only (Haller & Goulding 1981, EG&G 1981, H/F 1981, Decker et al. 1982, EMERTEC Schlumberger 1983). A sensitive thickness of 5 mm of silicon corresponds to the range of electrons with energies to about 2 MeV (even a 15 mm thickness represents the range of 6 MeV electrons in silicon) (Berger et al. 1969 and reference 24 therein). For β particles whose range in silicon exceeds the thickness of the sensitive layer, there is a small probability that they will be stopped in the active portion of

the detector and lose their energy there (low full peak efficiency). The probability of full energy deposition decreases rapidly as the energy of the incident β particles increases (Bertolini & Rota 1968; Berger et al. 1969). This incomplete energy loss causes severe distortions to the shapes of β spectra whose endpoint energies are higher than the electron energies that can be completely stopped within the detector active region (Bosch et al. 1963).

Stacking several transmission type silicon detectors in a telescope arrangement in order to obtain a sufficient sensitive thickness to stop energetic β particles results in several problems. Operating the detectors in a sum coincidence mode requires that the gains of all the detectors be perfectly matched. It also results in a deterioration in the resolution caused by the summing of the signals. In addition there are the problems of distortions of the shapes of β spectra due to the energy losses in the dead layers that exist on the front and back contacts of each of the detectors that are traversed in the stack. Another problem is that of matching the solid angles subtended by the active area of each of the detectors at the source. Using a small diameter front detector results in a large probability for energy loss through sidescattering while using a large diameter front detector and collimating the β particles incident on it results in distortions due the detection of β particles scattered from the collimator. In both cases the solid angle for detection is determined by the back detector (the last one in the stack). This solid angle will be quite small because of the separation between the back detector and the source.

Another solution for the limited thickness of silicon detectors has been attempted. In this approach, the β rays are made to enter through a flat edge on the side of the detector (the β particles enter the detector in a direction parallel to the plane of the contacts on the two faces of the detector). The incident β particles thus "see" a thickness of silicon almost equal to the diameter of the detector (Marlow & Waggoner 1967; Lund & Rudstam 1976). However, since the detector is rather narrow (its width being the thickness of the sensitive region $\sim$ 5 mm), there is a large probability for sidescattering out of the detector. To suppress this effect, anticoincidence electron detectors are arranged to surround the silicon spectrometer in order to veto any outscattered electrons (Lund &

Rudstam 1976).

Future Developments

Recent reports have demonstrated that with the availability of ultra high purity silicon (100 KΩ-cm), the manufacture of thick (up to 15 mm), totally depleted, silicon surface barrier detectors is now feasible (Shiraishi et al. 1983 and references 12, 14 therein). The excellent resolution of these detectors (a few keV for 1 MeV electrons), and the feasibility of making extremely thin contacts on both faces of the detectors (transmission type detectors suitable for stacking) make these newly developed detectors quite promising for use as high energy β spectrometers.

Finally, there has been a brief report recently on the use of a β spectrometer consisting of a 10 mm thick silicon detector and a thin (150 μm) silicon detector arranged in a telescope configuration (Nitschke 1983).

Germanium β Spectrometers

Although the very first semiconductor radiation detector was manufactured from germanium (see McKenzie 1979), the development of germanium detectors as radiation spectrometers lagged behind that of silicon detectors mainly because of the requirement that germanium should be operated at liquid nitrogen temperature. However, during the 1960's and early 1970's germanium γ ray spectrometers (first lithium drifted and then high purity) were developed and gained wide popularity.

In spite of the advanced stages of development that germanium γ ray spectrometers had reached by 1976, there had been only a few reports of electron spectra measured with germanium detectors. These early reports consisted mainly of measurements of internal conversion electron spectra to test the detector's performance and the thickness of the detector's contacts (see for example DeLyser et al. 1965; Strauss & Larsen 1969; Hansen 1971; Pehl & Cordi 1975). There were also reports on the use of conversion electrons and monoenergetic electron and positron beams (from a magnetic spectrometer) to measure the average energy required to create an electron-hole pair in germanium and the dependence (if any) of this energy on the species of particle depositing the energy (Ewan & Tavendale 1964; Pehl et al. 1968). Finally there were reports on the feasibility of using

a germanium detector as a β spectrometer or as an internal conversion electron spectrometer but without much in the way of applications (Camp & Armantrout 1965, Gruhn et al. 1969; Paris & Teherne 1969).

Thin germanium detectors were also used as conversion electron spectrometers and low energy beta spectrometers in nuclear orientation studies because of their good performance at low cryogenic temperatures (<10 K) (Frank et al. 1964; Brewer & Shirley 1970; Hung et al. 1976; Vydrik 1977; Boysen & Brewer 1977). However, there had been no published reports on the use of germanium detectors for precise β spectrometery measurements until 1976.

The development of the lithium drift processes for compensating germanium in the sixties made the production of planar Ge(Li) detectors with sensitive thicknesses of up to 20 mm quite feasible (Ewan 1979, Knoll 1979 p 416). This thickness corresponds to the range of electrons of about 20 MeV energy in germanium. (According to Ewan (1968), to a very good approximation the range of electrons in germanium is given by R = E - 0.2 where: R=Range in millimeters, E=Energy of the electrons in MeV. See also Evans (1955) p. 625). This energy range includes essentially all known β endpoint energies.

However, Ge(Li) detectors are quite difficult to fabricate and handle. The high mobility of lithium in germanium imposes that Ge(Li) detectors be kept at cryogenic temperatures (usually liquid nitrogen temperature) continuously after the lithium compensation process (Knoll 1979 p.416). Otherwise, if the Ge(Li) detector is warmed up to a room temperature even for a few minutes, the high mobility of lithium would result in the precipitation of the lithium and the decompensation of the sensitive region (Haller & Goulding 1981). This implies that Ge(Li) detectors should be maintained in the same cryostat in which they were mounted immediately following manufacture.

Ge(Li) detectors are also very sensitive to any surface contamination and therefore should be kept at a high vacuum at all time with special care taken to ensure that any condensable gases or vapors in the detector's cryostat are eliminated (Camp & Armantrout 1965; Boysen & Brewer 1977; McKenzie 1979; Haller & Goulding 1981). Their temperature and vacuum requirements cause severe handling problems and have hampered the use of Ge(Li) detectors as β spectrometers. Nevertheless, a Ge(Li)

detector (enclosed in its own, separate cryostat with a thin entrance window) has been used as a β spectrometer (D'Auria et al. 1976).

The development of high purity germanium (Ge(HP)) detectors in the early seventies eliminated most of the handling difficulties encountered with Ge(Li) detectors (McKenzie 1979, Haller & Goulding 1981). High purity germanium detectors can be easily recycled to room temperature and are less sensitive to surface contamination than Ge(Li) detectors.

Ge(HP) detectors are commercially available up to a sensitive thickness of 15 mm which implies that all β particles, even those emitted in the most energetic β decays, can be stopped within the sensitive region of the detector. All of these factors have paved the way for the application of germanium detectors to the field of β spectrometry.

The pioneering work done at the Foster Radiation laboratory in the mid seventies clearly demonstrated the potential of high purity germanium detectors as excellent β spectrometers especially for studies of nuclei far from stability (Moore et al, 1976; Rehfield 1977). Prior to that, there had been only one unpublished report on an unsuccessful attempt to use a germanium detector Ge(Li) for measurements of continuous spectra (see Otto et al. 1979 and reference 2 therein).

Since then, the use of high purity germanium detectors in β spectroscopy, and especially in regions far from stability, has been quite widespread. (See the following references for detailed instrumentation descriptions: Giarard & Avignone 1978; Blonnigen et al. 1980; Decker et al. 1982; Bom 1983; Trzaska et al. 1983; Avignone et al. 1983). (See the following references for examples on applications in β spectroscopy using Ge(HP) detectorss: Pardo et al. 1977; Wunsch & Wollnik 1977; Berg et al. 1978; Wunsch et al. 1978; Stippler et al. 1978b; Keyser et al. 1979; Davids et al. 1979; Sollnik 1980; Wollnik et al. 1980; Munnich 1980; AMCO 6 (1980) pp. 443-449, 485-492; Decker et al. 1980, 1981; CERN (1981) pp. 129-133, 141-147; Arai et al. 1981; Pahlmann et al. 1982; Moltz et al. 1982; Della Negra et al. 1982; Brenner et al. 1982; Iafigliola et al. 1983b; Nitschke 1983; Alkhazov et al. 1983; Blomquist et al. 1983).

Even with this broad popularity of Ge(HP) β spectrometers, in practically all of the cases mentioned above, the use of germanium spectrometers was confined to measurements of the endpoint energy of a single branch in the β decay. Indeed, only in investigations carried out

at this laboratory have germanium β spectrometers been used for branching ratios and shape factor measurements (Rehfield 1977, 1978; Hetherington et al. 1983; Hetherington 1984; and also in the work of Iafigliola et al. 1983b, a germanium β spectrometer was used for branching ratio measurements). The work of Decker et al. (1982) and Bom (1983, 1984) clearly shows the sensitivity of measurements performed with germanium spectrometers to the deviation of the shape of the measured β spectra from the allowed shape. However, no actual shape factor measurement were undertaken in either case.

In another application of Ge(HP) detectors to β spectroscopy, the shape of the low energy (156 keV endpoint energy) β spectrum of ^{14}C has been studied using a germanium spectrometer. This experiment was a by-product of an investigation of the carbon impurities in high purity germanium crystals. The long lived ^{14}C isotope was used as a radioactive tracer and was incorporated into the detector material during the crystal growth process. Therefore the measurement was effectively an internal source measurement with no need for the application of any corrections to the raw data (Haller et al. 1982; Haller 1982).

The Appeal of Germanium β Spectrometers:

In addition to the small dimensions of Ge(HP) detectors (in comparison to scintillators) and their excellent resolution (resolutions of 4-5 keV at 1 MeV have been reported) (Moore et al. 1976; Rehfield & Moore 1978; Girard & Avignone 1978) they have two other qualities which make them quite attractive as β spectrometers. The first is the linearity of their energy response which has been verified to 200 ppm in the case of electrons incident on the detector (Decker et al. 1982). The second is the high full-energy-peak efficiency for γ ray detection in germanium detectors which allows the use of γ rays to calibrate the germanium β spectrometers rapidly and accurately, especially at high energies (the pulse generated by the germanium spectrometer is a function of the energy deposited in the detector and is independent of the species of radiation depositing the energy) (Moore et al. 1976; Wunsch & Wollink 1977; Rehfield & Moore 1978; Wohn & Talbert 1978; Wollnik 1980; Wollnik et al. 1980; Brenner et al. 1982; Decker et al. 1982; Iafigiola et al. 1983b; Bom 1983; Trzaska et al. 1983).

The use of high purity germanium detectors as β spectrometers however is hampered by several factors:

1. Low Temperature Operation

Although Ge(HP) detectors can be stored at room temperature without any adverse effects, nevertheless they require cooling (usually down to liquid nitrogen temperature) for proper operation; the small band gap in germanium results in a leakage current that is too high at room temperature to allow the use of germanium diodes as radiation detectors (Goulding & Pehl 1974). In fact the resolution of germanium spectrometers deteriorates very rapidly as their termperature rises above 150 K because of the considerable increase in the leakage current (Goulding & Pehl 1974).

Therefore, germanium detectors have to be placed in a special cryostat in order to be cooled during their operation. They also have to be operated in vacuum to provide thermal insulation and to eliminate the possibility of contaminants condensing on the cold surface of the detector.

As a result of this vacuum requirement, Ge(HP) β spectrometers are usually installed in a separate cryostat with a thin entrance window through which the β particles have to pass before being detected and analyzed by the spectrometer (Girard & Avignone 1978; Moltz et al. 1982; Trzaska et al. 1983). Typical window thicknesses are several tens of microns of a low Z material (aluminum, titanium, berelium, nickel, or mylar) (D'Auria et al. 1976; Davids et al. 1979; Brenner et al. 1982; Decker et al. 1982, Bom 1983; Nitschke 1983; Arai et al. 1984). Beta particle scattering, energy losses, straggling and variation of energy losses with incident β particle energy in these windows result in distortions to the β spectrum for which correction have to be made, especially at low energies. Such corrections are not easy to calculate theoretically with precision (Decker et al. 1982; Bom 1983).

2. Problems Caused by the Relatively High Z or Germanium

a) A More Complicated Response Function

The higher Z of germanium in comparison to that of silicon or plastic scintillators results in: an increase in the backscattering

coefficient (a backscatter ratio of about 25%-35% at 1 MeV is observed in the different Germanium spectrometers depending on the angles of incidence and is in agreement with the formula of Kuzminikh & Vorobiev (1975) see Moore et al. 1976; Rehfield & Moore 1978; Noma et al. 1983; Bom 1983, 1984), an increase in the amount of sidescattering, an increase in bremsstrahling production and escape (Berger & Seltzer 1965, 1968; Grosswend 1974), and an increase in 511 pile-up (in the case of positrons) (Rehfield & Moore 1978; Noma et al. 1983; Bom 1983, 1984). The shape response function of germanium detectors will therefore deviate quite considerably from the ideal delta function shape. The determination of the shape of the response function at various energies and unfolding the distortions it causes to the shape of the continuous β spectrum is a very important task in the analysis of data collected with a germanium β spectrometer.

Different approaches to the problem of the determination of the shape of the response function of germanium spectrometers to β particles have been taken:

1) Monte Carlo Simulations

Detailed Monte Carlo studies of the response function of germanium detector to β particles have been performed (Varley et al. 1981; Noma et al. 1983). These are sophisticated computer simulations which take into account all the possible interactions of the β particles and the secondary particles that they produce during their interaction with the germanium crystal (secondary electrons, positrons and photons). Monte Carlo codes designed to simulate one specific type of the β particle interactions (such as 511 summing or sidescatter probability) have also been written (Avignone et al. 1981; Bom 1984).

2) Measurement of the Response Function

Using monoenergetic electron beams from magnetic β spectrometers, the response functions of different germanium spectrometers to β particles have been measured (D'Auria et al. 1976, Otto et al. 1979, Blonnigen et al. 1980, Varley et al. 1981; Decker et al. 1982). A crucial aspect in the measurement of the shape of the response function is the determination of the background spectrum and its subtraction from the true spectrum generated by the incident monoenergetic electrons in the germanium spectrometer. The component of the background that is caused by electron

scattering and bremsstrahlung production in the magnetic spectrometer is particularly important in this context. (Blonnigen et al. 1980; Varley et al. 1981; Decker et al. 1982). Furthermore, during measurements of the response function of the detectors, special attention has to be paid to reproducing the angles of incidence of the β particles on the face of the detector that result from the particular source-detector geometry which is used when the actual β spectra measurements are performed (D'Auria et al. 1976; Decker et al. 1982).

The excellent energy resolution of germanium β spectrometers requires that the monoenergetic beams used for the response function measurements have a very narrow momentum spread (i.e. the magnetic spectrometer has to have an excellent resolution). Otherwise, particular features in the shape of the response function would be smeared out. In addition, the shape of the monoenergetic electron line produced by the magnetic spectrometer has to be symmetric with no high or low energy tails which, if present, would be superimposed on the response function of the germanium detector.

3) The Generation of a Semiempirical Response Function

In this approach, an approximate general shape for the response function is determined from physical arguments concerning the type of interactions between the β particles and the germanium detector. The different parameters describing the shape of the response function (e.g. the relative intensities of the different parts of the response function), and the variation of these parameters with energy, are then adjusted such that a set of standard β spectra measured with the spectrometer can be deconvoluted using the same response function after the adjustment (Moore et al. 1976; Rehfield & Moore 1978; Rehfield et al. 1980; Arai et al. 1981, 1984; Bom 1984).

This approach is hampered by the lack of an adequate set of standard sources whose β spectra shape have been accurately measured and well established, especially for high endpoint energy decays (Moore et al. 1976).

Other techniques for analyzing the β spectra measured with germanium spectrometers have been attempted as well. (Pardo et al. 1977; Girard & Avignone 1978; Davids et al. 1979: Avignone et al. 1981; Trzaska et al. 1983). These techniques do not take into account the response

function of the spectrometers (at least not directly). They have been used mostly for rapid determination of the endpoint energy of the β spectrum with modest accuracy and without a detailed analysis of the spectrum but are too rudimentary to be used in shape factor measurements or even for precise endpoint energy determinations.

b) High Sensitivity to γ Rays

The high sensitivity of germanium detectors to γ rays requires that certain measures be taken so that counts resulting from γ ray detection in the germanium β spectrometer do not end up distorting the β spectrum to such an extent that extraction of any useful information from it becomes impossible.

In certain cases, the effects of γ ray interaction with the germanium detector are taken into account in the β spectrum deconvolution procedure. However, such an approach requires complete knowledge of the decay scheme of the nucleus under study and the intensities and energies of the γ rays emitted from the radioactive source and the γ ray response function of the detector as well (Pardo et al. 1977; see also Davids et al. 1974 for a description of the analysis technique).

In another approach, the probability of γ ray interactions with the detector is minimized by using a detector with a small volume and not thicker than necessary to stop the most energetic β particles from the particular decay under investigation (Girard & Avignone 1978).

A much more fruitful approach to reducing the distorting effects of γ ray detection is to employ an effective γ suppression technique in conjunction with the germanium β spectrometer. The different γ suppression techniques that have been used with germanium spectrometers include:

1) Particle identification using two detectors in an ΔE-E telescope arrangement. The ΔE detectors that have been tried are: plastic scintillators (D'Auria et al. 1976; Otto et al. 1979), a multiwire proportional chamber (Bom 1983), thin surface barrier silicon detectors (Davids et al. 1979; Shahien 1981; Iafigliola et al. 1983b; Nitschke 1983) and a thick Si(Li) detector (Trzaska et al. 1983).

2) Magnetic transport using either an achromatic electron guide employing a superconducting solenoid (Moore et al. 1976, Rehfield 1977), or a sector

magnet with a wide (10%) momentum range transmission (Blonnigen et al. 1980; Wollnik et al. 1980).

3) $\beta - \gamma$ coincidence methods have been used to eliminate the non coincident γ ray background and to select specific β decay branches in order to simplify the data analysis (see for example Pardo et al. 1977; Girard & Avignone 1978; Moltz et al. 1982; Decker et al. 1982; Brenner et al. 1982; Avignone et al. 1983).

2.4 Methods of γ Ray Suppression in Energy Sensitive Detectors

One of the major problems encountered with energy deposition β spectrometers is their sensitivity to γ rays. This sensitivity can result in a severe contamination of the accumulated β spectrum with counts caused by the interaction of γ rays, emitted from the radioactive source, with the energy sensitive detector. Such effects are quite important in nuclei far from stability since their β decay usually leads to intense γ ray emission.

In order for a γ ray photon to deposit some or all of its energy in the detector material, it has first to transfer this energy to one or more electrons in the detector material (photoelectric or Compton effects). Alternatively, the photon can create an electron-positron pair in the detector material. The charged particles (electrons and positrons) to which the photon energy has been transferred, dissipate their energy as they travel through the detector material producing the ionization (and the scintillation in scintillation spectrometers) which provides the detection signal.

For a beam of photons incident on an absorber, the fraction of the beam that interacts with the absorber (and therefore causes a signal if the absorber is a detector) is given by

$$F = 1 - \exp (-\mu_o t) \qquad 2.1$$

where

F = The fraction of the photon beam interacting with the absorber

μ_o = The mass attenuation coefficient for the absorber material (cm^2/g)

t = The mass thickness of the absorber (g/cm^2)

The mass thickness (t) can also be written as

$$t = \rho x$$

where

ρ = The density of the absorber material (g/cm^3)

x = The thickness of the absorber material (cm)

The mass attenuation is given by

$$\mu_o = \frac{\tau}{\rho} + \frac{\sigma}{\rho} + \frac{\varkappa}{\rho}$$

where

τ , σ , $\varkappa$ = The linear attentuation coefficients resulting from the photoelectric, Compton, and pair production interaction respectively.

The compton term (σ/ρ)which dominates the mass attenuation coefficient in the γ ray energy region 0.5 - 2 MeV is practically independent of Z of the absorber for the common detector materials (gases except hydrogen, plastic scintillator, silicon, germanium and NaI).

The photoelectric term (τ/ρ)which is important at low energies, and the pair production term ($\varkappa/\rho$)which gains importance at energies above $\sim$ 4 MeV, can be written as

$$(\tau/\rho) = {}_a\tau \ (N/A)$$

$$(\sigma/\rho) = {}_a\varkappa \ (N/A)$$

where

a^τ , $a^\varkappa$ = The fundamental compton and pair production cross sections per atom

N = The number of atoms per mole = constant

A = The mass number of the absorber

The fundamental cross sections ${}_a\tau$, ${}_a\varkappa$ can be expressed as follows:

$${}_a\tau = \text{constant} \ (Z^n / E^3)$$

$${}_a\varkappa = \text{constant} \quad Z^2 \ \overline{P}$$

where

Z = The atomic number of the absorber

E = The energy of the incident γ ray

$\overline{P}$ = A complicated function of the energy of the incident γ ray energy. It increases approximately logarithmically with γ ray energy but is nearly independent of Z.

n = An exponent with a value between 4-5 depending on the γ ray energy

Therefore

$$(\tau/\rho) \approx \text{constant} \quad (Z/A) \; (\; Z^{n-1}/E \;)$$

$$(\varkappa/\rho) \approx \text{constant} \quad (Z/A) \quad Z \quad \overline{P}$$

$Z/A = 0.45 \pm 0.05$ for all elements (except hydrogen $Z/A \approx 1$)

It is clear from the arguments above that in order to minimize the probability of γ ray interaction with an absorber, the thickness, density and atomic number of the absorber have to be made as small as possible. (The preceeding development closely follows that given by Evans 1955).

Different approaches to the Problem of γ ray suppression have been tried. Some of these approaches are:

2.4.1 The β Absorber Method

This is one of the most common methods for correcting for the contamination of the β spectrum with counts caused by γ rays emitted from the radioactive source. A low density, low Z absorber (polyethelyne, prespex, lucite, beryllium, carbon, and aluminium have been used for example), thick enough to stop the most energetic β rays emitted in the decay, is interposed between the radioactive source and the detector. Since no β particles will penetrate through the absorber to be detected by the β detector, the spectrum accumulated with the abosrber in place

results from γ rays penetrating through absorber and interacting with the detector. This spectrum is therefore subtracted from the original spectrum accumulated by the β spectrometer (containing both β and γ counts) to yield a β spectrum with no γ contamination (see for example Freedman et al. 1956; Ricci 1957; Gardner & Meinke 1958; Cramer et al. 1962; Kantele et al. 1964; Persson 1964; Wohn et al. 1972; Bosch et al. 1973, 1974; Dakubu & Gilboy 1978).

One of the problems with the β absorber method is the need for an accurate normalization procedure to adjust the intensity of the spectrum accumulated with the absorber in place, so that this intensity corresponds to the intensity of the γ ray background component of the spectrum taken without the aborber.

Another problem is caused by the fact that the β absorber method does not account for the effects of β -γ summing (both random and coincident) in the β detector (Kantele et al. 1964). Furthermore, the β ray absorber itself contributes to the background in the detector. This contribution comes from the bremsstrahlung radiation emitted as the β particles are stopped in the absorber, from the annhiliation photons produced in the absorber if a positron spectrum is under study, and from γ ray scattering in the absorber which can be accompanied by secondary electron production (O'Kelley 1961 p. 426).

Finally, for highly energetic β decays, the thicknesss of the absorber required to stop the β particles can be large enough that the attenuation of the γ rays by β absorber can be significant (see for example the calculation of the γ sensitivity of plastic scintillators). A thickness equivalent to 22 mm of aluminum is required to stop 10 MeV electrons. This thickness results in a 30% attenuation of 1 MeV γ rays. Accounting for this attenuation is especially troublesome in cases where collimators are used between the source and the β spectrometer (Persson 1964).

2.4.2 β - γ Coincidence Method

Another method for suppressing the effects of γ ray detection in energy sensitive β spectrometers is through the use of β -γ coincidence techniques. In this approach the β spectrum counts are acccumulated only if they are in coincidence with the full energy peak of a γ ray detected

in a separate γ ray detector. Such coincident γ rays are emitted during the deexcitation of the excited levels of the daughter nucleus that are fed by the β decay of the parent.

The $\beta - \gamma$ coincidence method eliminates most of the distortions to the β spectrum that would be caused by the gating γ ray if no coincidence condition was imposed. This method also helps in suppressing most of the adverse effects of non coincident γ ray detection. Furthermore, the $\beta - \gamma$ coincidence technique is quite useful in eliminating the detection of β rays emitted by any radioactive contaminants in the source and β rays emitted in the decay of the daughters of the nucleus whose decay is under investigation (Brenner et al. 1982). And, if the data acquisition is done in a multiparameter event mode, then the $\beta - \gamma$ coincidence data can also be used to verify the β feeding values to the various excited states (Brenner et al. 1982).

Both NaI(Tl) and germanium γ spectrometers have been used in such coincidence studies.

In addition to the obvious complexity of such a system it suffers from several other drawbacks:

1. Low Efficiency

The requirement of coincident detection of two radiations (β and γ) in two separate detectors results in a reduction in the efficiency of the spectrometer system. The efficiency of the $\beta - \gamma$ coincidence set-up is proportional to the product of the efficiencies of the β and γ detectors.

2. Variation of Efficiency with Pulse Height

The possible dependence of the efficiency of the coincidence system on the pulse heights of signals generated in the β detector can result in serious distortions to the shape of the β spectrum. Such a dependance can result from the details of the working of the coincidence circuit (Spejewsski 1966; see also Knoll 1979 pp 690-704).

3. Knowledge of the Decay Scheme

In order to be able to use the $\beta - \gamma$ coincidence method for γ suppression, complete knowledge of the decay scheme is needed. This requirement comes about because of the fact that the $\beta - \gamma$ coincidence

technique is completely ineffective in suppressing the effects resulting from the interaction (with the β detector) of γ rays that are coincident with the γ ray used in gating the β spectrometer. Therefore the choice of the appropriate gating γ ray is crucial. Such a γ ray should obviously be in prompt coincidence with the β decay branch under consideration. Furthermore, it should not be in coincidence with any other events that can result in counts in the β spectrometer (e.g. β particles from other β branches feeding higher levels that deexcite through a γ ray cascade to which the gating γ ray belongs, and other γ rays in such a cascade) (Gils et al. 1972). Using a γ ray that is part of such a cascade to trigger the β - γ coincidence results in the collection (in the β detector) of β spectrum composed of more than one branch. It also results in the usual γ ray distortions affecting the β spectrum (a superimposed background and a summing contribution) caused by the other γ rays in the cascade (Pardo et al. 1977; Keyser et al, 1981; Pahlmann et al, 1982).

Gating the β spectrum with a sum peak representing the sum of the energies of all the γ rays in a cascade has been used in Q_β masurements (Lund & Rudstam 1976). However, unless a very large solid angle for γ ray detection is available (~4π), the efficiency of such a β - γ coincidence method would be very small (as a result of the multiplication of the efficiency for detecting the γ rays). The technique of sum peak gating is not very useful if the β feeding to each individual high energy level is small.

Finally, in using the sum peak as a trigger one is choosing a β branch which is in the low energy region and which is therefore more susceptible to the different causes of distortion (higher energy loss in dead layers, more straggling, higher backscattering coefficient, etc.)

4. Ground State Branches

The β - γ coincidence technique obviously can not be used to suppress γ rays when the β branch feeding the ground state of the daughter nucleus is sought. However, if a β - γ anticoincidence is used, the ground state branch can be enhanced but without exclusive branch selection or very effective γ ray suppression. This is because the efficiency for γ ray detection is never 100% (Lund & Rudstam 1976).

5. Chance Coincidences

Depending on the count rate and the time resolution of the coincidence system, some of the counts accumulated in the β spectrum will result from accidental (as opposed to true) coincidences between the β and γ branches of the coincidence circuit. The chance-to-true coincidence ratio can be as high as several to 10% in a typical β - γ coincidence experiment (Gils et al. 1972; Bosch et al. 1973, 1974; Dakubu & Gilboy 1978).

6. Internal Bremsstrahlung

All β decays are accompanied by the coincident emission of a continuous spectrum of photons extending up to the endpoint energy of the β spectrum. This phenomena results from the electromagnetic interaction between the emitting nucleus and the β particle and is referred to as Internal Bremsstrahlung (Pettersson 1965).

Photons emitted during the internal bremsstrahlung processes can be detected in the γ ray detector and result in a β - γ coincidence. The effects of such coincidences have to be taken into account when the data is analyzed (Bosch et al. 1973).

7. Compton Background

The Compton continuum of a high energy γ ray, detected in coincidence with a β particle, contributes to all the coincidence gates of lower energies. This contribution is especially important in cases of low intensity β branches (Bosch et al. 1963; Persson 1964; Charoenkwan 1965; Keyser et al. 1981; Pahlmann et al. 1982). Sometimes anticompton guards (veto detectors) are used around the γ detector to reduce the magnitude of this effect (Lund & Rudstam 1976).

In 4π β spectrometers using β - γ coincidence techniques, there is the added possibility of a γ ray Compton scattering in the β detector and then causing a trigger signal in the γ detector (as a result of the wide energy window settings that are usually used when low resolution NaI γ ray detectors are employed). Such events can result in counts above the endpoint and shape distortions of the β spectrum (Rhode & Johnson 1962; Spejewski 1966; Gils et al. 1972).

8. Random Summing

The $\beta - \gamma$ coincidence technique does not reduce the adverse effects of the random pile-up of pulses in the β spectrometer. The importance of this effect depends on the singles count rate in the β detector and is therefore unaffected by he coincidence condition.

2.4.3 Particle Identification Methods

Particle identification methods have been used to distinguish between β rays and photons incident on energy sensitive β spectrometers and therefore to help suppress the detection of γ rays in such spectrometers. In this approach a thin detector (ΔE detector, or dE/dx detector) is interposed between the radioactive source and the main β detector (E detector) where the β particles are eventually stopped. This ΔE-E arrangement is referred to as a "telescope system."

Beta particles passing through the ΔE detector deposit some of their energy there before being stopped in the E detector where they deposit the rest of their energy. As for γ rays, because of the small thickness of the ΔE detector, there is only a very small probability that the photons will interact with it and cause a detection signal. Therefore by gating the E detector signals with the signals from the ΔE detector, events resulting from β rays can be differentiated from those caused by a γ ray interaction in the E detector since the spectrometer will be activated only if a charged particle passes through the E detector.

The reduction in the γ ray detection probability in a telescope system in comparison to the case when a single β detector (with the same thickness as the E detector) is used is called the γ ray suppression ratio. It is equal to the ratio of the probabilty of a γ ray causing a detection signal in both the E and ΔE detector to the probability of the same γ ray causing a signal in the E detector only. The γ ray suppression in telescope systems therefore comes about because of the small probabilty for a γ ray interaction with the ΔE detector as a result of its small thickness.

A γ ray interaction with the ΔE detector is very likely to produce signals in both the ΔE and the E detectors. For electrons produced by the photoelectric interaction of a γ ray with the ΔE detector, there is a high probabilty that the photoelectrons will be emitted in the forward

direction (i.e. the original direction of the incident γ ray). This is especially true for γ ray energies above 0.5 MeV (Evans 1955 pp. 695-697). In the case when the γ ray undergoes a Compton scattering in the ΔE detector, there is a high probability for the photon to be scattered either in the forward or the backward direction but a low probability for scattering sideways (i.e. perpendicular to the direction of the incident γ ray). As a result, the probability for the emission of a Compton electron is highest in the forward direction (Evans 1955 pp. 682-684, pp. 690-692). Similarly, for γ rays undergoing pair production interactions in the ΔE detector, the angular distribution of the emitted electron-positron pairs (with respect to the incident photon direciton) is strongly forward peaked (Evans 1955 p 703).

The forward directed secondary electrons that are produced by the processes described above have a high probability for traversing the small thickness of the ΔE detector and interaccting with the E detector . In the case of Compton scattering, the forward scattered photons themselves can also interact with the E detector. Among all of these possible processes. Compton events in which the incident photon is scattered backwards and a high energy electron is produced in the forward direction are the ones with the highest probability for producing signals in both the E and ΔE detectors (Toriyama et al. 1980; Ohya et al. 1982).

In comparison to the processes described above (production of forward directed electrons in the ΔE detector), there is a negligibly small probability for events in which the incident γ ray passes through the E detector without an interaction and then undergoes an interaction with the E detector which generates a detection signal in both the E and ΔE detectors. These improbable events can cause a detection signal in the ΔE detector as a result of the interaction (with the ΔE detector) of a photon, Compton scattered in the backward direction, or a secondary electron or positron emitted from the E detector in the direction of the ΔE detector. The occurance of such events is highly unlikely because of the small cross section for the production of backward directed secondary electrons, the large thickness of the E detector which insures that most of the secondary electrons produced in the E detector will be stopped there as well, and finally the small probability for interaction with the thin ΔE detector in the case of a backward scattered photon.

It follows from the preceeding discussion that, to first order, the γ ray suppression ratio of a telescope system is equal to the probabilty for a γ ray interaction with the ΔE detector alone divided by the probability for a γ ray interaction in the E detector by itself.

Using equation (2.1), we have

$$F_1 = 1 - \exp (-\mu_1 t_1)$$

$$F_2 = 1 - \exp (-\mu_2 t_2)$$

where

F_1, F_2 = The probabilty for γ ray interaction with the ΔE detector and the E detector respectively (i.e. the γ ray efficiens of the two detectors).

μ_1, μ_2 = The mass attenuation coefficient for the ΔE detector and the E detector materials respectively.

t_1, t_2 = The mass thickness of the ΔE and E detectors respectively.

Therefore, the γ ray suppression ratio = $\dfrac{1- \exp (-\mu_1 t_1)}{1- \exp (- \mu_2 t_2)} \approx \dfrac{\mu_1 t_1}{\mu_2 t_2}$

Hence, if the E and ΔE detectors are manufactured from the same material, then the suppression ratio is simply equal to the ratio of their thicknesses (Kantele & Passoja 1971; Dickey et al. 1978; Borovoy et al. 1979; Ohya et al. 1982). Typical γ ray suppression ratios for telescope spectrometers are of the order 100.

It is quite clear then, that in order to achieve a high γ ray suppression ratio, the ΔE detector has to be made from a low Z, low density material and its thickness has to be minimized. However using a ΔE detector with a small mass thickness results in small energy deposition by the β particles in the ΔE detector. This in turn causes the signals generated by the interaction of the β particles with the ΔE detector to be comparable in size to the electronic noise in the detector and associated circuitry. As a result there is an increase in the probability that the coincidence circuit will be triggered by a noise pulse in the ΔE detector (Dickey et al. 19878). The use of a very thin semiconductor ΔE detector can also cause other problems as will be seen later.

The arguments that have been used above to calculate the

suppression ratio for γ ray originating from the radioactive β source are abviously not applicable to the calculation of the effective suppression of γ rays which originate from other sources and which do not traverse the ΔE detector (as is the case for the ambient γ rays in a high background area). Telescope systems are most effective when such γ rays represent a problem since their suppression ratios for these γ rays is much higher than the values that are calculable from the equations used above (Kantele & Passoja 1971).

The energy loss suffered by β particles in passing through the ΔE detector has to be accounted for accurately so that the energy obtained with the telescope system does truly represent the energy spectrum of the incident β particles. In practice, there have been two approaches for accomplishing this. In telescope spectrometers where the energy loss of the β particles in the ΔE detector is small (e.g. if the ΔE is a thin plastic scintillator or a proportional counter), then the energy loss in the ΔE detector (including losses in dead layers such as entrance windows and reflectors) is calculated and added to the energy of the energy of the β particles detected by the E detector. In the second approach, the E - ΔE telescope is operated in a sum coincidence mode and the coincident pulses from both detectors are added to each other to account for the total energy of the β particles.

Both these methods suffer from problems which can cause distortions to the shapes of β spectra measured with telescope spectrometers.

1. Coincidence Mode Operation

In this mode, the ΔE detector is used simply to gate the E detector in the coincidence circuit. No pulse height information from the ΔE detector is retained. The energy loss of the β particles in the ΔE detector in this mode of operation is obtained from a calculation rather than direct measurement.

The problems with this approach are:

a) Dependence of the energy loss on the energy of the incident β particles.

The energy loss suffered by β particles in passing through the E is dependent on their initial energy especially for β particle energies below 0.5 MeV. Therefore adding a constant energy corresponding to the energy loss of minimum ionizing electrons in the ΔE detector to the energy

measured by the E detector (as is frequently done: see example Otto et al. 1979) would cause the telescope spectrometer to have a non-linear energy response, particularly in the low energy region.

Using the Bethe-Bloch formula (see for example Knop & Paul 1965 p. 12) to calculate the energy loss in the ΔE detector and the dependence of this energy loss on the energy of the β particles does not yield very accurate results either since the formula holds rigorously only for infinitesimal energy losses (infinitesimal layer thicknesses). The Bethe-Bloch formula does not include the effects of the slowing down of the β particles during their interaction with the finite thickness of the ΔE detector. Neither does the formula take into account the variations in energy loss experienced by monoenergetic electrons as a result of the differences in the length of the paths that they follow in the ΔE detector. (Such path length differences are caused by electron scattering in the ΔE detector material). The deviations of the actual energy loss from the energy loss calculated from the Bethe-Bloch formula will be most pronounced at low energies where the energy loss is greatest (Bom 1983).

Among the effects causing deviations from the energy loss as calculated from the Bethe-Bloch formula, the variation in the energy loss caused by electron scattering in the ΔE detector is perhaps the most important since it can cause serious distortions to the shape of the β spectrum. Because of the small mass of the electron, it can suffer significant deflections in its interaction with matter and its path as it passes through the ΔE detector can be very tortuous. In fact, the path length can be as large as 4 times the thickness of the ΔE detector (Evans 1955 p. 611). The energy losses of β particles traversing the ΔE detector will therefore vary widely depending on their path lengths (Beck 1969 Fig. 2; Hoyle et al. 1983 Figs. 8, 14). Moreover the amount of variation in the lengths of the paths of the β particles in the ΔE detector is a function of the primary energy of the β particles.

To account properly for all the variations in energy loss in the ΔE detector, the spectrum of energies deposited by monoenergetic β particles in this detector has to be carefully calculated (using Monte Carlo techniques for example) at different incident β particle energies. The spectra thus obtained should then be used to convolute the β particle energy spectrum accumulated by the E detector.

As an alternative, Beck (1969) used a single channel analyzer to set a window on the heights of the pulses accepted in the ΔE detector so that pulses generated by scattered electrons with long path lengths are excluded. This technique of pulse height selection in the ΔE detector has also been used to discriminate against backscattered β particles. A more detailed discussion of the technique will be given later in this section. The major shortcomings of the pulse hieght selection method are the reduction in efficieny and the dependence of efficiency on β particle energy as will be shown later.

b) Straggling

Even if the effects of large angle scatterings are eliminated and all the electrons follow paths of the same length in the ΔE detector there would still be large variations in the energy losses experienced by monoenergetic electrons passing through the ΔE detector. These differences in energy loss are due to the statistical nature of the interactions between the incident β particles and the detector material. Since the individual ionization energy losses suffered by the electrons (in single collisions) vary over a wide range of energies (from zero up to one half of the electron's kinetic energy because of the small mass of the electron) the total energy loss experienced in collision can be quite different from one electron to the other. In addition to this, the electron may also lose any fraction of its energy in a radiative collision.

According to the treatment of Landau, the spectrum of the energy losses of monoenergetic β particles in a thin absorber is a nonsymmetric distribution with a peak corresponding to the most probable energy loss and a full width at half maximum (fwhm) equal to about 20-25% of the most probable energy loss. Furthermore, the asymmetry of the distribution of energy losses in the thin absorber increases with a decrease in the energy of the incident β particle. Therefore for a fixed absorber thickness, the importance of straggling increases with a decrease in the primary energy of the β particles. (Bethe & Ashkin 1953 pp. 255-259; Evans 1955 pp. 621-622; Seltzer & Berger 1974).

The straggling of the energy loss of β particles during their passage through the ΔE detector has the effect of broadening the resolution of the telescope spectrometer in comparison to the resolution of the E detector alone (Toriyama et al. 1980; Bom 1983). It can also

result in an energy dependent resolution due to the dependence of straggling on the incident β particle energy (see Toriyama et al. 1980 Fig. 5)

2. Sum-Coincidence Mode Operation

The alternative to calculating the energy loss of β particles in the ΔE detector and adding it to the measured energy is to operate the ΔE and E detectors in a sum-coincidence mode. In this mode, the pulse heights from both detectors are added to each other to account for the total energy lost by each individual β particle in the telescope system (Kantele & Passoja 1971; Dickey et al. 1978; Borovoy et al. 1979; Clifford 1981; Ohya et al. 1982; Hoyle et al. 1983; Iafigiola et al. 1983b).

Some of the problems encountered with this approach are the usual problems encountered when signals from two detectors are summed. These include the need for gain matching and stabilization (Iafigiola et al. 1983b) and the deterioration in resolution due to summing. The problem of gain matching over a wide energy range is complicated further in this case as a result of the small thickness of the ΔE detector and therefore its small full energy peak efficiency for high energy (above 0.5 MeV) conversion electron lines. As for the deterioration in resolution, the problem is most severe in telescope systems where the ΔE detector is a semiconductor detector. The largest contribution to the resolution of these detectors comes from electronic noise which increases rapidly with an increase in the value of the capacitance with which the input of the preamplifier is loaded (Knoll 1979 pp. 651-652). The small thickness of the semiconductor ΔE detector results in a large capacitance and therefore in a signficant deterioration in resolution (Kantele & Passoja 1971; Ohya et al. 1982). (The large capacitance causes an increase in the rise time of pulses generated in the ΔE detector as well (Knoll 1979 p. 652). This in turn results in the use of long resolving times in the E-ΔE coincidence circuit and therefore in an increase in the ratio of random to true coincidences. It can also cause problems if the telescope spectrometer is used in timing applications (Kantele & Passoja 1971)). Using ΔE detectors with smaller surface areas helps to reduce the capacitance but also results in a lower efficiency (smaller solid angle) and an increase in the side scattering.

Finally, when operating the telescope system in the sum-coincidence mode, one has to account also for the small energy losses in the two extra dead layers (on the front and back of the ΔE detector) that are added as a result of the introduction of the ΔE detector.

Attempting to alleviate the problems resulting from the use of thin semiconductor detectors by increasing the thickness of the ΔE detector has the following disadvantages:

- A reduction in the γ ray suppresion capability of the telescope spectrometer.
- An upward shift in the spectrometer's low energy cut off to higher β particle energies.
- A strong dependence of the transmission of the ΔE detector on the energy of the transmitted β particles.
- An increase in the scattering of β particles during their traversal of the ΔE detector resulting in an energy dependent spectrometer efficiency (Bom 1983).

Problems Experienced by Telescope Spectrometers in General

Telescope β spectrometers, indpendent of the type of the E or ΔE detectors used or whether they are operated in a sum-coincidence or a coincidence mode, suffer from several problems in common with each other:

1. β - γ Summing

a) Coincident γ Rays

Telescope spectrometers are not effective in suppressing the detection of coincident γ rays if they strike the detector simultaneously with their coincident β particle. Such a situation occurs when the coincident β and γ rays are both emitted into the finite solid angle subtended by the telescope at the radioactive source. The β ray then triggers the coincidence circuit and the energy deposited by the β and γ rays is detected simultaneously and summed. The probability for the occurence of such events is proportional to the square of the solid angle which the telescope subtends at the source. Therefore in order to reduce the effects of coincident $\beta - \gamma$ summing the solid angle of acceptance of the telescope spectrometer has to be made quite small resulting in a

decrease in the spectrometer's efficiency.

b) Non-Coincident γ Rays

Telescope spectrometers are ineffective in suppressing β - γ random pile-up caused by the detection of a β particle and a γ ray in the spectrometer in a period of time shorter than the resolving time of the coincidence circuit. Therefore the γ suppression capability of telescope spectrometers is effectively count rate dependent (especially at high counting rates) (Borovoy et al. 1979).

2. Scattering from Solid Materials in the Vicinity of the Spectrometer

The addition of a ΔE detector between the source and the main β ray detector increases the probability of β ray scattering from the ΔE detector mounting and connections (Bom 1983). Very effective collimation is needed to reduce such effects. It was found necessary to use active collimators (plastic scintillation veto detectors) in order to avoid the use of thick inactive collimators from which β particles can scatter (Kaina 1977; Kaina et al. 1977; Clifford 1981; Bom 1983).

3. The Dependence of the Telescopes Efficiency on the Energy of the Particles

The detection efficiency of a telescope spectrometer for β particles is dependent on the energy of the incident β particles (see for examples Toriyama et al. 1980 Fig. 5; Clifford 1981 Fig. 3-6; Ohya et al. 1982, Fig. 6; Bom 1983). This energy dependence can cause serious distortions to the shapes of continuous β spectra and complicate measurements of shape factors. The variation in efficiency with β particle energy is caused by three distinct effects.

a) Low Energy Cut Off

As a result of the finite thickness of the ΔE detector, the telescope spectrometer will have a low energy cut off limit corresponding to the energy of β particles whose range in the ΔE detector material is equal to the thickness of the ΔE detector. Beta particles with energies less than the low energy threshold are not transmitted through the ΔE detector and therefore are not detected in the E detector. Hence if the

telescope is operated in a coincidence mode gated by signals from both detectors, counts resulting from such low energy β particles are not accumulated.

Typical values for ΔE detector thicknesses are 200 μm for silicon detectors and 0.5 mm for plastic scintillators. These thicknesses correspond to the range of β particles of energies of 175 keV and 220 keV respectively.

b) Energy Dependent Transmission of the ΔE Detector

Even for β rays whose range exceeds the thickness of the ΔE detector, some of the incident β particles will not be transmitted through the ΔE detecctor. The reason for this incomplete transmission is that some of the incident β particles are backscattered from the ΔE detector while some of the other incident β particles are completely stopped in the ΔE detector as a result of the long path lengths that they follow in the ΔE detector (caused by large angle scattering) (see Kantele & Passoja 1971 Fig. 2a, Ohya et al. 1982 Fig. 2).

As an example, using the empirical formula of Tabata and Ito (1975), for a beam of 1 MeV electrons perpendicularly incident on a 200 μm thick silicon detector, about 4% of the incident electrons are not transmitted through the detector. (The percentage is higher for oblique incidence angles (Tabata & Ito 1976)). The fraction of transmitted electrons is also a function of the incident electron energies and increases with a decrease in the energy.

The energy dependence of the transmission of β particles through the ΔE detector can cause serious distortions to the shape of the β spectrum measured with a telescope system.

c) Scattering in the ΔE Detector

A beam of electrons passing through a thin absorber (such as the ΔE detector) will emerge with a certain angular spread as a result of scattering. Because of this angular spread, some of the β particles that are transmitted through the ΔE detector miss the E detector altogether. The shape of the angular distribution of the β particles emerging from the ΔE is dependent on their primary energy (Seltzer & Berger 1974) (more forward directed at higher incident energies). Therefore the percentage

of β particles missing the E detector and the efficiency of the telescope are energy dependent as well (Dickey et al. 1978; Bom 1983).

The Use of Telescope Spectrometers to Reduce the Effects of Backscattering

Telescope β spectrometers have also been used to reduce the effects of β particle backscattering from the E detector. This is accomplished by making use of the fact that the energy loss per unit path length for β particles is nearly independent of their energy for energies above about 0.5 MeV. Thus by selecting the ΔE pulses such that the only events retained are those where the energy loss in the ΔE detector corresponds to the most probable energy loss of minimum ionizing β particles passing through the ΔE detector, it is possible to discriminate against backscattered β particles (which would have a high energy loss due to the double passage through the ΔE detecctor) (Knott et al. 19709; Kantele & Passoja 1971).

The ΔE pulse height selection also improves the γ ray suppression of the E - ΔE telescope. The improvement in γ ray suppression is achieved because of the fact that the most probable γ ray interactions with the ΔE detector are Compton scatterings. The spectrum of energies deposited by the Compton events in the ΔE detector forms a flat continuum most of which is discriminated against if a pulse height window is set on the ΔE detector (Knott et al. 1970; Kantele & Passoja 1971).

Furthermore, the pulse height selection method can be useful in eliminating the coincident summing of β particles and conversion electrons since the amount of energy deposited by two particles passsing through the ΔE detector falls outside the window set on the pulse height in the E detector (Michaelis et al. 1969).

The difficulties encountered with the pulse height selection technique are:

1. Reduction in Efficiency

The efficiency of an energy sensitive β spectrometer with an ideal antibackscattering system is lower than the efficiency of the same spectrometer without the antibackscattering by a factor equal to the backscattering coefficient. This is due to the fact that no information from events in which the β particles are backscattered is retained or used

in the spectrum analysis.

2. Variation in the Energy Loss of Monoenergetic β Particles in the ΔE Detector

Even for monoenergetic β particles incident on the ΔE detector, the energy loss experienced by the different particles varies greatly as a result of both straggling and the large difference in the path lengths of the β particles in the ΔE detector. The pulse height selection method discriminates against any events in which there had been a large energy loss in the ΔE detector, without distinguishing between single pass or backscattered events. Therefore, there is a reduction in the spectrometer's efficiency for detecting events in which the β particles are not backscattered out of the spectrometer since some of the single pass events are also rejected.

3. Dependence of the Efficiency on the Energy of the β Particles (see Kantele & Passoja 1971 table 1).

The energy dependence of efficiency is caused by two effects: the first is the dependence of the backscattering coefficient of β particles on their energy. Therefore, even for a spectrometer with an ideal system which rejects only events in which backscattering takes place whose rejection is 100% efficient, the efficiency is energy dependent.

The second effect results from the dependence of the shape of spectrum of energy losses of monoenergetic β particles passing through ΔE detector on the primary energy of the β particles (Berger et al. 1969; Seltzer & Berger 1974). Thus the percentage of single pass events with a high energy loss which are inevitably discriminated against by the pulse height slection method is also a function of the incident β particle energy.

4. Inapplicability of the Technique at Low Energies

At energies below 500 keV, the energy loss of β particles per unit path length is strongly dependent on the β particle energy (Evans 1955 p. 609; Knop & Paul 1965 p. 13). Therefore the pulse height selection method for discrimination against backscattered electronS is impractical.

5. The Escape of Backscattered β Particles

Depending on the solid angle subtended by the ΔE detector at the position of the E detector, some of the backscattered β particles can escape from the spectrometer without traversing the ΔE detector a second time, thus reducing the effectiveness of the pulse height selection method for rejecting backscattered β particles (Kantele & Passoja 1971). Also, since for a low Z materials ($Z \leqslant 30$) the angular distribution of backscattered electrons (at saturation) is dependent on the primary energy of the incident β particles (Tabata 1967 and reference 8 therein), the fraction of backscattered β particles escaping detection will be energy dependent as well, resulting in distortions to the shape of the β spectrum.

2.4.4 Gamma Ray Suppression Using Magnetic Fields

The bending of β particle trajectories in magnetic fields has been exploited in many γ ray suppression schemes that are used in conjunction with energy sensitive β detectors. Among energy deposition β spectrometers, semiconductor detectors and particularly silicon spectrometers have been the ones most widely used with magnetic field γ ray suppressors.

The differentiation between γ ray and β ray trajectories as they traverse a magnetic field located between the radioactive source and the energy sensitive detector is the basic property that is used in magnetic γ ray suppression. In most (but not all) cases the β particle trajectories are bent on an arc of a circle (due to the magnetic field) which allows one to interpose a γ ray absorber along the straight line joining the source and the detector in order to shield the β ray detector.

Energy sensitive β ray detectors utilizing a magnetic field for γ ray suppression differ from the hybrid β spectrometers described previously in two main aspects. The first is that unlike hybrid spectrometers, the magnetic field in γ suppressors is not used in the determination of the momentum of the β particles (i.e. no measurement of the magnetic rigidity is performed). The magnetic field serves simply to transport the β particles to the energy deposition β spectrometer where the energy determination takes place.

The second aspect in which magnetic γ ray suppressors differ from hybrid β spectrometers is that the magnetic field is usually held constant

in a suppressor and varied in hybrid spectrometers. This is not always the case (as will be seen later in this section). Since some magnetic transporters have a narrow momentum range at a constant magnetic field value, the field value has to be varied to cover the full momentum range, if a study of a wide energy spectrum is attempted.

Many of the basic ideas used in the design of magnetic γ ray suppresors were taken from concepts that had been developed in conjunction with magnetic β spectrometers. Some of the most common magnetic γ ray suppression methods will be discussed in what follows.

2.4.4a 1. Extended Focal Plane Devices

There are two types of these energy dispersive devices:

1) Sector Magnets

Sector dipole magnets which focus β particles of different energies along an extended focal plane have been used as magnetic γ ray suppressors. A large area energy sensitive β detector (usually a silicon spectrometer) is placed at the focal plane such that it covers a large portion of the focal plane and therefore receives a wide band of electron energies simultaneously.

The use of sector magnets in γ ray suppression offers several advantages (Mladjenovic 1979). One advantage is that both the source and the detector are in a field free region which provides easy access to both of them. A second advantage arises from the fact that positrons and electrons are deflected in different directions so that intense conversion electron lines do not hamper measurements of weak positron activities. Another benefit derived from the use of sector magnets is the ease of selection of a momentum range covering a region of interest through the use of slits or baffles. This allows one to study a specific part of the β spectrum (e.g. the endpoint) without the problems of pile up caused by intense emission of low energy β particles and electrons. Stronger sources and higher counting rates in the region of interest (hence shorter collection times) can therefore be used.

Other advantages associated with the use of sector magnets include excellent γ ray suppresion and small angles of incidence of β particles on the detector surface. Because of the particular geometry of sector

transport magnets, very effective γ ray shielding can be used between the source and the detector without interfering with the β ray transmission of the magnet. The small angles of incidence on the surface of the detector can be accomplished by orienting the detector such that the β particles are incident perpendicularly (or nearly so) on the detector (Mladjenovic 1979). The degree to which this is achievable depends on the orientation of the focal plane with respect to the central ray and the width of the transmitted momentum band. The small angles of incidence of the β particles reduce the probability of backscattering from the detector.

Some of the difficulties encountered with the use of sector magnets as magetic γ ray suppressors are:

1. The limited momentum range that can be covered with sector magnets at a constant magnetic field value ($\Delta p/p$ = 7% in the work of Sakai et al. as quoted in Mladjenovic (1979), 8% in the work of Cambi et al. 1972, and 18% in the work of Fazzini et al. (1983)). The limited momentum range is caused by the physical extension of the focal plane on the one hand and the limited surface area of semiconductor detector on the other (Cambi et al. 1972; Fazzini et al. 1983).

To increase the width of the momentum band ($\Delta p/p$) that can be investigated with sector magnets, one can use either smaller magnets with smaller radii of curvature and therefore smaller dispersions (the radius of curvature is 4 cm in the work of Cambi et al. 1972, it is 14 cm in the work of Sakai et al. as quoted by Mladjenvoic (1979)), or detectors with larger surface areas (Fazzini et al. 1983). The problem with the use of smaller magnets is the reduction in source size and therefore the luminosity of the spectrometer-transporter system (Mladjenovic 1979). The use of larger surface area detectors is limited by the availability of such detectors (the surface areas of the detectors that have been used are: 100 mm in the work of Cambi et al. (1972) and 500 mm^2 in the work of Fazzini et al. 1983) and by the problems of increased sensitivity to γ rays of the larger detectors (Fazzini et al. 1983).

2. Difficulties with the fringing magnetic fields which increase in importance as the width of the gap between the magnet poles is increased. As a result, magnets with smaller gaps have to be used resulting in the low transmission values that are typical for sector magnets ($< 1\%$) (Mladjenovic 1979; Fazzini et al. 1983).

3. Problems of β particles scattering from the walls of the vacuum chamber and from the baffles that are used to define the β particle trajectories (Cambi et al. 1972).
4. The dependence of the focusing properties of the sector magnet on the position of the focus along the focal plane (i.e. on the β particle energy) (Fazzini et al. 1983; see also Armini et al. 1967).
5. Complications in the response function of the energy sensitive β detector resulting from the energy dependence of the position of the entry points of β particles into the detector.

Due to all of these problems, the use of sector magnets in γ ray suppression has been limited to in-beam conversion electron studies (Cambi et al. 1972; Mladjenovic 1979; Fazzini et al. 1983). Sector magnets have also been used in "orange" systems to increase efficiency. In these systems several sectors are arranged symmetrically in the azimuthal direction around an axis with the source placed on the symmetry axis and a separate detector for each sector (Mladjenovic 1979 and references 34, 35 therein).

b) Semicircular Magnets

A semicircular homogeneous field magnet has also been used as an extended focal plane β transporter (Catura 1965). In this case, both the source and the detector are placed in the uniform magnetic field (along the focal plane), and an energy range is selected by placing a baffle in front of the detector.

Like sector magnets, semicircular magnets have the advantages of electron positron separation and good γ ray shielding. Semicircular magnets have the added advantage that the β particles enter the detector perpendicular to its surface and therefore suffer less backscattering. The perpendicular incidence results from the fact that the focal plane of semicircular magnets is perpendicular to the trajectories of the β particles.

Semicircular magnets also suffer from many of the problems encountered with sector magnets including low transmission (0.3% in the work of Catura 1965) and narrow momentum band width ($\Delta p/p$ = 8.8% in the work of Catura 1965). To overcome the drawbacks of a limited momentum range, Catura (1965) used a swept magnetic field to cover the full β spectrum.

2.4.4b "Mini-Orange" Transport Systems

"Mini-Orange" transport systems resemble the high transmission "Orange" (toroidal) type β spectrometers. (For a detailed description of orange β spectrometers see for examples Siegbahn 1965 pp. 119-139; Mladjenovic 1976 Chap. 11; Mladjenovic 1979). In both cases, a toroidal magnetic field is generated by several sector magnets that are arranged in an azimuthally symmetric configuration around an axis on which both the source and the detector are positioned. A lead γ ray absorber is placed along the symmetry axis between the source and the β detector to shield the detector.

In the mini-orange systems, small permanent magnets are used, instead of electromagnets, to generate the magnetic field. The toroidal magnetic field produced by these permanent magnets is no longer used to resolve electrons of different energies. Instead it is used simply to transport electrons from a wide energy range by causing electrons emitted from the radioactive β source to converge onto the detector in a fashion somewhat analogous to the action of an optical lens (Van Klinken & Wisshak 1972, Van Klinken et al. 1975). The toroidal magnetic field also acts to separate the positrons from the electrons by bending the trajectories of particles of one charge sign toward the detector and those of the opposite charge away from the detector.

Because of the focusing action of the magnetic field of mini-orange transporters, the number of β particles incident on the detector is considerably larger than that determined by the geometrical solid angle subtended by the detector at the source (see Ishii 1975 Fig. 6 for example). Therefore the source and the detector can be separated by a considerable distance without an appreciable loss in transmission. At the same time the small geometrical solid angle subtended by the detector at the source and the attenuating effect of the γ ray absorber result in a large reduction in the flux of γ rays incident on the detector (Van Klinken & Wisshak 1972). However, due to the dependence of electron transmission and the γ ray attenuation on the energy of the electrons and the γ rays respectively, the enhancement in the ratio of electrons to the γ rays incident on the detector (the γ suppression ratio) is energy dependent in mini-orange systems. Typical values of the γ ray suppression

ratio vary between 300 and 25 for energies betweem 0.5 and 1 MeV (Ishii 1975).

Different shapes and types of permanent magnets have been used in the construction of mini-orange systems. The most popular type of permanent magnets used have been $SmCo_5$ because of its attractive magnetic characteristics (high remnance, near constant magnetization for large demagnetizing fields, and its availability in the form of small, thin and strong permanent magnets (see Van Klinken et al. 1975 Fig. 10: Ishii 1975 Fig. 2)). The small size, low price and simplicity of mini-orange systems have made them quite popular (Mladjenovic 1979).

Problems Encountered with Mini-Orange Transport Systems:

Despite their attractive features, there are some major problems encountered with the use of mini-orange transport systems in β spectroscopy. Some of these problems are:

1. Low Transmission

Typical values for the maximum transmission of mini-orange transport systems are usually less than 10% (Van Klinken et al. 1975; Neumann et al. 1979) and can even be less than 1% (Van Klinken & Wisshak 1972; Ishii 1975).

2. Narrow Momentum Band and Strong Dependence of the Transmission on the β Particle Energy

The transmission of mini-orange transport systems is quite strongly dependent on the energy of the incident β particles. The exact dependence of transsmission on energy is determined by several factors including the geometry of the set-up (the distances of the source and the detector from the magnets, dimensions of the detectors and magnets, shape of the magnets, etc.) and the strength of the magnetic field (Van Klinken & Wisshak 1972, Van Klinken et al. 1975). In general, the transmission versus energy curve is asymmetric with a sharp low energy cutoff. It is also characterized by a broad maximum with a full width at half maximum (fwhm) of a few hundred keV (Van Klinken & Wisshak 1972 Figs. 4, 5; Van Klinken et al. 1975 Figs. 2, 7, 8, 14; Van Klinken et al. 1978 Figs. 4,5; Neumann et al. 1979 Figs. 2, 4).

Increasing the momentum range of the transmitted electrons (i.e. the width of the transmission curve) requires the use of magnets of

special shapes, the use of fewer magnets (so that the defocusing influence of non toroidal field components becomes more noticeable) or the use of a non-symmetric configuration with varying gap widths between the magnets. In all of these cases, the shape of the magnetic field becomes more complicated and harder to calculate. Moreover, the peak of the transmission curve is shifted to lower energies (Van Klinken & Wisshak 1972; Van Klinken et al. 1975, 1978).

3. Low Transmission at High Energies

As a result of the particular shape of the transmission curves of mini-orange systems, the transmission at electron energies above ~ 2 MeV is quite small. Therefore such systems are not very suitable for the study of energetic β particles.

The peak of the transmission curve can be shifted to a limited extent to higher energies. This shift to higher energies can usually be accomplished by increasing the source and detector distances from the magnets or by increasing the strength of the magnetic field through the use of more magnetic material (increasing the number of magnets or their thickness). These steps, however, result in a significant reduction in the overall transmission and in a decrease in the width of the transmission curve (Van Klinken & Wisshak 1972; Van Klinken et al. 1975; Ishii 1975; Neumann et al. 1979).

4. Problems Caused by the Use of Permanent Magnets.

a) The dependence of the magnetic properties of the permanent magnets on their history and on the ambient temperature.

b) The difficulty involved in calculating the exact shape and strength of the magnetic field generated by the permanent magnets. This difficulty is brought about by the complicated fashion in which the permanent magnets are magnetized. Therefore when a calculation of the transmission curve of a mini-orange system is attempted, it is necessary to use a crude approximation of the shape of the magnetic field (e.g. purely toroidal fields) (Van Klinken et al. 1975; Ishii 1975). Considerable discrepencies between calculated and measured transmission curves have been observed as a result of the rough approximations used in calculating the magnetic fields (Van Klinken & Wisshak 1972; Neumann et al. 1979).

5. Gammy Ray Related Background

The γ ray background is caused mainly by two effects. The first is the penetration of high energy γ rays through the central absorber. The second effect is the production of secondary electrons through the interaction of γ rays with the magnets ($SmCo_5$ has a high density and a high effective Z) or other parts of the transport system that lie between the source and the detector (Van Klinken et al. 1978; Neumann et al. 1979).

6. Beta Particle Scattering from the Magnet Surfaces

The large surface areas offered by the multiple magnets that are used in a mini-orange system result in a large probability for the β particles to scatter from these surfaces and reach the detector after their energies have been degraded (Van Klinken et al. 1975).

7. Trochoidal Orbits

Electrons that reach the detector after executing multiple loop in the magnetic field (trochoidal orbits) cause irregularities and fluctuations in the transmission curve. Such irregularities are quite hard to detect (Van Klinken et al. 1975).

8. Large Angles of Incidence on the Detector

As a result of the large angles of incidence of β particles on the detector in a mini-orange system, the probability for β particle backscattering is quite large (Van Klinken & Wisshak 1972; Van Klinken et al. 1975). Special detectors with unconventional shapes (e.g. conical or cylinderical sensitive surface) have been propossed and used to reduce backscattering (Van Klinken et al. 1975, 1978).

As a result of all of these difficulties that are experienced by mini-orange transport systems, the use of such systems in the field of β spectroscopy has not been popular. Beta spectra measurements with mini-orange systems have been undertaken mostly to determine the transmission curves of mini-orange spectrometers (Van Klinken & Wisshak 1972; Van Klinken et al. 1975.

2.4.4c Archromatic Magnetic Transport Systems

There are four types of these non dispersive magnetic transport systems.

a) Triple Focusing Systems

Triple focusing transport systmes are generally constructed from

flat, uniform field magnets. The deflection angle of a beam of electrons passing through such a system is greater than 180°. The action of the magnet results in triple focusing: double-focusing in space (axial and radial directions) and momentum focusing at the location of the energy sensitive detector. Thus unlike the case of extended focal plane devices, a wide range of energies can be accumulated with a small surface area detector.

Triple focusing systems usually have an energy dispersive intermediate focus where the width of the momentum band can be set with a diaphragm system (Ejiri et al. 1976; Mladjenovic 1979). Triple focusing systems with reasonably wide momentum bands have been constructed ($\Delta p/p_{av}$ = 10%, 40%, 57-80%, and 140% in the works of Blonnigen et al. 1980; Ejiri et al. 1976; Nagai et al. 1982; and Komma 1978 respectively).

Some of the other advantages of triple focusing spectrometers are:

- Large distances between the source and the detector which allow excellent γ ray shielding of the detector (Blonnigen et al. 1980; Wollnik et al. 1980).
- Electron-positron separation as a result of their different deflection directions.
- The possibility of orienting the detector such that the electrons have perpendicular incidence onto the detector surface thus reducing the percentage of backscattered electrons (Mladjenovic 1979; Nagai et al. 1982).
- Sharp time signals generated by the electrons incident on the detector as a result of their well defined trajectories and the small differences in path length between particles of different energies. Moreover, the time signals generated by the electrons may be well separated from those due to γ rays originating from the source (as a result of differences in the time of flight). These excellent timing characteristics of triple focusing systems are quite important in coincidence measurements (Ejiri et al. 1978).
- Elimination of intense but undesired parts of the spectrum through the selection of the transmitted momentum band (Komma 1978). This can be quite useful in eliminating the effects of pile-up in studies of endpoint energies of β spectra (Blonnigen et al, 1980; Wollnik et al. 1980).

The major difficulties encountered with triple focusing systems are:

- The requirement of a triple focus of small physical extension imposes

stringent restrictions and tolerances on the design and construction of the magnets. The effects of the fringing field of the magnet are especially important in this context (Ejiri et al. 1976; Komma 1978; Blonnigen et al. 1980; Wollnik et al. 1980; Nagai et al. 1982).

- The restricted momentum band nature of triple focusing spectrometers renders them incapable of covering the full energy range of a high endpoint β spectrum at a fixed magnetic field value (for a spectrum with a 6 MeV endpoint, the low energy cutoff is about 1 MeV even for the widest band system in use $\Delta p/p_{av} = 140\%$). This quality makes triple focusing systems unattractive for shape factor measurements.
- Their small solid angle of acceptance. This is perhaps the most serious drawback of triple focusing systems. Typical values for transmission are less than 0.5% resulting in very low efficiences.

2) Boomerang Systems

In these zero dispersion systems, both the radioactiave source and the energy sensitive detector are placed in a homogeneous magnetic field. The source and the detector are positioned one above the other (in the case of a vertical magnetic field), along a straight line parallel to the direction of the magnetic field such that electrons emitted from the source are focused at the detector's location after a deflection of 360° (hence the name "boomerang" systems) (Elbek 1967; Paris & Treherne 1969; Plochocki et al. 1971).

The operation of the boomerang transport systems is based on a characteristic property of the uniform magnetic field. The trajectory of a charged particle, emitted in a plane perpendicular to the uniform magnetic field, describes a circle that passes through the point of emission and is tangential to the original direction of emission. Therefore, β particles emitted in different directions in a plane perpendicular to the magnetic field of the boomerang system, are focused back to the source position after one complete revolution irrespective of their energy or angle of emission in the plane (Mladjenovic 1979). By accepting β particles with a small component of velocity parallel to the magnetic field direction, the non dispersive focus at 360° is extended above the position of the radioactive source. If an energy sensitive detector is placed at this location, then the full energy range of the

focused β particles can be studies simultaneously. Because of the source-detector separation, a γ ray absorber can be inserted between the source and the detector to shield the detecctor (Elbeck 1967). Another attractive feature of boomerang systems is that electron-positron differentiation can be easily achieved by accepting only particles that have the correct sense of rotation in the magnetic field (Paris & Treherne 1969; Plochocki et al. 1971).

Some of the difficulties encountered with boomerang systems are:

1. Low Effective Transmission

Boomerang systems provide momentum focusing and spatial focusing in the radial direction only (no axial focusing at all) and therefore have inherently low transmission in comparison to triple focusing devices. Because of the lack of axial focusing, the non dispersive image (formed at 360°) has a large physical extension in the axial direction and can not be fully contained within the surface area of the detector. As a result, the effective transmission of the spectrometer is quite small (less than 0.2% in the work of Plochocki et al. 1971).

In order to increase the transmission of a boomerang system, Elbek (1967) proposed the use of a detector with a cylinderical sensitive surface so that β particles emitted in any radial direction can be detected. This, however, is achieved only at the expense of the loss of the ability to distinguish between positrons and electrons. Furthermore, even with cylinderical detectors, the transmission of boomerang systems is still expected to be quite small (Elbek 1967).

Using flat semiconductor detectors with larger surface areas to increase the effective transmission results in a derioration in resolution.

2. Difficulties with Momentum Band Selection.

As a result of the wide angles of acceptancce in the radial direction, the intermediate (energy dispersive) focus at 180° is no longer well defined. Hence only a rough energy selection through the use of baffles is possible at this location.

3. Inadequate γ Ray Shielding

The small source-detector separation (35 mm and 15 mm in the works of Paris & Treherne (1969) and Plochocki et al. (1971) respectively) does not allow for adequate absorber thickness and therefore the γ ray suppression is not very effective (Plochocki et al. 1971).

4. Large Angles of Acceptance and Incidence

The large angles of acceptance in the radial direction (up to 90° if a flat detector is used and 180° with the use of a cylindrical detector) are reproduced as angles of incidence on the detectors surface. The large angles of acceptance aggrevate the problems of energy loss and scattering in the source and the source backing. The large angles of incidence result in an increase in backscattering from the detector and a deterioration in resolution as a result of the increase in energy loss in the detector's entrance window.

5. Dependence of Transmission on Energy

As a result of the energy dependence of the effective axial solid angle of acceptance (Paris & Treherne 1969), the transmission of boomerang systems is strongly dependent on the energy of the transmitted β particles (see Plochoki et al. 1971 Fig. 1B).

6. Dependence of Time of Flight on Energy

For a charged particle moving in a uniform magnet field, the time taken to complete one revolution is given by (Jackson 1975 p. 581)

$$T = \frac{2\pi E}{ecB}$$

where

T = The time required to complete one revolution

E = The total energy of the charged particle (kinetic + rest mass)

e = The charge of the particle

B = The magnetic field value

c = The speed of light

Since all of the β particles execute only one revolution in the homogeneous magnetic field of the boomerang system, their flight times are independent of the radial or axial angles of emission. However, as is evident from the equation above, the time of flight of the β particles is dependent on the energy of the β particles. This time dependence can cause problems in timing and coincidence experiments especially when boomerang transport systems with weak magnetic fields are used.

3) Trochoidal Guides

The basic principles of the trochoidal motion of electrons in magnetic fields with azimuthal symmetry and high field gradients ($B \propto r^{-n}$,

$n \geq 1$) have been quite thoroughly studied and applied to the design of electron-positron separators, pair spectrometers, and a few magnetic β ray spectrometers (Malmfors 1958; Malmfors & Nilsson 1958; Siegbahn 1965 pp. 139-=145; Mladjenovic 1971 pp. 58-64; Mladjenovic 1972 pp. 596-602; Mladjenovic 1976 pp. 201-220, Mladjenovic 1979).

The high transsmission and low dispersion properties of trochoidal β spectrometers made them quite attractive for use as magnetic transporters in conjunction with energy sensitive detectors (trochoidal guides).

Trochoidal transport systems are achromatic steering devices in which the electrons are guided in the fringing field of a cylindrically symmetric magnet. These electrons travel along the arc of a circle from the source to the detector following trajectories consisting of multiple loops with a precessing center of gyration (Watson et al. 1966, 1967; Allan 1970; Gono et al. 1975; Mladjenovic 1979).

The motion of the electrons in the high gradient field is a superposition of a trochoidal motion in the median plane (the magnetic symmetry plane between the pole faces the magnet) and a vertical oscillation about this plane (Malmfors 1958). In other words, the electrons travelling in the fringing field region of the radially decreasing magnetic field experience two types of drift motion: an azimuthal drif along the circumference of the magnet and a vertical drift consisting of a spiralling motion about the magnetic field lines. The field lines are highly convergent in the fringing field region near the magnet's pole tips. Therefore, depending on their axial angles of emission, some of the electrons reaching this region are reflected back to the median plane because of the magnetic mirror effects (Watson et al. 1967). The magnetic mirror effect thus causes a vertical oscillation about the median plane and results in an effective axial focusing at 1/2 period of the vertical oscillation (Watson et al. 1966).

In the radial direction, the acceptance solid angles is 180° (i.e. any electron emitted in the median plane is accepted irrespective of its angle of emission in the plane) (Watson et al. 1966). Therefore the transmission of trochoidal guides is usually quite high and can ideally reach 30% or higher (see Watson et al. 1967; Allan 1970 Figs. 4-5; Gono et al. 1975).

Some of the other attractive features of trochoidal guides include:
- An energy independent transmission and a broad momentum range (Watson et al. 1967; Allan 1970; Gono et al. 1975). Moreover, the transmission is independent of the angular separation between the source and the detector (Allan 1970).
- Electron-positron separation. The direction of the azimuthal precession of the particles in the magnetic field depends on their electric charge, therefore only particles of one charge sign are transported to the detector (Allan 1970; Gono et al. 1975).
- Effective γ ray shielding. As mentioned before, in trochoidal guides, β particles are steered around the arc of a circle from the source to the detector. And since the transmission is independent of the source-detector angular separation, very effectiave γ ray shielding of the detector can be achieved by providing a large angular separation between the source and the detector (usually > 90°) and placing a γ ray absorber along the straight line extending between the source and the detector.

Some of the problems encountered with trochoidal guides are:

1. The Dependence of Transmission on the Dimensions of the Magnet.

Unlike other types of magnetic β spectrometers, trochoidal orbit spectrometers have transmissions that are dependent on the phyisical dimensions of the spectrometer (Malmfors 1958). Similarly, the transmission of trochoidal guides is also dependent on the size of the magnet used, specifically its radius of curvature and pole gap width (Watson et al. 1967 eqn. 8; Gono et al. 1975 eqn. 9).

2. The Dependence of the Image Width on Energy.

The width of the image produced by the trochoidal guide for an electron point source is approximately equal to twice the radius of curvature of the electrons in the magnetic field of the guide (Watson et al. 1967). The width of the image is therefore dependent on the magnetic rigidity of the β particles and hence their energy. As a result, if high energy β particles are to be studied with trochoidal transporters, one has to use either very high magnetic fields or large surface area detectors (the magnetic rigidity of a 10 MeV electron is about 35000 guass cm).

Distortions in the shape of the magnetic field due to saturation effects in the magnet poles at high magnetic fields limit the strength of the magnetic fields that can be employed in trochoidal guides. On the

other hand the use of large area semiconductor detectors is limited by their availability and by the deterioration in resolution resulting from their large capacitances.

The use of a detector whose width is less than the width of the image at the highest electron energy under study results in an effective transmission which is energy dependent and which has a sharp drop at high energies (Allan 1970 Fig. 4; Gono et al. 1975 Fig. 5).

3. The Dependence of Time of Flight on β Particle Energy

The time of flight of β particles from the source to the detector in trochoidal systems is independent of their initial direction of emission. However, the transit time is strongly dependent on the energy of the β particles (Malmfors 1958; Watson et al. 1967 eqn. 4, Table 1; Allan 1970 Fig. 6; Gono et al. 1975). In fact, trochoidal β spectrometers were first proposed as time of flight spectrometers (Malmfors 1958; Malmfors & Nilsson 1958). Variations in the time of flightof β particles can cause problems in timing experiments and especially coincidence circuits (Allan 1970; Gono et al. 1975).

4. Large Angles of Incidence on the Detector.

Since all angles of emission in the median plane are acccepted, the angles of incidence on the detector will vary greatly. Some of the electrons will impinge on the detector at very shallow angles resulting in an increase in backscattering (Gono et al. 1975).

5. The Increase in the Effective Thickness of Dead Layers.

Because of the trochoidal motion that the β particles execute in the magnetic field, their paths in any dead layers that they traverse are quite curved. This results in an increase in the effective thickness of the dead layers as seen by the β particles passing through them (Allan 1970). Moreover, for a low energy electron, the radius of curvature of the trochoidal orbit can be larger than the drift displacement along the radial path after one revolution. This causes low energy electrons to traverse a dead layer several times losing energy and scattering every time they re-enter the dead layer (Watson et al. 1966; Gono et al. 1975).

The "magnification" of the thickness of the dead layers that results from the two effects described above is strongly dependent on the energy of the β particles. It has been observed to cause a deterioration in resolution, energy shifts, low energy tails in the spectra of

monoenergetic electron lines, a reduction in efficiency and an energy dependent transmission (Watson et al. 1966, 1967; Allan 1970; Gono et al. 1975).

6. Problems with the Radioactive Sources.

Since trochoidal transport system accept electrons emitted in the backward as well as the forward direction, some of the accepted electrons will traverse the source and the backing at least once. Furthermore, some of the low energy electrons traverse the source and the backing several times (as explained above). The source backing therefore represents a dead layer through which some of the electrons must pass. In fact, the attenuation of low energy electrons (as a result of their multiple passes through the source backing) was used to limit the transmission of the trochoidal guide at low energies (Gono et al. 1975). In addition, unless extreme care is exercised in the design and positioning of the source holder, some of the electrons (especially at low energies) can collide with it and undergo large energy losses and scattering (Watson et al. 1967; Allan 1970).

7. Coincident Summing

As a result of the large solid angles of acceptance of trochoidal guides, coincident summing of conversion electrons and β particles can become a serious problem (Allan 1970).

4) Solenoidal Tranposrt Systems

a) Modifid Lenses

Lens type β spectrometers have been modified for use as magnetic transport systems and operated in conjunction with energy sensitive detectors (Picone et al. 1972; Avignone et al. 1973). The shape of the magnetic field is maintained but the momentum selection slit is either removed completely (Picone et al. 1972) or replaced with a wide pass baffle (Avignone et al. 1973). The spectrometer can then be operated in a high transmission, low resolution (wide band) mode relying on the energy dispersive detector to analyze the β particle energies. The γ ray absorbers that are usually placed along the axis of lens β spectrometers are retained to help in the suppression of γ rays.

The transmission of the modified lenses is typically a few percent.

The momentum band, transported at a constant magnetic field value, is usually quite narrow ($\Delta E/E$ = 14% in the work of Picone et al. (1972)). Therefore, the magnetic field value has to be swept in order to be able to cover the full energy spectrum under study. This in turn results in problems of normalization of the different segments of the spectrum. Nevertheless, the narrow band nature of the modified lenses can be quite useful in reducing the effects of pulse pile- up caused by the intense emission of low energy electrons.

The problems of modified lens transporters are quite similar to those of hybrid spectrometers. In fact the only difference between these spectrometers and the hybrid spectrometers described previously is that in the modified lens type, the determination of the β particle energy is performed exclusively in the energy sensitive detector with no reliance on the measurement of the magnetic rigidity.

b) Axial Magnetic Guides

Burginyon and Greenberg (1966) were the first to suggest the use of strong, cylindrically symmetric magnetic field as a high transmission, broad range electron transporter to guide electrons from a radioactive source to an energy sensitive detector. In that work, both the radioactive source and the detector were placed in a uniform magnetic field which acts as an electron guide maintaining a high transmission for electrons but at the same time allowing the source and detector to be far from each other in order to reduce the solid angle for γ ray detection. In the particular set-up used by Burginyon and Greenberg, the magnetic field was generated between the poles of a cylindrically symmetric, iron-core magnet. The detector was oriented with its sensitive surface parallel to the direction of the magnetic field and a small γ ray shield was placed between the source and the detector. However, that specific source-shield-detector geometry resulted in a strong dependence of transmission on the energy of the β particles including oscillations in the transmission as a function of energy at high β particle energies.

Following the pioneering cited above, the use of axial magnetic fields as electron guides became quite popular. In most cases, the strong magnetic field is generated by a long solenoid and the detector is oriented with its sensitive surface perpendicular to the magnetic field

direction (Burson 1968; Goudsmit 1969; Michaelis et al. 1969; Kotajima & Beringer 1970; Waldschmidt & Osterman 1970; Morozov and Pelekov 1972; Klank & Ristinen 1972; Morozov 1973; Konijn et al. 1975; Lindbald & Linden 1975; Hamilton 1975; Fromm et al. 1975; Popeko et al. 1976; Moore et al. 1976; Hung et al. 1976; Maté et al. 1978; Backe et al. 1978; Hagemann et al. 1979; Arvay et al. 1980; Ercan et al. 1981; Henry et al. 1982; Guttormsen et al. 1983). Solenoidal magnetic transporters have also been used in conjunction with 4π semiconductor β spectrometers (Shera et al. 1967; Andersen 1968; Andersen & Christensen 1968; McMillan 1970) (see the section on 4π silicon spectrometers for a detailed description). Axial magnetic guides have been used for in-beam measurements, using neutron beams from reactors (Burson 1968; Goudsmit 1969; Michaelis et al. 1969; Popeko et al. 1976) and proton or heavy ion beams from accelerators (Burginyon & Greenberg 1966; Kotajima & Beringer 1970; Klank & Ristinen 1972; Konijn et al. 1975; Lindbald & Linden 1975; Maté et al. 1978; Backe et al. 1978; Arvay et al. 1980; Ercan et al. 1981; Henry et al. 1982; Guttormsen et al. 1983).

Axial magnetic guides used in conjunction with semicondcutor β spectrometers have resolution, transmission, and luminosity values that are comparable to the high transmission, large orange type magnetic β spectrometers (Andersen & Christensen 1968; Burson 1968; Hamilton 1975). However, the multichannel nature of axial magnetic guides results in much higher figures of merit than those for magnetic spectrometers (von Egidy 1969).

The spectrometer system on which this thesis reports is composed of an axial magnetic transport system used in conjunction with an energy sensitive Ge(HP) β detector.

Beta particles emitted from a radioactive source placed on the axis of the solenoid follow helical trajectories as they spiral around the magnetic field lines of the solenoid. An energy dispersive detector placed on the solenoid axis intercepts these trajectories, detects the β particles and analyzes their energy. The radii of the helical orbits of the β particles are determined by the energy of the β particles (their magnetic rigidity), their angle of emission with respect to the solenoid axis, and the strength and geometry of the magnetic field. In order to

achieve an energy independent transmission, the radius of the β detector should be larger than the maximum diameter of the helical orbits of the most energetic β particles under study. Therefore a strong magnetic field is needed to confine the energetic β particles to orbits small enough in diameter that a detector with a resonable size surface area can be used to the study β spectra with high endpoint energies. Both normal and superconducting solenoids have been used to furnish the required magnetic fields. Typical field strengths achieved are several kiloguass for normal magnets and several tens of kiloguass (several tesla) for superconducting magnets.

The widespread use of transport solenoids can be attributed to their many attractive features some of which are:

1. High Transmisison

Very high transmission values for β particles can be achieved with transport solenoids. Typical transmission values for a single solenoid vary from 4% to 40% (Goudsmit 1969; Kotajima & Beringer 1970; Morozov & Pelekhov 1972; Konijn et al. 1975; Popeko et al. 1976; Moore et al. 1976; Hagemann et al. 1979) and values as high as 50% can be easily achieved (Morozov 1973; Andersen 1974). Transmission values exceeding 50% can be obtained with two solenoidal transport systems (magnet + detector) placed on either side of the source (Maté et al. 1978; Arvay et al. 1980). A 100% transmission (i.e. 4π detection) can be realized with a single transport system with two detectors on either side of the radioactive source (see section on 4π silicon spectrometers for full details).

The high efficiency of solenoidal transport systems makes them ideal instruments for coincidence measurements. They have been frequently used in electron-gamma coincidence experiments (Burson 1968; Goudsmit 1969; Klank & Ristinen 1972; Lindbald & Linden 1975; Konijn et al. 1975; Popeko et al. 1976; Backe et al. 1978; Arvay et al. 1983); Henry et al. 1982; Guttormsen et al. 1983) and electron-electron coincidence experiments (Maté et al. 1978; Array et al. 1980; Guttormsen et al. 1983). In the latter case, the source is sandwiched between two transport systems.

2. Broad Range and Energy Independent Transmission

If a combination of a strong magnetic field and a large surface area detector are used, then the transmission of a solenoidal transport system is independent of the energy of the β particles (see Arvay et al.

1980 Fig. 10). The range of transmitted β particle energies extendss from zero up to a maximum value determined by the radius of the detector and the strength and geometry of the magnetic field. Since magnetic fields of 5 tesla can be easily achieved with modern superconducting solenoids, and Ge(HP) detectors with surface areas of 2000 mm^2 (2.5 cm radius) are commercially available, β particles of energies up to about 18 MeV can be studies with an axial guide system.

3. Good γ Ray Suppression

The large distance separating the radioactive source from the detector in a solenoidal transport system, ranging form 10 cm to 50 cm for the various existing sytems, results in a very small geometrical solid angle for γ ray detection. The γ ray suppression ratio (the ratio of the solid angle of acceptance for β particles to the solid angle for γ ray detection) varies from several hundred to 1000 or more (Morozov & Pelekhov 1972, Maté et al. 1978, Arvay et al. 1980). The use of the large surface area detectors that are needed to study high energy β decays would of course result in an increase in the solid angle for γ ray detection.

Secondary electrons that are produced by γ rays incident on the walls of the spectrometer chamber in the region between the source and the detector have a small probability of reaching the detector and contributing to the background. The magnetic field of the solenoid forces any electron emitted from the chamber walls to follow a helical trajectory which intercepts the chamber wall after one revolution. There the electron scatters again undergoing some energy loss and follows a tighter orbit before its next collision with the wall. This process is repeated until the electron loses all of its energy and is stopped in the chamber wall. Because of the large source-detector distance, the probability of the Compton electron being intercepted by the detecctor before it is stopped in the wall is quite small (Burginyon & Greenberg 1966; Klank & Ristinen 1972; Lindbald & Linden 1975; Hung et al. 1976.

Problems encountered with axial guide systems

Like any other β spectroscopy system, axial magnetic guides suffer from certain problems and limitations some of which are discussed below (see also Mladjenovic 1979).

1. Large Angles of Acceptance.

With a uniform magnetic field of sufficient strength, the transmission of an axial transport system is as high as 50%. In this case, all of the β particles emitted in the direction of the detector at any angle (from 0° to 90°) with respect to the solenoid axis are intercepted by the detector. Such large angles of acceptance can cause problems since they result in an increase in scattering and energy losses in the source and the detector (Lindbald & Linden 1975; Popeko et al. 1976). The large angles of acceptance can also cause problems with coincident summing of β particles and conversion electrons (Michaelis et al. 1969; Konijn et al. 1975).

In order to overcome the problem of large acceptance angles, the particular profile of the magnetic field of a solenoid can be used to limit the angles of acceptance. To achieve this, the radioactive source is placed at a location along the axis of the solenoid where the magnetic field is less than its maximum value, with the maximum magnetic field location lying somewhere between the source and the detector. In this configuration, the magnetic mirror effect, which is produced by the variation of the magnetic field strength along the axis of the solenoid, causes electrons that are emitted at large angles with respect to the solenoid axis, to be reflected back or botteled out of the solenoid. The maximum angle of acceptance then is given by:

$$\theta = \sin^{-1}\left(\frac{B_z}{B_o}\right)^{1/2} \qquad 2.2$$

where

θ = The maximum angle of acceptance

B_z = The magnetic field strength at the location of the source

B_o = The maximum value of the magnetic field along the solenoid axis (Michaelis et al. 1969; Goudsmit 1969; Kotajima & Beringer 1970; Morozov & Pelekhov 1972; Klank & Ristinen 1972; Lindbald & Linden 1975; Guttormsen et al. 1983). To first order, the angles of acceptance are also energy independent.

The use of the magnetic mirror effect to limit the solid angle of acceptance is quite an elegant solution, especially since it avoids the use of baffles from which β particles can scatter.

2. Large Angles of Incidence

The large angles of incidence of β particles on the surface of the energy sensitive detector in axial guide systems represent a problem for two reasons. The first is the deterioration in resolution resulting from the increase in the effective thickness of the detector's entrance window as seen by the β particles which are incident at large angles. The second and more important effect is the increase in the backscattering of β particles from the detector as a result of the increase in the angles of incidence.

In analogy to the large angles of acceptance, the problem of large angles of incidence can be solved by placing the detector in a lower magnetic field region along the axis of the solenoid. The maximum angle of incidence in this case is also given by equation (2.2) where B_z now is the magnetic field at the detector's location (Klank & Ristinen 1972; Lindbald & Linden 1975; Popeko et al. 1976; Guttormsen et al. 1983).

If the location of the maximum magnetic field value lies somewhere between the source and the detector, then the positioning of the detector in a low field region has the added advantage that some of the β particles that are backscattered from the surface of the detector will be reflected back to the detector. This is again the result of the magnetic mirror effect that is experienced by the backscattered particles in travelling from the low magnetic field at the location of the detector to the location of the maximum field value. The re-entry of these reflected β particles into the detector increases the probability that they will deposit their full energy in the detector (Guttormsen et al. 1983; Hetherington 1984).

However, the lower field value at the detector's position results in an increase in the radii of the orbits of the β particles. The radius of an electron's orbit is given by (Jackson 1975 pp. 588-593; Guttormsen et al. 1983)

$$\frac{r}{r_o} = \left(\frac{B_o}{B_z}\right)^{1/2}$$

where

r = The radius of the orbit of the β particle at the location of the detector.

r_o = The radius of the orbit of the β particle at the location of the

magnetic field maximum

B_o = The maximum value of the magnetic field

B_z = The value of the magnetic field at the detector's location.

Therefore, detectors with larger surface area have to be used if they are to be located in a lower field region.

3. Problems with Dead Layers.

The helical trajectories of β particles in the magnetic field of a solenoid force them to follow curved paths in any dead layers intervening between the source and the detector. The curved paths combined with the large angles of acceptance and incidence result in an increase in the path lengths of β particles in the dead layers and therefore in an increase in the energy loss and scattering experienced by the β particles. consequently, it is quite advantageous to have the source and the detector in the same vacuum chamber with no entrance windows separating them from each other. Such an arrangement, however, can result in difficulties when cooled detectors are used and when the source introduction is to be performed rapidly and frequently.

5. Difficulties Associated with Electron-Positron Differentiation

Since the only difference between the trajectories of electrons and positrons is the sense of rotation about the magnetic field lines, particles of either charge will be transported by the axial guides. This lack differentiation between electrons and positrons can cause problems when nuclei with weak positron activities and intense conversion electron emission are under study.

Helical baffles that distinguish between the two charge states have been used to overcome this problem. Their use, however, results in several drawbacks. The helical baffles transmit particles of the right charge only in a narrow momentum band. Therefore in order to study a wide energy range, the magnetic field of the transporter has to be varied over a wide range. This in turn introduces the problems of normalization of the different segments of the spectrum and the problems of variations in the transmission of the baffle with the magnetic field strength.

- The use of the charge selection baffle reduces the overall transmission of the guide system quite considerably (Konijn et al. 1975; Backe et al. 1978).

- The helical baffles provide large surface areas from which the β

particles can scatter.

5. Pile-Up Problems

The high transmission - broad band nature of axial guide systems and the extension of the range of transmitted β particles down to zero energy, can result in high counting rates in the detector and severe spectral distortions due to pulse pile-up. This is particularly problematic in cases where there is an intensive emission of low energy electrons (Auger electrons or intense low energy β particles).

The flux of low energy electrons incident on the detector can be significantly reduced by placing a small diameter circular baffle on the solenoid axis between the source and the detector. Such a baffle, however, would also stop some of the high energy β particles and result in oscillations in the value of transmission with changes in the β particle energies. A sweeping magnetic field component (with all the associated problems) has to be introduced to smooth these oscillations. In addition to the overall transmission at high energies is reduced considerably by the introduction of the baffle (Kotajima & Beringer 1970; Klank & Ristinen 1972; Konijn et al. 1975; Lindbald & Linden 1975; Backe et al. 1978; Arvay et al. 1980). Another important drawback of using a small diameter baffle on the solenoid axis is that the baffle intercepts most of the β particles with small acceptance angles while allowing particles with large angles of acceptance to pass through (Klank & Ristinen 1972). As a result the fraction of β particles that backscatter from the detector is increased.

Axial guides can also be operated in a long lens mode such that they transmit only a well defined momentum band. The narrow band transmission can be achieved by incorporating a set of momentum selection baffles in the transport system. Operating the solenoid as a long lens, however, reduces the overall transmission of the system and requires that the magnetic field be swept in order to cover a wide momentum range (Backe et al. 1978; Ercan et al. 1981; Henry et al. 1982).

6. Timing Problems

Beta particles travelling between the source and the detector in a solenoidal transport system follow helical trajectories that can be of considerable length. Moreover, the lengths of these trajectories vary considerably even for β particles of the same energy. The flight paths are longest for particles emitted at the maximum acceptance angle and

shortest for particles emitted along the axis of the solenoid. As a result, the time of flight between the source and the detector is quite long and variable depending on the length of the specific trajectory, consequently no sharp time signal is produced (Michaelis et al. 1969).

The long time of flight and its variation with energy can cause problems in 4π systems using axial guides (see section on 4π silicon spectrometers and Shera et al. 1967). It can also be a problem in measurements of short nuclear lifetimes and coincidence experiments (Konijn et al. 1975, Lindskog & Svensson 1976; Kantele et al. 1982).

7. Complications in the Determination of the Response Function of the β Detector

The dependence of the points of entry of β particles into the detector on their energy, and the large angles of incidence complicate the calculations of the response function of the detector (using Mote Carlo techniques for example).

CHAPTER 3

THE SUPERCONDUCTING MAGNET SYSTEM:

THE SOLENOID, THE CRYOSTAT, AND THE SUPPORT STRUCTURES

3.1 Design Aims

As was mentioned in the first chapter, the present spectrometer design is based on an idea that has been tried and proven in a previous superconducting solenoid spectrometer which was constructed and used at this lab (Moore et al. 1976). The main motivations behind the design of the present spectrometer were: resolving the problems encountered with the former, enhancing the capabilities of the whole system further and improving the mobility, flexibility and adaptability of the spectrometer in general.

The former spectrometer employed a 13.6 cm long vertical solenoid with a usable bore of 3.67 cm diameter (Fig 3.1). The maximum operating magnetic field produced by the solenoid was 4.3 tesla at 120 ampere (Rehfield 1977). The cryostat design was a conventional one using liquid nitrogen cooled radiation shields. Both the radioactive source and the detector were contained within the cold (liquid helium temperature) bore of the solenoid. The detector was maintained at liquid nitrogen temperature by mounting it on the end of a cold finger attached to the liquid nitrogen reservoir. The enhancement ratio of β rays to γ rays incident on the detector was about 50.

Based on the experience gained from operating the previous vertical spectrometer, some of the main problems identified were:

(1) The inconvenience of using liquid nitrogen cooled heat shields. The shields and the liquid nitrogen reservoir add extra weight to the total weight of the spectrometer and therefore restrict its mobility.

(2) The vertical configuration of the spectrometer. This complicates the engineering problems of the source introduction mechanism especially if the spectrometer is situated in an area where space is limited. The vertical height of the system places a demand for large overhead space and makes the system quite awkward to operate. These are very

Figure 3.1

Sectional view of a previous superconducting solenoid beta spectrometer developed at this laboratory

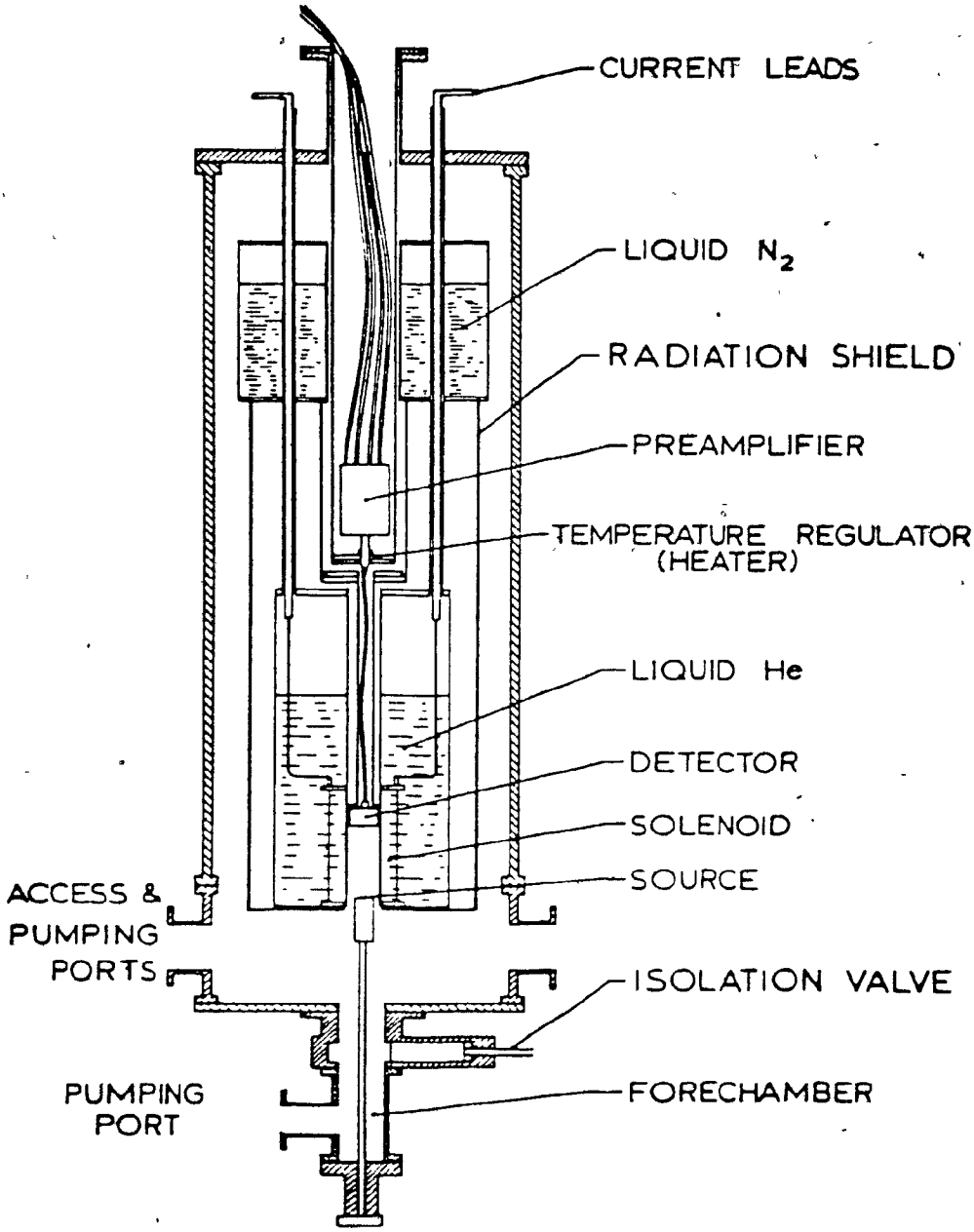
CURRENT LEADS
LIQUID N_2
RADIATION SHIELD
PREAMPLIFIER
TEMPERATURE REGULATOR (HEATER)
LIQUID He
DETECTOR
SOLENOID
SOURCE
ACCESS & PUMPING PORTS
ISOLATION VALVE
PUMPING PORT
FORECHAMBER

important considerations if experiments are to be performed at different laboratory sites.

(3) The presence of the source and the detector inside the low temperature part of the magnet. This hampers access to the detector for its alignment, variation of its position along the axis of the solenoid, or for electronic connections.

Introducing calibration sources with long half lives into the bore of the solenoid resulted sometimes, through accidents, in the contamination of the spectrometer with long lived activities. In order to remove such activities, the whole magnet system has to be dismantled to clean or replace the contaminated parts and then rebuilt afterwards.

Along the line of solving these problems, some of the development goals of the present spectrometer were:

(1) To change the cryostat design in such a way as to eliminate the need for the liquid nitrogen cooled shields.

(2) To achieve a higher magnetic field in a solenoid of greater length. The higher magnetic field enables one to study β transitions with higher endpoint energies (for a fixed detector surface area), while increasing the distance between the source and the detector results in improved supression of γ rays and therefore less γ ray contamination of the β spectrum.

(3) The use of a magnet with a larger diameter, room temperature, bore. The large diameter simplifies quite a few engineering problems and permits the use of detectors of larger surface area. The diameter of the detector is a major factor in determining the maximum energy of the beta rays that can be studied with the spectrometer. The room temperature bore allows the separation of the source-detector assembly from the magnet part of the system. This in turn facilitates access to the source and the detector positions and eases the problems of varying the location of either one of them with respect to the other or with respect to the magnetic field. Gaining this ease in access is crucial since different source introduction methods and different detector systems are contemplated for use in conjunction with the new magnet. The room temperature bore also has the advantage of rendering the superconducting solenoid system

completely independent from the rest of the spectrometer and thus freeing it for other uses in the lab as a high field magnet.

(4) To have the whole system in a horizontal configuration for ease of adaption to different experimental set-ups and convenience during operation.

(5) Increasing the versatility and mobility of the system. This is quite necessary since it is the norm in studies involving nuclei far from stability that experiments have to be carried out at various remote locations. These include accelerators, reactors and isotope separators (often in on-line combination with an accelerator or a reactor) wherever the method of production of the desired isotope is available and most suited for the specific spectrometer.

3.2 The Choice of a Superconducting Solenoid

The use of a superconducting solenoid instead of a water cooled normal conductor type is even more justified in the present spectrometer than it was in the previous one because of the larger volume and higher intensity of the desired magnetic field. The choice of a superconducting coil is more attractive on the basis of simpler design, lower cost, mobility, compactness, lack of requirements for complicated water cooling facilities and high power current supplies (Montgomery 1969, p.37). (For a detailed comparison of the merits of superconducting vs. normal magnets see Wood 1971.)

The use of a normal solenoid cooled with a cryogenic fluid (liquid nitrogen or liquid hydrogen) represents an even less attractive option than a normal magnet. This is because of the sophisticated design required and the fact that cryogenic magnets suffer from most of the drawbacks of both the superconducting and normal types (Parkinson & Mulhal 1967, p.5, 13, 69; Montgomery 1969, p.218; Taylor & Post 1962).

The use of rare earth permanent magnets was also given some consideration. However, because of several factors including: the high initial cost, the inflexibility of the design, the magnet weight, the delicate nature of the rare earth magnets, their temperature dependence, the lower magnetic fields attainable and the need for accurate magnetic field mappings, it was concluded that the disadvantages of the use of such magnets far outweigh the advantages.

3.3 The Solenoid

The solenoid used in this spectrometer was supplied by Canada Superconductor & Cryogenics Company Limited (CSCC). Some of the relevant parameters of the solenoid are listed in Table 3.1. The solenoid is wound from a vapor deposited (CVD) niobium tin (Nb_3Sn) composite conductor tape with a rectangular cross section. The critical temperature of Nb_3Sn is 18.3 K (Dew-Hughes 1979, p.143). The structural element in the ribbon is a substrate of Hastelloy in the center. The cladding is made up of two layers of high conductivity copper (CSCC; Brechna 1973, p.20). The copper cladding provides the adiabatic (enthalpic), dynamic and cryogenic stabilization required for the satisfactory performance of the superconductor (Wood 1971, p.304; Hancox & Catteral 1971, p.536; Brechna 1973, p.22, 301; Parkinson & Mulhal 1967, p.113). It also limits the voltages developed during a quench (Iwasa & Montgomery 1975, p.436).

Some of the parameters of the superconductor tape appear in Table 3.2.

The superconducting tape is wound around an anodized aluminum bobbin (see Table 3.1 for dimensions). The electrical contacts for the solenoid are located on an insulator ring (1/4 inch thick bakelite) which is fixed to one end of the bobbin. The current leads of the magnet are of the vapor cooled type supplied by American Magnetics Inc. (Type L-150). Each current lead is connected to the corresponding solenoid contact by two bus extensions. The extensions (supplied by AMI) are comprised of a high transition temperature superconductive Nb_3Sn tape sandwiched between copper strips. The bus extensions are joined by a wood's metal solder to the solenoid contacts.

The rated field of the magnet was 7 tesla (nominal) at 150 ampere current. Commissioning test performed with the solenoid installed a temporary liquid helium cryostat verified that the solenoid can be operated at 150 ampere. However, during the initial testing of the magnet after it was installed in the present cryostat, it was found that the solenoid consistently quenched (lost its superconductivity) at about 115 ampere (a detailed description of the processes involved in a quench is given in another section of this chapter). Since the quality of the wood's metal solder joint is suspect, and because it is located in a high

Table 3.1 Parameters of the Superconducting Solenoid

Windings: length (cm)	25.4
inner diameter (cm)	10.8
outer diameter (cm)	15.0
Numbers of turns (along the axis)	100
Number of layers (radially)	100
Bobbin: diameter of bore (cm)	17
length (cm)	27.3

Table 3.2 The Superconducting Composite Ribbon

Ribbon thicknesss (cm)	0.021
Ribbon width (cm)	0.230
Copper cladding thickness	0.005
Substrate	Hastelloy (a high strength nickel alloy)

magnetic field region, the quench was probably initiated at the contact as a result of the solder changing from the superconducting to the normal state.

The solenoid was therefore usually operated at a current of 100 ampere producing an axial magnetic field of 4.4 Tesla at its centre. Tests indicate that the solenoid would operate satisfactorily at currents of up to 110 ampere.

The inductance of the solenoid was calculated to be 4.7 henry using the method of Grover (1964, p.105). This value was also verified experimentally by monitoring the voltage across the solenoid while the current increased at a constant rate. From the rate of current change (0.056 Ampere/sec) and the voltage (0.25 ± 0.01 volt), the inductance is estimated to be 4.5 ± 0.2 henry in agreement with the calculation above.

Rapid changes in the current flowing through a superconducting magnet lead to excessive flux jumping and the generation of heat which can drive parts of the windings back into the normal (resistive) state (Wood 1971, p.302; Williams 1969, p.41; Parkinson & Mulhal 1967, p.112). Therefore the charging of the magnet (build up of the magnetic field and current) was done at a conservative pace. The rate of change of current was usually limited to about 3 ampere per minute. However, charging rates of up to 6 ampere/min ($\sim$0.5 volts inductive voltage) have been used without an indication of excessive flux jumping (which would manifest itself in rapid voltage changes across the solenoid). The current can therefore be taken up to its operating value (100 amp) in about 15 minutes.

3.4 The Current Supply

Two types of current supplies were used. The first consisted of 18 storage cells from 3 large truck batteries (2 volts per cell) connected in parallel with each other and in series with both the solenoid and a large carbon rehostat that was used to vary the current (Parkinson & Mulhal 1967, p.61).

In spite of the true D.C. nature of the current they supply (i.e. no ripple noise) and their low initial cost, the impracticality of the use of these batteries (the need for frequent adjustments of the rehostat, heavy weight, maintenance requirements, corrosive fluids and fumes emanating from the cells) and their unsuitability for extended operation

(limited charge storage capacity) led to the testing of an electronic power supply as a replacement for the batteries.

The power supply chosen was a Hewlett Packard model 6260B. Its operation in conjunction with the superconducting solenoid was quite satisfactory with good current regulation and long term stability. No significant increase in the electronic noise of the β ray detector or its associated counting circuitry was observed during the operation of the power supply.

A heat sunk reverse diode was installed across the output terminals of the power supply to protect it from the effects of high voltages that might be generated in the magnet during a quench (Donadieu & Rose 1962).

The magnet current was measured from the voltage drop across a 0.1 milliohm shunt resistor in series with the solenoid. The accuracy of the current determination and reproducibility is about 1 ampere, however its stability and regulation are much better.

3.5 The Cryostat

The superconducting solenoid employed in this spectrometer is cooled by immersing it in liquid helium during its operation. Therefore, a suitable cryostat for holding the liquid helium had to be designed in accordance with the general guidelines outlined in the beginning of this chapter.

The cryostat design used (figures 3.2, 3.3) is a pool type reservoir at atmospheric pressure. The cryostat reservoir is a horizontal cylinder with an eccentric circular hole running horizontally along its length. The reservoir is enclosed in a vacuum chamber and is held in its position by six vertical stainless steel support tubes. The cryostat is built from several pieces of polished stainless steel (type 304) welded together (TIG Welds).

Stainless steel is the conventional choice in cryostat design because of its excellent mechanical and thermal properties (Wigley & Halford 1971). These include a low thermal conductivity, a low thermal contraction coefficient, and a high tensile strength (Wigley 1971). Type 304 stainless steel was used because of its non-magnetic nature (low magnetic permeability and susceptibility) (Wigley 1971, p.60; White 1968, p.203; Collings & Hart 1979).

Figure 3.2

Sectional view of the present superconducting solenoid spectrometer (side view)

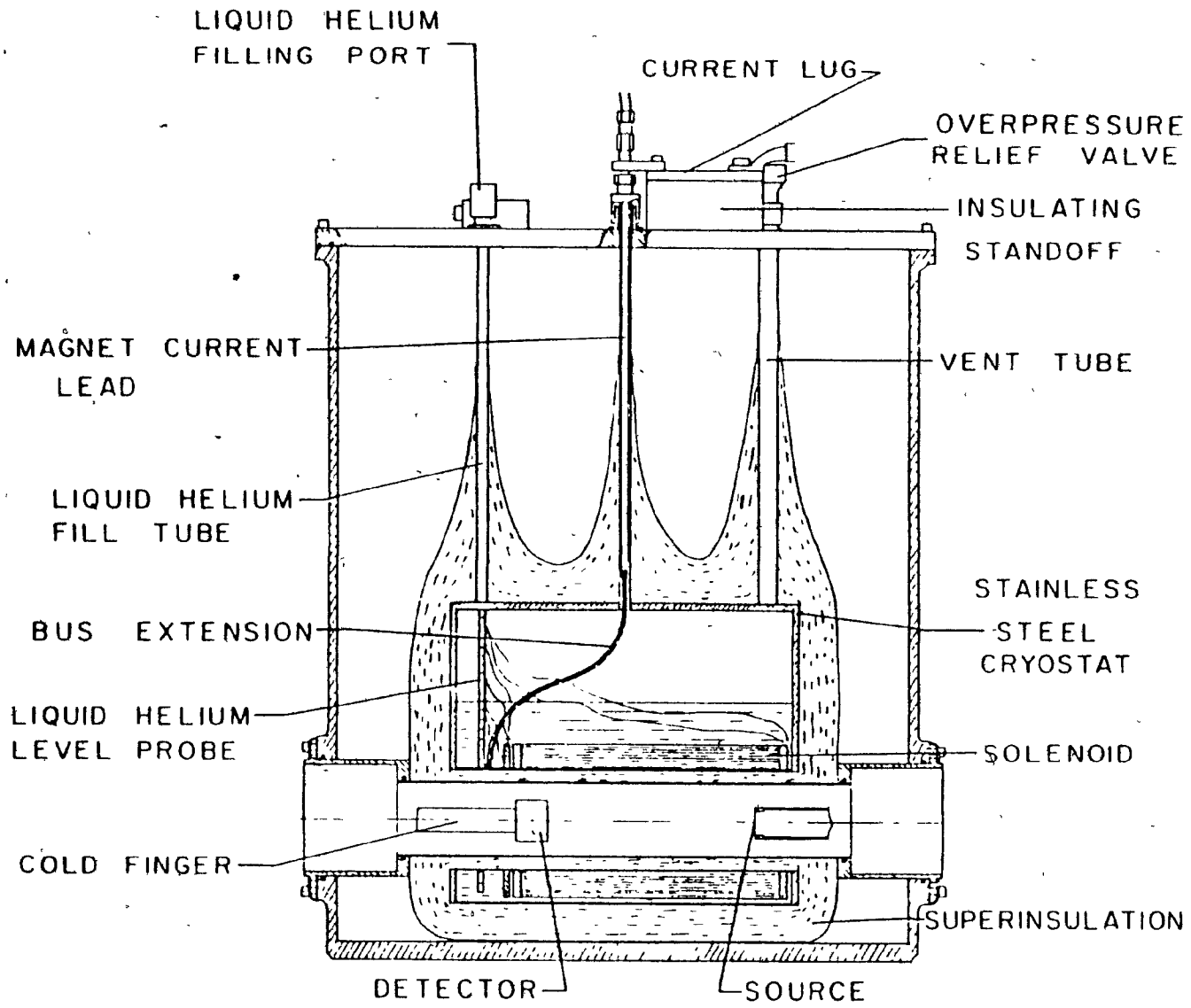
LIQUID HELIUM
FILLING PORT
CURRENT LUG
OVERPRESSURE
RELIEF VALVE
INSULATING
STANDOFF
MAGNET CURRENT
LEAD
VENT TUBE
LIQUID HELIUM
FILL TUBE
STAINLESS
STEEL
CRYOSTAT
BUS EXTENSION
LIQUID HELIUM
LEVEL PROBE
SOLENOID
COLD FINGER
SUPERINSULATION
DETECTOR
SOURCE

Figure 3.3

Sectional view of the present superconducting solenoid spectrometer (front view)

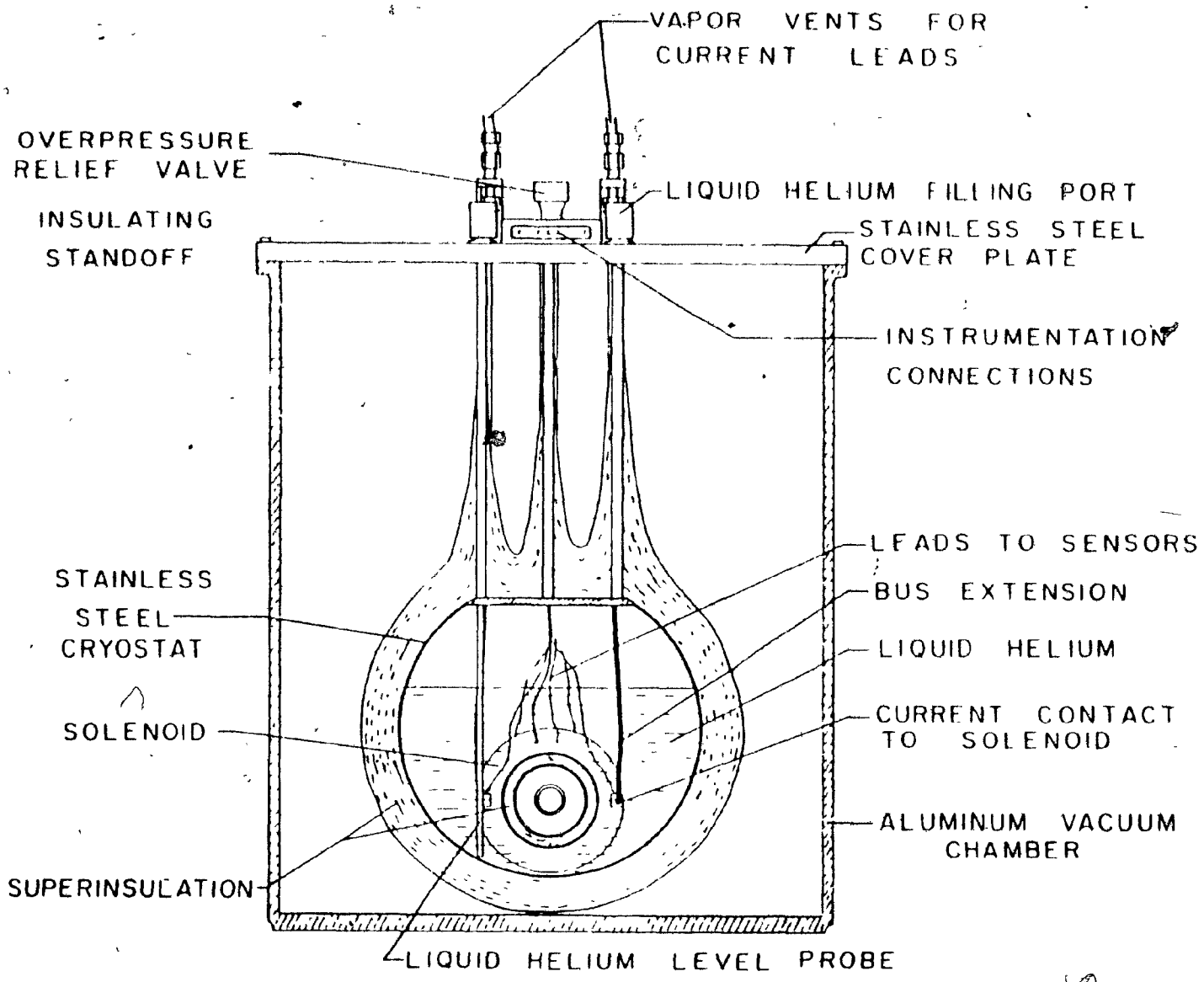
VAPOR VENTS FOR CURRENT LEADS
OVERPRESSURE RELIEF VALVE
INSULATING STANDOFF
LIQUID HELIUM FILLING PORT
STAINLESS STEEL COVER PLATE
INSTRUMENTATION CONNECTIONS
LEADS TO SENSORS
BUS EXTENSION
LIQUID HELIUM
CURRENT CONTACT TO SOLENOID
ALUMINUM VACUUM CHAMBER
STAINLESS STEEL CRYOSTAT
SOLENOID
SUPERINSULATION
LIQUID HELIUM LEVEL PROBE

The solenoid is enclosed within the helium reservoir with the inside diameter of the bobbin tightly fitting around the outside diameter of the horizontal bore of the cryostat. This, in addition to the teflon wedges inserted between the cryostat walls and the solenoid, fixes the solenoid in its position. The eccentric location of the solenoid (Fig. 3.3) places it low in the cryostat so that it is possible to continue operating until the reservoir is nearly empty.

The six support tubes from which the cryostat is suspended also provide access to the magnet and the liquid helium reservoir. These tubes are utilized as follows: 2 tubes are taken up by the magnet current leads, one tube is used to place a liquid helium level meter into the reservoir, one tube is used as a conduit for the leads to different sensors in the cryostat (a cryothermometer, a magnetoresistance, leads for measuring the voltage drop across the solenoid), one tube for liquid cryogen filling and the last tube is used as a helium vapor vent.

The level of liquid helium in the cryostat was monitored with a superconductive filament level sensor (figures 3.2, 3.3). The monitoring of the temperature inside the cryostat was done with a platinum resistance cryothermometer mounted on one end of the solenoid bobbin. Both the level meter and the cryothermometer were supplied by American Magnetics Inc. The liquid capacity of the helium reservoir is about 18.5 liters and its total surface area is about $0.56 m^2$.

The introduction of cryogenic fluids into the cryostat causes thermal contractions which might lead to misalignment of the different parts of the system. The data of Wigley (1971, p.301) for the total linear thermal contraction of type 304 stainless steel, combined with the dimensions of the cryostant and the support tubes indicate that the axis of the solenoid will be displaced by no more than 1 mm from the axis of the room temperature bore after being cooled down to liquid helium temperature.

3.6 The Vacuum Chamber

The body of the vacuum chamber is constructed from welded aluminum while the top lid is made from stainless steel. The cryostat support tubes are welded to this lid and therefore the whole magnet system can be removed from the vacuum chamber by lifting the lid. A stainless steel

tube makes up the room temperature free bore of the magnet system.

Rubber (Buna - N) "O" rings were used for all demountable, room temperature seals. The free volume of the vacuum chamber is about 145 liters. A pressure of 2.5×10^{-3} Pa (2×10^{-5} torr) is maintained in the vacuum chamber by evacuating it through a 2.5 cm pump out port. This port is connected through a 10 cm long pumping line to a small diffusion pump which is equipped with liquid nitrogen cooled baffles. The pressure inside the vacuum chamber was measured with a cold cathode ionization guage (PIG) situated at the pump out port. A complete description of the vacuum system of the whole spectrometer is given in chapter 5.

The overall dimensions of the magnet system are about 56 cm diameter and 72.5 cm height. The free room temperature bore of the magnet has a diameter of about 7.3 cm. The masses of the various parts of the magnet system are given in Table 3.3. The total mass of the whole system is less than 125 kg which makes it quite mobile and eases the structural requirements on the frame needed to support it. The mass of this spectrometer system represents only a small fraction of the mass of magnetic beta spectrometers (see for example Langer & Cook 1948; Wegstedt 1957; Siegbahn et al. 1964).

3.7 Thermal Insulation and Heat Transfer in the Cryostat

Because of the low heat of vaporization of liquid helium (2.6 Joule/cm^3 or 0.72 watt-hr/liter) (Rose-Innes 1964, p.140), even a small amount of heat input into a reservoir containing liquid helium would cause excessive boiling and rapid consumption of the liquid helium. The low boiling point of liquid helium (4.22 K) (Rose-Innes 1964, p.140) complicates the thermal insulation problems further. It results in a large temperature difference between the liquid helium reservoir and the environment and therefore a high heat input into the reservoir unless special precautions are taken.

Hence the aim of the cryostat design is to eliminate, or reduce to a minimum, all possible sources of heat leak into the helium reservoir in order to prolong the operating time of the magnet as much as possible. The sources of heat flow into the cryostat can be summarized as follows (Wexler 1961):

(1) Conduction and convection through the gas in the space surrounding

Table 3.3 Masses of Different Components of the Magnet System

Component	Material	Mass (kg)
Cryostat	Stainless steel	12.5
Solenoid windings	Assumed copper	20.7
Solenoid bobbin	Aluminum	1.3
Vacuum chamber	Stainless steel	43.8
Vacuum chamber lid	Stainless steel	44.1
Room temperature bore tube	Stainless steel	1.3
total		123.7

the cryogenic reservoir.

(2) Solid conduction along the tubes supporting the cryostat.

(3) Heat radiation through the aperture of the tubes connected to the cryostat.

(4) Conduction along the magnet current leads.

(5) Joule heating of the current leads when electric current is flowing through them.

(6) A.C. losses whenever the current in the solenoid is changing.

(7) Radiant heat incident on the helium reservoir walls.

(8) Conduction of heat through any material in contact with the liquid helium reservoir.

In what follows each of these sources will be discussed in the same order in which they appear above.

3.7.1 Gas Conduction and Convention

The thermal leakage caused by heat transfer through the gas is reduced to a negligible amount by enclosing the cryostat in a high vacuum tank. At the operating pressure of this vacuum chamber (2.5×10^{-3} Pa) direct heat transfer by the residual gas is totally insignificant (Scott 1959, p.144-147; Kropschot 1962, p.154-156). However, the contribution of gas conduction to heat flow across the multilayer superinsulation used in this cryostat is more significant and will be discussed at length later in this section.

3.7.2. The Support Tubes

3.7.2a Conduction

In order to reduce the amount of heat conducted along the support tubes, they were constructed from thin walled (0.05 cm wall thickness) stainless steel pipes and made as long as is compatible with the constraints of the general design (about 40cm long).
Since for solid conduction (White 1968, p.213)

$$W = K(t)\ A\ (dT/dl) \qquad 3.1$$

where

W = The rate of heat flow by solid conduction

K(T) = The thermal conductivity of the tube material

A = The cross sectional area of the tube wall

dT/dl = The temperature gradient along the length of the tube.

By using stainless steel tubes K(T) is made quite small (Wigley 1971, p.304); using thin walled tubes minimizes (A); and finally by increasing the length of the tubes (dT/dl) is decreased since the total temperature change across the length of the tube is fixed (room temperature to liquid helium temperature).

In addition to these measures, the effluent helium vapor from the reservoir is vented through two of these tubes (the ones housing the magnet current leads) to help remove some of the heat conducted along the tubes. The heat exchange betweeen the rising cold vapor and the stainless steel tube walls reduces the heat input into the liquid quite considerably (Scott 1959, p.239-242).

In order to estimate the heat input into the liquid helium reservoir caused by solid conduction along the support tubes, the method of Conte et al. (1970) was used. In their work, the authors take into account the variation of thermal conductivity of stainless steel with temperature. Following their approach, the amount of heat conducted by the stainless steel tubes used in our cryostat was calculated and the results are given in Table 3.4.

These values overestimate the heat flux conducted through the support tubes; they do not take into account the vapor cooling of two of the tubes since it was difficult to estimate the efficiency of the heat exchange between the gas and the tubes (Conte et al. 1970). A better estimate of the total heat conducted down the tubes would be perhaps around 0.6 ~ 0.55 watt (0.8 ~ 0.75 liters of liquid helium/hr).

3.7.2b Thermal Radiation

To estimate the heat load on the liquid helium cryostat caused by radiation through the aperture of the support tubes, we first assume a "worst case" condition. In this case, the apertures of all the tubes are assumed to be exposed to black body radiation at room temperature (i.e. the tubes are assumed to be open to the atmosphere with no covers or plugs on top). The inside surfaces of the tubes are assumed to be specular reflectors with very low emissivity therefore causing all the radiation

Table 3.4 Heat Conducted by the Support Tubes

	Number of tubes	Diameter (cm)	Heat conducted per tube (watt)	Total heat conducted (watt)
	1	1.6	0.19	0.19
	2	1.3	0.15	0.30
	3	1.0	0.11	0.33
total	6			0.82

- Vapor cooling was not included
- All tubes have a length of 38.7 cm and wall thickness of 0.051 cm

incident on the top opening of the tubes to be funnelled down to the cryostat. In this case, the heat input from this source can be calculated from the Stefan-Boltzman Radiation law (White 1968, p.230).

$$W = \varepsilon \sigma A (T_2^4 - T_1^4) \qquad 3.2$$

where

W = The rate of heat input (watt)

ε = emissivity of the radiant surface (assumed 1 here)

σ = The Stefan-Boltzman constant 5.67×10^{-8} W/m^2 K^4 (Anderson 1981, p.4)

T_2 = The temperature of the hot emitting surface (300 K)

T_1 = The temperature of the cold absorbing surface (4.2 K)

A = The surface area of the top aperture of the tube

The results of this "complete funnelling" calculations appear in Table 3.5.

In reality the heat input from this source is much less than the estimates above. The top openings of two of the tubes are covered with polished brass plugs. The surfaces of these plugs have an emissivity of about 0.05 or less (White 1968, p.220; Thornton 1971, p.495; Scott 1959, p.347; Kropschot 1962, p.154; Monlar 1971, p.210). Three of the other tubes have inserts inside them (two magnet current leads and one liquid helium level sensor) which act as radiation traps reducing the radiation heat flux piped down the tubes (White 1968, p.53). Furthermore, the inside surfaces of the tubes were not polished but were diffuse reflectors with high emissivity. This coupled with the length of the tubes ($\sim$ 40cm) results in the funnelling of only a small fraction of the reflected radiation only.

If one assumes that no reflected radiation is transmitted through the tubes and that the surfaces of the tubes are non radiating (i.e. "best case" condition), then the amount of radiant heat that reaches the bottom of the tube will be that emitted in the small solid angle subtended by the lower opening of the tube at the upper aperture. In this case the radiant heat reaching the bottom of the tubes is (Conte et al. 1970)

$$W = \varepsilon \sigma A (T_2^4 - T_1^4) \frac{\Omega}{2\pi} \qquad 3.3$$

Table 3.5 Estimates of Heat Transfer by Radiation through the Support Tubes

Number of tubes	Diameter (cm)	Heat transfer per tube (complete funnelling) (watt)	Total heat transfer per tube (complete funnelling) (watt)	$\Omega/2\pi$ (reduction factor) (absorbing walls)
1	1.6	0.09	0.09	2.1×10^{-4}
2	1.3	0.05	0.10	1.3×10^{-4}
3	1.0	0.03	0.09	7.5×10^{-3}
6			0.28	

where all the parameters are the same as the ones defined in 3.2 and Ω is the solid angle subtended by the bottom opening at the top of the tube.

$$\Omega = 2\pi \left[1 - \left(\frac{1}{1 + \frac{r^2}{L^2}} \right)^{1/2} \right] \qquad 3.3a$$

where

r = The radius of the tube

L = The length of the tube

The results of applying 3.3 to the cryostat described here are given in Table 3.5. They show that the radiation flux will be reduced by a factor of about 5000 or more compared to the case of complete funnelling. If this was the case, then the contribution of radiation from the aperture of the tubes to the total heat flux would be completely negligible. However, the inside surfaces of the tubes are not perfectly absorbing and the actual situation lies somewhere between the two extreme estimates (Kuraoka et al. 1979).

The additional heat radiated by the inside walls of the tubes themselves can be accounted for as well. In the case of a tube with diffuse reflecting or black walls, Perlmutter & Siegel (1963) show that with negligible solid conduction (not a totally unreasonable approximation for thin walled stainless steel tubes), the total amount of heat radiated through the low temperature aperture is less than 5% of the total heat incident on the high temperature aperture if the ratio of length to diameter of the tube (L/2r) exceeds 20 (which is the case in our cryostat). For specular reflecting walls, the authors show that the radiation heat reaching the low temperature aperture is less than 50% of radiant heat incident on the high temperature aperture if the emissivity is 0.1 or higher.

After accounting for all of these effects, the amount of heat radiated down the tube is estimated to be less than 0.1 watt (about 0.1 liter of liquid helium/hr or less).

3.7.3 The Magnet Current Leads

The current leads chosen for this solenoid are the helium vapor

cooled type similar to those described by Efferson (1967). The helium vapor emanating from the boiling liquid passes through cooling channels in the leads. The large heat capacity of the vapor is used to extract some of the Joule heat generated by the current flowing through the leads and some the heat conducted by the leads. The heat flow into the cryostat per pair of leads at the operating current (100 ampere) is about 0.25 ∿ 0.3 watt (liquid helium consumption of about 0.35 ∿ 0.4 liters/hr) and 30-40% of this value when no current is passing through them (AMI 1, p.9).

3.7.4 A.C. Losses

A.C. heating, caused by changes in the magnetic field of the solenoid whenever the current is varied, can provide a significantly large heat load on the cryostat system and has therefore to be considered carefully (Colyer 1967). The A.C. heating is caused by several factors. The first factor is common to all superconducting, current-carrying elements and results from the presence of normal-state regions in the superconductor when it is placed in a magnetic field above a few kiloguass. Any movement of the magnetic flux caused by varying the transport current in the superconductor results in heat generation in the normal-state regions (Iwasa & Montgomery 1975, p.449). Another factor is the A.C. heating due to eddy currents that are set up by the varying magnetic field in the normal conductor matrix (the cladding) surrounding the superconductor (Brechna 1973, p.250). This is especially important in our case since the solenoid was wound from a single filament tape rather than a twisted multifilamentary composite which would have reduced the effect. Heat is also generated by eddy currents flowing in the metallic parts of the magnet and the cryostat (normal conductors) when the solenoid current (and therefore the magnetic field) is changing (Brechna 1973, p.274). These parts include the aluminum bobbin around which the solenoid is wound and the stainless steel reservoir that surrounds the magnet.

It is quite difficult to calculate a reasonably accurate estimate of all these A.C. effects. Order of magnitude calculations of the heat dissipated in the magnet due to some of the factors mentioned above is given by Smith and Lewin (1967). Following their method, the rate of heat generation by the A.C. loss in the superconductor material itself is calculated to be of the order of 0.1 watt during the 15 minutes it takes

to charge up the magnet to full field. Contributions from the other factors are harder to estimate but in general the heat load resulting from their effects increases as the rate of current change is increased. In the magnet described in this thesis the helium consumption increased quite perceptibly during the time when the solenoid current was being changed. This was evident from the increased frost formation on the vent lines indicating an increase in the liquid helium boil off rate.

3.7.5 The Superinsulation

Installation

As mentioned earlier in this chapter, replacing the liquid nitrogen cooled radiation baffles was one of the major aims of the new cryostat design. In order to be able to achieve this, laminar multilayered radiation shields were. These multiple layers, when used in combination with high vacuum, are commonly referred to as superinsulation. The type chosen was NRC-2 superinsulation commercially supplied by KST Co. It is made up of mylar foils 0.0064mm (1/4 mil) thick each, with high purity aluminum deposited on one side to a thicknesss of about 250 Å.

The foils are wrapped in successive layers around the cold surfaces of the cryostat, thoroughly covering the liquid helium reservoir (including the bore) and the support tubes. Each layer is made up of several separate pieces taped together to fit the shape of the cryostat. The joints between these pieces are lap joints which were offset in successive layers during application. This type of joint (staggered lap joint) is considered to be one of the most efficient joints with respect to thermal conductivity (Price 1968; Hammond 1971). The successive layers were fastened to each other using a metallized polyester adhesive ribbon (3M #850) (see figures 3.4, 3.5).

The consecutive layers of insulation applied around the support tubes did not all extend to the same height of the tube, rather each successive layer was terminated at a slightly higher point along the tube than the preceeding layer. Thus each layer would reach only to the point at which the temperature of the tube wall is the same as the rest of the extended layer. This configuration eliminates any lateral conduction in the superinsulation (KST). The offsetting of the successive layers was

Figure 3.4

Photograph of the liquid helium cryostat showing the multilayer superinsulation (side view)

Figure 3.5

Photograph of the liquid helium cryostat showing the multilayer superinsulation (front view)

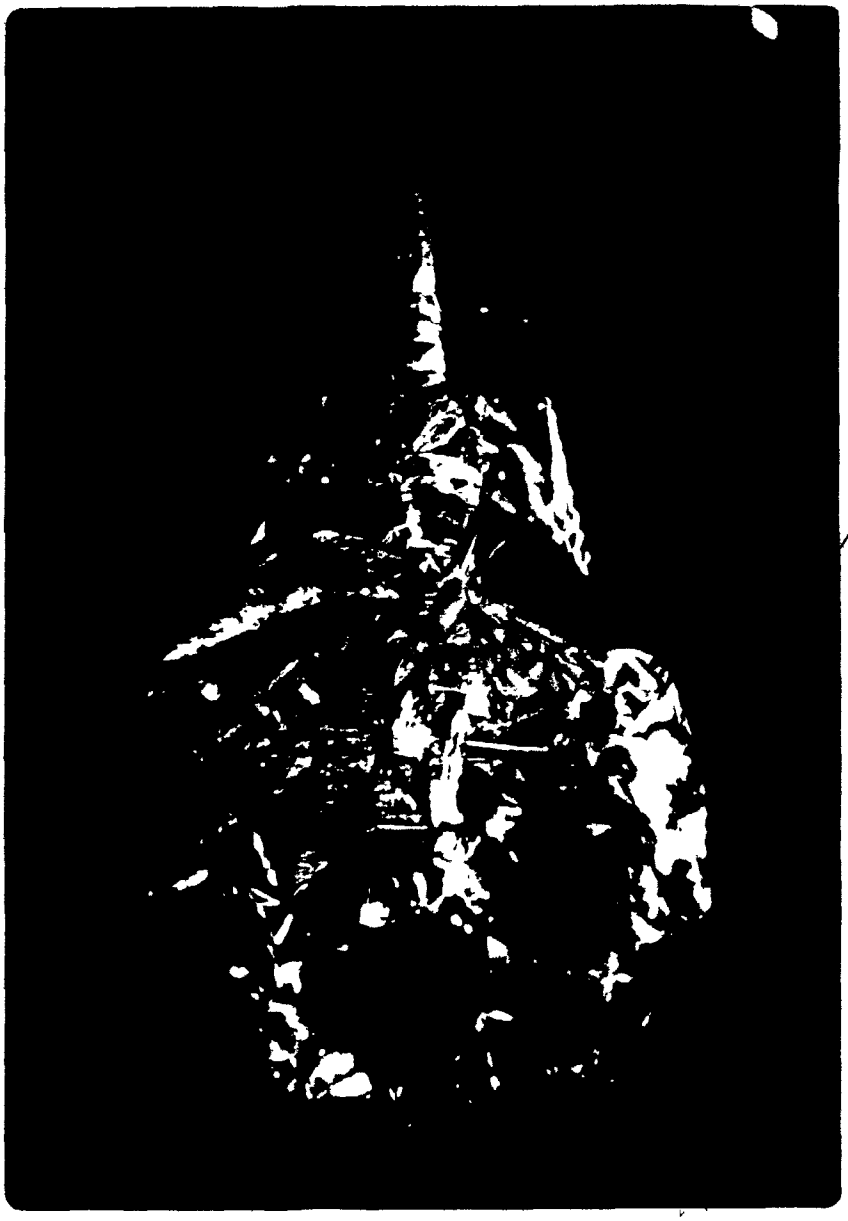

done only approximately since the profile of the temperature variation across the thickness of the multilayered superinsulation blanket could not be easily determined (Hammond 1971; Kropschot 1961).

The bottom parts of the insulation layers covering the support tubes formed skirts which were interleaved with the rest of the superinsulation at the regions where the tubes penetrated it. This was done in order to eliminate the adverse thermal effects of penetrations through the superinsulation (thermal shorting) (Price & Lee 1967).

The number of layers of superinsulation used was 80, each installed individually. The average thickness of the multilayered blanket was about 3.75 cm on the outside surfaces of the cryostat and about 1.25 cm around the bore. The resulting packing densities are 60 layers/cm covering an area of about 1000 cm^2 and 20 layers/cm covering an area of about 4600 cm^2. The total mass of the superinsulation used is about 0.4 kg.

Heat Transfer in the Superinsulation

Because of the high reflectance (low emissivity) of the aluminum deposit and the low thermal conductivity between successive foils, the superinsulation layers act as thermally floating radiation shields; each shield reflects a large part of the radiation incident on it and radiates the rest to the next layer. By having a large number of such shields in series, most of the heat incident in the form of electromagnetic radiation is be reflected back to the warm outer surfaces. The thermal conductivity between neighbouring layers is minimized by crinckling the foils so that the area of contact between the layers is reduced (Bailey 1971, p.151). Thus, after equilibrium is reached, each foil establishes itself as a constant temperature shell (isotherm) around the cryostat.

In our cryostat, the multilayer superinsulation is the only means of reducing the heat radiation incident on the surface of the cryostat from the room temperature vacuum chamber walls. It is also the only material (besides the support tubes) that comes in contact with the liquid helium reservoir. Therefore careful determination, and reduction, of the heat transfer through the superinsulation is necessary in order to circumvent the effects of two of the heat input sources listed in the beginning of this section (points (7) and (8)).

The heat transport through the multiple layers superinsulation

arises from (Kropschot 1961):

(1) Heat conduction by the residual gas between neighbouring layers

(2) Solid conduction across the layers

(3) Heat radiation across the superinsulation.

3.7.5a Residual Gas

At low pressures, when the mean free path of the gas molecules is large compared to the dimensions of the space in which they are travelling (free molecular flow region), the rate of heat transfer between two parallel surfaces due to gas conduction is given by (Kropschot 1962, p.155):

$$W = A\, G\, \alpha\, P\, (T_2 - T_1) \qquad 3.4$$

where

W = The rate of heat transfer

A = The surface area

α = An accommodation coefficient which depends on the species of gas and temperature of the surface (Scott 1959; p.147)

P = The pressure of the gas

G = A constant which depends on the type of gas

T_2, T_1 = The temperatures of the hot and cold boundaries between which heat is conducted, respectively.

The extension of this formula to multilayered superinsulation is given by Ruccia et al. (1967). However, this extension did not prove to be useful in our case due to lack of knowledge of the values of several parameters appearing in the formula given by the authors.

In general, the heat transported by gas conduction in multilayer superinsulation decreases as the absolute pressure of the gas between the layers is lowered and becomes quite small below 0.013 Pa (10^{-4} torr) (Leonhard & Tatro 1970; Kropschot 1961; Hnilicka 1960; Getty et al. 1966; Barron 1972).

At an interlayer pressure of 10^{-4} torr and lower, the gas conduction within the insulation is the result of a process of free molecular flow and an effective thermal conductivity can be ascribed to the gas. The effective thermal conductivity has a value of the order of 0.1 μ w/cm K at 10^{-4} torr and decreases linearly with pressure (Scurlock &

Saull 1976; Barron 1972).

The heat flux due to gas conduction can be calculated from theeffective thermal conductivity attributed to the gas as follows:

$$W = \frac{A K (T_2 - T_1)}{t} \qquad 3.5$$

where

W = The rate of heat input due to residual gas conduction (watt)

A = The area covered by the superinsulation (cm^2)

t = The thickness of the superinsulation (cm)

T_2 = The hot boundary temperature 300 K

T_1 = The cold boundary temperature 4.2 K

K = effective thermal conductivity due to the gas = 0.1 μ w/cm K

For the superinsulation used in the cryostat described in this thesis, the residual gas conduction calculated from equation 3.5 amounts to about 0.07 watt if the interlayer pressure is 0.01 Pa or less ($<10^{-4}$ mm Hg).

Measurement of the pressure in the tank surrounding the superinsulation does not provide a realistic estimate of the pressure in the interspaces within the insulation (Price 1968). In general, the local interlayer pressure which is responsible for the gas conduction is considerably higher than the pressure measured in the vacuum container (Black & Glaser 1961; Barlcerek & Rafalowicz 1976). The relationship between the two is determined by the different parameters of the particular set up (geometry, outgassing, pumping speed, etc.) (Mikhalchenko et al. 1976; Coston 1966; Price 1968).

The major causes of the high residual gas pressure in the superinsulation are the outgassing from the large surface areas of the foils (Price 1968; Scurlock & Saul 1976; Leonhard & Tatro 1970) and the tortuous path that the gas molecules have to follow through the multilayers before being removed from the system. Because of the lap joint configuration used in installing the multilayers in our cryostat, the evacuated gas must change direction in each lapped layer before being removed. This reduces the pumping speed and results in high interlayer pressures.

In order to reduce the rate of outgassing from the superinsulation,

repeated purges with dry, room temperature, nitrogen gas were used (Price 1968) followed by long periods of continuous pumping. The dry nitrogen purges help to remove the absorbed water vapor molecules from the metallic surfaces of the superinsulation without the nitrogen itself being preferentially absorbed (Kutzner et al. 1973).

The ultimate operating pressure attained was about 2.5×10^{-3} Pa measured in the vacuum chamber. At this value, the interlayer pressure is probably higher than 0.01 Pa and therefore the contribution of gaseous conduction to heat transfer is considerably higher than the 0.07 watt estimate above.

3.7.5b Solid Conduction

Solid conduction in the multilayer superinsulation is the result of: conduction from one layer to another across the surfaces of these layers at the points of contact, conduction along the individual layers themselves (Kutzner et al. 1973), and conduction across any impurities or cryopumped gases that bridge the gap between successive layers (Kropschot et al. 1960).

Solid conduction in the superinsulation is dominated by the contact resistance between neighbouring layers. The thermal conductance across each point of contact depends on the area of contact (and hence the microstructure of the layers) and the local mechanical pressure (and therefore the wrapping layer density) (Scurlock & Saul 1976). Since the thermal contact between adjacent foils is an important factor in conductive heat transfer, increasing the packing density results in an increase in the conductive component as a result of an increase in the number and intensity of contact point (Brechna 1973, p.460, 461).

Rigorous treatment of the solid conduction problem in superinsulations is not possible (Barron 1972). This is especially true in the case of crinckled aluminized mylar because the conduction takes place in contact points between alternating layers of dissimilar materials (aluminum and mylar) (Getty et al. 1966). In addition the temperature varies across the thickness of the superinsulation causing variations in the conduction coefficient (Balcerek & Rafalowicz 1976). The variation of the thermal conductivity of the contact points with temperature is not very well understood (Kropschot 1961).

If one assumes that the thermal conductivity coefficient between two successive layers is independent of temperature, an approximate expression for the amount of heat transferred by solid conduction across the superinsulation, can be written as follows (Getty et al. 1966):

$$W = \frac{A(T_2 - T_1)}{(N + 1) f(r)} \qquad 3.6$$

where

W = The rate of heat transfer due to conduction

A = The surface area covered by the superinsulation

T_2, T_1 = The hot and cold boundary temperatures respectively

N = The number of superinsulation layers

f(r) = A term representing the total local resistance to conduction heat flow. It is made up of contributions from both the solid conduction in the aluminum deposit, and the contact resistance between neighbouring layers. It generally decreases with increasing wrapping density.

However, because of the assumptions made in the derivation of the formula, and the difficulty in determining f(r), equation 3.6 serves only to illustrate the general trend and can not be used for an accurate determination of the contribution of solid conduction.

In general, the contribution of solid conduction decreases with temperature, therefore conduction is the dominant factor in heat transfer in the innermost layers while radiation is more important in the outer ones (Leonhard & Tatro 1970). Over the whole thickness of the superinsulation, estimates for the contribution of solid conduction vary between 20%-80% of the total heat transfer across the superinsulation. This fraction is dependent on several factors including the type of superinsulation, the packing density and the boundary temperatures (Getty et al. 1966; Price & Lee 1967; Thomas & Weitzman 1967; Ruccia et al. 1967, Kutzner et al. 1973).

In order to minimize the contribution of solid conduction to heat transfer in the multilayer insulation, each layer was installed separately instead of wrapping the multilayers around the cryostat in a spiral fashion. The installation of individual layers reduces conduction from one layer to another (Hofmann 1970). In addition, only the minimum

packing density (number of layer per cm) needed for dimensional stability (20 layers/cm) was used around the surfaces where space was not restricted (the outer surfaces of the cryostat). Where space was restricted (along the bore), the layer density used (60 layers/cm) was the one that results in the lowest overall effective thermal conductivity (including the radiation contribution) (Hnilicka 1960, KST).

The method used to wrap the superinsulation (no exposed edges, interleaved skirt joints around penetrations) eliminates the heat transfer that results from "end effects". This is the increase in the amount of heat transported by the superinsulation when the edges of the layers are exposed to room temperature (Getty et al. 1966, KST). The increase is caused by solid conduction parallel to the layers and by radiation being funnelled in the space between the reflective layers (Vilet & Coston 1968). The radiation contribution is quite significant since the edge of a stack of superinsulation layers represents an absorbing blackbody to the incident radiation (Barron 1972, KST). The heat input due to edge effects, if not dealt with appropriately, can cause a serious deterioration of the insulating properties of superinsulation. This is because of the high effective parallel thermal conductivity of superinsulations (typically three orders of magnitude greater than the transverse conductivity (Vilet & Coston 1968; Kutzner et al. 1973; Barron 1972; Long 1972).

Radiation

The primary function of the superinsulation is to act as a set of successive shields to reduce the amount of heat transferred to the cryostat by means of electromagnetic radiation. This reduction results from the fact that the temperature difference between successive layers is quite small. And, since according to the Stefan-Boltzman law (3.2) the amount of heat transferred by radiation is very stronly dependent on the temperature difference, the heat radiated from one layer to another in the superinsulation is quite small.

For a number (N) of radiation shields, the Stefan-Boltzman law can be written as follows (Kutzner et al. 1973; Getty et al. 1966):

$$W = \frac{\sigma A (T_2^4 - T_1^4)}{(N - 1)\left(\frac{1}{\epsilon_1} + \frac{1}{\epsilon_2} - 1\right)} \qquad 3.7$$

where

W = The rate of heat transfer due to radiation

σ = The Stefan Boltzman constant = 5.67×10^{-8} W m^{-2} K^{-4}

N = The number of superinsulation layers (the number of freely floating radiation shields is N - 2 since the layers adjacent to the warm and cold surfaces are not considered freely floating (Caren 1968; Brecha 1973, p.459)

T_2, T_1 = The temperature of the hot and cold boundaries respectively

A = The area covered by the superinsulation

ϵ_1, ϵ_2 = The emissivities of the two sides of the radiation shields (the mylar and the aluminized side).

This formula is only an approximation in the case of superinsulation since the different layers are not truly thermally floating (some conduction takes place between layers). In addition the emissivities of the different layers are not identical (as this formula assumes). The emissivity changes from one layer to another due to the difference in temperature among the foils and the dependence of the emissivity on temperature (Kropschot et al. 1960). A detailed discussion of the limitations of (3.7) is given in Caren (1969).

Nevertheless, the trends indicated by the formula are valid. Increasing the number of shields results in the reduction of the amount of heat transferred by radiation through the superinsulation provided that the increase does not result in a higher packing density and therefore a larger contribution from solid conduction.

The estimates for the contribution of radiation to the total heat flow in superinsulation vary quite widely (Black et al. 1960; Kropschot 1961; Adelberg 1962, p.369; Kutzner et al. 1973; Getty et al. 1966; Price & Lee 1967; Thomas & Weitzman 1967; Ruccia et al. 1967). This contribution is quite dependent on the type of superinsulation used (emissivity of the radiation shields) and the characteristics of the set-up (boundary temperature, temperature profile across the superinsulation, number of layers, etc.).

Overall Performance of the Superinsulation

For standard conditions of boundary temperatures (300-77 K, 300-2 K, 300-4.2 K) and a thickness t of the superinsulation, it is convenient to define an effective thermal conductivity K_e that will take into account the different modes of heat transfer. K_e is defined by

$$W = \frac{K_e \; A \; (T_2 - T_1)}{t} \qquad 3.8$$

where

W = The rate of heat transfer across the superinsulation

K_e = The effective thermal conductivity of the superinsulation

T_2, T_1 = The hot and cold boundary temperatures respectively

t = The thickness of the superinsulation

The justification for using such an effective thermal conductivity is based on the results of experiments which show that the overall heat transfer is inversely proportional to the thickness of the multilayered superinsulation blanket, when all other parameters are held constant (Hnilicka 1960). The reason for this is that, to a first approximation, the contributions of radiation and conduction heat transfer increase linearly with the thickness of the insulation (assuming a constant packing density) (see euqations 3.6, 3.7). Therefore the apparent thermal conductivity should be independent of the thickness (Kropschot et al. 1960). It must be kept in mind that this effective thermal conductivity is merely a mathematical convenience and applies only between specific boundary temperatures and for a specific packing layer density (Hnilicka 1960; Adelberg 1962, p.369; Bailey 1971, p.151; Adelberg 1967).

Experimental data on the effective mean thermal conductivity of NRC-2 type superinsulation are available for boundary temperatures of 300-77 K (Hnilicka 1960; Monlar 1971, p.209; Leonhard & Tatro 1970, KST; Price & Lee 1967; Ruccia et al. 1967; Nast & Williams 1967; Thomas & Weitzman 1967; Vilet & Coston 1968; Getty et al. 1966; Hammond 1971; Barron 1972) or 77-4.2 K (Leung et al. 1980). In our cryostat the boundary temperatures were 300-4.2 K. In general, however, decreasing the temperature of the cold boundary of the multilayered superinsulation results in a decrease in the effective mean thermal conductivity (Riede & Wang 1960; Kropschot 1961; Black & Glaser 1961; Caren 1969; Vilet & Coston

1968). A possible reason for this is the decrease in the emissivity of aluminum with temperature (Kropschot et al. 1960). Another reason is the increased cryopumping effect of the layers adjacent to the low temperature boundary as the temperature of the boundary is reduced (Black & Glaser 1961). Because of the decrease in the effective thermal conductivity when the temperature of the cold boundary is lowered, estimates taken from the published values for boundary temperatures 300-77 K will probably overestimate the heat flux into the helium vessel through the superinsulation. Indeed even for identical conditions of boundary temperatures and packing density the published values are not in good agreement.

Price & Lee (1967) give an empirical formula for heat transfer by radiation and conduction in NRC-2 superinsulation which seems to agree with most of the available data. The formula can be written (after a slight modification to convert to MKS units):

$$\frac{W}{A} = \frac{\sigma\,(T_2^4 - T_1^4)}{(N-1)\left(\frac{1}{\varepsilon_1}+\frac{1}{\varepsilon_2}-1\right)} + \frac{5.98\times10^{-6}\, n^{1.18}\,(T_2 - T_1)}{(N-1)} \qquad (3.9)$$

where

W = The rate of heat transfer (watt)

A = The surface area covered by the superinsulation (m^2)

N = The number of superinsulation layers

n = The layer packing density (layers/m)

σ = The Stefan Boltzman constant

T_2, T_1 = The temperatures of the hot and cold boundaries respectively

ε_1, ε_2 = The emissivities of the two sides of the radiation shield.

This formula was used to calculate the total rate of heat transfer across the superinsulation in our cryostat. Total number of layers N = 80, and boundary temperatures of T_2 = 300K and T_1 = 4.2K were used. Several values for the emissivity of the two surfaces of singly aluminized mylar sheets similar to the ones used appear in the published literature (Ruccia & Hinckley 1967; Vilet & Coston 1968; Ruccia et al. 1967; Barron 1972; Hammond 1971; Caren 1969; Getty et al. 1966; Hnilicka 1960). The values chosen for the calculation above were ε_1 = 0.04 for the aluminized

side and $\epsilon_2 = 0.3$ for the mylar surface. The formula was applied separately for the two regions of the cryostat surface which are covered with superinsulation of different layer densities.

For the regions of the cryostat covered with superinsulation at a packing density of 20 layers/cm (i.e. the outer surfaces), the rate of heat transfer is 0.40 watt/m^2, while for the regions covered with superinsulation at a packing density of 60 layers/cm (i.e. the bore) the rate of heat transfer is 0.88 watt/m^2. Thus the total rate of heat transfer through the superinsulation is estimated to be 0.27 watt (0.4 liters of liquid helium per hour). It should be kept in mind that equation 3.9 used for this estimate does not take into account the variation of emissivity with temperature or the contribution of residual gas conduction.

3.8 The Overall Heat Input into the Cryostat

The overall heat input into the cryostat system is summarized in Table 3.6. Other sources of heat input not included in the table are negligible. These include: the liquid helium level meter which results in a liquid helium consumption rate of about 0.02 litres/hr (0.015 watt heat input) (AMI 2); the cryothermometer, whose heat input is about 0.005 watt (maximum current of about 50 mA, resistance 2 ohm at 4.2 K (Gerald et al. 1981)); and finally the heat dissipated by the passage of current in the leads connected to these and other sensors which is the order of microwatts (~50 milliampere current, 38 B&S copper leads (see White 1968 p. 231)).

3.9 Performance of the Cryostat

3.9.1 Precooling

The temperature of the cryostat (and the solenoid within it) was first reduced using liquid nitrogen (a cheap coolant) before the introduction of liquid helium into the cryostat. Great savings in the amount of liquid helium required to cool and fill the cryostat can be thus achieved. This is because of the rapid decrease in the specific heat of materials at low temperatures which results in a decrease in the total enthalpy of the system. Therefore after cooling with liquid nitrogen the

Table 3.6 Summary of Sources of Heat Input into the Cryostat

Source	Heat Input (watt)
Support tubes (radiation)	0.1
Support tubes (conduction)	0.6
Superinsulation (total)	0.27
Magnet current leads (100 amp)	0.30
Total	1.27

1.27 watt = Liquid helium consumption rate of 1.75 litres/hr

total enthalpy that has to be removed before the system reaches liquid helium temperature is quite small and less helium has to evaporate in the process of cooling (Rosenberg 1971, p.88; Rose-Inns, p.41) (Table 3.7).

Hence before every run, the cryostat was first filled with liquid nitrogen and left for several hours to reach thermal equilibrium. The liquid nitrogen was then removed from the cryostat just prior to the initiation of liquid helium transfer.

The latent heat of vaporization of helium is quite low, while the change in enthalpy of the helium vapor as it warms up to room temperature is much larger. Therefore it is necessary to ensure that the cold gas, generated by the rapid evaporation of liquid helium before the system reaches 4.2 K, is used to cool the cryostat and the solenoid. To achieve this, the opening of the liquid helium transfer tube is placed at the bottom of the cryostat so that the rising vapor sweeps by the solenoid and the warm parts of the cryostat and cools them (Brechna 1973, p.358). In addition, the helium filling is carried out slowly particularly at the start of the fill to allow the cooling capacities of the liquid and vapor to be utilized more fully (White 1968, p.63).

3.9.2 Liquid Helium Consumption

The liquid capacity of the cryostat is calculated to be about 18.5 liters. This was verified by measuring it with liquid nitrogen. However, with liquid helium, the cryostat is usually filled up with about 16.5 liters only. This is because of the large losses associated with overfilling with liquid helium which prevent further transfer of the liquid efficiently (Wexler 1961, p.153; Fuller & McLagan 1962, p.230).

A total of about 35 liters of liquid helium was required for a fill starting at liquid nitrogen temperature. Out of this total about 18.5 liters were lost during the fill. The loss can be attributed to the following:

(1) The evaporation loss of liquid helium during the cooling of the cryostat and the solenoid from liquid nitrogen to liquid helium temperature.

(2) The evaporation loss during the cooling down of the liquid helium transfer line from room temperature to 4.2K.

(3) The heat input into the liquid helium associated with the transfer

Table 3.7 Enthalpy Changes for Different Temperature Changes

Component	Material	Mass	Enthalpy Change (kJ)		
		(kg)	300-77 K	80-4 K	40-4 K
Magnet windings	Assumed copper	20.7	1490.7	124.6	12.6
Solenoid bobbin	Aluminum	1.2	90.6	11.6	0.9
Cryostat	Stainless Steel	12.5	943.7	72.1	4.9
total		43.4	2525.0	208.3	18.4

- Data for enthalpy changes are taken from CRC-49, and Fuller & McLagan 1962 p. 231
- For type 304 stainless steel (18-8 steel), values used are those for γ-iron as recommended by Wigley & Halford (1971 p. 316)

line.

Of these three factors, the first is by far the most serious.

Using the values for the enthalpy change given in table 3.7, the heat of vaporization of helium (2.6 J/cm^3), the change of enthalpy of the helium vapor between 4.2 K and 80 K (17.5 J/(cm^3 of liquid helium before evaporation)) (Hoare et al. 1961, p.359) and assuming that the 18.5 liter loss was all due to evaporation during the cooling down of the solenoid and cryostat, the efficiency with which the cooling capability of the helium vapor was used is calculated to be 17%. This value is perfectly within the accepted range (Fuller & McLagan 1962; Montgomery 1969, p.186).

The consumption rate of liquid helium after a fill is complete is measured by monitoring the level of the liquid in the cryostat vs. time. The liquid helium level sensor position is shown in figures 3.2, 3.3. The calculated calibration relationship between the height of the liquid as measured by the sensor and the volume of the liquid remaining in the cryostat is shown in figure 3.6.

The total holding time of the cryostat after a complete fill is about 9.5 hours yielding an average rate of loss of 1.7 liters of liquid helium per hour which is quite compatible with the calculations of the total heat input into the system (see table 3.6). The increase in the helium boil off rate during the time when the current was varied was quite noticeable. However, no significant dependence of the consumption rate on the value of the D.C. current flowing through the magnet and its current leads was observed. This is in agreement with previous assertions.

A typical consumption curve is shown in figure 3.7. As can be seen from the figure, the rate of consumption of liquid helium decreases over time from a starting value of about 2.7 liters/hr soon after the completion of a fill to about 1.4 liter/hr several hours afterwards. This reduction in the rate of consumption with time is due to several factors some of which are:

(1) The time period needed for the establishment of: a stable vapor flow pattern in the vent tubes (Boardman et al. 1973), the proper temperature gradients in the cryostat especially along the support tubes (Lynman et al. 1969; Klein 1967), and the proper thermal gradient across the multiple layer superinsulation. Reaching thermal equilibrium requires several hours in the case of the

Figure 3.6

Calibration curve for the volume of liquid helium in the cryostat vs. the height of the liquid level (as measured by the level sensor)

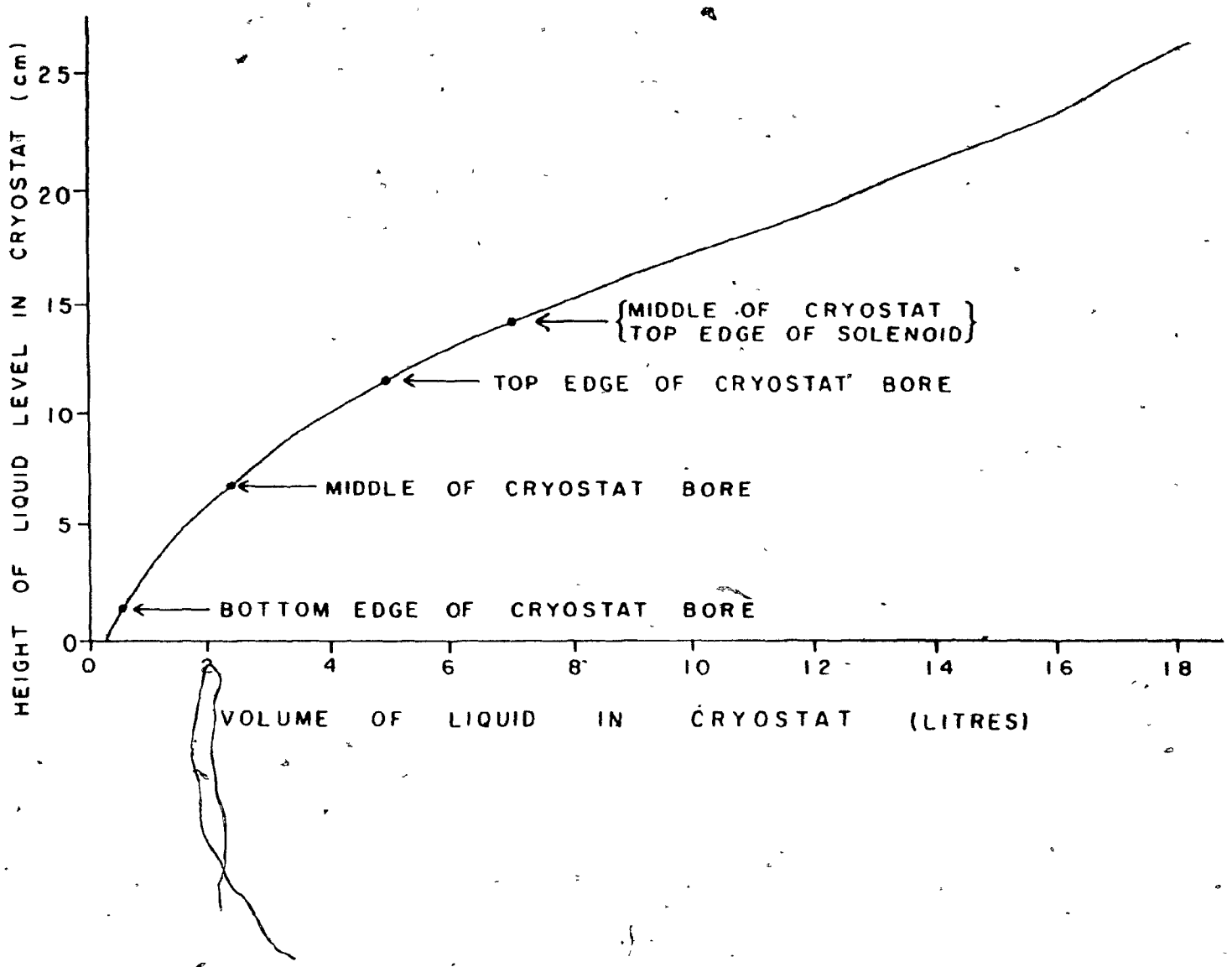
HEIGHT OF LIQUID LEVEL IN CRYOSTAT (cm)
0
5
10
15
20
25
0
2
4
6
8
10
12
14
16
18
VOLUME OF LIQUID IN CRYOSTAT (LITRES)
BOTTOM EDGE OF CRYOSTAT BORE
MIDDLE OF CRYOSTAT BORE
TOP EDGE OF CRYOSTAT BORE
MIDDLE OF CRYOSTAT
TOP EDGE OF SOLENOID

Figure 3.7

Liquid helium consumption vs. time

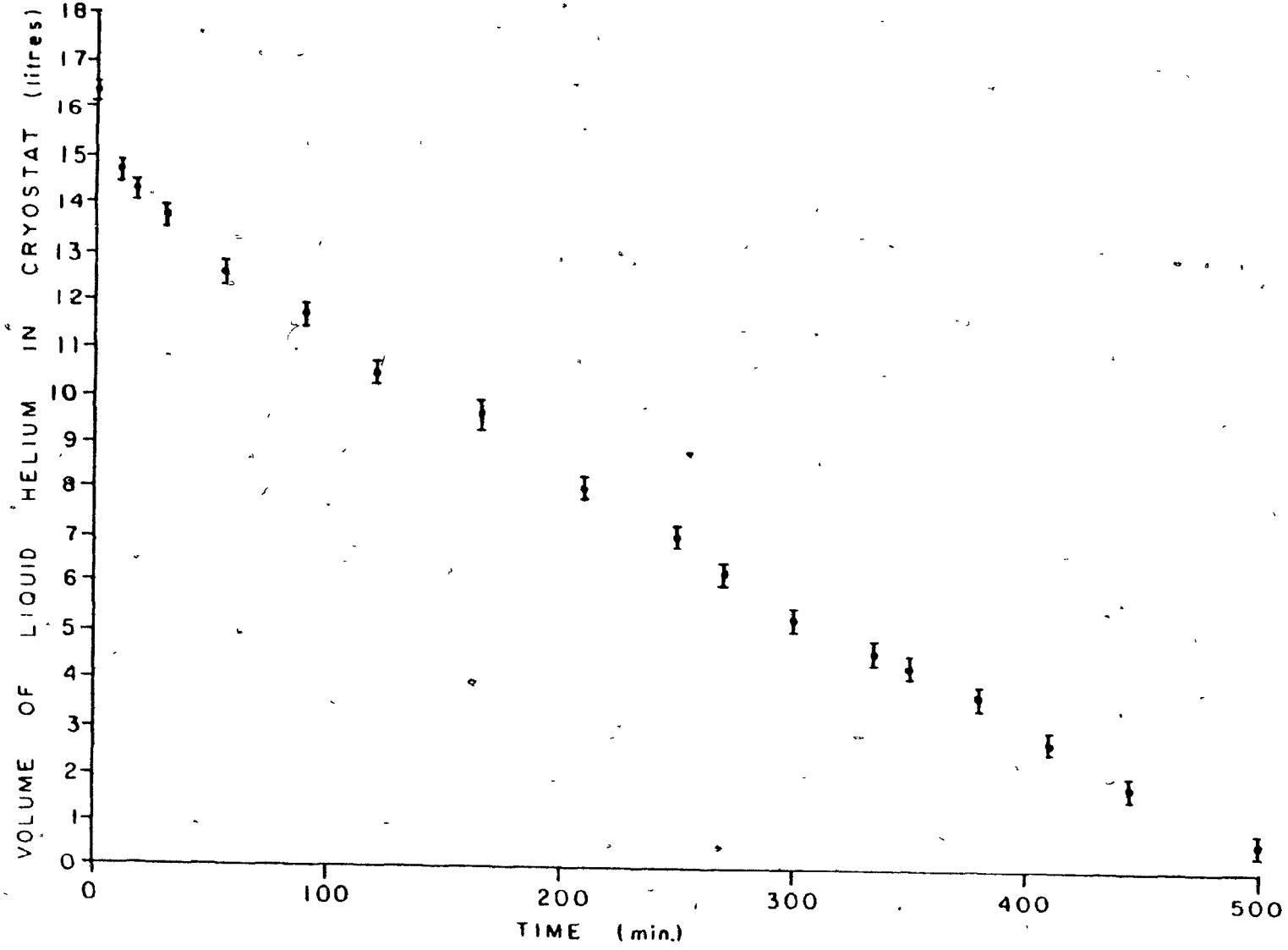
VOLUME OF LIQUID HELIUM IN CRYOSTAT (litres)
0
1
2
3
4
5
6
7
8
9
10
11
12
13
14
15
16
17
18
0
100
200
300
400
500
TIME (min.)

superinsulation, during this time the actual heat flux can be several times higher than its value at steady rate (Stoy 1960).

(2) The thermal load caused by cryosorption, on the superinsulation's inner cold layers, of gas molecules evolved from the outgassing of the warmer outer layers. This causes a net molecular flow, and hence heat transport, from the warm to the cold parts of the superinsulation (Sculock & Saull 1976). The net flow is higher in the beginning and tends to decrease with time since the rate of outgassing decreases after prolonged periods of pumping.

(3) Thermal oscillation of the helium vapor in the support tubes. These oscillations were noticed to occur (distinguished by the low frequency oscillatory sound they produced) soon after the completion of a fill. The oscillations would stop only after the level of the liquid helium had dropped some distance below the bottom opening of the tubes. These oscillations can provide enough heat transfer to the liquid helium to increase the rate of evaporation by hundreds of cubic centimeters per hour (White 1968, p.226; Wexler 1961, p.155; Rose-Inns 1964, p.7, 46; Wexler 1951).

(4) The increase in the distance between the room temperature end of the support tubes and the surface of the liquid helium as the level of the helium drops. This results in a reduction in the thermal gradient dT/dl and therefore a decrease in the amount of heat conducted down the tubes (equation 3.1). The low thermal conductivity of the stainless steel cryostat and tubes helps in establishing this thermal stratification within the cryostat.

(5) The heat load due to the A.C. losses associated with the variation of the current in the solenoid. Since the current is usually increased from zero to its desired value soon after the completion of a liquid helium fill, the heating effects caused by such a current change result in a higher consumption rate in the first half hour or so following a fill. They also cause a delay in the establishment of thermal equilibrium in the cryostat.

3.9.3 Quench Performance

One of the design criteria for superconducting magnet cryostats is that they should be able to withstand a quench of the magnet at maximum

operating current. In a quench a small region of the superconducting windings suddenly reverts to the normal (resistive) state. Because of the high current passing through the magnet, the resistive region dissipates some of the energy stored in the magnetic field through Joule heating. The low specific heats and low thermal conductivities of materials at low temperatures result in the Joule heat not dissipating away to the helium pool rapidly enough. The heat thus generated causes the temperature of neighbouring regions of the solenoid to rise above the superconducting transition temperature and turn resistive as well (Williams 1969). This runaway process, driven by the energy stored in the magnetic field, propagates rapidly throughout the coil converting the energy of the collapsing magnetic field to Joule heat in the solenoid. The time scale during which this process takes place is of the order of 1 sec for magnets similar to the one used in this work (Hancox & Catteral 1971, p.554).

The heat generated during a quench causes rapid boiling of the liquid helium and therefore a sudden large increase in the pressure inside the cryostat if the vapor is not vented adequately (Donadieu & Rose 1962, p.362). A subsequent rise in the temperature of the solenoid will ensue if the enthalpy change of helium is less than the energy that was stored in the magnetic field.

The cryostat described in this thesis is connected to a 1.5 cm (I.D.) vent tube equipped with an overpressure relief valve. Furthermore the design of the cryostat enables it to withstand internal pressures in excess of 7×10^5 Pa (100 psi) in order to ensure that it does not rupture during a quench, in case of blockage of the venting tube.

Using the value of the inductance of the solenoid (4.7 henry), the energy stored in the magnet at the operating current (100 ampere) is calculated to be 32.5 kJ.

This energy is equivalent to the heat of vaporization of 9 liters of liquid helium. However, if the magnet quenches with no liquid helium left in the cryostat and assuming that all the energy of the magnetic field is dissipated in the coil windings, then this energy will cause the temperature of the coil to rise to about 50 K only (this value is calculated from the change of enthalpy of the solenoid). For such a small temperature rise there is no need for special precautions (the introduction of an external dump resistor for example to dissipate the

energy outside the magnet and prevent excessive heating) (Montgomery 1969, p.183).

During the initial testing of the magnet system, the solenoid quenched at a current of 116 Amp. This quench caused the evaporation of about 8.7 liters of helium only indicating that some of the enthalpy of the vapor was also utilized. In normal operation, the solenoid usually quenches at around 9.5 hours after a complete liquid helium fill. The temperature rises to about (30 $\sim$ 40 K) after such a quench suggesting that the quench occurs before the liquid helium has evaporated completely. The amount left just prior to such a quench is probably less than 0.5 liters.

The fact the that temperature rise after such a quench was small was exploited to save liquid helium. The cryostat was refilled shortly after the quench and usually up to three runs were scheduled consecutively to maximize the savings. About 7.5 liters of liquid helium were lost in each of these refills to cool the solenoid, the cryostat and the transfer system (i.e. a saving of 11 liters of liquid helium per refill).

3.10 A Comparison between Multilayered Superinsulation and Liquid Nitrogen Cooled Radiation Shields

Multilayered superinsulation extending between bounderies at liquid helium and room temperature cannot match the reduction of heat flux achieved in systems utilizing liquid nitrogen cooled shields and high vacuum insulation (Kutzner et al. 1973; Kropschot 1960; Colyer 1967).

The main source of heat influx into the liquid helium reservoir in cryostat systems employing liquid nitrogen cooled shields is the heat radiation from those shields. In multilayered superinsulation heat input through radiation is reduced considerably because of the large number of successive shields. However, solid conduction through the multilayers is unavoidable and contributes quite significantly to the heat load.

Nevertheless, multiple layer superinsulation can present a more attractive option than liquid nitrogen cooled radiation shields when judged by the overall benefits it offers. Some of these benefits are:

(1) Bypassing quite a few engineering and construction problems associated with the cooled shields.

(2) A great reduction in the weight of the cryostat system.

(3) For the excellent thermal performance of cooled radiation shields to

be realized, it is crucial that the surface emissivities of the liquid helium reservoir and the radiation shields be as low as possible. Achieving this low emissivity quite often is not an easy task. Metals with low surface emissivity (e.g. Cu, Al, etc.) (Kropschot 1962, p.154; White 1968, p.220; Thornton 1971, p.495) are usually good heat conductors as well. Therefore their use in the construction of the liquid helium reservoir results in a considerable heat load due to solid conduction unless some special techniques are used. One of these techniques is to construct the support tubes from stainless steel (low thermal conductivity) and weld them to rest of the cryostat (Wexler 1961, p.157). Such welds, between two metals with different thermal expansion coefficients and which are subjected to thermal cycling, are not easy to make.

Achieving a low emissivity also requires very careful surface treatment (Wexler 1951, p.157; White 1968, p.219; Scott 1959, p.151; Leung et al. 1980) and the prevention of surface contamination and tarnishing during use or storage or even simple exposure to air (Thornton 1971, p.495). The strong dependence of the emissivity on surface contamination (Kropschot 1962, p.154) places strict demands on the vacuum system used in conjunction with the cooled shields. Certain measures have to be taken to prevent the formation of cryodeposits through the condensation of cryopumped gases or contaminents on the cold surfaces (Clark & Thorogood 1971, p.146; Long 1972).

The problem of surface contamination is not as severe in systems using superinsulations. Aluminum which is the most common reflector material in superinsulations forms, upon exposure to air, a thin protective oxide layer. This layer is transparent to infrared radiation and therefore does not increase the emissivity of the surface (Ruccia & Hinckley 1967; Leung et al. 1980). Exposure of multilayered superinsulations to different gases and storage in gaseous environments which are less than ideal (e.g. high humidity atmospheres) seems to have a very minor effect on the emissivity of the metallic deposit (Ruccia & Hinckley 1967). The problems caused by the formation of cryodeposits are also less severe in superinsulators. This is due to the large total surface area of the

foils and the fact that the cold layers (which do most of the cryosorption) are the innermost ones. These layers are not directly exposed to the contaminents which have to traverse the spaces between the outer layers before being absorbed on the inner ones. Finally, surface contamination of a few boundary layers (reduction in their emissivity) will not affect the overall performance of the superinsulation noticeably because of the large number of layers that are usually installed (Hnilicka 1960).

(4) In general, the requirement for high vacuum is more relaxed in superinsulation systems for two reasons. The first is that the multiple layers act as dividers reducing the temperature difference across which gas conduction by molecular flow is taking place so that higher pressures can be tolerated without an increase in the heat flux (see equation 3.4). The second reason is the increased tolerance to higher pressures as a result of the extension of the range of the free molecular flow region of the gas (Hnilicka 1960). Gases enter the molecular flow region when the mean free path of the molecules becomes comparable to the dimensions of the space in which they are travelling. Because of the small separtion between the successive layers of the superinsulation, the mean free path can be quite small (i.e. the gas pressure is high) when the gas enters the molecular flow region. Since it is in this region that the rate of heat transfer by the gas is diminished, its extension to higher pressures is quite desirable (Bailey 1971, p.138-142).

3.11 The Choice of NRC-2 Superinsulation

Several kinds of multilayered superinsulation are available commercially. In general, they can be classified into two types: in the first type, separate radiation shields (aluminum foils) and spacer materials (an insulator e.g. fiber glass paper) are applied in alternate layers. In the second type (similar to the one used here), the reflective shield and the spacer material are integrated into one foil (layer) by depositing aluminum on a plastic foil (e.g. mylar). Under similar conditions the second type is somewhat inferior to the first type in its thermal insulating properties (Kropschot et al. 1960; Stoy 1960; Scurlock & Saul 1976; Kropschot 1961). It would seem that this is the result of

the higher emissivity of the aluminized plastic in comparison with aluminum foils (Black & Glaser 1961).

Nevertheless, there are several advantages to using the aluminized plastic foil type. One of these advantages is the ease of installation (Leung et al. 1980), and the fact that this type does not restrict the method of application in any way (Hofmann 1970). Reflector plus spacer types require special skills and more sophisticated methods and instruments for application because of their low tensile strength in comparison to aluminized mylar (Hofmann 1970).

Another advantage offered by the aluminized mylar superinsulation is its lower bulk density and therefore lower total mass. The lower mass combined with the inherently low specific heat of aluminized mylar results in a low total heat capacity and therefore less cool down losses and a much faster approach to thermal equilibrium (Hnilicka 1960, KST).

An additional benefit derived from using aluminized mylar superinsulation is the ease with which the gases in the interlayer spaces can be evacuated in comparison to the foil plus spacer type. This is the result of the higher mean permeability and mean diffusion coefficient for gases in the aluminized mylar type due to the lack of spacers which tend to impede the diffusion of gas molecules through the insulation (Coston 1966; Nast & Williams 1967).

In comparison to other kinds of aluminized plastic superinsulation, NRC-2 foils are aluminized on one side only and the thickness of the aluminum deposit is smaller. This causes the NRC-2 superinsulation foils to have higher emissivities than other kinds with thicker deposits and therefore to be less effective in reducing heat transfer by radiation. However, because it is aluminized on one side only, the total surface area of the aluminum deposit in NRC-2 superinsulation is reduced by half and hence the total rate of outgassing is much lower than it is in other kinds (Kutzner et al. 1973). The small thickness of the aluminum deposit (250 A) results in less heat transfer by lateral and transverse solid conduction than in other types with thicker deposits (Vilet & Coston 1968; Black & Glaser 1961; Kutzner et al. 1973).

3.12 Suggestions for Further Improvements of the Cryostat System

Although the performance of the cryostat was quite satisfactory,

there is still room for some additional improvements. These proposed improvements center around decreasing the heat flux into the liquid helium reservoir through certain modifications that can be implemented in a new cryostat design. Some of these modifications would be:

(1) Increasing the length of the support tubes considerably (by a factor of two for example). Since solid conduction along these tubes is a major source of heat input, doubling the length would cut this contribution by a factor of two at least (the increased length improves the heat exchange between the rising vapor and the tube walls as well). It would also reduce the amount of radiant heat funnelled down the tubes. On the other hand, however, increasing the length of the tubes would result in an increase in the mass and size of the spectrometer.

(2) Reducing the number of tubes connected to the liquid helium reservoir by using the overpressure vent tube as a conduit for the different sensor leads and as a filling port.

(3) Blackening the inside surfaces of the support tubes with aquadag paint and/or adding radiation baffles inside their bores, would greatly reduce the thermal radiation funnelled into the cryostat (White 1968, p.230; Lynam et al. 1969; Kuraoka et al. 1979). The radiation baffles would also promote better heat exchange during precooling and speed up the approach to equilibrium evaporation conditions (Lynam et al. 1969).

(4) Using detachable current leads and operating the solenoid in a persistent current mode would certainly increase the holding time by 25% at least (table 3.6) (Colyer 1967). However, the suitability of this particular solenoid for such operation is not certain since it may have a short field decay time (depending on the number and quality of the superconductor joints).

(5) Improving the insulating properties of the superinsulation.

(a) Using a different number of layers to insulate different parts of the cryostat according to space limitations and without increasing the layer packing density (i.e. a larger number of layers than preseuntly used around the outer surfaces). The increased number of layers would reduce the contributions of both the radiation and the conduction modes of heat transfer

(equations 3.6, 3.7, 3.9) (Adelberg 1962, p.357; Stoy 1960; Hnilicka 1960, KST). However, the increase in the number of layers would also result in a reduction in the pumping speed in the interlayer spaces and in an increase in the overall outgassing rate (due to the increase in the surface area). This would give rise to higher residual gas pressures between the superinsulation foils, and therefore more residual gas conduction.

(b) Perforating the multilayered superinsulation would help to overcome the problem of residual gas quite considerably by providing more passageways for evacuating the gas (Hofmann 1970, Adelberg 1962, p.372; Mikhalchenko et al. 1976; Bailey 1971, p.152; Price 1968; Barron 1972, KST). Notwithstanding, perforating the superinsulation causes an increase in the contribution of radiation to the total heat. The presence of holes exposes regions of a radiation shield to radiant heat emanating not from a neighbouring shield but from ones further away and which therefore at higher temperatures (Barron 1972; Ruccia et al. 1967). A compromise between the reduction in residual gas conduction and the increase in radiant heat flux has to be arrived at. Barron (1972) gives some useful indications as to how such a compromise can be reached.

(c) Interleaving the aluminized mylar foils with getter loaded spacer material (thermal insulator). This would result in a reduction in the residual gas pressure in the interlayer spaces especially after the introduction of cryogenic fluid into the cryostat (Scurlock & Saul 1976).

(d) A further reduction in the amount of heat conducted by the residual gas can be achieved through the use of heat sealable polyester base tape for fastening the superinsulation layers instead of the pressure sensitive type used.

(6) Using multishielding techniques. In this technique a combination of multilayer superinsulation with one or more vapor cooled radiation shields interleaved among the multilayers is used. It can improve the effectiveness of the insulation to the extent that it will surpass both the performance of the superinsulation alone and that of liquid nitrogen cooled heat shields (Colyer 1967).

The vapor cooled radiation shields are usually constructed from thin, reflective, highly conductive sheets (of Al or Cu) attached to heat exchangers placed at suitable levels in the vent tube (Paivanas et al. 1965). Thus some of the enthalpy of the rising helium is used to intercept and extract a significant portion of the heat inflow through the superinsulation before it reaches the liquid helium reservoir. This technique would also result in a considerable reduction in the weight of the superinsulation (Niendorf & Choksi 1967) and therefore would speed up the approach to thermal equilibrium and minimum helium loss conditions. However, the construction of the heat exchangers and their connections to the vent tube and the shields might pose some technical problems (Thornton 1971, p.499).

CHAPTER 4

THE SOURCE-DETECTOR SYSTEM

The energy dispersive element used in the spectrometer described in this thesis is a high purity germanium diode. It was chosen because of the outstanding characteristics of semiconductor detectors, especially Ge(HP), as spectrometers.

Semiconductor detectors figure prominently among the detector types most widely used in the study of nuclear radiation today. They are solid state analoges of the gaseous ionization chamber and enjoy several advantages over other types of radiation spectrometers. The most important advantages that they offer over other multichannel energy deposition spectrometers are their linearity and superior energy resolution. Furthermore, as a result of the high density of semiconductor materials (especially germanium), detectors with small dimensions can be used to study even the most energetic β decays.

Silicon and germanium have been the choice materials for the manufacture of semiconductor detectors, with silicon detectors predominating in the field of charged particle spectroscopy and germanium detectors being the type most commonly used in gamma ray spectroscopy (Knoll 1979 p. 360). This situation, however, is rapidly changing with the increase in the popularity of Ge(HP) β spectrometers (see Chapter 2).

4.1 Principles of Operation of Semiconductors Radiation Detectors

In analogy to gaseous ionization chambers, the operation of semiconductor radiation detectors is based on the principle of using the energy deposited in the detector material by the incident radiation to generate electron-hole pairs. By collecting these charge carriers on electrical contacts on the surfaces of the semiconductor, an electric signal is produced which is proportional to the amount of energy deposited in the detector.

This section will briefly review the principles involved in the working of semiconductor detectors concentrating mainly on high purity germanium detectors.

4.1.1 The Band Structure

The preriodic lattice of crystalline materials establishes allowed energy bands for electrons within the solid. These energy bands arise from the allowed energy levels for electrons in the individual atoms which make up the crystal. In an isolated atom, the allowed energies are very sharply defined, however, when a collection of atoms is brought together to form a crystal, the Pauli principle imposes that no two electrons can have exactly the same set of quantum number values. The atomic energy levels therefore change to an extent dictated by the closeness of the atoms and the periodicity of the atomic field generated by the atomic nuclei. The sharply defined energy levels of the separate atoms are broadened into bands of levels each of which is non-localized and is a propoerty of the whole crystal (Dearnaley & Northrop 1963 p. 58). These bands of allowed energy levels are separated from each other by forbidden gaps. The width of the forbidden gaps is related to the nature of the chemical bond in the solid.

Both silicon and germanium crystals are particularly simple in their structure. Each atom in a pure crystal of either of these semiconductor materials is tetrahedrally surrounded by four other similar atoms and shares one covalent bond with each of them (Diamond type crystal structure) (Restelli 1968 p. 14).

At very low termperatures ($\approx$0 K), in a perfect crystal, all of the valancy electrons are bound into the structure and no electons are available for electric conduction. These bound valancy electrons occupy an allowed energy band called the valance band. In the case of pure crystalline silicon and germanium, the valance band is completely filled at very low temperatures. The next allowed, higher lying band is called a conduction band and represents electrons that are free to migrate through the crystal. An energy band gap separates the valance and the conduction bands. The characteristic property of a monocrystalline semiconducting material, such as silicon or germanium, is the small size of the band gap. The gap, at 0 K, is 1.165 eV for silicon and 0.746 eV for germanium. The band gap in these two semiconductors increases with temperature reaching a value at 300 K which is about 10% larger than its value at 0 K (Restelli 1968 p. 14).

4.1.2 The Generation of Charge Carriers

4.1.2a The Thermal Generation of Electron-Hole Pairs

At any non-zero temperature a small number of the covalent bonds in the crystal are broken by thermal excitations so that charge carriers are present in the material and are free to drift throughout the crystal. This breaking of the bond can be viewed alternatively as the elevation of an electron from the valancy band to the conduction band due to the fact that the thermal energy of this electron is greater than the gap between the two bands. The excitation of the electron into the higher band not only creates an electron in the otherwise empty conduction band but it also leaves a vacancy (a hole) in the otherwise full valance band. The combination of the two charge carriers thus created is called an electron-hole pair. If an external electric field is applied to the crystal, the electron and the hole will drift in opposite directions parallel to the applied field.

For an intrinsic semiconductor (perfect crystal with no electrically active impurities), the number of electrons that are thermally excited to the conduction band (which is equal to the number of holes left in the valance band) is given by: (Dearnaley & Northrop 1963 p. 60; Kittel 1976 p. 229; Haller 1982)

$$n_i = \sqrt{N_C N_V}\ T^{3/2}\ \exp(-E_g/2kT) \qquad 4.1$$

where

n_i = The number of conduction electrons per unit volume (concentration of conduction electrons)

N_C, N_V = The effective density of states in the conduction and valance bands respectively

T = The absolute temperature

k = The Boltzman constant

E_g = The band gap

The introduction of electrically active impurities into the crystal structure (doping) changes the relative concentration of charge carriers (increases the concentration of electrons in the case of a donor impurity and the concentration of holes in the case of an acceptor impurity)

however, the product of the concentrations of the two kinds of charge carriers remains constant. Thus the product

$$n_i p_i = N_c N_v \exp(-E_g/kT) \qquad 4.2$$

where

P_i = The concentration of holes

(The rest of the symbols are the same as in equation 4.1)

remains constant and is the same whether the semiconductor is intrinsic or doped (extrinsic) (Restelli 1968 p. 15; Kittel 1976 p. 229, Knoll 1979 p. 368). For germanium the product of the concentrations of the two charge carriers, at room termperature, is 5.8×10^{26} cm^{-6} (Knoll 1979 p. 366).

In high purity germanium detectors, the concentration of impurities (doping) is usually of the order of 10^{10} impurities/cm^3 (Knoll 1979 p. 493). Due to the small band gap of germanium, the number of thermally generated charge carriers (intrinsic carrier density), at room temperature (300 K), is much higher (2.4×10^{13} /cm^3) (Knoll 1979 p.363). Therefore, the electrical conductivity of high purity germanium at room temperature is dominated by the intrinsic charge carrier density which results in a value of 47 Ω cm for the resistivity of germanium at room temperature (Goulding 1966; Restelli 1968; Knoll 1979 p. 363). Consequently, germanium detectors must be operated at cryogenic temperatures (typically liquid nitrogen temperatures) to decrease the number of thermally generated charge carriers (i.e. reduce the leakage current) in order to be able to detect charge carriers that are produced by the ionizing radiation (Knoll 1979 p. 391; Haller & Goulding 1981 p. 811; Haller 1982).

4.1.2b The Generation of Charge Carriers by Ionizing Radiation

Ionizing radiation incident on the semiconductor material can generate charge carriers in excess of those generated by thermal excitations. The details of the mechanisms through which the incident radiation deposits its energy during its interaction with the semiconductor material are quite complicated. However, the following simplified model can serve to illustrate the charge production process during such an interaction (see Restelli & Rota 1968 p. 76).

A high energy charged particle incident on a semiconductor, or an

electron produced by a γ ray interaction with the semiconductor material produces secondary electrons of lower energy in the semiconductor by impact ionization. Subsequently, these electrons can produce more electron-hole pairs in the semiconductor by imparting enough energy to some elctrons in the crystal lattice to raise them from the valance band (or lower lying states) to the conduction band. The energetic electrons and holes thus generated can produce further ionization and so on. This shower process continues until the kinetic energy of the charge carriers is no longer sufficient to excite an electron across the forbidden energy gap (and therefore to create an electron-hole pair).

During the ionization events that take place in the semiconductor material, the energy of the incident charged particles is reduced by an amount equal to the band gap energy plus the kinetic energy acquired by the electron-hole pair. The sharing of the energy between the ionizing charged particle and the electron-hole pair can be considered to be random in nature, while the division of energy between the electron and the hole in the pair is dependent on the details of the band structure of the material.

Electrons travelling through the semiconductor material can also lose some of their energy through interactions with the crystal lattice itself and the production of phonons (lattice vibrations). Such interactions dissipate a considerable amount of energy without producing a useful signal since they do not result in the production of charge carriers. Furthermore, the large number of electrons produced at the end of the shower process, not having sufficient energy to produce secondary ionization, quickly (after $\sim 10^{-12}$ sec) reach thermal equilibrium with the lattice by losing their kinetic energy through the generation of more phonons. Because of all of these energy losses in nonionizing events, the average energy required to produce an electron-hole pair (ϵ) is considerably greater than the band gap energy. In germanium, at 77 K, ϵ is more than 4 time the band gap energy (Knoll 1979 p. 363) i.e. the energy used in the ionizing events makes up only about 25% of the total energy deposited by the radiation in the detector material.

The model describing the ionization processes used above is due to Shockley and Van Roosbroeck. It was summarized here from the information given in the following references: Dearnaley & Northrop (1963 p. 65);

Goulding (1966); Restelli & Rota (1968). An alternative model for the ionization processes in semiconductors has been proposed by Klein (see Restelli & Rota 1968 p. 80). This model explains the production of electron-hole pairs in irradiated semiconductors in terms of the generation and subsequent decay of plasmons (collective oscillations of the electron paritcle density in the solid.

The average energy required to produce an electron-hole pair, is experimentally observed to be largely independent the type of incident radiation and the energy deposited in the material (Price 1964 p. 217; Restelli & Rota 1968; Goulding & Pehl 1974 p. 305; Knoll 1979 p. 372; Haller & Goulding 1981 p. 812). This is mainly due to the fact that the dominant production of electron-hole pairs occurs at the low energy "tails" of the shower process and these tails are quite insensitive to the details of the high energy processes that led to their existance (Haller & Goulding 1981 p. 812). The average energy per electron-hole pair (ϵ) (sometimes also referred to loosely as the ionization energy) has a value of 2.96 eV for germanium and 3.76 eV for silicon at 77 K (Restelli 1968 p. 14).

The fact that ϵ is independent of energy is responsible for the excellent linearity of the energy response of semiconductor detectors. It is this linearity that makes these semiconductor detectors excellent radiation spectrometers. The independence of the value of ϵ of both the type and the energy of the incident radiation eases the problems of calibrating semiconductor β spectrometers quite significantly.

The small value of ϵ in semiconductor detectors in comparison to gas filled detectors (ϵ in semiconductors $\approx$1/10 of the amount of energy required to create an electron-hole pair in gases), results in a 10 fold increase in the mean number of charge carriers produced by a given amount of energy deposited in the detector. This increase in the number of charge carriers has two beneficial effects on the energy resolution attainable with semiconductor detectors. The greater amount of charge produced per unit deposited energy leads to a larger signal to noise ratio , and therefore better resolution, especially at low energies. In addition, as the mean number of charge carriers per unit energy increases, the statistical fluctuation in the number of these information carriers becomes a smaller fraction of the total number, thus leading to better

resolution.

In semiconductor materials the statistical fluctuations in the number of charge carriers per unit energy loss is smaller than the value expected on the basis of Poisson statistics alone. Poisson statistics would hold if all the events along the track of the ionizing particle were indpendent of each other (i.e. if there were no correlations in the formation of consecutive electron-hole pairs). This is not the case in semicondcutors since the ionizing events can not be regarded as completely indpendent as was clearly shown above in the description of the ionization processes in semiconductors. As a result of the interdependence of the ionization events, the standard deviation of the number of charge carriers produced is given by:

$$\sigma = \sqrt{F\,N} = \sqrt{\frac{F\,E}{\epsilon}} \qquad 4.3$$

where

σ = The standard deviation in the number of charge carriers

ϵ = The average energy required to produce an electron-hole pair

E = The energy deposited in the semiconductor

N = The number of electron-hole pairs produced

F = The Fano factor; a numerical factor $0 < F < 1$

The measured values for the Fano factor in germanium at 77 K are typically around 0.1 (Tavendale 1967 p. 84; Restelli & Rota 1968 p. 97; Goulding & Pehl 1974 p. 305; Pehl 1977; Knoll 1979 p. 363; Haller & Goulding 1981 p. 812; Tsoulfanidis 1983 p. 280).

The full width at half maximum of the distribution in N (the number of electron hole pairs) is given by

$$FWHM = 2\sqrt{2\ln 2}\,\sigma \qquad 4.4$$

Therefore

$$\frac{\Delta E}{E} = 2\sqrt{2\ln 2}\sqrt{\frac{F}{N}} = 2\sqrt{2\ln 2}\sqrt{\frac{F\epsilon}{E}} \qquad 4.5$$

where

E = The energy deposited in the detector

ΔE = the fwhm of energy distribution

(Haller & Goulding 1981 p. 811; Tsoulfanidis 1983 p. 280). The ratio $\Delta E/E$ represents the contribution of the statistics of electron-hole production

to the resolution of the semiconductor detector. It is therefore the ultimate resolution attainable with semiconductor detectors. The contributions of electronic noise and detector leakage current to the resolution of semiconductor spectrometers are usually considerably larger than the contribution of charge production statistics, especially at low energies (Knoll 1979 p. 374, 423). Furthermore, problems in charge collection caused by electron-hole recombination and charge trapping can also contribute to the resolution as well.

At an energy of 1 MeV, $\Delta E/E$ calculated from equation 4.4 above is 0.13%. The measured resolution of the germanium spectrometer used in this work is 0.45% at 1 MeV.

4.1.3 Charge Collection

An electric field applied to the semiconductor material will separate the two types of charge carriers that are created (either thermally or by ionizing radiation) in the semiconductor and will cause them to drift in opposite directions parallel to the applied electric field. The drift velocity of the charge carriers in the applied electric field is a function of the field strength. In germanium, the drift velocity reaches a saturation value of about 10^7 cm/sec at an applied electric field of about 1000 V/cm. This high saturation velocity (which is easily achievable in typical germanium detectors) is responsible for the fast rise times of the pulses that are generated in the semiconductor detectors.

4.1.4 Radiation Detector Construction

In order to be able to measure the amount of energy deposited by the ionizing radiation in the semiconductor medium, the charge carriers that are produced by the incident radiation have to be collected at either end of the material and counted. To achieve a rapid and efficient charge collection, a strong electric field ($\sim$ 1000 V/cm) has to be applied to the semiconductor medium through the electric contacts on which the charge is collected. If ohmic (i.e. non rectifying) contacts are used, the strong applied electric fields result in large currents, of the order of 1 ampere, flowing through the semiconductor medium, even at liquid nitrogen temperature. Such high currents make the detection of the very small

currents (10^{-6} amp) that are generated by radiation produced charge carriers totally undetectable (Pehl 1977, Knoll 1979 p. 375).

To overcome this problem, "blocking" contacts that do no inject charge into the semiconductor material must be used. One common method of achieving a blocking contact structure is to form a p-n junction in the semiconductor material (or a surface barrier junction on the surface of the semiconductor material) and operate it as a reverse biased diode (Goulding & Pehl 1974 p. 312).

4.2 The β Detector Used in the Present Spectrometer

The energy sensitive detector used in this work is a Ge(HP) diode supplied by Aptec Engineering Ltd. (Canada). It is a planar detector with a 15 mm sensitive thickness and 500 mm^2 active area (2.54 cm diameter). The detector is manufactured from high purity P-type germanium with a diffused p-n junction structure. The n^+ contact is the back contact; it is made by the diffusion of a thin layer of lithium on the back surface of the detector. The front contact, through which the β particles enter the detector, is a thin evaporated metallic contact.

Voltage pulses from the Ge(HP) detector were fed to a Princeton γ-Tech model RG-11 preamplifier and from there to an Ortec model 572 amplifier. The pulse shaping time constant of the amplifier was set to 1 μsec. From the amplifier, the pulses were routed to a Tracor Northern TN-1212 A.D.C. interfaced to a PDP-15 computer. The "inhibit" pulse output from the amplifier was connected to the A.D.C. to gate it in an anticoincidence mode in order to reduce pulse pile up. In all experiments, the output of an electronic pulser was connected to the "test" input of the preamplifier to enable corrections for dead time lossses and pile up and to monitor gain stability. An Ortec model 459 high voltage power supply was used to bias the detector.

When a volatage is applied to the detector, a depletion layer starts to from at the p-n junction near the back contact and advances to the front of the detector as the voltage is increased. At the recommended operating voltage (1000 V volts), the detector is over depleted and only a very thin dead layer ($\sim$1 μm of germanium) is left at the entrance surface.

Since no information was available from the manufacturer on the depletion bias of the detector (the minimum voltage at which the depletion

layer extends to cover the full sensitive thickness of the detector), it was directly measured using the conversion electron lines from a ^{207}Bi source. The depletion voltage was measured by varying the bias on the detector and observing the changes in the shape and position of the conversion electron lines as measured by the detector. The onset of such changes in the electron peaks as the voltage of the detector is lowered would indicate that the depletion layer does not extend all the way to the front contact and that the electrons are traversing the dead layer left between the front edge of the depletion layer (the sensitive thicknesss) and the front surface of the detector. At biases below 450 volts, the K conversion line of the 569.6 keV transition disappears completely indicating that the thickness of the dead layer is larger than the range of 0.5 MeV electrons in germanium. Since this range is quite small ($\sim$ 0.5 mm) in comparison to the thickness of the detector, 450 volts was taken as the depletion voltage of the detector (the punch through voltage).

Using the value of the depletion voltage (450 volts) and the total depletion thickness of the detector (15 mm), and with the aid of equations (11-13, 11-15) from Knoll (1979 p. 383), the values of the net concentration of the electrically active impurities (acceptor type) in the detector material is calculated to be $N_A = 3.5 \times 10^9$ impurities/cm^3. Similarly the value of the detector's capacitance is calculated to be 4.7 pf.

The typical resolution values achieved with the detector are 4 $\sim$ 5 keV for a 1 MeV γ ray and a slightly worse resolution for electrons of the same energy (due to energy losses in the dead layers in the source and the detector's front contact). The resolution of an electronic pulser peak ($\sim$ 4 keV) is only slightly better than that of the γ ray peak indicating that the charge collection processes in the detector do not contribute significantly to the resolution.

The major contributions to the spectrometer's resolution come from the leakage current of the detector (especially the surface leakage current) and the preamplifier noise. Since the preamplifier noise is a strong function of the capacitance with which the input of the preamplifiers is loaded (Knoll 1979 p. 652), it is particularly important in this spectrometer. The length of the cable connecting the detector to the preamplifier ($\sim$ 30 cm) contributes significantly to the input

capacitance. This cable length was necessary since the preamplifier had to be kept in a low magnetic field region.

In order to improve the resolution of a spectrometer system similar to the one described in this thesis (a superconducting solenoid plus a solid state detector system), Andersen (1968) installed the first stage of the preamplifier (the FET) on the cold finger very close to the detector. A significant improvement in resolution is achieved in this case as a result of two effects: the reduction in the thermal noise of the preamplifier due to cooling, and the decrease in the input capacitance to the preamplifier that results from the elimination of the capacitance of the long cable connecting it to the detector.

One of the advantages gained from the use of the superconducting solenoid in the present spectrometer is the reduction in detector background count rate. Because of the location of the detector inside the bore of the magnet surrounded by the solenoid and the liquid helium cryostat, it is quite well shielded from the ambient background. The typical background count rate is 3 to 5 c.p.s.

The detector was calibrated at energies below 1.5 MeV using conversion electron lines from ^{207}Bi. At higher energies, γ rays from standard sources and from ^{66}Ga were used for calibration. Under the influence of the strong magnetic field of the solenoid, a small difference between the calibrations obtained using electrons versus those obtained with γ rays was noticed. This β ray calibration shift was thoroughly investigated and accurately corrected for (Hetherington 1984).

The choice of a detector with a 15 mm sensitive thickness in the present spectrometer was motivated by the desire to study β decays with high endpoint energies (>10 MeV). However, there is a limit on the maximum β ray energy that can be studied with the spectrometer without introducing excessive distortions to the β spectrum. This limit is imposed by the strength of the magnetic field of the solenoid and the surface area of the detector. Its value is slightly less than 6 MeV in the present spectrometer (see section 5.4). Hence, the use of a thinner detector ($\sim$8 mm for example) would have probably been a better choice. The thinner detector would be less sensitive to γ rays, have a smaller capacitance; better resolution and faster pulse risetime, and show a smaller β ray calibration shift in the strong magnetic field of the

solenoid.

4.3 The Source-Detector Chamber

The radioactive source and the cold (liquid nitrogen temperature) germanium detector are mounted in the same vacuum chamber with no windows separating them from each other. This was necessary in order to avoid the β spectrum distortions that are caused by β particle scattering in the window material. The source-detector vacuum chamber consists mainly of a 70 cm long stainless steel tube (5 cm I.D.) which fits inside the room temperature bore of the superconducting solenoid and is completely separate from the magnet's vacuum chamber (see Figure 4.1).

One end of the stainless steel tube is connected through a gate valve to a forechamber through which new radioactive sources are introduced in the detector's vacuum chamber. On the other end, the stainless steel tube is coupled to the detector cryostat. The detector cryostate was taken from an old Ge(Li) spectrometer and modified so that the copper cold finger on which the Ge(HP) detector is mounted extends approximately 25 cm into the source-detector vacuum chamber. The other end of the cold finger dips into a liquid nitrogen reservoir. The bottom of the detector cryostat (around the cold finger) is filled with a small quantity ($\sim$ 50g) of zeolite to maintain the vacuum when the detector is at liquid nitrogen temperature. The pumping action of the cold cathode (PIG) ionization gauge which is mounted on the detector cryostat aids in maintaining the vacuum as well. An electrical feedthrough at one end of the vacuum chamber provides an electrical connection to the detector through a 20 cm long cable.

4.4 The Vacuum System

The vacuum system that was originally used with this spectrometer consisted of pumping station made up of a 2 inch (5 cm) oil diffusion pump equipped with a liquid nitrogen cooled baffle, and a mechanical rotary pump.

Severe problems, caused by condensation on the detector's surface, were experienced with this vacuum system. The condensation on the detector resulted in large leakage currents, a significant deterioration in resolution (10 $\sim$ 20 keV resolution), and most importantly, detector

Figure 4.1

Schematic drawing of the source-detector vacuum chamber.

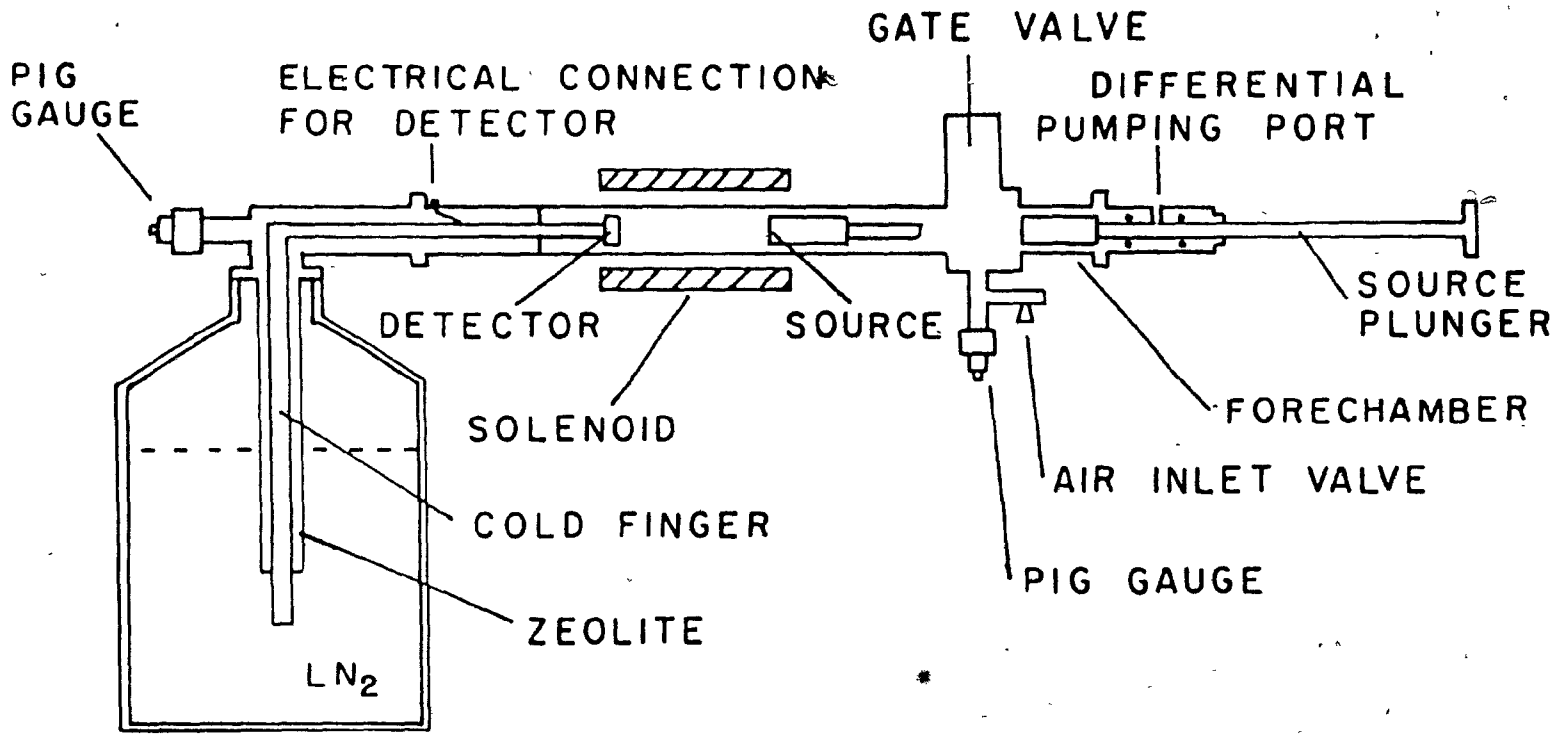
GATE VALVE
PIG GAUGE
ELECTRICAL CONNECTION FOR DETECTOR
DIFFERENTIAL PUMPING PORT
DETECTOR
SOURCE
SOURCE PLUNGER
SOLENOID
FORECHAMBER
AIR INLET VALVE
COLD FINGER
PIG GAUGE
ZEOLITE
LN_2

breakdowns at biases below the operating voltage.

A residual gas analysis of the gas in the vacuum chamber showed that the condensation had most likely been caused by hydrocarbons backstreaming from the pumps.

Following this finding, a complete overhaul of the vacuum system was undertaken. The detector was cleaned (after warming it up to room temperature) by carefully wiping its front surface with a cotton swab soaked in ethanol. The detector was then heated to 40°-60° C, under vacuum ($\sim 10^{-3}$ Pa), and maintained in this temperature range for several hours to remove any traces of condensation that were left. The vacuum chamber and the various pumping lines and components in the vacuum system were thoroughly cleaned with solvents and leak tested. And a new charge of zeolite (molecular sieve 5A) was placed in the bottom of the detector cryostat.

In addition to these measures, the possibility of replacing the diffusion pump station with an oil free pumping system was investigated. Two options for an oil free system were considered: a turbomolecular pump and a cryogenic pump. The turbomolecular pump that was tested caused excessive electronic noise in the detector. The detector's microphonic nature (Goulding & Pehl 1974), and the vibrations caused by the turbomolecular pump are responsible for this noise. The problems were further aggravated by the length of the cold finger on which the detector is mounted. Therefore, the decision was made to avoid the use of a turbomolecular pump. As for the cryogenic pump option, it was discarded because the need for frequent radioactive source changes (and therefore repeated pumping of the forechamber) can result in the saturation of a limited capacity cryogenic pump. In addition to these drawbacks, the two oil free pumping systems are also quite expensive.

The final pumping system design that was arrived at represented a compromise. The oil diffusion pumping station was maintained but only after significant improvements in its performance. The pumping system was also supplemented with a cryosorption pump that was installed at the forechamber (see Figure 4.2). Along the line of improving the performance of the oil diffusion pump station, two steps were taken to minimize the backstreaming of hydrocarbons from the diffusion pump and the mechanical pump. The first was the addition of a water cooled baffle between the

Figure 4.2

Schematic drawing of the spectrometer vacuum system

1. Thermocouple Vacuum Gauge
2. Cold Cathode Vacuum Gauge
3. Valve
4. Gate Valve
5. Oil Diffusion Pump
6. Mechanical Pump
7. Sorption Trap
8. Air Admittance Valve
9. Flexible Pumping Line
10. Sliding Source Plunger
11. Forechamber
12. Cryosorption Pump
13. Source-Detector Vacuum Chamber
14. Zeolite at Liquid Nitrogen Temperature in the Detector Cryostat
15. Superconducting Solenoid Vacuum Chamber
16. Liquid Nitrogen Cooled Baffle
17. Water Cooled Baffle

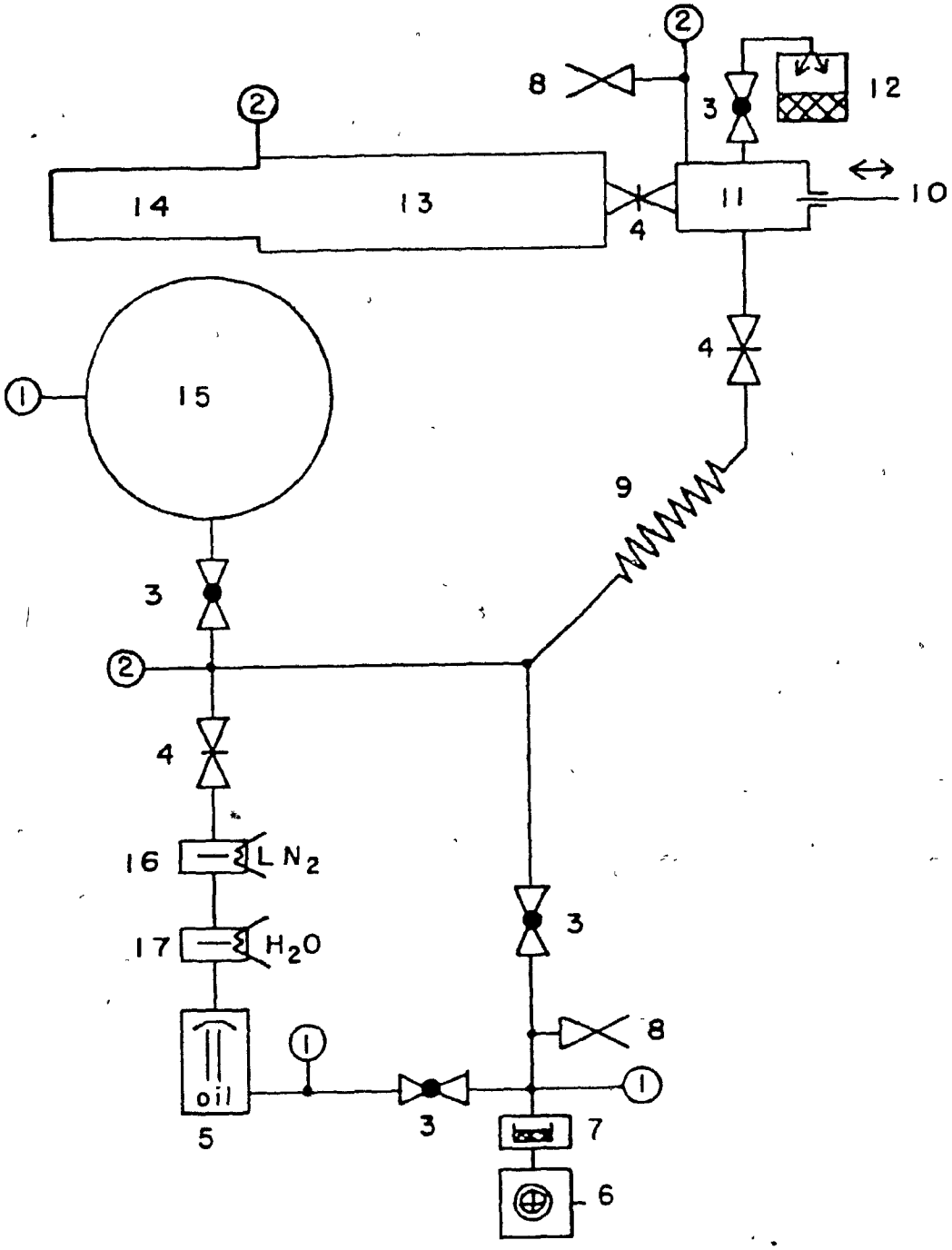
2
8
3
12
2
14
13
4
11
10
4
15
1
9
3
2
4
16
$L N_2$
17
H_2O
3
8
oil
1
1
5
3
7
6

diffusion pump and the liquid nitrogen cooled baffle. The second was the installation of a room temperature sorption trap (filled with type 13X molecular sieve) on the intake of the rotary pump. After these measures were effected, a residual gas analysis showed a drastic reduction in the concentration of hydrocarbons in the vacuum chamber.

The diffusion pump station is used to pump the source-detector vacuum chamber only when the detector is at room temperature (to avoid the posssibility of condensation on the detector completely). It is also used to reduce the pressure in the forechamber to $1x10^{-2}$ Pa after a new source is introduced.

When the detector is at liquid nitrogen temperature, the vacuum in detector chamber is maintained by the pumping action of the zeolite around the bottom of the cold finger. However, this small quantity of zeolite can not be relied on when frequent source changes are contemplated; the small gas leak that accompanies the introduction of a new source into the detector chamber can easily result in the saturation of the zeolite after a few source changes. Attempting to reduce the amount of gas admitted into the detector chamber after each source change by pumping out the forechamber with the diffusion pump until a high vacuum ($< 10^{-3}$ Pa) is achieved can also cause problems. In addition to the long waiting time ($\sim$ 20 minutes), prolonged pumping with the diffusion pump at low pressures (i.e. in the molecular flow region) increases the possibility of backstreaming from the diffusion pump. (The rate of backstreaming reaches a maximum at a pressure of $\approx 5x10^{-2}$ Pa; see Rettinghaus & Huber 1974). To alleviate these problems, a liquid nitrogen cooled sorption pump was installed at the forechamber.

Although cryosorption pumps are designed for use as oil free roughing pumps, it was found possible to use a cryosorption pump to achieve a high vacuum ($< 10^{-4}$ Pa) in our system. A small prototype sorption pump was built and its performance tested under different conditions. This prototype pump contained a small charge of molecular sieve type 5A placed in a wire screen basket that surrounds a liquid nitrogen cooled thimble. It was found that after baking the zeolite at a temperature of 250°C, in vacuum, for several hours, pressures of 10^{-4} Pa and less can be easily reached when the zeolite is cooled to liquid nitrogen temperature. No saturation effects were observed except when a deliberate leak was

introduced in the system. (The absorption capacity of molecular sieve 5A at liquid nitrogen temperature and a pressure of 10^{-3} Pa is $\sim$ 50 cm^3 of nitrogen gas (STP) per gram of zeolite; see Stern & DiPaolo 1967; Davey 1971 for more detailed data).

After these successful tests were completed, a commercially supplied cryosorption pump was installed at the forechamber. (The sorption pump was supplied by Varian Associates). This sorption pump is simply a large reservoir filled with about 1 Kg of zeolite (molecular sieve type 5A) It is efficiently cooled by immersing it in a liquid nitrogen dewar. The liquid nitrogen dewar was equipped with an automatic filling system to ensure the continuous operation of the pump for long periods of time.

The performance of the cryosorption system was quite satisfactory even after operating it continuously for periods of days with many source charge taking place during these periods. The zeolite showed no signs of saturation during normal operation and pressures of 10^{-3} Pa and less were easily achieved in the forechamber. The presence of atmospheric gases that are not efficiently adsorbed by the zeolite at liquid nitrogen temperature (mainly helium and neon) did not cause any problems since only minute quantities of these gases are left in the forechamber after it is evacuated by the diffusion pump.

Following each long run, the zeolite in the sorption pump was baked at 250° C, in vacuum ($\sim$0.1Pa), for several hours to expel the absorbed gases and reactivate the zeolite. Similarly, the zeolite in the detector cryostat was regenerated after each run by warming it up to $\sim$50°C, for several hours, in vacuum. The zeolite was warmed up by replacing the liquid nitrogen reservoir in (Figure 4.1) a hot water bath. (The presence of the Ge(HP) detector did not permit the use of higher temperatures during the reactivation of the zeolite).

A schematic drawing of the vacuum system is given (Figure 4.2). The vacuum system is built entirely from aluminum and stainless steel components. Copper gaskets and rubber seals (Buna-N and Viton 'O' rings) were used in the various demountable couplings in the vacuum system. The 5 cm (nominal diameter) flexible pumping line allows one to change the position of the source-detector chamber (and therefore the position of the detector) with respect to the superconducting solenoid (see also Figure

4.5). The strong magnetic field of the superconducting solenoid was not noticed to affect the operation of the cold cathode vacuum gauges.

The pressure in the source-detector vacuum chamber during the operation of the spectrometer was usually in the range 10^{-3} - 10^{-4} Pa. At these pressures, the scattering of β particles, as a result of their collisions with air molecules, is negligible and does not affect the measured shape of the β spectrum (Paul 1965; Booij 1970; Mladjenovic 1976 p. 31; Hughes 1980 and references therein).

Since the vacuum chamber of the superconducting solenoid cryostat needed occasional pumping to maintain its vacuum, it was connected, through a valve, to the diffusion pump station and evacuated during the time when the diffusion pump was not being used to pump the forechamber.

4.5 Source Mountings

Most of the radioactive sources used in this spectrometer were deposited on a thin (0.3 mg/cm^2) mylar film which was glued to an aluminum ring. The inner radius of the ring is larger than the maximum diameter of the orbit of the most energetic β particles that can be studied with the spectrometer. (The inner radius of the source ring is 1.4 cm, and the maximum diameter of the orbit of 5.8 MeV electrons at the source position is 1.28 cm). This prevents the scattering of β particles from the source ring. To avoid backscattering from the source holder, the source ring was mounted on a 10 cm long hollow aluminum tube whose inner diameter is slightly larger than the inner diameter of the source ring (see Figure 5.7). The hollow aluminum tube was fastened to the end of the source plunger (a hollow stainless steel tube, 1.8 cm inner diameter).

4.6 Source Introduction Methods

Two source introduction methods were used in conjunction with this spectrometer:

4.6.1 Manual Plunger System

For the introduction of long lived sources into the sspectrometer, a manual plunger system and a vacuum forechamber were used (see Figures 4.1, 4.3, 4.4, 4.5). Differential pumping was applied between the sliding seals on the plunger and the gate valve that separates the forechamber

Figure 4.3

A photograph showing a side view of the beta spectrometer and its associated equipment.

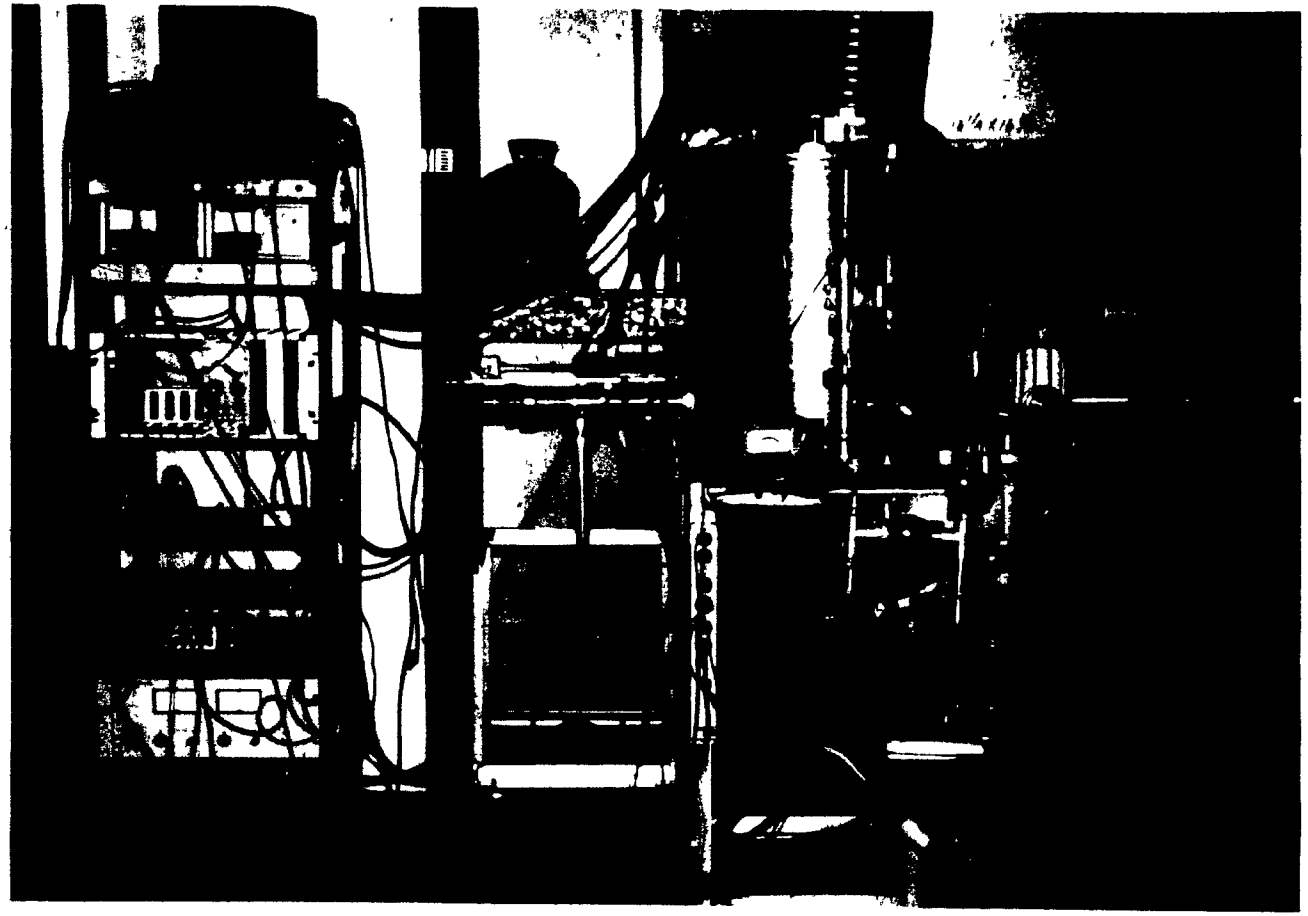

Figure 4.4

A front view of the beta spectrometer. The manual plunger, the forechamber and the sorption pump are shown in the foreground.

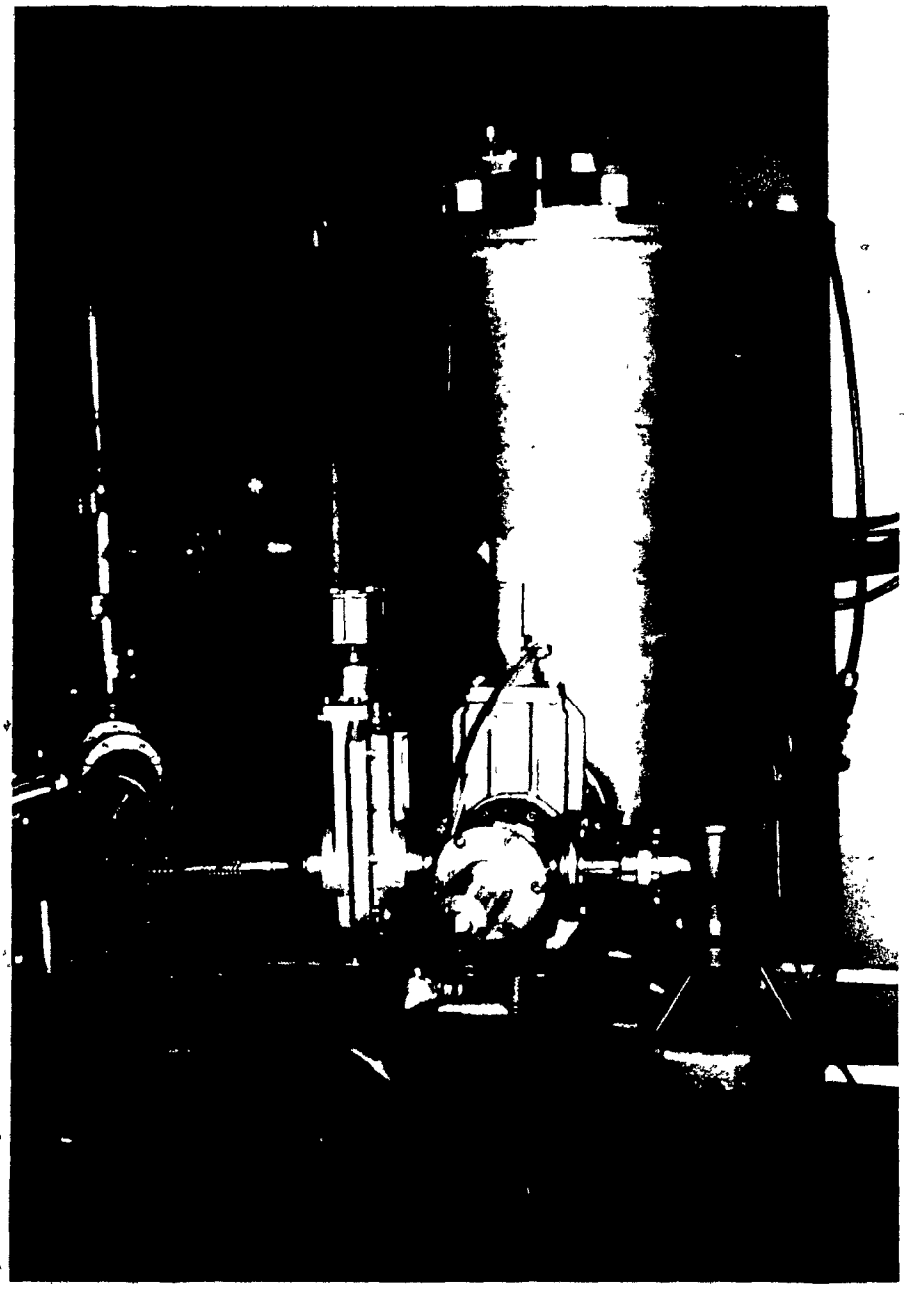

Figure 4.5

A top view of the beta spectrometer. The flexible pumping line, forechamber and manual plunger are clearly shown on the right side of the photograph.

from the detector vacuum chamber in order to reduce gas leaks into the system when new sources are inserted.

The manual plunger assembly is operated as follows (see Figure 4.2). After a new source, mounted on the end of the plunger, is introduced into the forechamber, the forechamber is evacuated using the diffusion pump station until a pressure of 10^{-2} Pa is reached. The forechamber was then isolated from the diffusion pump station (by closing a gate valve) and pumping was resumed using the sorption pump until a pressure $1 \sim 2 \times 10^{-3}$ Pa was reached in the forechamber. At this pressure, the gate valve between the forechamber and the detector vacuum chamber was opened and the source was introduced into the detector chamber for counting. A small volume forechamber (2" cross) was used in order to minimize the pumping time needed to reach the desired pressure.

The total time required to introduce a new source into the detector chamber is about 5 minutes. Whenever it was required to bring the forechamber to atmospheric pressure to charge sources, dry nitrogen gas was admitted into the forechamber through the inlet valve. The use of dry nitrogen reduces the pumping time that is needed to lower the forechamber pressure to 10^{-3} Pa as a result of the reduction in the rate of water vapor outgassing from the forechamber walls.

The manual plunger system was used to insert delicate sources and sources deposited on very thin backings into the detector vacuum chamber without any difficulty or any significant increase in the total time needed to change a source.

4.6 2 Automatic Plunger System

For the study of short lived sources, produced by on-line bombardment, an automatic plunger system was used (Figure 4.6). The system consists of three manual plungers and one pneumatic plunger that are coupled to a bombardment chamber (Figures 4.6, 4.7). The bombardment chamber is connected to the detector vacuum chamber through a pneumatic gate valve. The pneumatic plunger and gate valve are both activiated by a set of interlocked A.C. switches that can be controlled either manually or through a computer.

The automatic plunger shuttles the target-source, which is mounted on its end, between the bombardment chamber and the counting position in

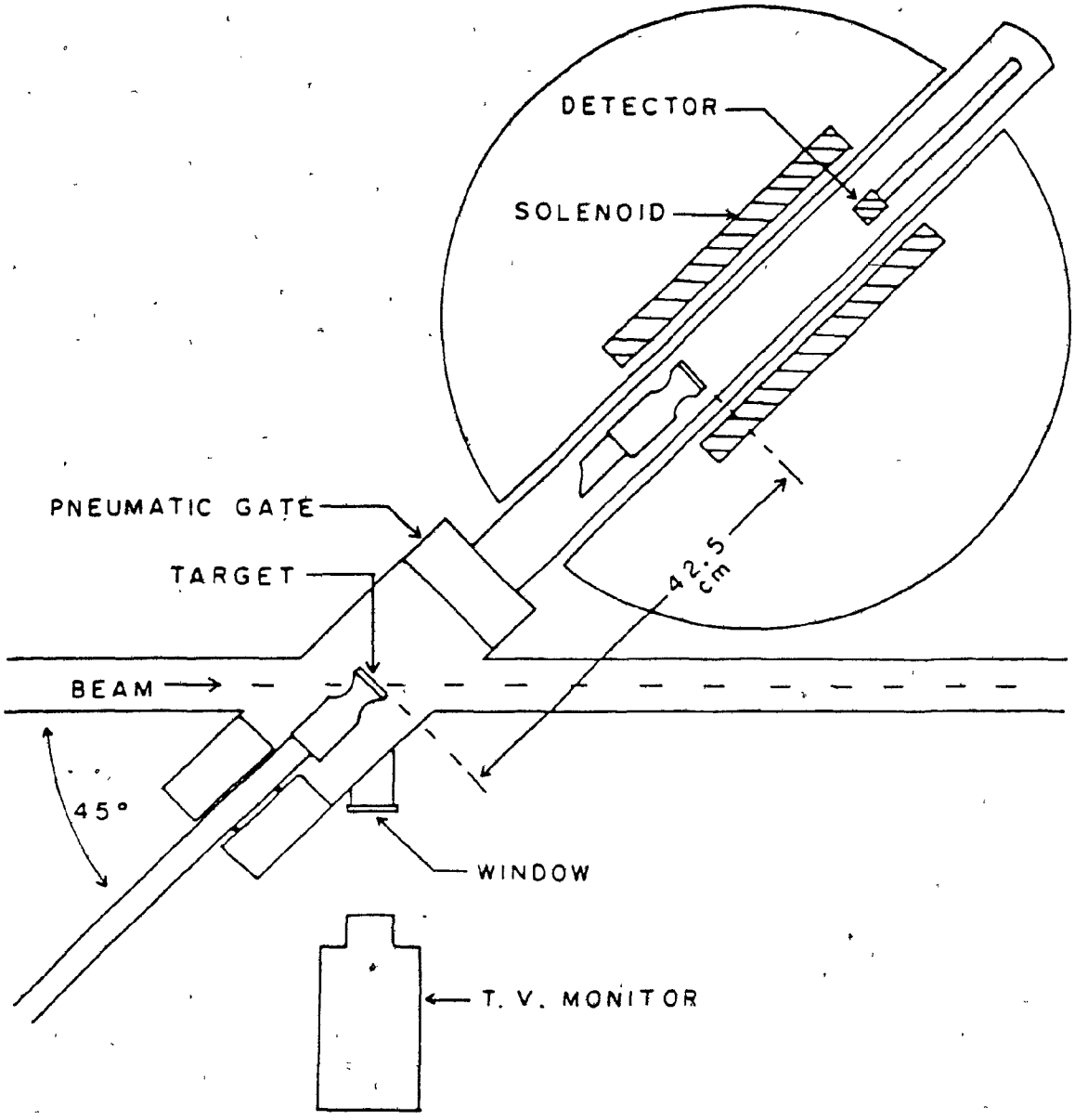

Figure 4.6

Layout of the automatic plunger system.

Figure 4.7

Design of the pneumatic plunger system.

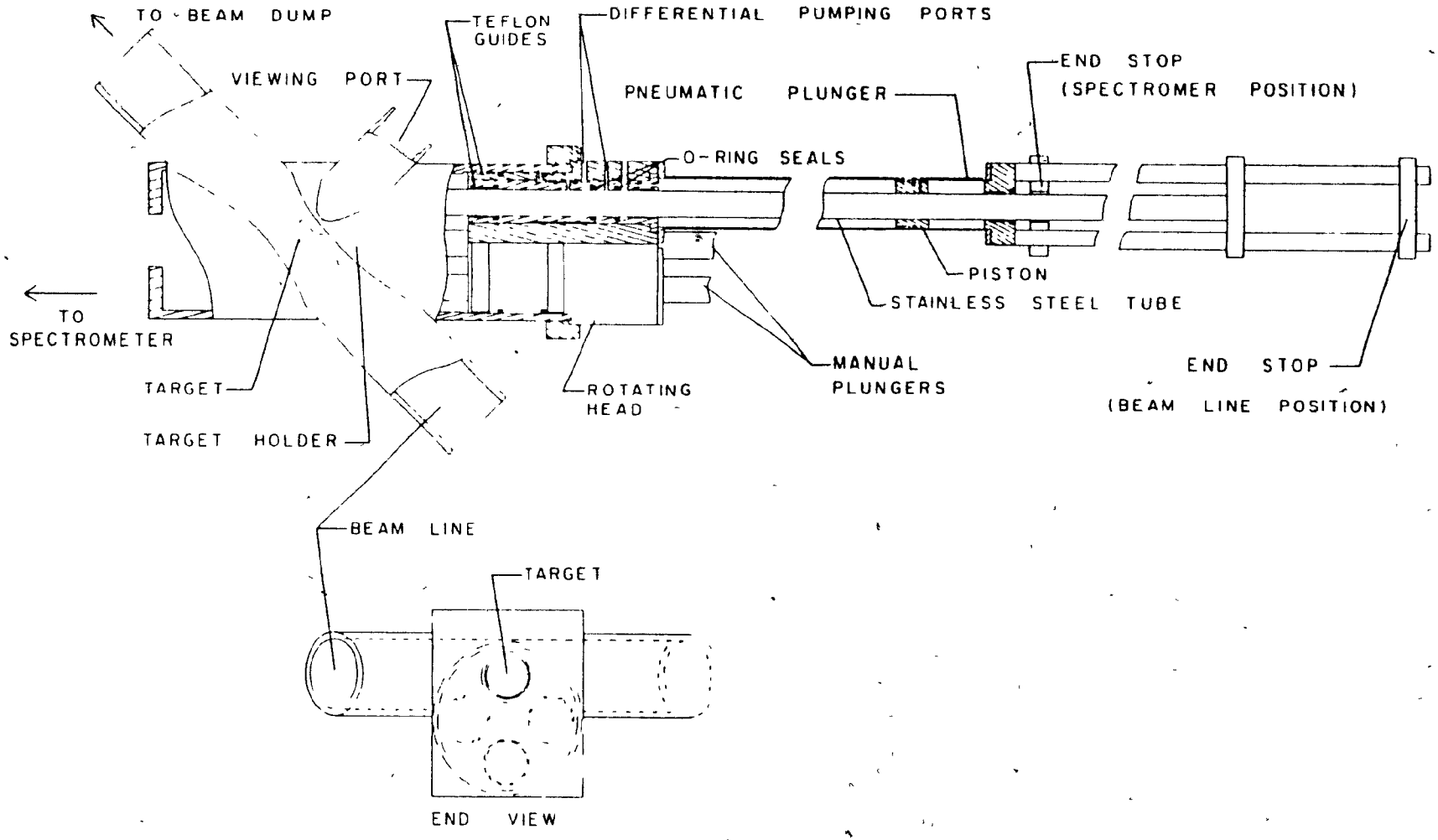
TO BEAM DUMP
VIEWING PORT
TEFLON GUIDES
DIFFERENTIAL PUMPING PORTS
PNEUMATIC PLUNGER
END STOP (SPECTROMER POSITION)
O-RING SEALS
TO SPECTROMETER
TARGET
TARGET HOLDER
ROTATING HEAD
MANUAL PLUNGERS
PISTON
STAINLESS STEEL TUBE
END STOP (BEAM LINE POSITION)
BEAM LINE
TARGET
END VIEW

the magnetic field of the solenoid. The pneumatic gate valve is closed automatically when the plunger is in the bombardment position to help suppress the very large background that was experienced when the beam was incident on the target. Differential pumping between the sliding seals of the plunger system allows the rapid movement of the plunger without any significant gas leak into the detector chamber.

The three manual plungers are used for the insertion of long lived sources or the verification of the position of the accelerator beam with a quartz crystal (mounted on the end of one of the manual plungers).

The autmoatic plunger systems permits the use of fragile targets and ensures the accurate and reproducible positioning of the sources (± 0.1 mm accuracy). It was used in the study of the β spectrum of ^{20}F (half life 11 sec) and can be used for sources with even shorter half lives (see Hetherington 1984 for a more detailed description of the automatic plunger system).

4.7 The $\beta - \gamma$ Coincidence System

A $\beta-\gamma$ coincidence system, built by Aptec Engineering Ltd. (Canada) was tested with the present spectrometer system. The $\beta - \gamma$ coincidence system is made up of two Ge(HP) detectors and fits inside the room temperature bore of the superconducting solenoid (see Figure 4.8). One of the two detectors (the γ detector) is an annular Ge(HP) detector (15 mm thickness, 30 mm I.D., 60 mm O.D.) which is located close to the center of the solenoid. The second detector (the β detector) is a planar Ge(HP) detector (15 mm thickness, 500 mm^2 surface area) and is placed close to the end of the solenoid. The distance between the two detectors is fixed (12.7 cm), but their positions relative to the solenoid can be easily changed. The two detectors are enclosed in the same hermetically sealed cryostat. The radioactive source is placed outside this cryostat in the center of the annular detector. The radioactivity is deposited on a thin mylar film which was stretched on a nylon ring. The nylon ring is mounted on the tip of a hollow nylon rod which is used to insert and retract the source. A thin (50 μm) titanium window separates the radioactive source from the β detector.

The high magnetic field at the location of the radioactive source forces the β particles to move in helical trajectories which clear the

Figure 4.8

The $\beta-\gamma$ coincidence system.

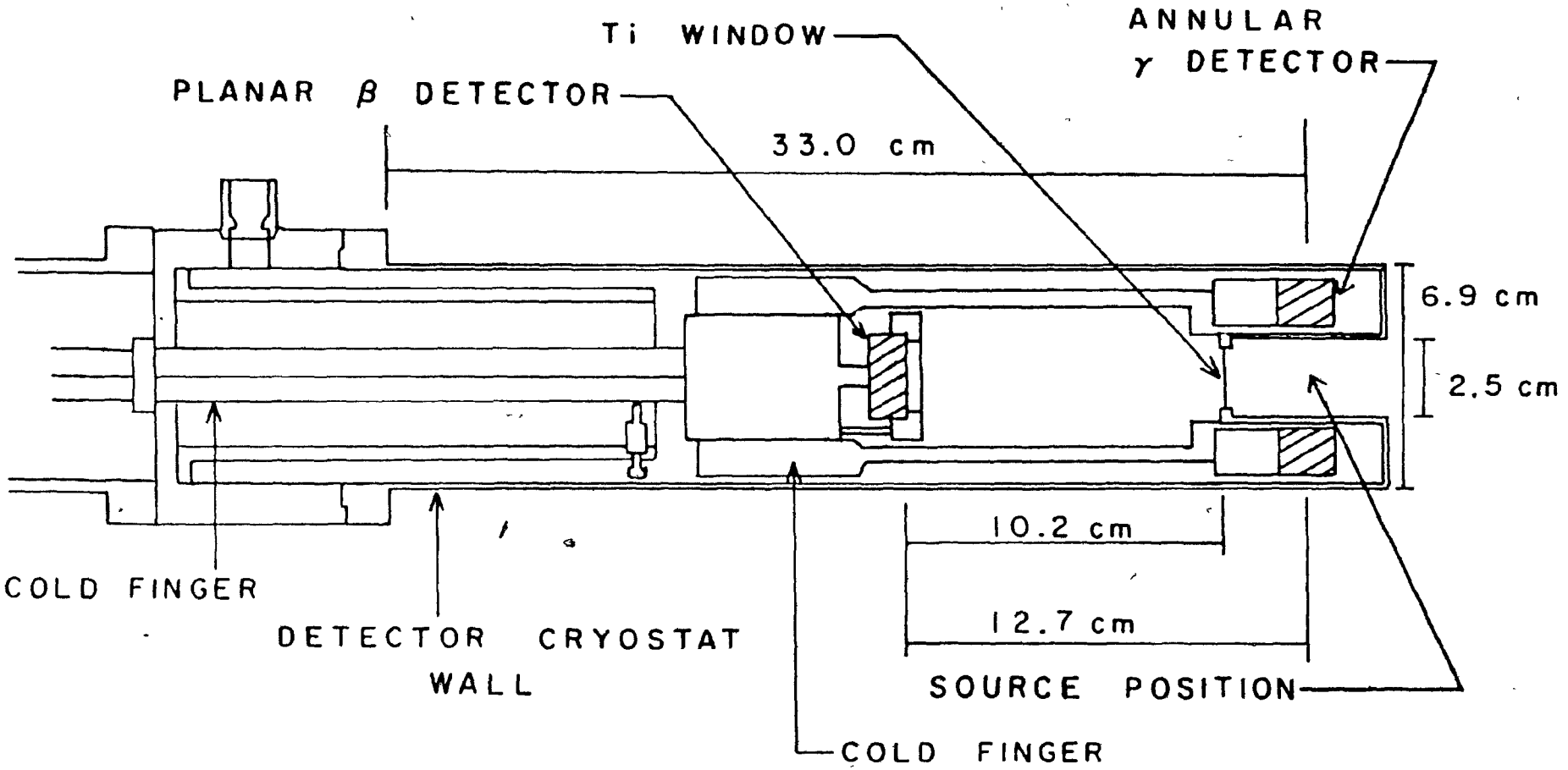
Ti WINDOW
ANNULAR
γ DETECTOR
PLANAR β DETECTOR
33.0 cm
6.9 cm
2.5 cm
10.2 cm
12.7 cm
COLD FINGER
DETECTOR CRYOSTAT
WALL
SOURCE POSITION
COLD FINGER

inner diameter of the annular detector (see Figure 4.9). The action of the strong magnetic field thus deflects all the β particles, emitted by the source, away from the γ detector and transports them to the β detector. As a result, the γ ray spectra collected with the annular detector are free from β ray contamination. And since no β rays are incident on the γ detector, a thin entrance window can be used in front of this detector making it suitable for the study of X rays and low energy γ rays.

Because of the size of the annular detector used in this set-up and its proximity to the radioactive source, the solid angle subtended by the γ detector at the source is approximately 2π steradian. The solid angle for β particle detection is dependent on the location of the source in the magnetic field and can easiy be as high as 1π steradian.

The β - γ dual detector system is intended for use in β - γ coincidence measurements. It can be used to select a single β branch in a multibranch decay, and to help in clarifying complicated decay schemes. Furthermore, the β - γ coincidence system can be used to measure the β decay energy (Q_β) in decays where the endpoint energy of the most energetic β branch exceeds the maximum electron energy that can be studied with the spectrometer. This can be acccomplished, in cases where the decay scheme is known the β detector with a specific γ ray so as to select a low energy β branch whose endpoint falls within the maximum energy range of the spectrometer.

Only a few, very preliminary tests of the β-γ coincidence system were undertaken, nevertheless, the exceptional β-γ coincidence efficiency of the system was clearly demonstrated. The results from these preliminary tests, however, seem to indicate that the resolution of the annular γ ray detector is strongly affected by the high magnetic field of the solenoid. The data available on the performance of the β - γ spectrometer is still inconclusive and more extensive testing is needed.

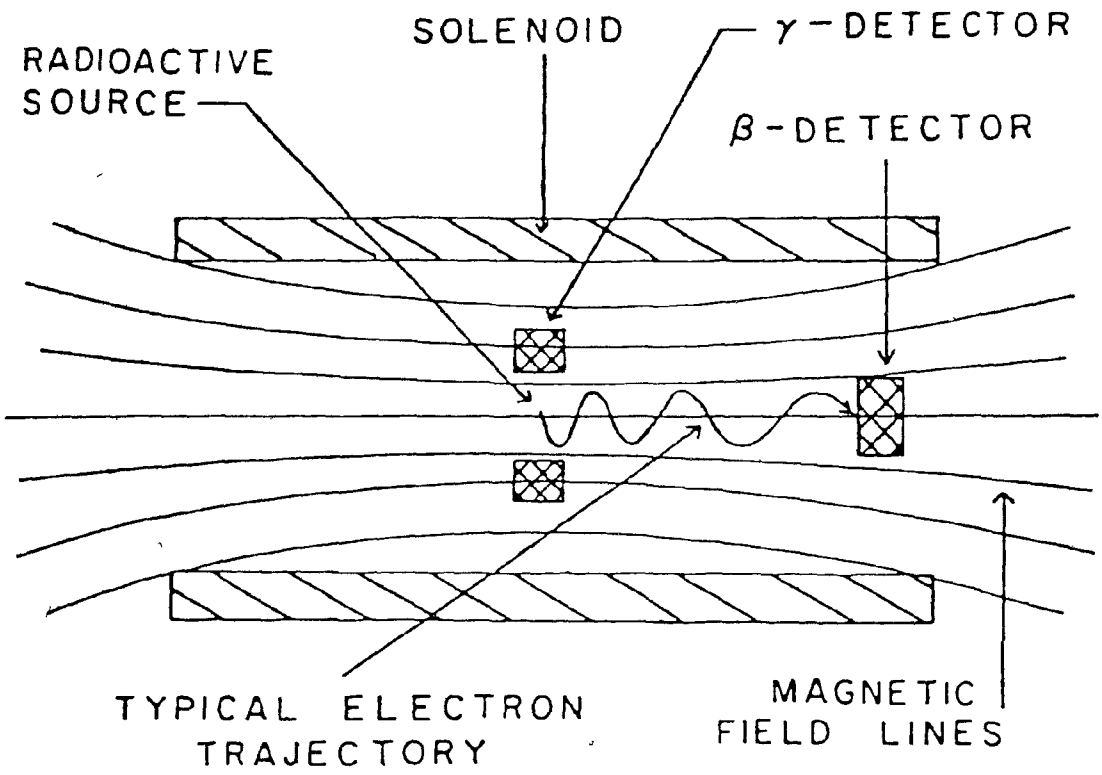

Figure 4.9

Illustration of the principle of operation of the beta-gamma coincidence system.

CHAPTER 5

THE SPECTROMETER'S PERFORMANCE

The principle aim that guided the design of the present β spectrometer and its support equipment was the resolution of the problems associated with the use of germanium detectors in β spectrometry (see Chapter 2 for a detailed discussion of these problems). The superconducting solenoid transport system effectively eliminates the difficulties that are caused by the high sensitivity of the germanium detector to γ rays. The elaborate vacuum system and source introduction mechanisms described in Chapter 4 solve most of the problems associated with the use of a liquid nitorgen cooled detector. The most important problem that remains to be addressed is the effect of the non-ideal shape of the response function of the germanium detector on the shapes of the β spectra that are measured with the spectrometer.

5.1 Distortions of the Beta Spectra Measured with the Spectrometer

Distortions of the shapes of the β spectra that are caused by the response function of the germanium detector are quite drastic. As an example, figure 5.1 shows the effect of the response function of the germanium detector used in the present spectrometer on a statistical beta distribution. Hence, in order to be able to extract the different parameters of the β spectrum (endpoint energies, branching ratios, and shape factors) precise knowledge of the response function is necessary.

An exhaustive study of the response function of germanium detectors to β^- particles was undertaken by Hetherington (1984). A major part of his work dealt with the investigation of the performance of the present β spectrometer, the distortions of the β spectra that are caused by the spectrometer, and the extraction of the maximum amount of information possible from these spectra.

The distortions of the β spectra were found to be caused by several factors besides the non-ideal response function of the germanium detector. These factors include β particle scattering in the source and backscattering from the source backing (both of which are affected by the

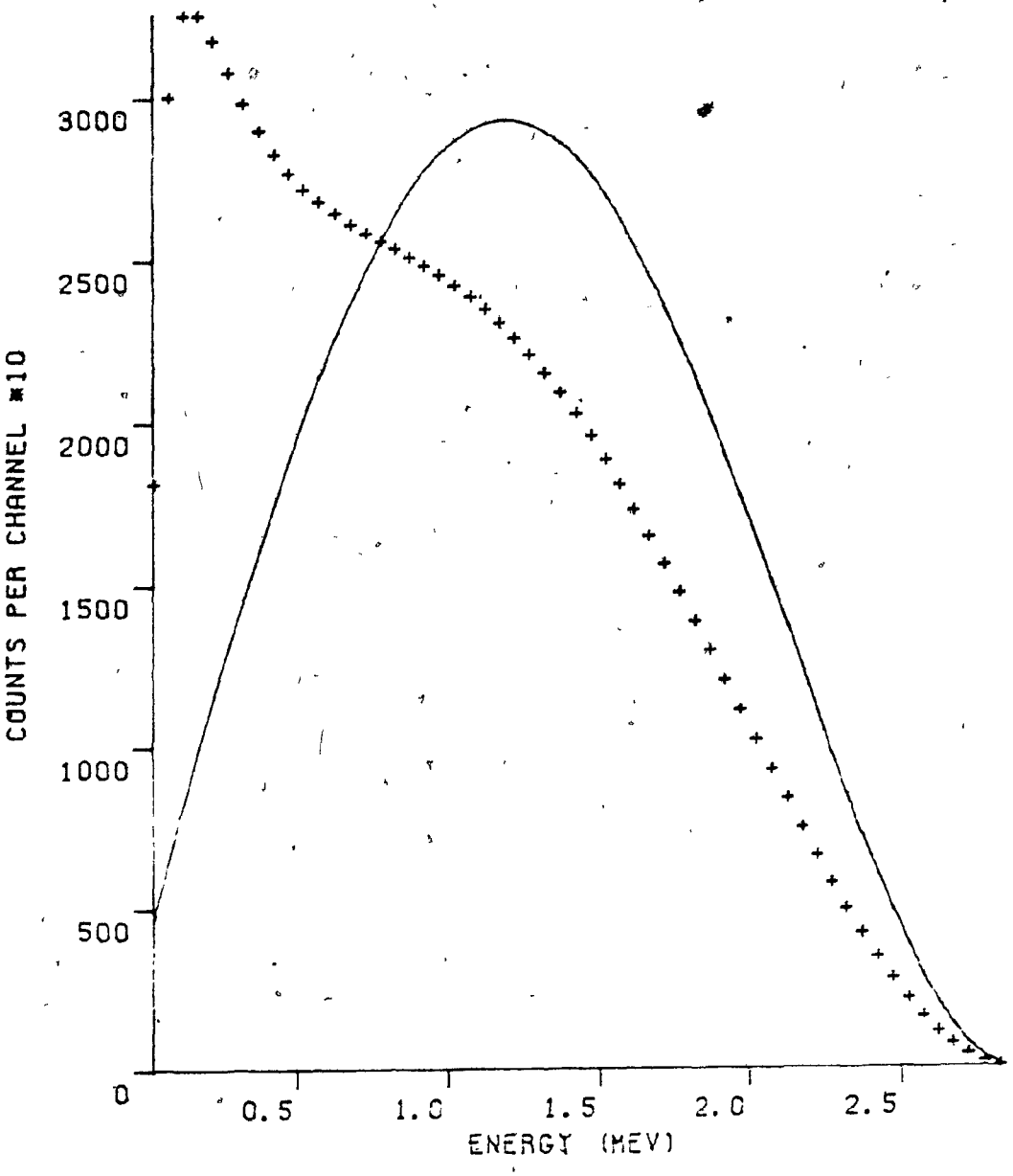

Figure 5.1

Statistical beta distribution (-) and corresponding distribution of pulses from detector (+++).

strong magnetic field), and the change in the beta ray calibration of the detector under the influence of the strong magnetic field of the solenoid. The effects of pulse pile up and gamma rays emitted from the source on the shape of β spectra measured with the present spectrometer were found to be negligible in most cases.

The approach followed by Hetherington (1984) for the determination of the response function of the superconducting solenoid spectrometer was a semi-empirical approach. First, the response function of the germanium detector is generated by a Monte Carlo simulation of the interactions of the β particles with the detector. The different parameters describing the shape of the response function are then adjusted in order to be able to fit the β spectra of several standard sources simultaneously.

Because of the presence of the source and the detector in the magnetic field of the solenoid, the trajectories followed by the β particles emitted from the source to the detector are determined by the magnetic field strength and geometry. Since the angles of incidence of the β particles on the surface of the detector, and their points of entry into the detector, are determined by their trajectories, it is clear that accurate calculations of the trajectories of the β particles are required for the generation of the response function through the Monte Carlo simulation. The precise calculation of trajectories is also necessary in order to reveal any dependence of the transmission of the solenoid on β particle energy.

Extensive computer codes for calculating the magnetic field of the solenoid and for simulating the trajectories of the β particles in this magnetic field were written in this laboratory under the direction of R.B. Moore. The codes were the result of the effort of several contributors, the principle contributor being L. Ouellet.

Some aspects of the trajectory calculations that are relevant to the performance of the spectrometer are reviewed here.

5.2 The Magnetic Field of the Solenoid

The first step in studying the trajectories of the β particles in the magnetic field of the solenoid is to obtain a map of this magnetic field. A computer program was written for this purpose.

The radial and axial components of the magnetic field (B_r and B_z respectively) were calculated using the standard form of the equations for these field components for a circular loop (Smythe 1968 p. 291):

$$B_r = \frac{\mu I}{2\pi} \quad \frac{z}{r\,[(a+r)^2 + z^2]^{1/2}} \quad \left[-K(k) + \frac{a^2+r^2+z^2}{(a-r)^2 + z^2} \; E(k)\right] \qquad 5.1$$

$$B_z = \frac{\mu I}{2\pi} \quad \frac{1}{[(a+r)^2 + z^2]^{1/2}} \quad \left[K(k) + \frac{a^2-r^2-z^2}{(a^2-r^2) + z^2} \; E(k)\right] \qquad 5.2$$

where

r, z = The cylindrical coordinates (relative to the center of the loop) of the point at which the field is calculated.

a = The radius of the loop

I = The current in the loop

μ = The permeability of the medium

(K)k, E(k) = The complete elleptical integrals of the first and second kind repsectively:

$$K(k) = \int_0^{\pi/2} (1 - k \sin^2\theta)^{-1/2} \, d\theta \qquad 5.3$$

$$E(k) = \int_0^{\pi/2} (1 - k \sin^2\theta)^{1/2} \, d\theta \qquad 5.4$$

$$k = 2\left[\frac{a\,r}{(a+r)^2 + z^2}\right]^{1/2} \qquad 5.5$$

K(k) and E(k) were evaluated by using the algorithm due to Carlson & Notis (1981) for computing incomplete elleptical integrals of the first and second kind and setting the arguments for these two integrals (R_F and R_D respectively) as follows:

$$K(k) = R_F\,(0,\ 1-k^2,\ 1) \qquad 5.6$$

$$E(k) = R_F\,(0,\ 1-k^2,\ 1) - (1/3)\ k^2\ R_D\,(0,\ 1-k^2,\ 1) \qquad 5.7$$

B_r and B_z values for the present solenoid were calculated by dividing the solenoid into ring segments and approximating each segment by a loop whose radius was equal to the mean radius of the ring. The field

calculated for all these loops was then summed to get the solenoidal field. The ring segments were 0.254 cm thick in the radial direction and 1.27 cm long in the axial direction. The field values were calculated at grid points separated by 0.4 cm radially and 1.27 cm axially.

To test the error that might be introduced by the finite size of the ring segments used in the calculations, a more accurate calculation was made for the most error sensitive point on the grid (r = 4 cm, z = 12.7 cm) using ring segments of one tenth the radial and axial thickness of the ring segments used in the previous calculation. The error introduced by the larger ring segments was found to be less than one part in 10^4.

Graphs of the field values resulting from these calculations are shown in figures 5.2, 5.3, 5.4. To check these values, a set of field lines was calculated from the values of B_r and B_z and the results are shown in figure 5.5. A graphical check on the divergence of these field lines shows that it is appropriate for $\vec{\nabla} \times \vec{B} = 0$.

5.3 The Acceptance Solid Angle of the Spectrometer

As was mentioned in the review of axial magnetic guides in Chapter 2, the magnetic field of the solenoid forces the particles to follow helical trajectories such that most of the particles emitted from the source in the direction of the detector will be intercepted by the detector regardless of the detector's location along the axis of the solenoid. On the other hand gamma rays are unaffected by the magnetic field so that the number of γ rays emitted from the source that impinge on the detector varies inversely as the square of the source-detector distance (see figure 5.6).

5.3.1 A First Order Calculation of the Solid Angle of Acceptance for Betas

If the radioactive source is placed at a position along the axis of the solenoid where the magnetic field is lower than its maximum value at the center of the solenoid, then some of the electrons emitted in the direction of the high field regior (the forward direction) will be reflected back as a result of the magnetic mirror effect (Jackson 1975 p. 592). In such a situation, electrons emitted at large angles with respect to the solenoid axis will have their forward momentum reversed as a result

Figure 5.2

The axial magnetic field calculated along the axis of the solenoid.

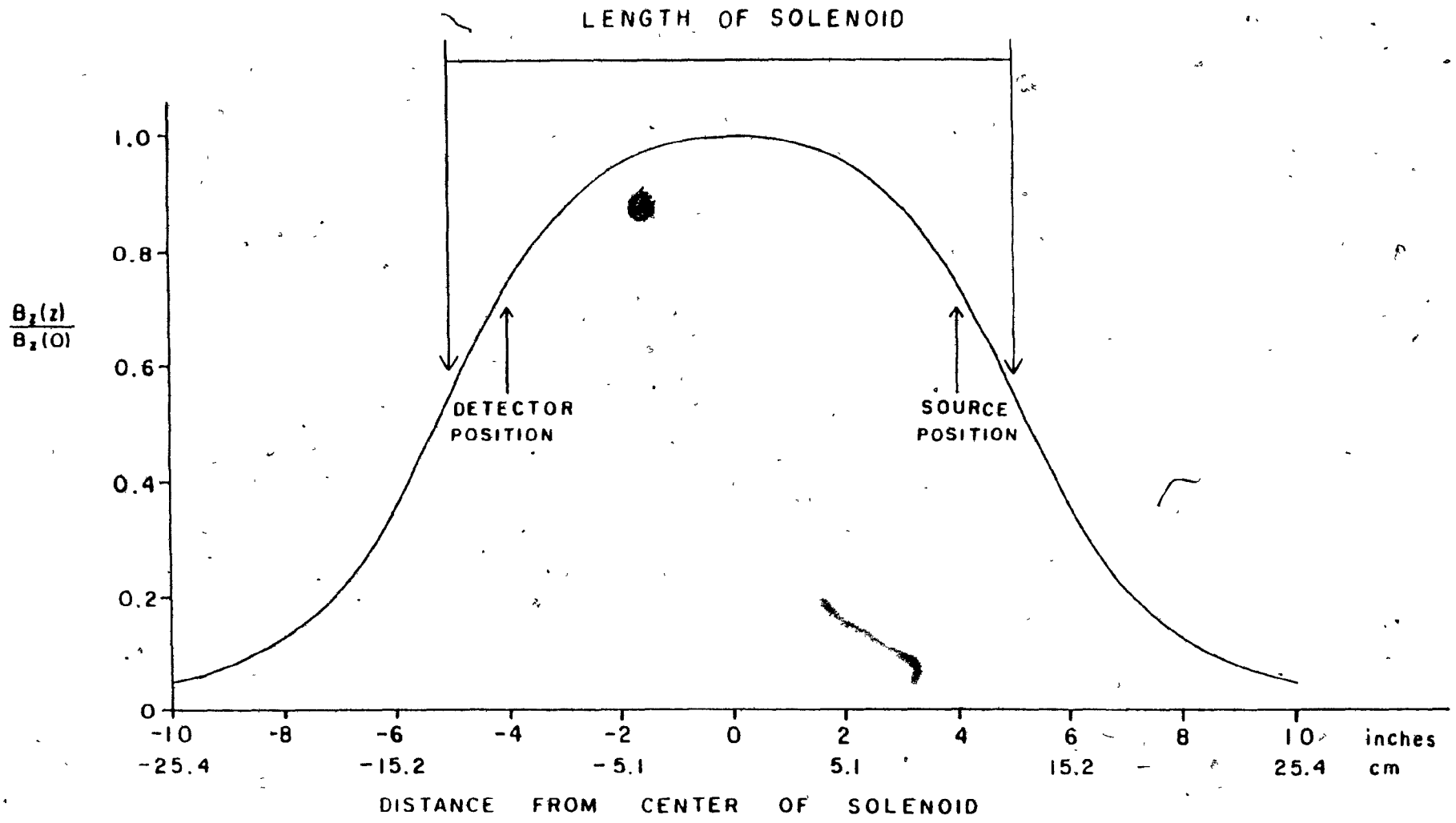
LENGTH OF SOLENOID
1.0
0.8
0.6
0.4
0.2
0
$\frac{B_z(z)}{B_z(0)}$
DETECTOR POSITION
SOURCE POSITION
-10
-8
-6
-4
-2
0
2
4
6
8
10
inches
-25.4
-15.2
-5.1
5.1
15.2
25.4
cm
DISTANCE FROM CENTER OF SOLENOID

Figure 5.3

The axial magnetic field of the solenoid as a function of the radial and axial distances from the center of the solenoid.

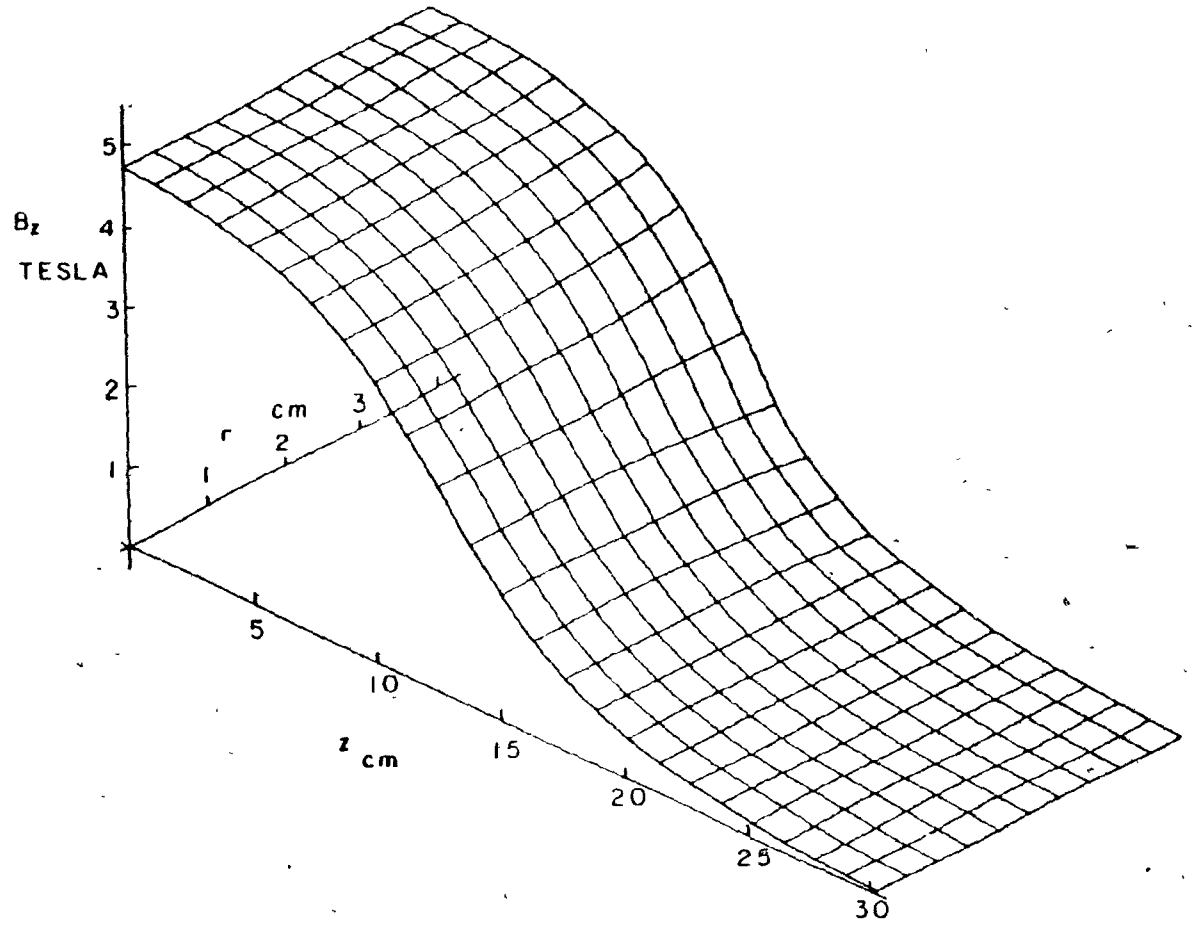
B_z
TESLA
5
4
3
2
1
r
cm
1
2
3
5
10
15
20
25
30
z cm

Figure 5.4

The radial magnetic field of the solenoid as a function of the radial and axial distances from the center of the solenoid.

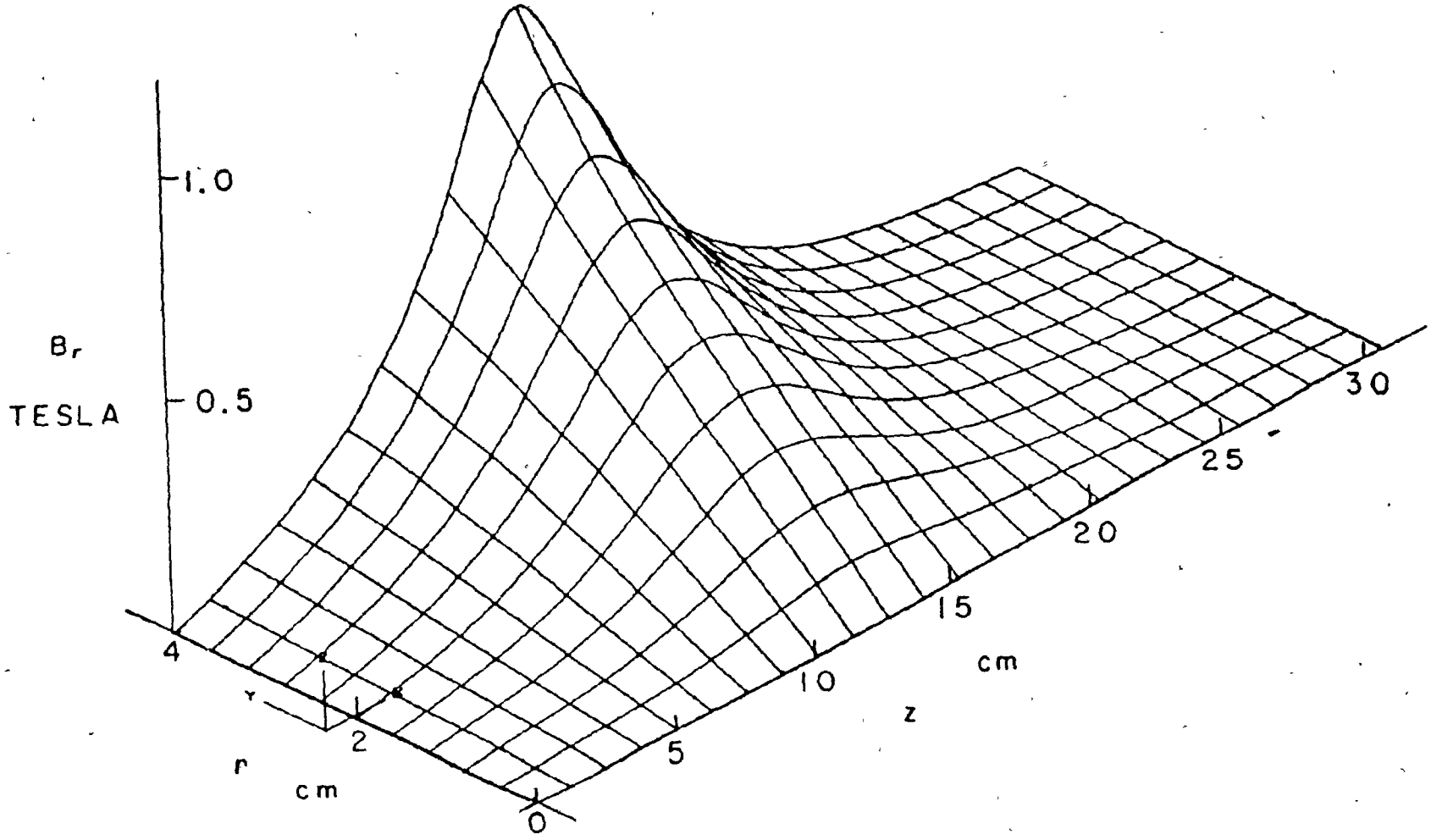
1.0
0.5
B_r
TESLA
4
2
0
r
cm
5
10
15
20
25
30
z
cm

Figure 5.5

The magnetic field lines of the solenoid.

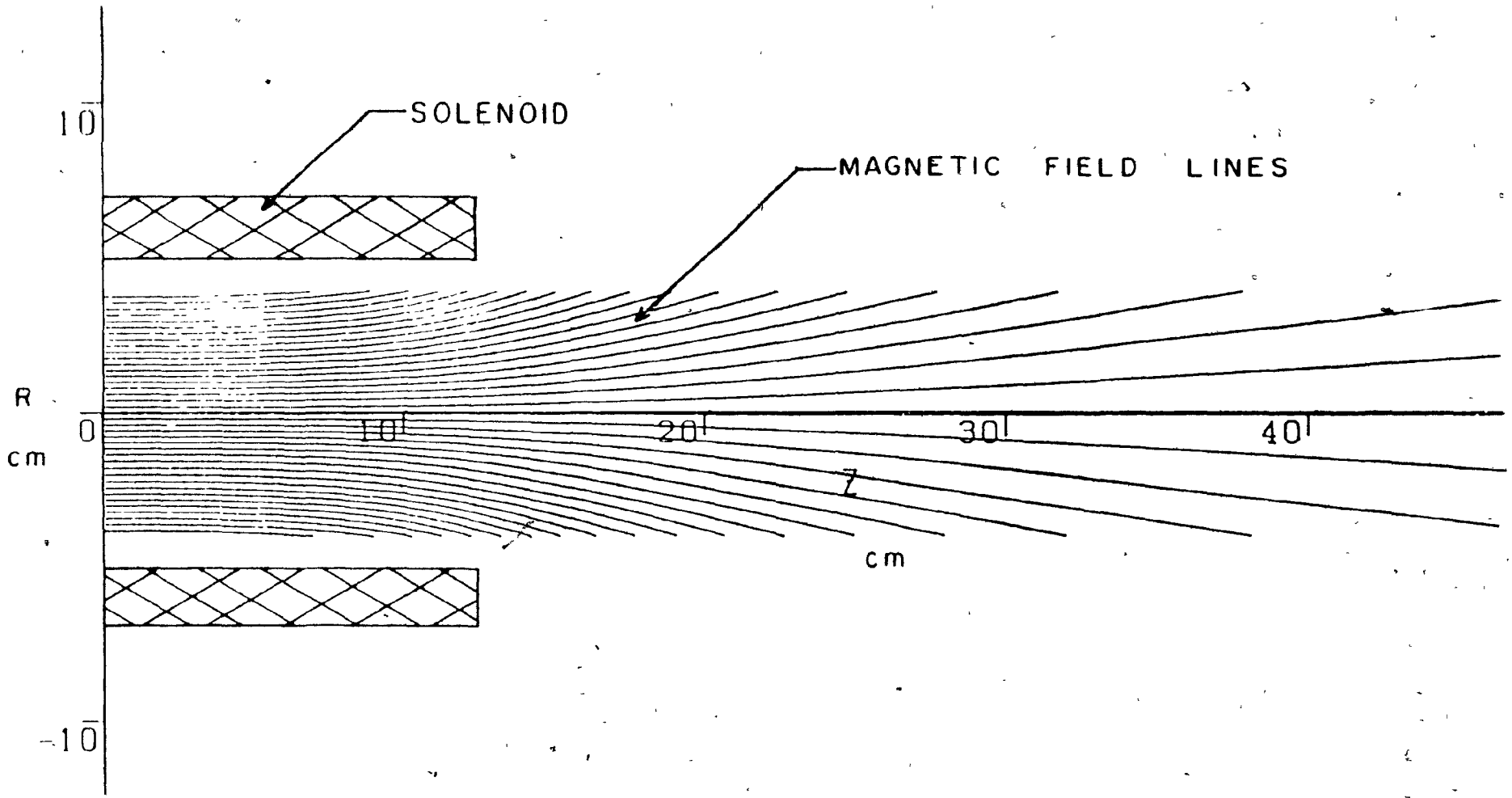
SOLENOID
MAGNETIC FIELD LINES
10
R
cm
0
10
20
30
40
Z
cm
-10

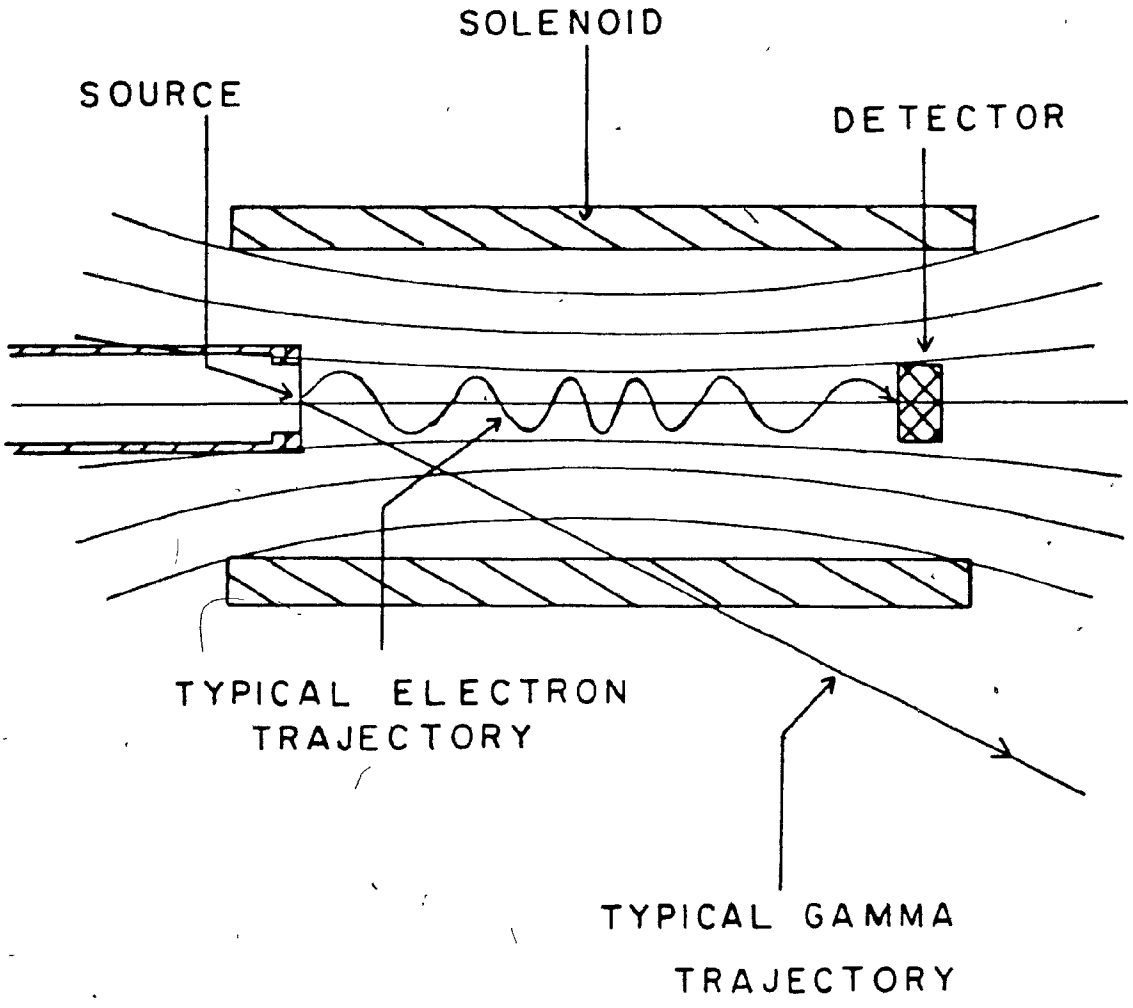

Figure 5.6

Typical beta and gamma ray trajectories in the magnetic field of the solenoid.

of the non-uniformity of the magnetic field.

Using the adiabatic approximation (i.e. invariance of the magnetic flux through the orbit of the electron, Jackson 1975 pp. 588-593), it can be easily shown (Reitz & Milford 1967 pp. 277-278) that all electrons emitted at angles larger than a critical angle (θ) will be reflected back irrespective of their energy. Electrons emitted at angles less than the critical angle will penetrate past the magnetic field maximum and hence will not reflected by the magnetic mirror effect. In this first order approximation the value of the critical angle θ is independent of energy and is given by (Rietz & Milford 1967 p. 278):

$$\theta = \text{Sin}^{-1} \left(\frac{B_z(z)}{B_z(0)} \right)^{1/2} \qquad 5.8$$

where

θ = The maximum angle of acceptance

$B_z(z)$ = The axial magnetic field at the location of the source

$B_z(0)$ = The maximum value of the magnetic field (i.e. the field value at the center of the solenoid-4.4 tesla at 100 ampere)

In the case of a solenoidal transport system, this critical angle represents the maximum angle of acceptance of the system (Kotajima & Beringer 1970, Mladjenovic 1979).

Using the axial magnetic field values of the superconducting solenoid of the present spectrometer (see figure 5.2) and equation 5.8 above, the solid angle of acceptance of the spectrometer as a function of the position of the source along the solenoid axis was calculated. The results of these calculations are shown in (figure 5.7).

In most of the experiments performed with this spectrometer, the position of the source was chosen to be on the axis of the solenoid, 1 inch (2.54 cm) from the end of the solenoid (inside the solenoid). At this location the axial magnetic field is 3.28 tesla and the maximum angle of acceptance (calculated form 5.8) is 59.7°. The solid angle of acceptance is about π steradians (25% transmission). (To achieve a 25% transmission without the magnetic field of the solenoid, the point source would have to be placed at a distance of 0.73 cm in front of the 500 mm^2 surface area detector).

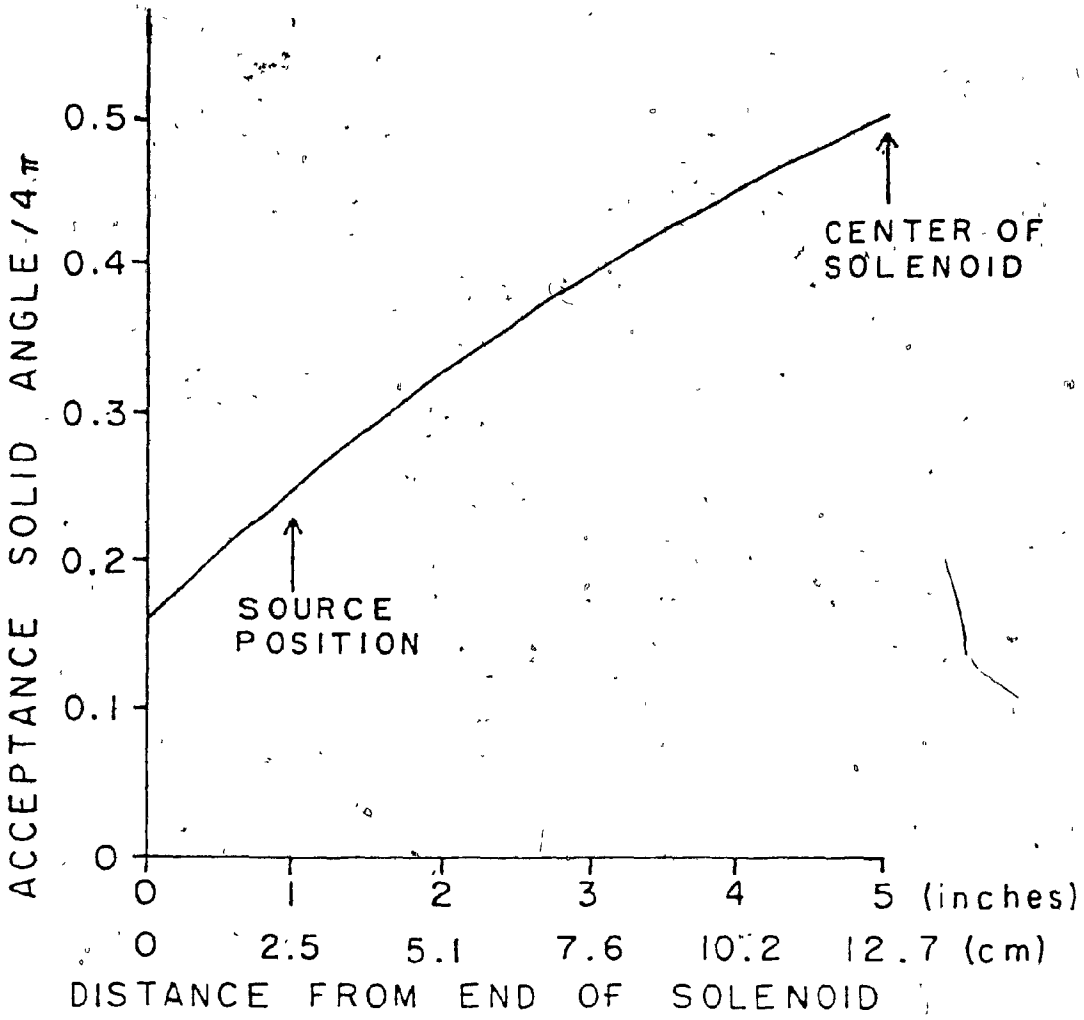

Figure 5.7

Solid angle for betas as a function of source position on solenoid axis.

5.3.2 Numerical Calculation of the Electron Trajectories

A direct numerical calculation of the electron trajectories in the solenoid was carried out to check the predictions of the first order calculation used above and to reveal any possible dependence of the solid angle of acceptance on electron energy.

The magnetic field map that was calculated by the method described in section 5.2 was used in a fourth order Runge-Kutta integration of the equations of motion of the electrons in the magnetic field. In what follows, a discussion of the principle features of the calculation will be given. Some examples illustrating the results of the calculation are also included.

The Runge-Kutta integration was carried out in a cylindrical coordinate system with the coordinate axis parallel to the axis of the solenoid but displaced from it so that the center of curvature of the electron orbit at any time was close to the axis of the displaced coordinate system. Although this necessitated a movement of the coordinate axis after typically each integration step, it allowed very large integration steps to be taken without loss of accuracy. With 45° steps, the computational accuracy (as checked by comparing with integrations using smaller steps) was typically of the order of 10^{-6} mm for trajectories that involved over one hundred orbits of the electron. Thus it was concluded that the primary error in the calculation of the electron trajectories was that due to inaccuracies in the magnetic field calculations and in the interpolations between the points of the calculated magnetic field grid. Judged on the basis of the consistency of the calculated electron trajectories and their close agreement with the adiabatic approximation (when this approximation was valid), the accuracy of the numerical calculations of the electron trajectory appears to be always better than 10^{-2} mm.

A typical set of electron trajectories is shown in figure 5.8. Figure 5.8a shows a family of 1 MeV electron trajectories while figure 5.8b shows a family of 5 MeV electron trajectories. In both cases all of the electrons are emitted from a point source on the solenoid axis at 20° with respect to the axis but their angles of emission with respect to the plane of the figure (the XZ plane) vary in steps of 30° around a full

Figure 5.8

Trajectories of electrons emitted at 20° to the axis and at different angles with respect to the plane of the figure.

a) 1 MeV electrons

b) 5 MeV electrons

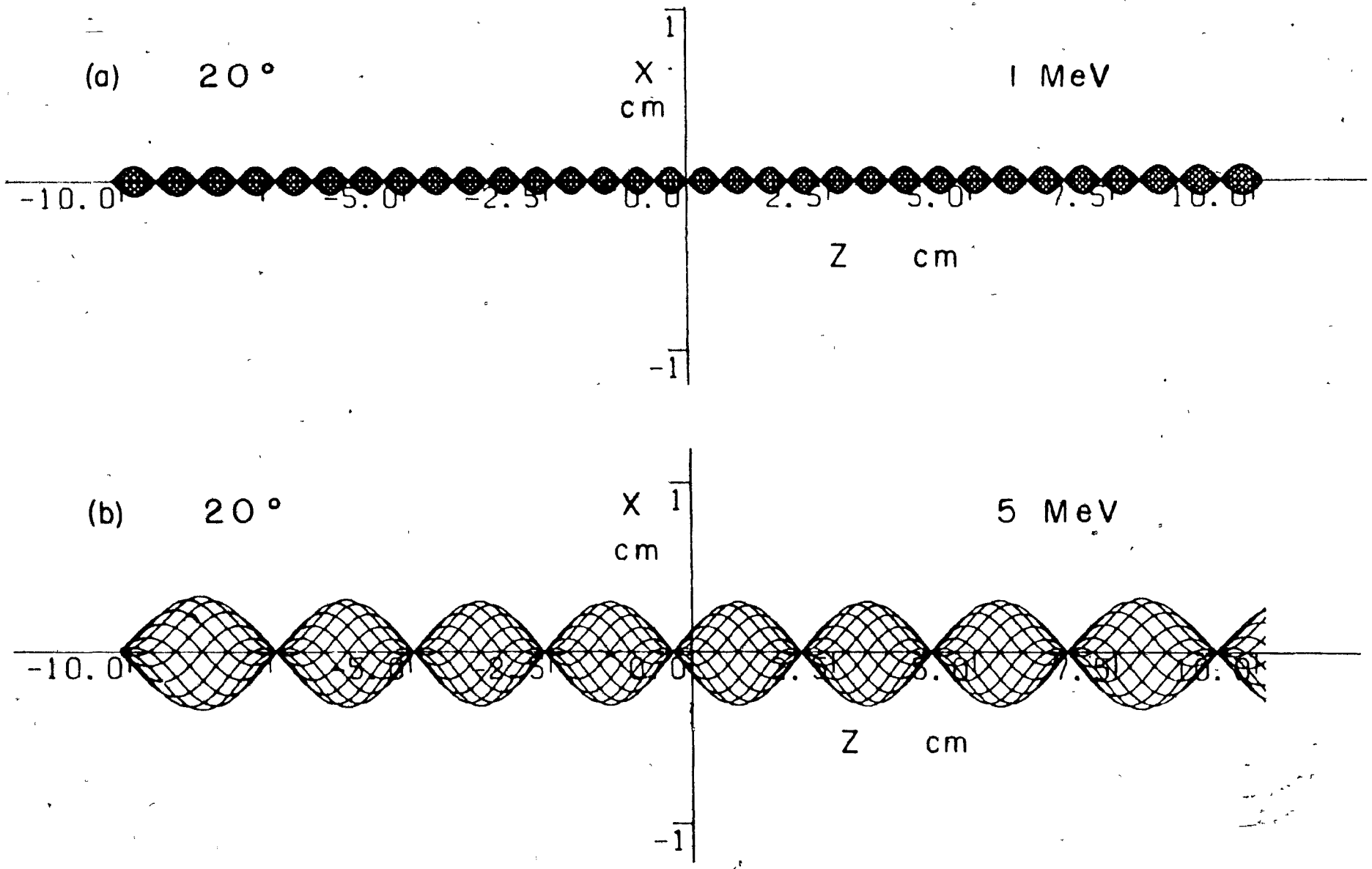
(a) 20°
1
X
cm
1 MeV
-10.0
-5.0
-2.5
0.0
2.5
5.0
7.5
10.0
Z cm
-1
(b) 20°
X 1
cm
5 MeV
-10.0
Z cm
-1

circle. This results in the 12 trajectories seen in each family. The plots shown in figure 5.8 are projections of the trajectories in the XZ plane. The X and Z axes are not drawn to the same scale in order to enhance the view of the radial displacement over the axial therefore the view of the angle that the electron velocity makes with the solenoid axis is a distorted one. The two families of trajectories clearly show the focusing effect of the solenoidal field (the nodes in the diagram), and the maximum diameter of the electron "beam" (the distance across the antinodes in the diagram). It can be seen from figure 5.8a,b that the maximum diameter of the beam for electrons emitted at 20° to the axis is 1.5 mm for 1 MeV electrons and 6 mm for 5 MeV electrons (i.e. 5 MeV electrons emitted from a point source at 20° to the axis of the solenoid impinge on a circular area on the detector surface which is centered on the axis of the solenoid and whose diameter is 6 mm).

Figure 5.9 shows similar sets of trajectories for electrons leaving the source at 45° to the solenoid axis. One can clearly see the shorter distance between the nodes (shorter focal length) and the wider extent of the electron beam (about 3 mm diameter for 1 MeV electrons and about 12.5 diameter for 5 MeV electrons.

5.3.3 Energy Dependence of the Solid Angle of Acceptance

Figure 5.10 shows an example of a numerical calculation which was performed to determine the solid angle of acceptance of the solenoid. Here it can be seen that 5 MeV electrons leaving the point source at angles less than 60° with respect to the axis of the solenoid are transmitted to the detector while electrons leaving at an angle of 60° or greater are reflected back by the magnetic mirror effect of the non-uniform field of the solenoid. Figure 5.10 shows that 59.8° is very close to the maximum angle of acceptance of the solenoid at 5 MeV for a point source placed on the axis of the solenoid 1 inch (2.54 cm) from the end of the solenoid (the standard source position). Iterations of this type show that the maximum angle of acceptance is 59.90° for 5 MeV electrons.

Similar calculations performed at different electron energies show that the maximum angle of acceptance ranges from 59.70° for 0.5 MeV electrons to 60.03° for 6 MeV electrons. The acceptance solid angles

Figure 5.9

Trajectories of electrons emitted at 45° to the axis and at different angles with respect to the plane of the figure.

a) 1 MeV electrons

b) 5 MeV electrons

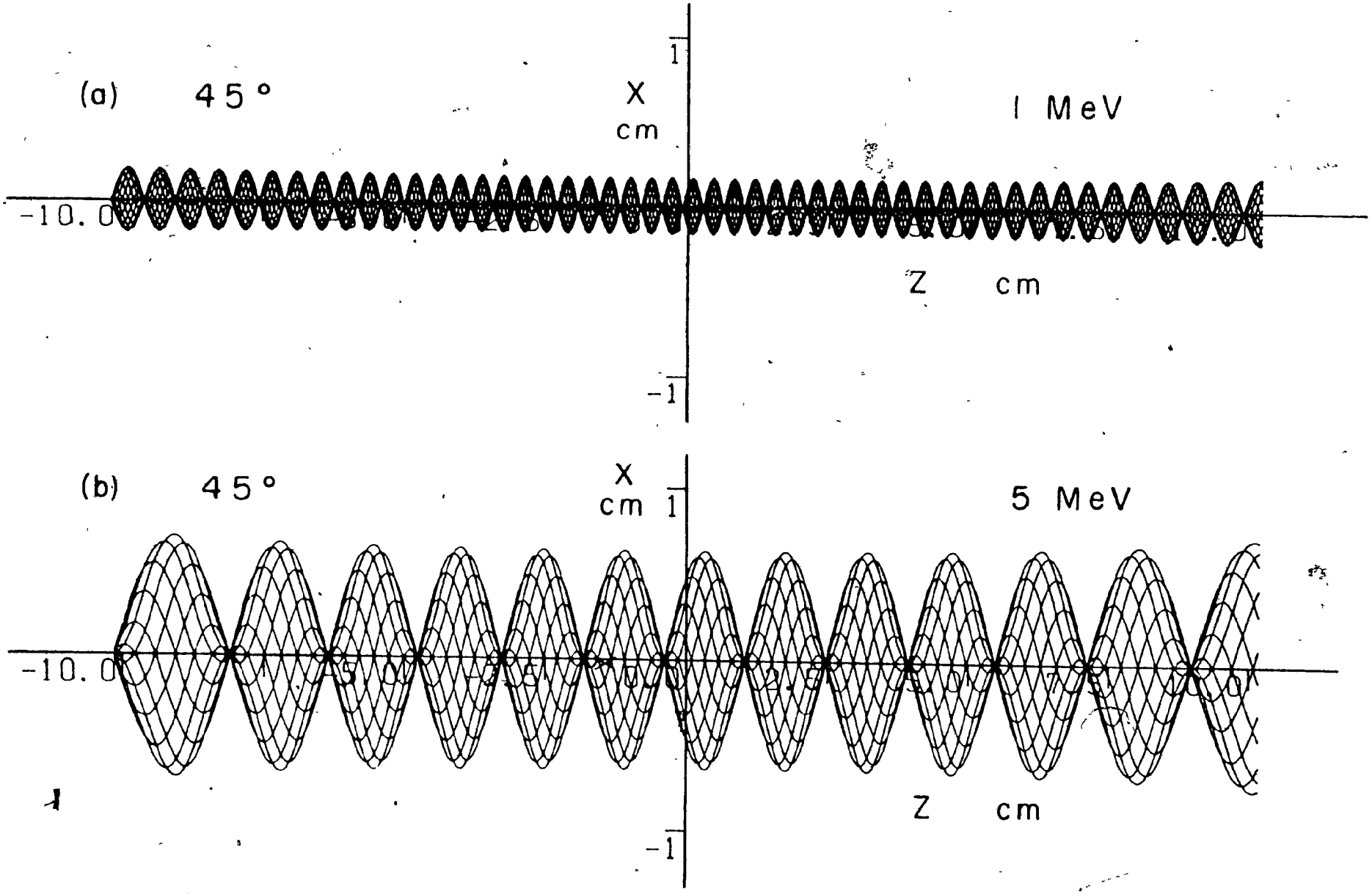
(a) 45°
X
cm
1
-1
1 MeV
-10.0
Z cm
(b) 45°
X
cm
1
-1
5 MeV
-10.0
Z cm

Figure 5.10

Trajectories of 5 MeV electrons emitted at angles around 60° with respect to the axis (the electrons are emitted in the plane of the figure).

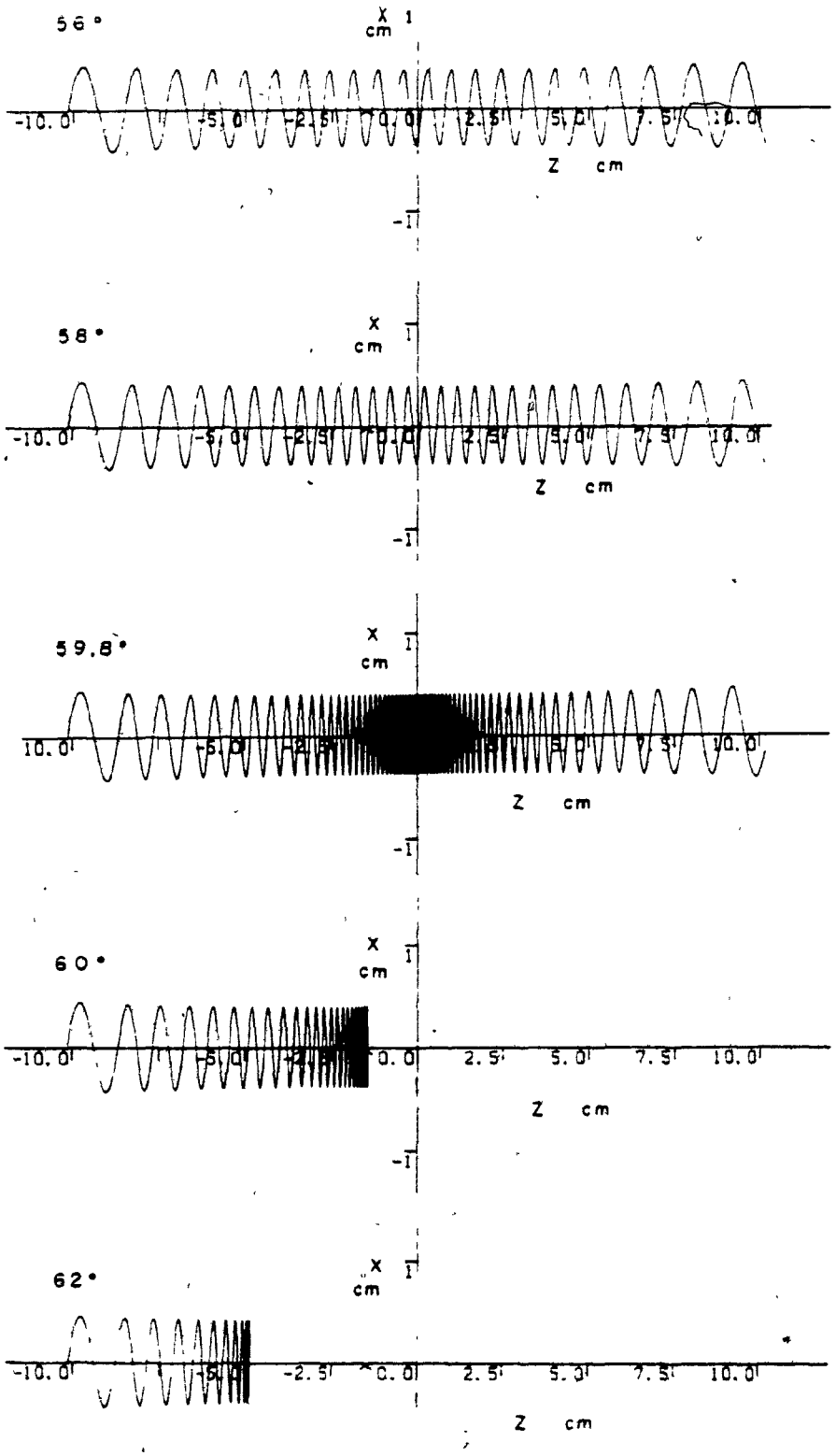
56°
X cm 1
-10.0
-5.0
-2.5
0.0
2.5
5.0
7.5
10.0
Z cm
-1
58°
X cm 1
-10.0
-5.0
-2.5
0.0
2.5
5.0
7.5
10.0
Z cm
-1
59.8°
X cm 1
10.0
-5.0
-2.5
5.0
7.5
10.0
Z cm
-1
60°
X cm 1
-10.0
-5.0
0.0
2.5
5.0
7.5
10.0
Z cm
-1
62°
X cm 1
-10.0
-5.0
-2.5
0.0
2.5
5.0
7.5
10.0
Z cm

corresponding to these values are shown in figure 5.11. As can be clearly seen from figure 5.11, the solid angle of acceptance of the spectrometer varies by about 1% only over the full energy range from 0 to 6 MeV.

The deeper penetration of high energy electrons into the solenoid is shown in figure 5.12 where it is seen that 5 MeV electrons emitted at 60° to the axis reach to within 1.2 cm of the center of the solenoid while electrons of 1 MeV energy emitted at 60° to the axis are reflected at a point 2 cm from he center of the magnet.

5.4 Diameters of the Electron Orbits and Maximum Beta Energy

The magnetic field of the solenoid confines β particles which are emitted from a point source on the axis of the solenoid to helical trajectories that are tangential to the axis. In order for the effective transmission of the spectrometer to be independent of the energy of the β particles, the detector must intercept all of the electrons emitted in the forward direction at angles less than the maximum acceptance angle. To achieve this, the radius of the detector must be greater than the maximum diameter of the orbits (at the detector's location) of the most energetic β particles under study.

If this condition is not met, then some of the β particles will scatter off the detector casing and some will miss the detector altogether. This will strongly distort the response function of the spectrometer. Therefore, an upper limit is imposed on the endpoint energies of the β spectra that can be studied with the present spectrometer.

Monoenergetic electrons leaving a point on the axis of the solenoid at different angles with respect to the axis, follow trajectories that have different orbit diameters (compare for example figures 5.8a 5.9a and 5.8b, 5.9b). The electrons that are emitted at the maximum angle of acceptance of the spectrometer have the largest diameter orbits (because they have the largest transvers velocity compcnents). The angle at which these elctrons enter the detector (maximum angle of incidence) is needed for the calculation of the maximum diameter of the orbits.

The maximum angle of incidence can be calculated from the following equation (Rietz & Milford 1967 pp. 277-278)

$$\theta = \mathrm{Sin}^{-1}\left(\frac{B_z(z)}{B_z(0)}\right)^{1/2} \qquad 5.9$$

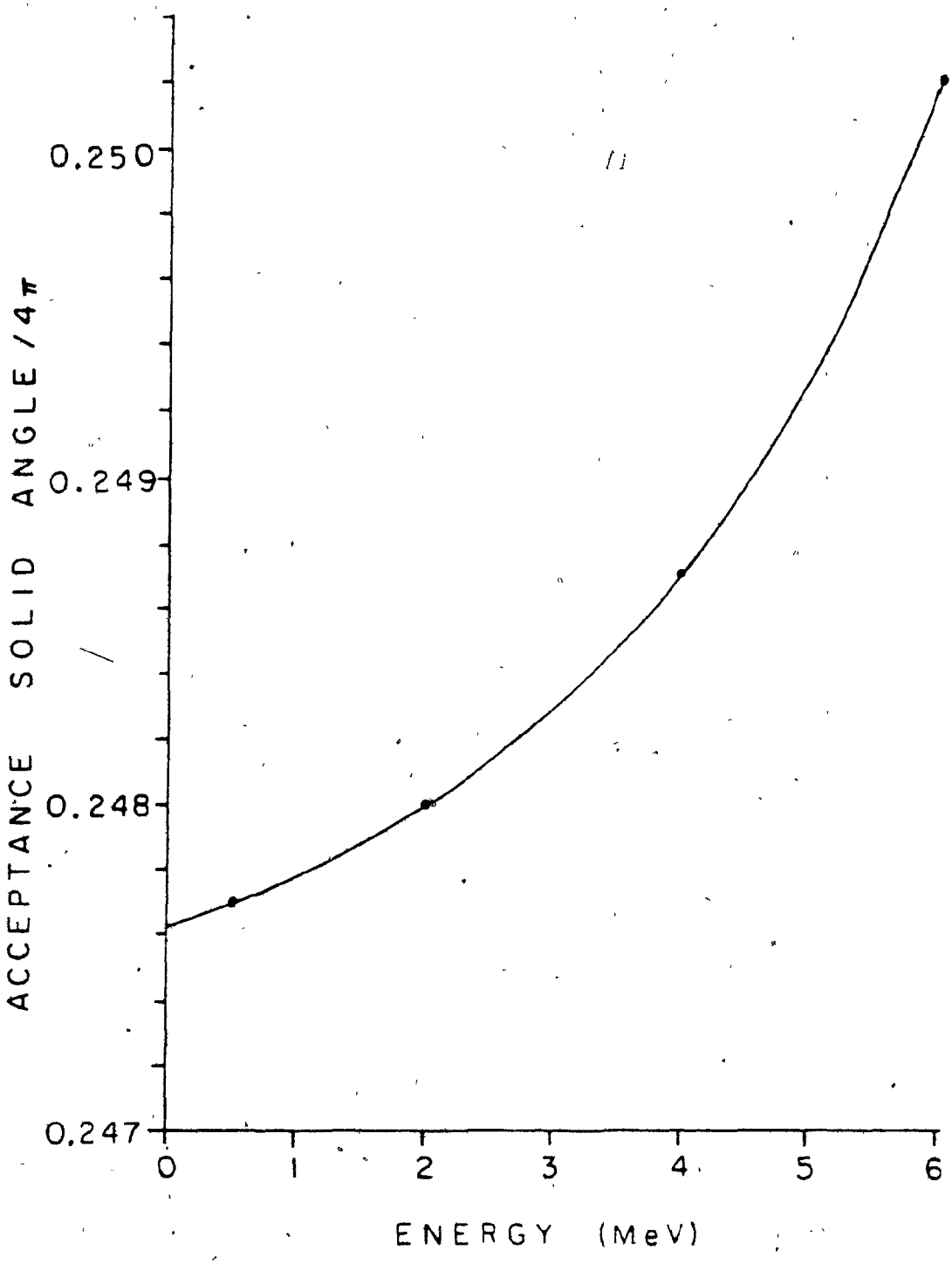

Figure 5.11

Solid angle for betas as a function of kinetic energy.

Figure 5.12

Penetration of the electrons into the solenoid at two different energies. The electrons are emitted at 60° to the axis in the plane of the figure.

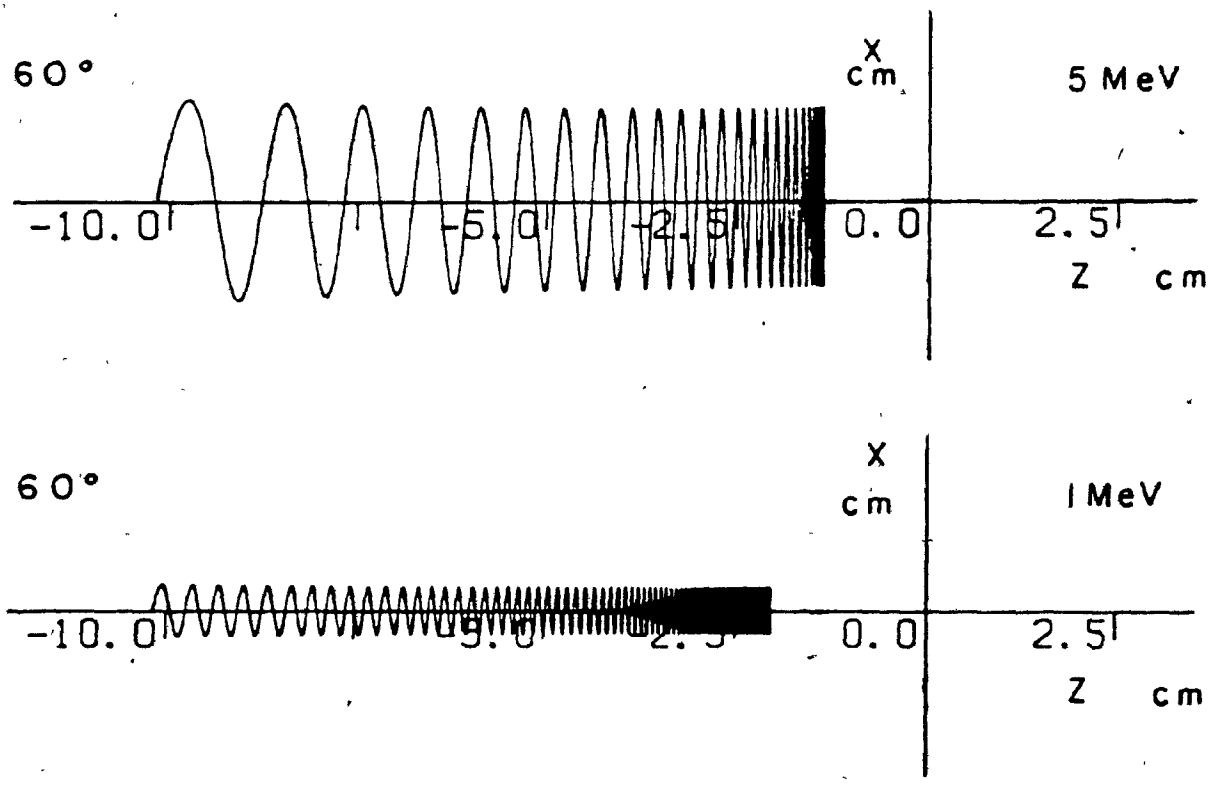
60°
X
cm
5 MeV
-10.0
-5.0
-2.5
0.0
2.5
Z cm
60°
X
cm
1 MeV
-10.0
0.0
2.5
Z cm

where

θ = The maximum angle of incidence

$B_z(z)$ = The axial magnetic field at the location of the detector

$B_z(0)$ = The magnetic field at the center of the solenoid

In the present spectrometer, the detector was placed just inside the solenoid, 1 inch (2.54 cm) from the end of the solenoid (i.e. the positions of the source and the detector are symmetric about the center of the solenoid). Therefore the maximum angle of incidence is the same as the maximum angle of acceptance (60°).

A good estimate of the radius of the electron trajectory at the detector position can be made by assuming that the magnetic field is locally uniform and using equation (12.42) from Jackson 1975, we then have:

$$r = \frac{p \ \mathrm{Sin}\ \theta}{3.0 \ B} \qquad 5.10$$

where

r = The radius of the elctron robit in cm

p = The momentum of the electron in MeV/c

B = The magnetic field strength, in tesla

θ = The angle between p and B

At the detector's location $\theta = 60°$, B = 3.28 tesla. Therefore for the detector used (1.27 cm radius) and with a point source placed on the solenoid axis, the maximum energy that can be studied with the spectrometer is 6.7 MeV (see figure 5.13). Using a source of finite size lowers this limit significantly. For a 3 mm diameter source, the limit on the maximum electron energy is 5.8 MeV.

Figure 5.14 shows the results of a numerical calculation of the trajectories of 5 MeV electrons illustrating the diameter of the orbits of electrons emitted at angles close to the maximum angle of acceptance. The two plots in the figure are the projections in the XZ plane of the trajectories of two 5 MeV electrons emitted at 58° with respect to the solenoid axis. Both electrons are emitted perpendicular to the plane of the figure (XZ plane); in one case the electron is emitted out of the XZ plane (towards the viewer) while in the other case it is emitted into the XZ plane (away from the viewer). The angle of emission of the electrons (with respect to the solenoid axis) shown in figure 5.14 (58°) is close to

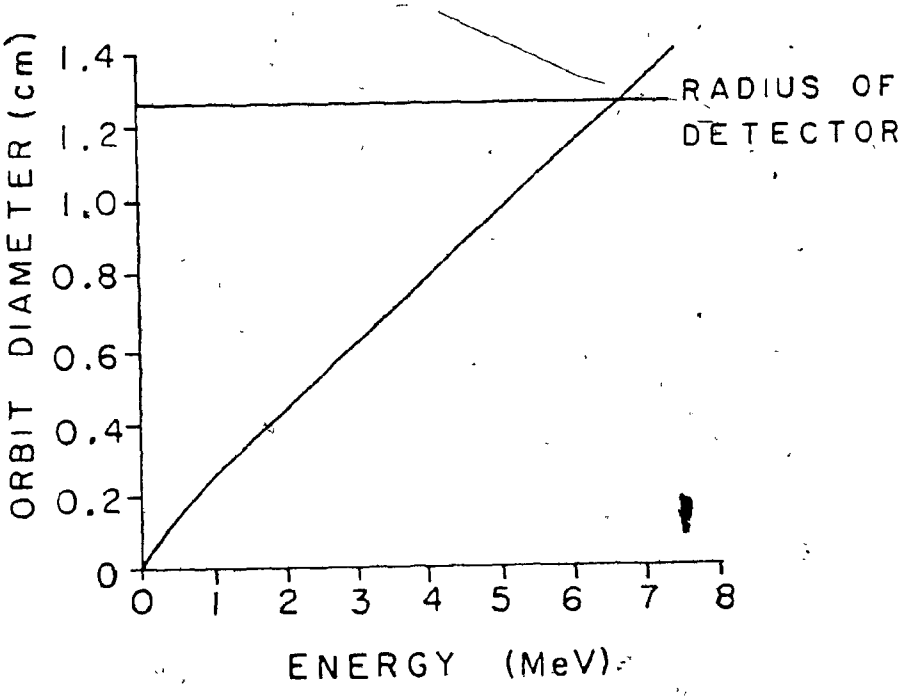

Figure 5.13

Diameter of electron orbits as a function of energy.

Figure 5.14

Trajectories of 5 MeV electrons emitted at 58° to the axis perpendicular to the plane of the figure.

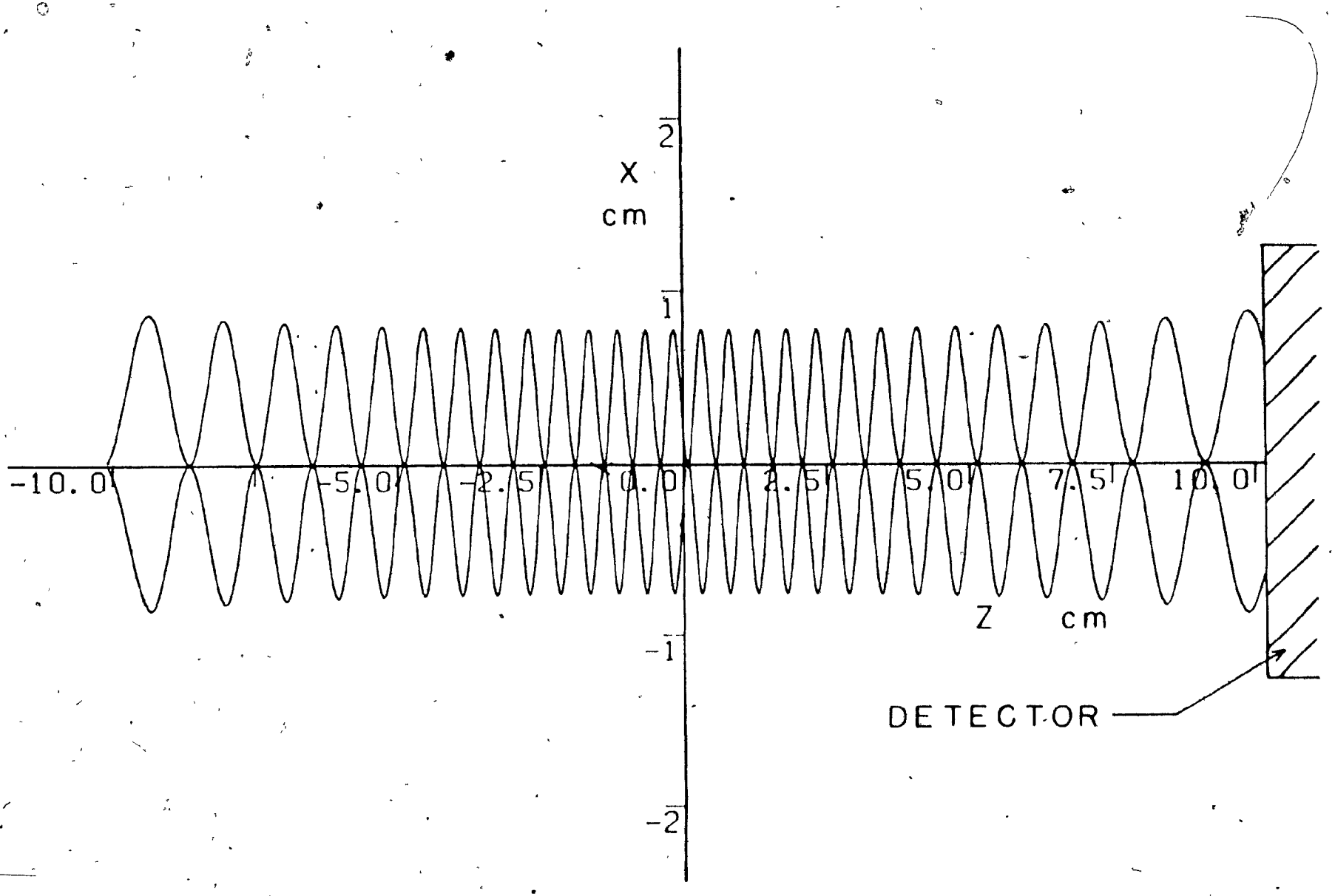
2
X
cm
1
-10.0
-5.0
-2.5
0.0
2.5
5.0
7.5
10.0
Z cm
-1
-2
DETECTOR

the maximum angle of acceptance of the spectrometer. Therefore the diameter of the "beam" that these electrons form ~15 mm is close to the diameter of the area on the surface of the detector inside of which all the 5 MeV electrons accepted by the spectrometer impinge. For reference the diagram shows the diameter of the detector used in the spectrometer Again, note that geometery is distorted in the figure because of the different scales used for the two axes.

5.5 Solid Angle for Gamma Ray Detection

The solid angle for γ ray detection is simply the geometrical solid angle subtended by the detector at the source. When the source and the detector are in their standard positions inside the solenoid 20.3 cm apart, the solid angle for γ ray detection is 9.7×10^{-4} steradians

The γ ray suppression that is brought about by this source-detector separation is equal to the reduction in the flux of 1 MeV rays that results from placing the source and the detector on either side of a slab of lead, 4 cm thick. Moreover, the reduction in the γ ray flux achieved by the large source-detector separation is independent of the energy of the γ rays.

5.6 Experimental Verification of the Performance of the Spectrometer

5.6.1 Solid Angle of Acceptance

The dependence of the solid angle of acceptance of the spectrometer on the electron energy is too small to be easily verified experimentally. However, the variation of the solid angle of acceptance with source position along the solenoid axis can be checked with a conversion electron source.

The conversion electron lines from ^{207}Bi were used to measure solid angle of acceptance of the spectrometer for several source positions along the axis of the solenoid. Since the detector is maintained in the same position throughout the measurements, the angular distribution of the electrons entering it remains constant (see Section 5.4) and the response function of the detector is unchanged (Hetherington 1984). The area of the conversion electron peaks in the spectrum can therfore be used as a direct measure of the relative solid angle of acceptance of the

spectrometer.

A thin ^{207}Bi source deposited on a thin mylar backing was placed at various positions along the axis of the solenoid starting at 1 inch (2.54 cm) outside the solenoid and progressing in 1 inch steps to the center of the solenoid. The relative peak areas of the K conversion electron lines as a function of the source axial position are shown in figure 5.15. The results are in good agreement with the solid angles of acceptance calculated from the constant flux approximation (see figure 5.7).

5.6.2 Axial Displacements of the Source

A direct check on the effects of small variations in the axial position of the source on a measured beta spectrum was made with two beta sources: ^{32}P with an endpoint of 1.7 MeV and ^{88}Rb with an endpoint of 5.3 MeV. The beta spectra were collected with the sources placed at the standard position and at axial displacements of 2 and 5 mm towards the center of the solenoid and away from it.

After background subtraction, the various spectra collected at different axial positions were compared with the spectrum collected at the standard position. The comparison is performed with a computer program, COMPARE (Hetherington 1984). The two spectra are first normalized by multiplying one of them by a constant sc that it has the same total number of counts as the second spectrum in a specified region. The program then calculates the difference between the two spectra for each channel and normalizes the difference by dividing it by the standard deviation for each channel:

$$D = \frac{s N_2 - N_1}{\sigma} \qquad 5.11$$

$$\sigma = \sqrt{N + s^2 N} \qquad 5.12$$

where,

D = The normalized difference

N_1 = The number of counts/channel in spectrum 1

N_2 = The number of counts/channel in spectrum 2

s = The scale factor used to normalize the two spectra

Figure 5.16 shows the comparisons for the ^{32}P source. No systematic trends in the normalized differences plots are detected for any of the

Figure 5.15

Solid angle vs source position on solenoid axis. Data from ^{207}Bi K conversion lines:

x 0.482 MeV

o 0.976 MeV

I 1.682 MeV

Solid line calculated by constant flux approximation.

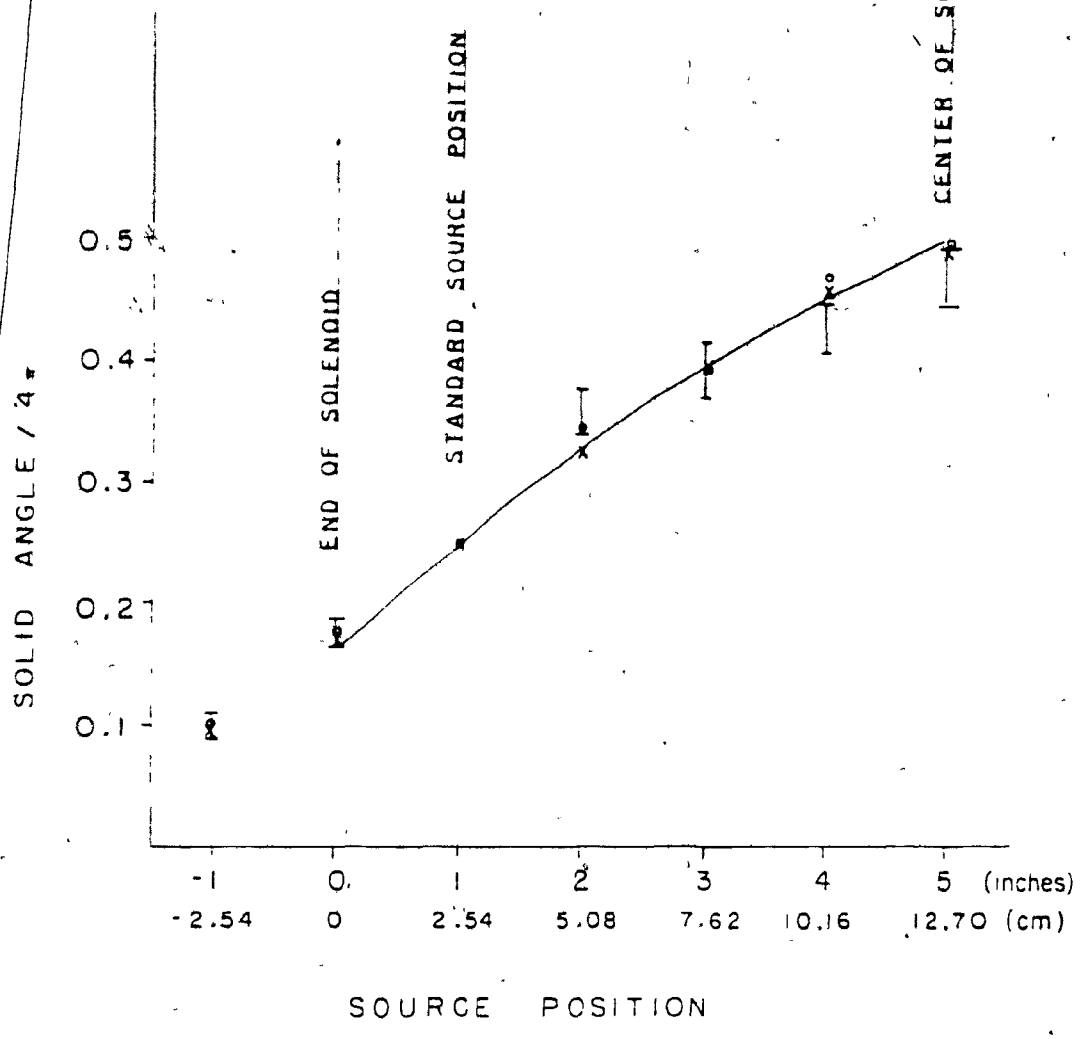
SOLID ANGLE / 4π
0.5
0.4
0.3
0.2
0.1
END OF SOLENOID
STANDARD SOURCE POSITION
CENTER OF SOLENOID
-1
-2.54
0
0
1
2.54
2
5.08
3
7.62
4
10.16
5 (inches)
12.70 (cm)
SOURCE POSITION

Figure 5.16

Comparison of ^{32}P spectra for different axial source positions:

(a) 5 mm out from standard position
(b) 2 mm out from standard position
(c) 2 mm in from standard position
(d) 5 mm in from standard position

Each graph shows the normalized differences between the spectrum taken at the stated position and one taken at the standard position.

(a)

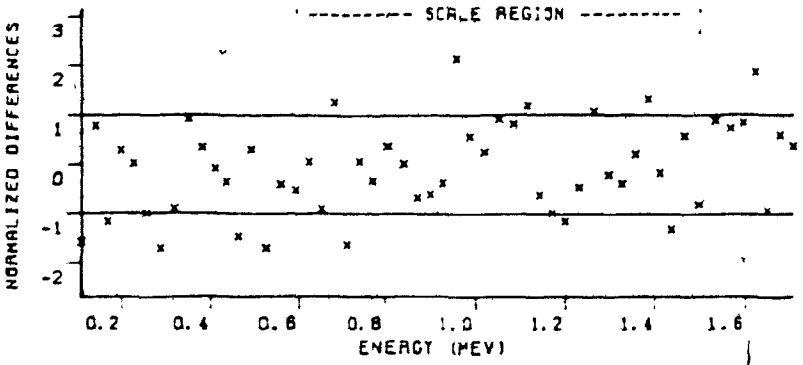
SCALE REGION
NORMALIZED DIFFERENCES
3
2
1
0
-1
-2
0.2
0.4
0.6
0.8
1.0
1.2
1.4
1.6
ENERGY (MEV)

(b)

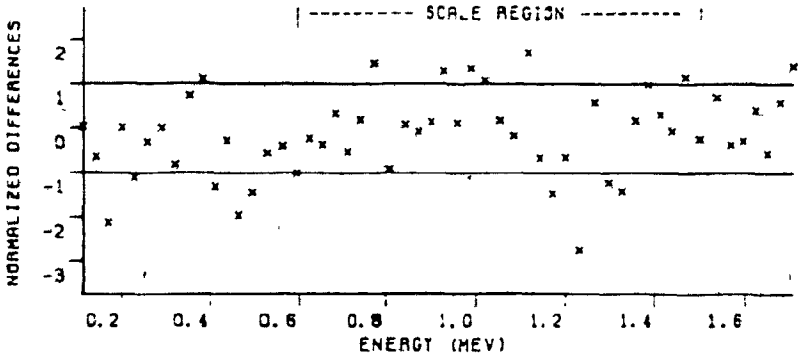
SCALE REGION
NORMALIZED DIFFERENCES
2
1
0
-1
-2
-3
0.2
0.4
0.6
0.8
1.0
1.2
1.4
1.6
ENERGY (MEV)

(c)

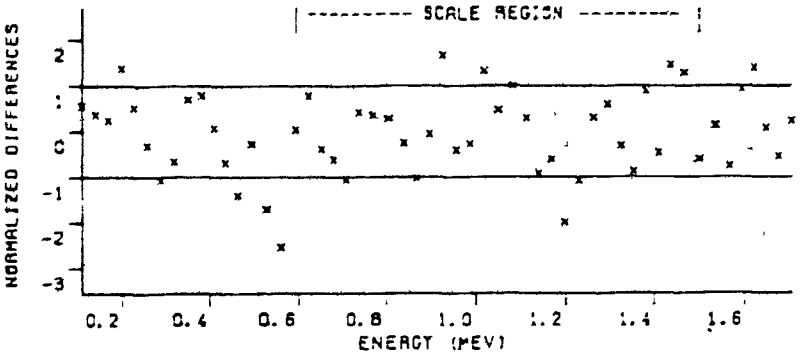
SCALE REGION
NORMALIZED DIFFERENCES
2
1
0
-1
-2
-3
0.2
0.4
0.6
0.8
1.0
1.2
1.4
1.6
ENERGY (MEV)

(d)

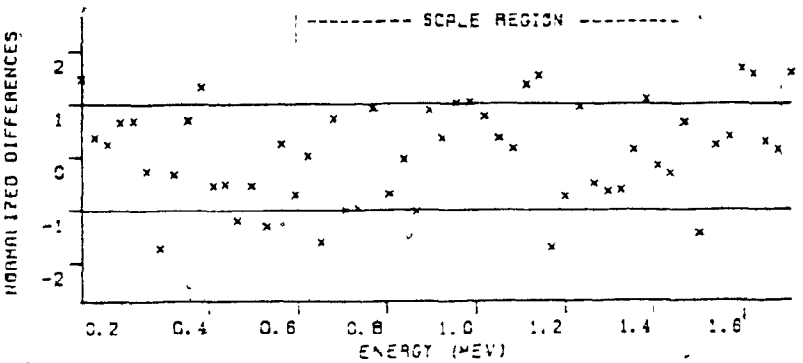
SCALE REGION
NORMALIZED DIFFERENCES
2
1
0
-1
-2
0.2
0.4
0.6
0.8
1.0
1.2
1.4
1.6
ENERGY (MEV)

spectra collected from the axially displaced sources. Therefore, it can be concluded that displacements of up to 5 mm in either direction along the solenoid axis will not result in any observable changes in the shapes of the measured β spectra of ^{32}P. From the statistics of the collected data at low energies (i.e. the value of σ/N_1, for channels in the low energy region) it was estimated that the normalized differences plots are sensitive to distortions of the order 0.5%.

The same measurements were repeated for a ^{86}Rb β source. The results are displayed in figure 5.17 and they confirm the conclusions drawn from the measurements perfomred with the low endpoint energy β source ^{32}P.

These results clearly show that the small energy dependence of the solid angle of acceptance is not perceptibly influenced by the axial position of the source for displacements of 5 mm or less from the standard position.

5.6.3 Radial Displacements of the Source

The effect of the radial displacement of the sourcce on the the measured β spectra was studied using ^{32}P and ^{86}Rb β sources.

Four ^{32}P sources were prepared; in one source, the activity was centered on the axis while in others it was located at distances of 2 5, and 10 mm respectively from the center. Spectra collected from the different off axis sources are compared with the spectrum collected from the centered source using the same method of normalized differences described in section 5.6.2. The results are displayed in figure 5.18. All of the plots show an excess of counts at the lower end of the spectrum. Even for a radial displacement of 2 mm there is an excess of about 1.7% in the lowest channel. The distortion for the 10 mm displacement is extreme and a deficiency of counts at high energies indicates that some of the β particles are missing the edge of the detector.

Similar measurements were performed using ^{86}Rb sources. All sources were 2 mm in diameter and included one centered source and five off-center sources. In four of the off-center sources, the radioactivity was located at 1, 2, 4, and 6 mm to the right of the axis while in the fifth, the radioactivity was deposited 2 mm to the left of the axis. The

Figure 5.17

Comparison of ^{88}Rb spectra for different axial source positions:

(a) 5 mm out from standard position
(b) 2 mm out from standard position
(c) 2 mm in from standard position
(d) 5 mm in from standard position

Each graph shows the normalized differences between the spectrum taken at the stated position and one taken at the standard position

(a)

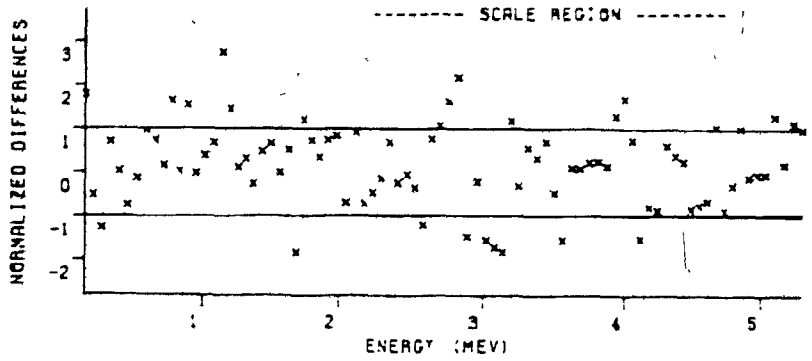
-------- SCALE REGION --------
NORMALIZED DIFFERENCES
3
2
1
0
-1
-2
1
2
3
4
5
ENERGY (MEV)

(b)

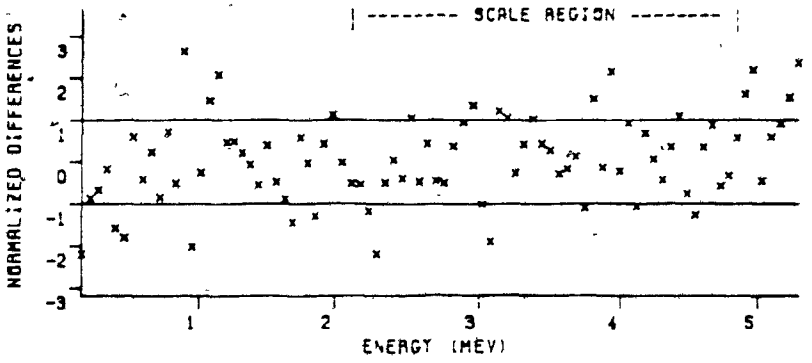
-------- SCALE REGION --------
NORMALIZED DIFFERENCES
3
2
1
0
-1
-2
-3
1
2
3
4
5
ENERGY (MEV)

(c)

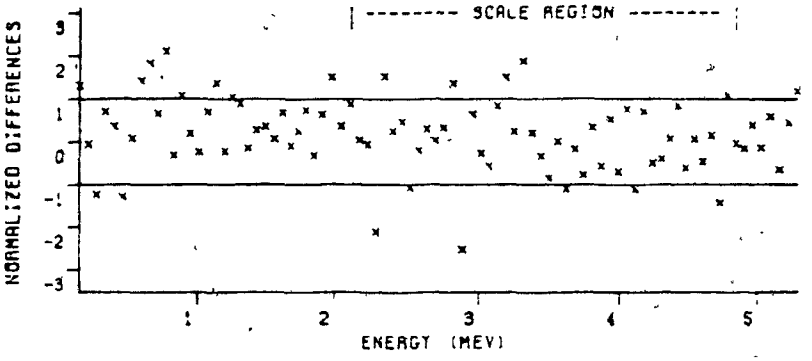
-------- SCALE REGION --------
NORMALIZED DIFFERENCES
3
2
1
0
-1
-2
-3
1
2
3
4
5
ENERGY (MEV)

(d)

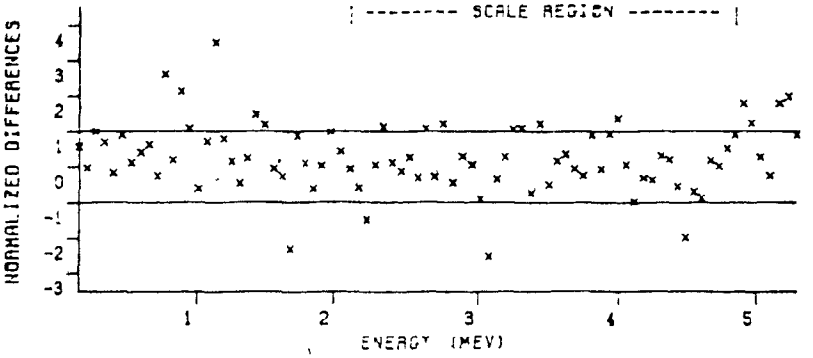
-------- SCALE REGION --------
NORMALIZED DIFFERENCES
4
3
2
1
0
-1
-2
-3
1
2
3
4
5
ENERGY (MEV)

Figure 5.18

Comparison of ^{32}P spectra for different radial source positions:

(a) 2 mm off axis
(b) 5 mm off axis
(c) 10 mm off axis

Graphs show the normalized differences between the spectrum taken at the stated position and one taken on the axis.

(a)

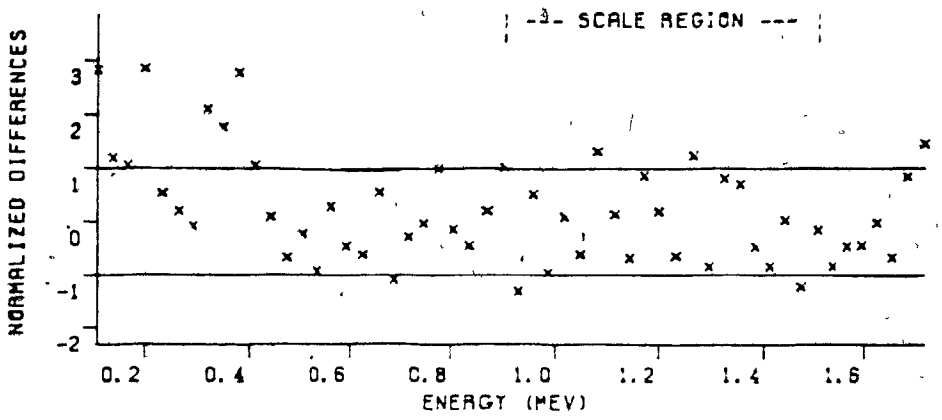
SCALE REGION
NORMALIZED DIFFERENCES
3
2
1
0
-1
-2
0.2
0.4
0.6
0.8
1.0
1.2
1.4
1.6
ENERGY (MEV)

(b)

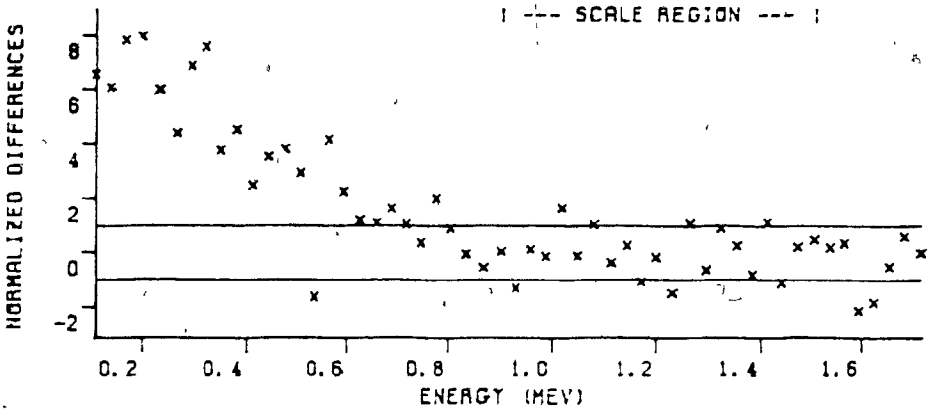
SCALE REGION
NORMALIZED DIFFERENCES
8
6
4
2
0
-2
0.2
0.4
0.6
0.8
1.0
1.2
1.4
1.6
ENERGY (MEV)

(c)

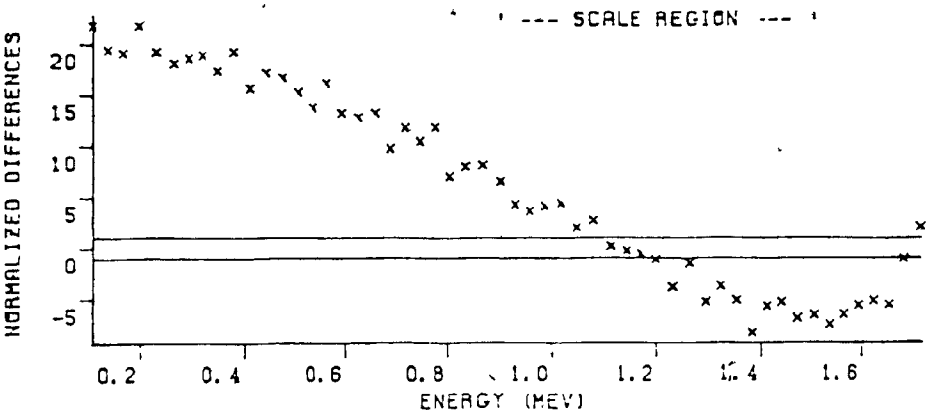
SCALE REGION
NORMALIZED DIFFERENCES
20
15
10
5
0
-5
0.2
0.4
0.6
0.8
1.0
1.2
1.4
1.6
ENERGY (MEV)

normalized differences plots are shown in figure 5.19. A 1 mm displacement produces no distortions while the 2 mm displacements show an excess of counts at the low energy end of the spectrum of 1% and 3% for the left and right displacements respectively. The distortions at 2 mm displacements are comparable to that seen in ^{32}P at the same radial displacement. The difference between the deviations measured for the right and left sources is probably due to the fact that the "centered" source was not perfectly centered on the solenoid axis. An educated guess would put the centering error at about 0.5 mm.

The spectrum collected with the 4 mm off-axis source shows a 4.5% excess in the number of counts at the low energy end and a deficiency of about 3.5% in the number of counts at energies above 4 MeV. For the 6 mm off-center source, the same deficiency in the number of counts is seen down to 3 MeV. This effect is due to the fact that some of the electrons at the higher energies miss the sensitive area of the detector. To verify this, equation 5.10 can be used to calculate the maximum diameter of the electron orbits. For a 2 mm diameter source, displaced by 4 mm from the axis of the solenoid, 4 MeV electrons incident at the detector at an angle of 60° to the axis (i.e. electrons with maximum diameter orbits) will have a maxium displacement from the solenoid axis of 1.29 cm. This is larger than the radius of the sensitive area of the detector (1.27 cm). Similarly, for a 2 mm diameter source, 6 mm off-axis, the maximum displacement of 3 MeV electrons is 1.31 cm.

It can be concluded from the β spectra measurements performed at different radial source positions that the accuracy of the positioning of the source in the radial direction is critical. At large radial displacements some of the energetic electrons miss the sensitive area of the detector resulting in distortions to the spectra. At small radial displacements (~2 mm) the excess of counts in the lower part of the spectrum is probably caused by changes in the angular distribution of electrons incident on the detector face. It is necessary therefore to ensure that the 3 mm sources usually used in the spectrometer are acccuarately centered on the axis of the solenoid with a centering error of no more than 1 mm.

Figure 5.19

Comparison of ^{88}Rb spectra for different radial source positions:

(a) 1 mm to right of axis
(b) 2 mm to right of axis
(c) 4 mm to right of axis
(d) 6 mm to right of axis
(e) 2 mm to left of axis

(a)

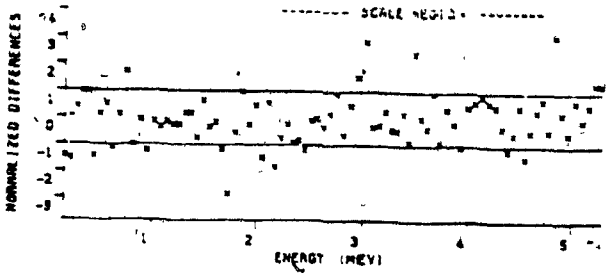
SCALE REGION
NORMALIZED DIFFERENCES
ENERGY (MEV)

(b)

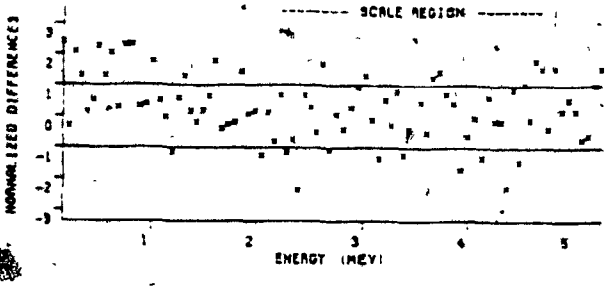
SCALE REGION
NORMALIZED DIFFERENCES
ENERGY (MEV)

(c)

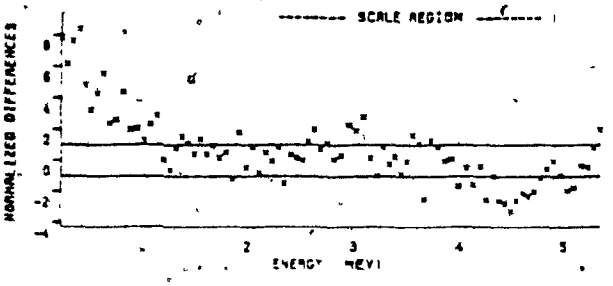
SCALE REGION
NORMALIZED DIFFERENCES
ENERGY (MEV)

(d)

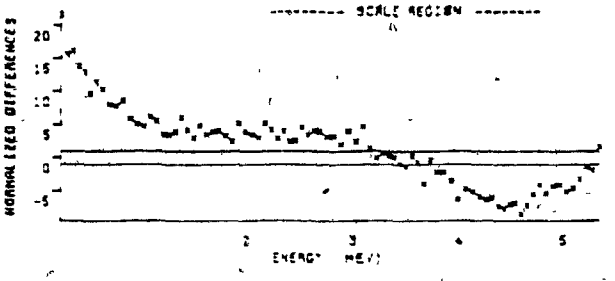
SCALE REGION
NORMALIZED DIFFERENCES
ENERGY (MEV)

(e)

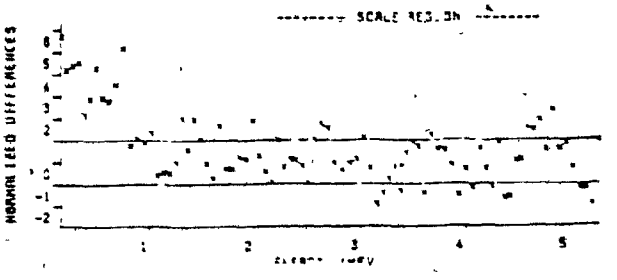
SCALE REGION
NORMALIZED DIFFERENCES

5.6.4 Axial Displacements of the Detector

The position of the detector along the axis of the solenoid determines the maximum angle of incidence and the angular distribution of the electrons impinging on its surface (see Jackson 1975 eqns. 12.70-12.72). This in turn has a strong effect on the response function of the detector. As was mentionned in the review section on axial magnetic guides, moving the detector closer to the center of the solenoid (i.e. to a higher field region) increases the maximum angle at which electrons enter the detector (see equation 5.9 and figure 5.2). The increase in the angles of incidence results in an increase in the probability for backscattering and therefore in a reduction in the peak fraction (the intensity of the full energy peak) in the response function (see Chapter 2). Moving the detector away from the center of the solenoid has the opposite effect.

During most of the experiments performed with the present spectrometer, the source and detector were placed at symmetric points in the magnetic field. As a result, the directional distribution of the beta particles at the detector is the same as that at the source. This simplifies the problem of determining the points and angles of entry of the β particles into the detector.

As a result of the importance of the angles of incidence and the points of entry of electrons into the detector on the determination of the response function, an experiment was performed to evaluate the effect of the detector's axial position on the response function.

A ^{207}Bi conversion electron source was placed in the standard source positions on the solenoid axis. The detector was moved in 1 inch (2.54 cm) increments from an initial position at the end of the solenoid (i.e. 1 inch outside the standard position) to a final position of 2 inches from the center of the solenoid. Since the source position was fixed, the solid angle of acceptance of the spectrometer is constant (equation 5.8) and the areas of the conversion electron peaks are a measure of the intensity of the full energy peak of the response function. (The highest energy peak in the conversion electron spectrum of ^{207}Bi that was used in this measurement is at 0.976 MeV. At this energy the diameters of the orbits of the electrons are small enough that their variation, as a result of changes in the detector position (equation 5.10,

figure 5.2) does not result in a reduction in the effective transmission i.e. the orbits are still confined within the sensitive surface area of the detector).

The data is displayed in figure 5.20. The peak areas were normalized to a value of 1.0 at the standard detector position. The intensities of the peaks at the different locations relative to the intensities at the standard detector position are shown in the figure. The expected decrease in the intensity of the peaks as the detector is moved from a low magnetic field region to higher magnetic field regions is clearly seen. The change in the peak fractions (peak intensities) is the same for both the 0.482 MeV and the 0.976 MeV lines.

It is quite clear from the preceeding measurements that changes in the axial position of the detector result in significant changes in the response function of the detector. In order to examine the effects of such changes on the β spectra measured with the present spectrometer, spectra from a ^{88}Rb source were collected at different detector positions. The detector was moved 2 and 5 mm from the standard position, along the axis of the solenoid, into and out of the solenoid. The normalized differences between the spectra collected at the different detector positions and the spectrum collected at the standard position are shown in figure 5.21. Displacements into the higher field region show the expected excess of counts at low energies caused by the increase in the backscattering probability. Displacements to low field regions show the opposite effect.

It is quite clear that the axial position of the detector in the solenoid strongly affects the response function of the detector. It is estimated that the detector position in the present spectrometer was reproducible to within ±1 mm. This causes a variation of about 0.5% in the peak fraction (see figure 5.21).

5.7 Measurements of Standard Beta Spectra

The spectrometer response function and the beta spectrum analysis programs developed by Hetherington (1984) were used to analyze the β spectra of two standard sources: ^{32}P, ^{88}Rb. Complete descriptions of the analysis programs and the development of the response function are given in Hetherington (1984). A brief review of some of the relevant points is given here.

Figure 5.20

Relative peak fraction for response function vs detector position on axis. Data from ^{207}Bi conversion electron lines (•,x) and ^{88}Rb beta spectrum (Δ). Solid line is a visual aid only.

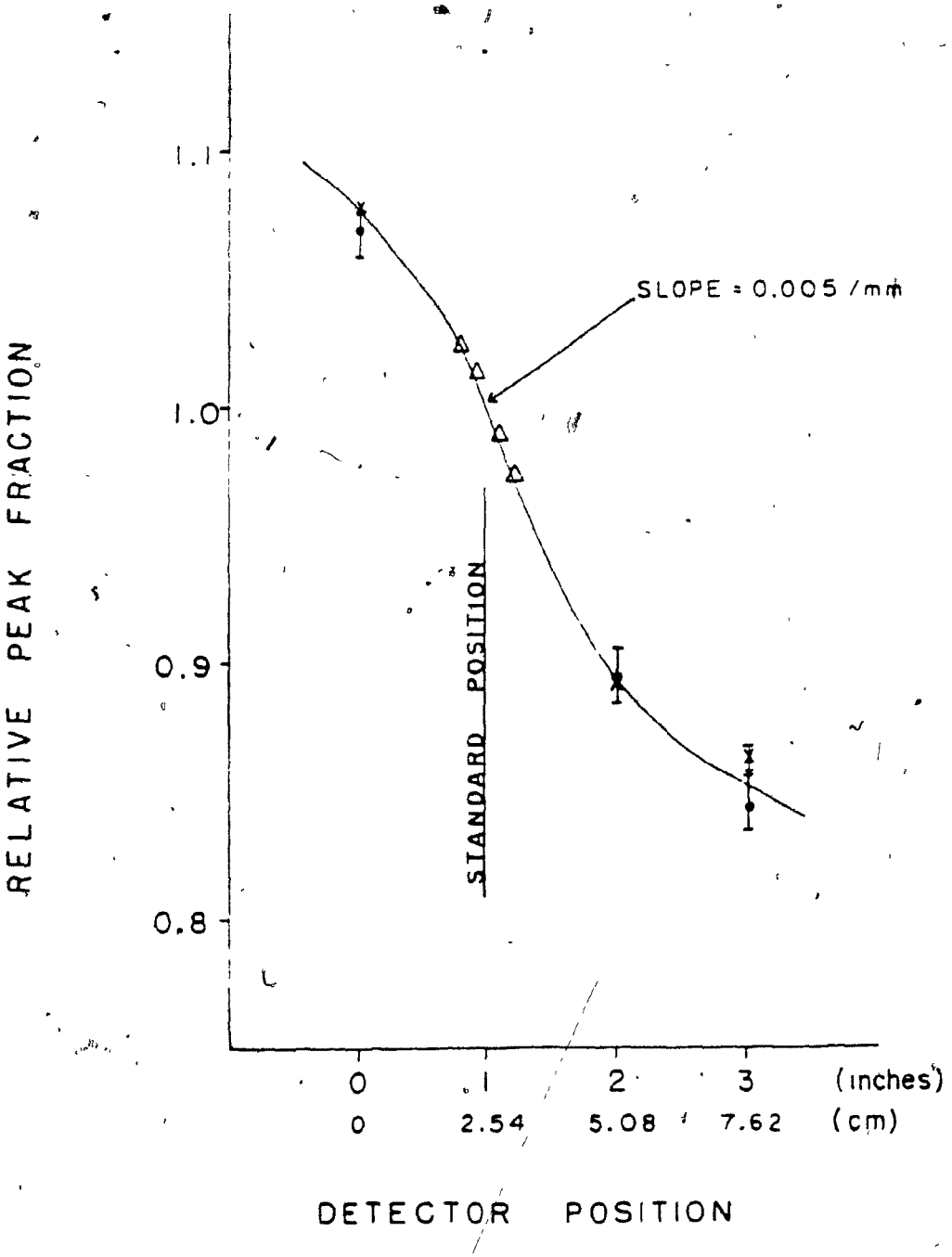
RELATIVE PEAK FRACTION
1.1
1.0
0.9
0.8
SLOPE = 0.005 /mm
STANDARD POSITION
0
1
2
3
(inches)
0
2.54
5.08
7.62
(cm)
DETECTOR POSITION

Figure 5.21

Comparison of ^{88}Rb spectra for different detector positions on solenoid axis:

(a) 5 mm in from standard position
(b) 2 mm in from standard position
(c) 2 mm out from standard position
(d) 5 mm out from standard position

Graphs show the normalized differences between the spectrum taken at the stated position and one taken at the standard position.

(a)

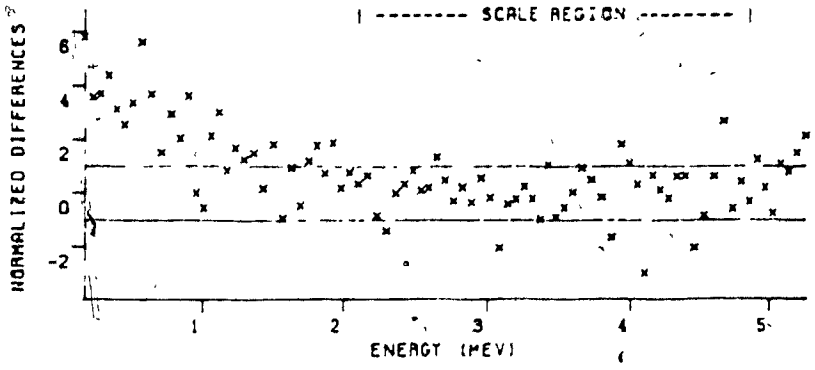
SCALE REGION
NORMALIZED DIFFERENCES
6
4
2
0
-2
1
2
3
4
5
ENERGY (MEV)

(b)

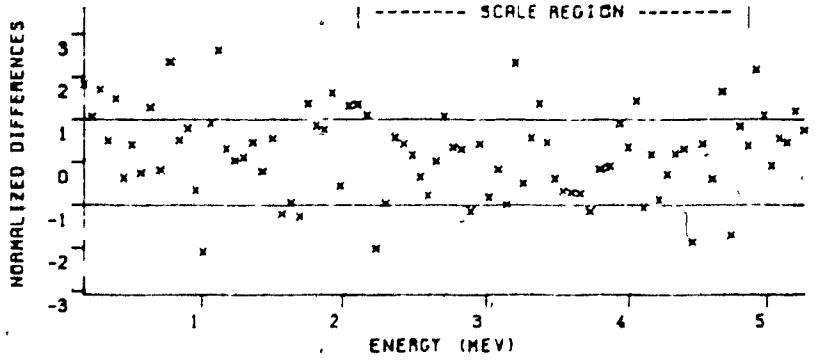
SCALE REGION
NORMALIZED DIFFERENCES
3
2
1
0
-1
-2
-3
1
2
3
4
5
ENERGY (MEV)

(c)

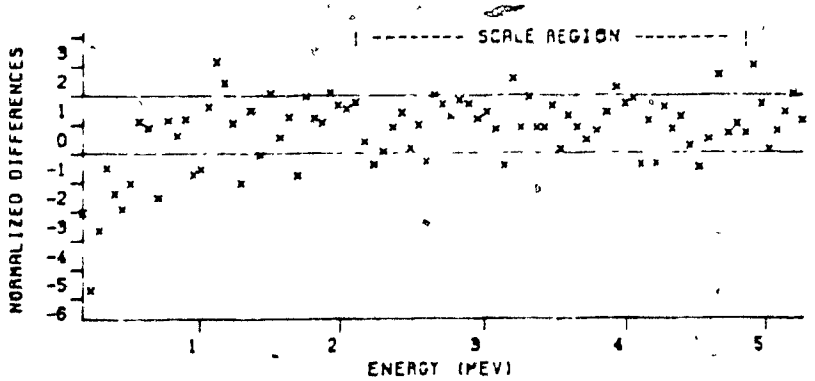
SCALE REGION
NORMALIZED DIFFERENCES
3
2
1
0
-1
-2
-3
-4
-5
-6
1
2
3
4
5
ENERGY (MEV)

(d)

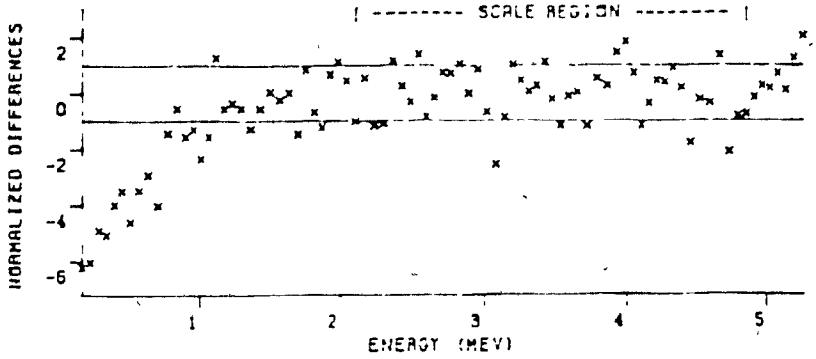
SCALE REGION
NORMALIZED DIFFERENCES
2
0
-2
-4
-6
1
2
3
4
5
ENERGY (MEV)

As mentioned in the beginning of this chapter, the response function was developed semi-empirically starting with a Monte Carlo simulation and then varying the parameters describing the shape of the response function until a simultaneous fit to several standard β spectra was obtained. Figure 5.22 shows the shapes of response function at different electron energies. The changes in the shapes at the different stages of development and modification are also indicated.

In order to acccount for the distortions to the β spectrum caused by the response function of the spectrometer, the spectrum analysis program (BETABRAN) uses the following procedure: A theoretical undistorted beta distribution (or distributions) is generated first, the response function is then folded into this distribution. The distorted distributions thus obtained are fitted directly to the raw data using least squares techniques. The goodness of the fit is tested by calculating the reduced chi-squared (χ^2_ν) over a specified fit region. For a good fit, the reduced chi-squared value is usually between 0.9 and 1.1. The fitting program also calculates the "residuals" [(data - fit)/standard deviation] for every channel in the fit region and plots them as part of the output. For a perfect fit, the residuals should be randomly distributed about zero with 2/3 of them lying between plus and minus one. A square root plot of the data and the fit is generated by the fitting program to enhance the display of the β spectrum and the fit near the end point.

5.7.1 ^{32}P

A solution containing ^{32}P (14 days half life) was purchased to prepare the source. The source was prepared by placing a small drop of the solution in the center of a thin mylar backing (0.3 mg/cm^2) and drying it in an oven. The resulting source was 2 mm in diameter and invisibly thin. The small amount of ^{33}P contamination (<1%) was accounted for in the analysis program.

The β spectra were collected using the standard electronics described in section 4.2. The count rates were between 1000 and 1500 c.p.s. Pulse pile up corrections were negligible and the background was substracted before analysing the data.

The data and the fit are shown in figure 5.23. The measured

Figure 5.22

Electron response functions for the present spectrometer.

x Monte Carlo calculations

.... original parametrization

--- after correction for reflected electrons

___ after modification of parameters to fit standard spectra

Note that the full energy peak is not drawn to scale.

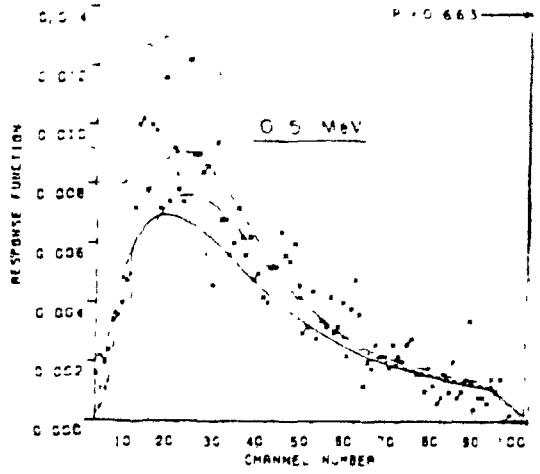
P = 0 663
0 5 MeV
RESPONSE FUNCTION
CHANNEL NUMBER

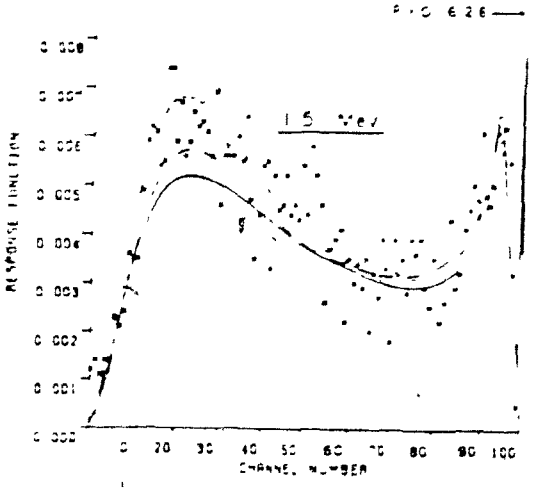
P = 0 626
1 5 MeV
RESPONSE FUNCTION
CHANNEL NUMBER

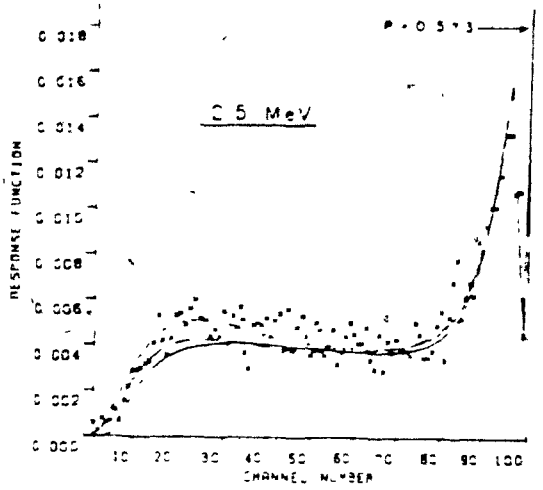
P = 0 573
2 5 MeV
RESPONSE FUNCTION
CHANNEL NUMBER

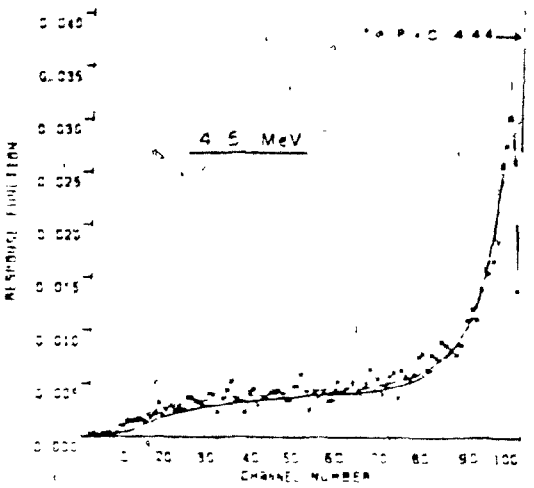
P = 0 444
4 5 MeV
RESPONSE FUNCTION
CHANNEL NUMBER

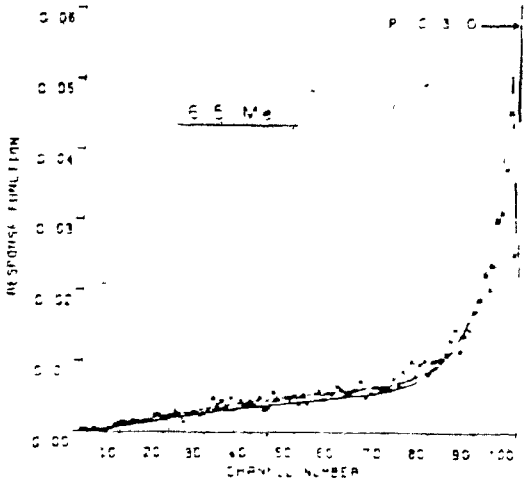
6 5 Me
RESPONSE FUNCTION
CHANNEL NUMBER

Figure 5.23

Data, fit and residuals for ^{32}P.

$E_o = 1.7101 \pm .0003$

$\chi^2_\nu = 1.072$

total counts = 7.63×10^6

^{33}P intensity = 0.8%

source thickness = 0.

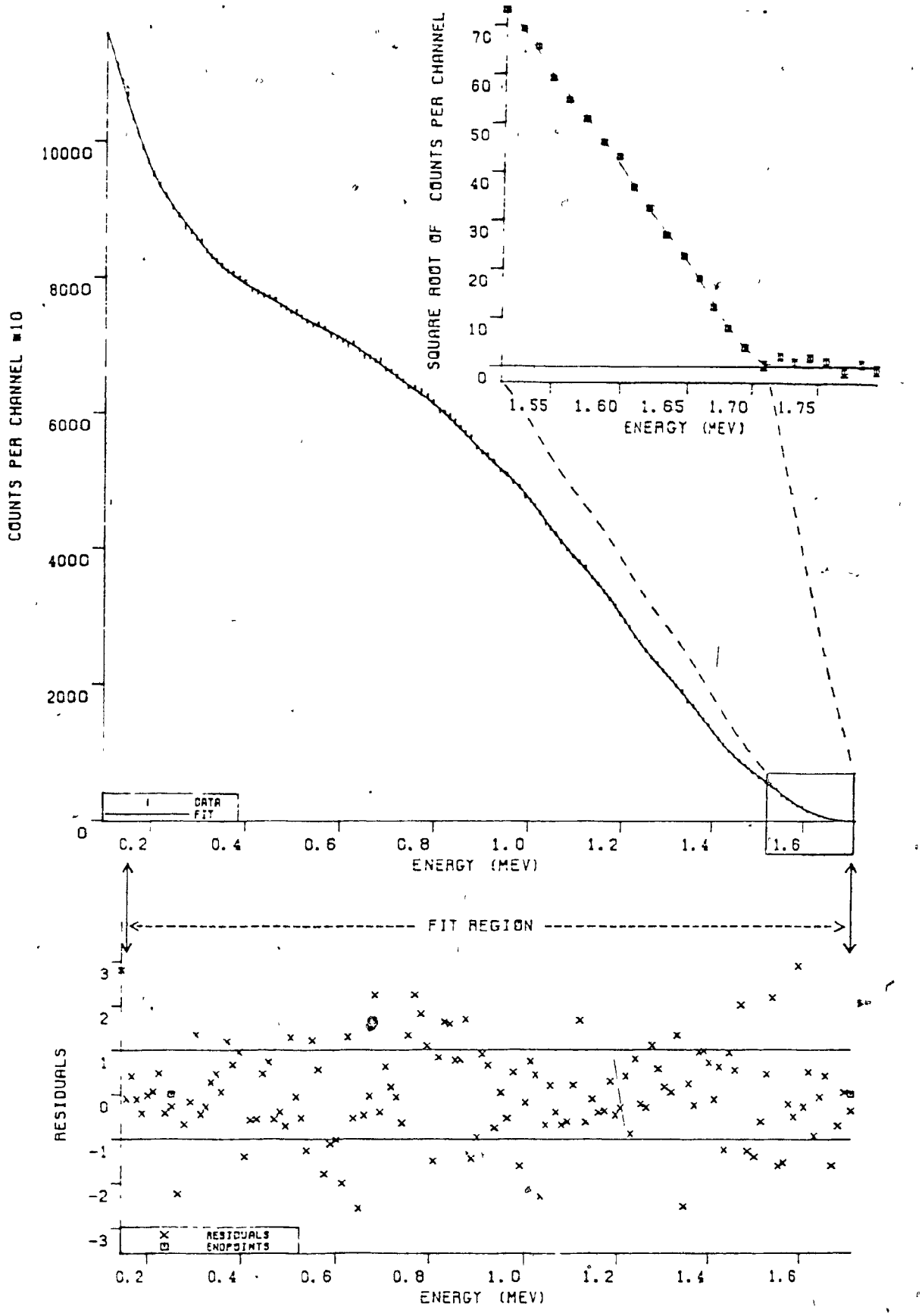
COUNTS PER CHANNEL *10
10000
8000
6000
4000
2000
0
DATA
FIT
0.2
0.4
0.6
0.8
1.0
1.2
1.4
1.6
ENERGY (MEV)
SQUARE ROOT OF COUNTS PER CHANNEL
70
60
50
40
30
20
10
0
1.55
1.60
1.65
1.70
1.75
ENERGY (MEV)
FIT REGION
RESIDUALS
3
2
1
0
-1
-2
-3
RESIDUALS
ENDPOINTS
0.2
0.4
0.6
0.8
1.0
1.2
1.4
1.6
ENERGY (MEV)

endpoint energy (1.7101 ± 0.0003 MeV) is in agreement with the value given in the Table of Isotopes (Lederer & Shirley 1978). The shape factor obtained (1 - 0.013 W) is in agreement with the results of previous measurements (the average of all but the most extreme values of the results that appear in the compilation of Behrens & Szybisz (1976), and the results of Hughes (1980)).

5.7.2 ^{88}Rb

The ^{88}Rb (half life 17.8 min) was produced by particle induced fission of ^{238}U (using 100 MeV protons or 50 MeV dueterons from the McGill Synchrocyclotron). The sources used were mass separated sources obtained from the on-line isotope separator at this laboratory. The ^{88}Rb ions were deposited on a thin mylar backing (0.3 mg/cm^2). A collimator ensured that the activity was centered and not more than 3 mm in diameter. The data collection was performed in a manner similar to that used for ^{32}P. Pile up corrections were negligible and the background was substracted before analysing the data.

The data and the fit are shown in figure 5.24. The end point energy (5.3176 ± 0.0015 MeV) and the branching ratios for the two highest energy branches are in good greement with the previous measurements (Lederer & Shirley 1978; Decker et al. 1980. 1982).

Figure 5.24

Data, fit and residuals for ^{88}Rb.

$E_o = 5.3176 \pm .0015$

$\chi^2_\nu = 0.827$

total counts = 10.0×10^6

Branches:

Endpoint (MeV)	Fraction	Shape Coefficients a	b	c
5.3175	0.78	-0.0045(13)	0.	0.
3.4816	0.0429(6)	-0.274(25)	0.	0.029(3)

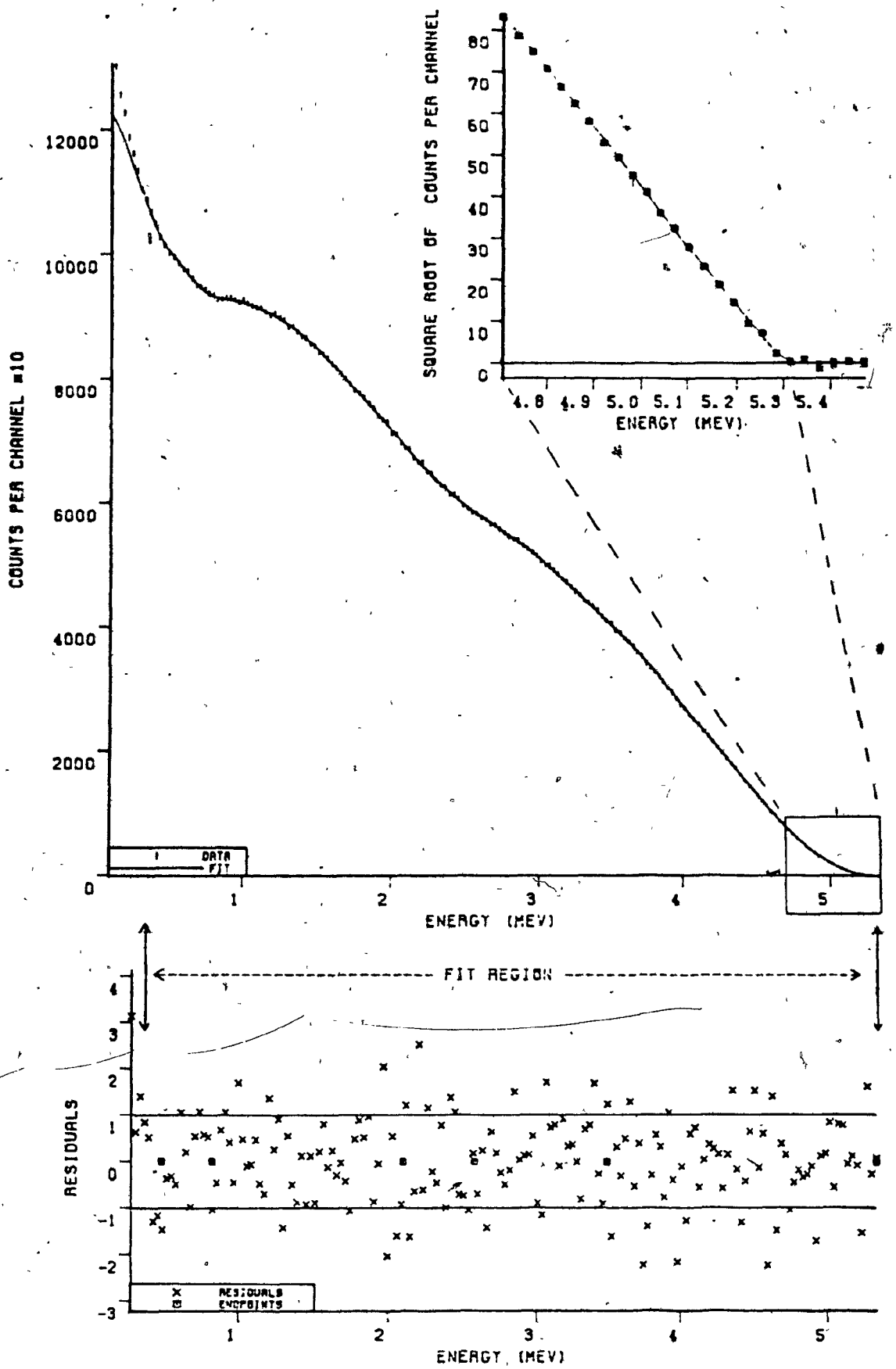
SQUARE ROOT OF COUNTS PER CHANNEL
80
70
60
50
40
30
20
10
0
4.8 4.9 5.0 5.1 5.2 5.3 5.4
ENERGY (MEV)
COUNTS PER CHANNEL *10
12000
10000
8000
6000
4000
2000
0
DATA
FIT
1
2
3
4
5
ENERGY (MEV)
FIT REGION
RESIDUALS
4
3
2
1
0
-1
-2
-3
RESIDUALS
ENDPOINTS
1
2
3
4
5
ENERGY (MEV)

CHAPTER 6

CONCLUSIONS

It is clear from the discussion presented in the introduction to this thesis (Chapter 1) that the information which can be extracted from β spectra measurements is of great importance in nuclear spectroscopy and fundamental physics. This fact has provided the motivation for the continuous development of new methods and techniques in β spectrometry.

The different types of β spectrometers that have been reviewed in Chapter 2 show certain shortcomings and deficiencies that are particular to each type. It is quite evident, however, that the capabilities of multichannel type spectrometers give them a clear advantage in the field of β spectrometry of nuclei far from stability. Among these energy sensitive detectors, high purity germanium detectors offer, in addition to other benefits, the best resolution.

The present spectrometer was therefore built with the aim of exploiting the exceptional capabilities of Ge(HP) detectors and overcoming the drawbacks that are associated with their use in β spectrometry. The superconducting transport solenoid used in the spectrometer solves the problem of γ ray sensitivity of the germanium detector. At the same time it provides a high transmission for β particles (25%) which is very nearly independent of the energy of the particles within a maximum energy limit of about 6 MeV.

The major difficulty associated with the use of a germanium β spectrometer is the distortion of the measured spectrum caused by the incomplete deposition of the energy of the β particles incident on the detector. This problem was resolved by determining the response function of the present spectrometer to a high degree of precision (Hetherington 1984).

The superconducting solenoid β spectrometer described in this thesis has been used for the measurement of the shape factor of the β spectrum of ^{20}F. The result of this experiment represents the most accurate determination to date of this small shape factor. It clearly illustrates the high accuracy with which the response function was

determined and gives a good indication of the limit of precision achievable with this type of spectrometer.

While little can be done to further improve the precision of the spectrometer (Hetherington 1984), its versatility can be enhanced quite considerably. A substantial improvement in the capabilities of the present spectrometer can be achieved through the implementation of new source delivery mechanisms such as a tape transport system. Another possibility is the use of the spectrometer in an on-line configuration in conjunction with an isotope separator and the injection of the radioactive ions directly into the bore of the magnet. With these source introduction techniques, isotopes with half lives as short as 1 sec or less can be easily studied with the spectrometer.

The present spectrometer has only been used to measure β^- (i.e. electron) spectra. This is mainly because the response function of the spectrometer to positrons is much more complicated than that for electrons (see Chapter 2). Determining the positron response function of the spectrometer even to a much lower accuracy than was achieved for β^- particles, can still be extremely useful. It can widen the range of applications of the spectrometer to include measurements of the endpoint energies of β^+ decays for example.

Using a combination of a larger surface area detector and a stronger magnetic field (either by operating the present solenoid at higher currents or by using a more powerful magnet) can extend the limit on the maximum β energy that can be studied with the spectrometer to well above 10 MeV.

The $\beta-\gamma$ coincidence capability of the spectrometer should be developed further since it can result in a considerable increase in the amount of information obtainable. The deterioration in the resolution of the γ detector in the strong magnetic field is most likely caused by the reduction in the mobility of the charge carriers as a result of the magnetoresistance of germanium (Hetherington 1984). The resolution can improved considerably by a judicious choice of the detector material, the detector's bias, and the amplifier pulse shaping time constant. Alternatively, the problem can be solved by using γ detectors placed in a low magnetic field region outside the solenoid. To accomplish this, a split coil pair magnet can be used. In this case, the radioactive source

would be placed at the center of the solenoid in the gap between the two coils. The γ ray detectors can then be placed outside the solenoid such that they view the source through the radial access ports. And because of the possibility of introducing the radioactive sources through one of the radial access port, the split pair magnet can be equipped with two β detectors at either end of the solenoid. This arrangement would be quite useful in 4π β spectrometry and electon-electron coincidence measurements. A β spectrometer using a split pair magnet and a single high purity germanium detector is currently under development at the Brookhaven National Laboratory (Gill 1984).

The use of a superconducting solenoid equipped with a persistent current mode switch and a liquid helium cryostat with a long holding time can simplify the operation of the spectrometer quite considerably. In addition, it would highly enhance the capabilities of the spectrometer as a result of the unlimited time available for data collection.

The technical aspects of the present spectrometer are summarized in table 6.1.

In comparison to other multichannel β spectrometers (energy sensitive detectors), the high transmission, excellent resolution, and exceptional γ ray suppression capabilities of the present spectrometer clearly set it apart from the rest.

When contrasted with the different types of magnetic β spectrometers, the superconducting solenoid spectrometer is distinguished by its high transmission. Among magnetic spectrometers only the large toroidal (orange) type is comparable to the present spectrometer on the basis of transmission (Siegbahn 1965). The Argonne iron free toroidal β spectrometer is perhaps the best of this type (Freedman et al. 1960; Siegbahn 1965). Nevertheless, its performance parameters (0.9% resolution, 18% transmission, 3.5 MeV maximum β energy, and 1 mm source diameter) are inferior to those of the superconducting solenoid spectrometer. Moreover, the single channel nature of the Argonne spectrometer and the complicated support equipment needed for its operation (Freedman et al. 1967a,b) put it at a clear disadvantage.

Finally, it is felt that an instrument with the exceptional capabilities and the breadth of applications of the present spectrometer should be given a name of its own. It is proposed to name this spectrometer the SHEEP (Superconducting High Energy Electron Positron) spectrometer (see Fig. 3.4).

Table 6.1 Technical Data for the Spectrometers

Solenoid (superconducting)	
windings: length (cm)	25.4
inner diameter (cm)	10.8
outer diameter (cm)	15.0
normal operating current (A)	100
field at center of solenoid (T)	4.4
Detector (hyperpure gemanium)	
surface area (mm^2)	500
depletion depth (mm)	15
operating bias (V)	1000
Source and Detector Position	
(distance from the center of solenoid)	
source (cm)	-10.16
detector (cm)	+10.16
Solid Angle/4 π	
β rays	0.25
γ rays	9.7×10^{-4}
ratio (β/γ)	255
Transmission	25%
Resolution	4.5 keV at 1 MeV
Source Diameter (mm)	3
Maximum Beta Energy (MeV)	
point source	6.7
3mm diameter source	5.8

REFERENCES

Abecasis, S., and Krmpotic, F., Nucl. Phys. A151 (1970) 641.

Adelberg, M., Applied Cryogenic Engineering, R.W. Vance and W.M. Duke, eds., John Wiley & Sons, New York (1962) 344.

Adelberg, M., Advances in Cryogenic Engineering 12 (1967) 252.

Agarwal, Y.K., Baba, C.V.K., and Mirta, S.K., Nucl. Phys. A127 (1969) 652.

Alburger, D.E., Rev. Sci. Inst. 27 (1956) 991.

Alkhazov, G.D., Mezilev, K.A., Novikov, Yu.N., Ganbaatar, N., Gromov, K. Ya., Kalinnikov, V.G., and Potempa, A., Z. Physik A310 (1983) 247.

Allan, C.J., Nucl. Inst. & Meth. 85 (1970) 181.

AMCO 4, Atomic Masses and Fundamental Constants 4, Proceedings of the Fourth International Conference on Atomic Masses and Fundamental Constants, Teddington, England (1971), J.H. Sanders, and A.H. Wapstra, eds., Plenum Press, London (1972)

AMCO 5, Atomic Masses and Fundamental Constants 5, Proceedings of the Fifth International Conference on Atomic Masses and Fundamental Constants, Paris (1975), J.H. Sanders, and A.H. Wapstra, eds.,Plenum Press, London (1976)

AMCO 6, Atomic Masses and Fundamental Constants 6, Proceedings of the Sixth International Conference on Atomic Masses and Fundamental Constants, East Lansing, Michigan (1979), J.A. Nolen, Jr., and W. Benenson, eds., Plennum Press, London (1980)

A.M.I.1, Selection Guide: Superconducting Magnets, Cryogenic Instruments and Accessories, American Magnetics, Inc., Oak Ridge, Tennessee (no date).

A.M.I.2, Operation Manual: Model 110 Liquid Helium Lever Meter, American Magnetics, Inc., Oak Ridge, Tennessee (no date).

A.M.I.3, Cryothermometer Model 210 Manual, Oak Ridge (no date).

Andersen, V., and Christenssen, C.J., Nucl Inst.& Meth 61 (1968) 77.

Andersen, V., Nucl. Inst & Meth. 65 (1968)

Andersen, V., Nucl. Inst. & Meth. 122 (1974) 543.

Anderson, H.L., ed., Physics Vade Mecum, American Institute of Physics, New York (1981).

Antman, S., Grunditz, Y., Johansson, A., Nyman, B., Pettersson, H., Svahn,

B., and Siegbahn, K., Nucl. Inst. & Meth. 82 (1970) 13.

Antman, S., and Svahn, B., Nucl Inst. & Meth. 82 (1970) 24

Arai, Y., Fujioka, M., Tanaka, E., Shinozuka, T., Miyatake, H., Yoshii, M., and Ishimatsu, T., Phys. Lett. 104B (1981) 186.

Arai, Y., Tanaka, E., Miyatake, H., Yoshii, M., Ishimatsu, T., Shinozuka, T., and Fujioka, M., Nucl. Phys. A420 (1984) 193.

Armini, A.J., Polichar, R.M., and Sunier, J.W., Nucl. Inst. & Meth. 48 (1967) 309.

Arnould, M., See AMCO6 (1980) 375.

Arvay, Z., Fenyes, T., Fule, K., Kibedi, T., Laszlo, S., Mate, Z., Morik, Gy., Novak, D., and Tarkanyi, F., Nucl. Inst. & Meth 178 (1980) 85.

Avignone, F.T., Pinkerton, J.E., and Trueblocd, J.H., Nucl. Inst. & Meth. 107 (1973) 453.

Avignone, F.T., and Greenwood, Z.D., Phys. Rev. C22 (1980) 594.

Avignone III, F.T., Noma, H., Moltz, D.M., and Toth, K.S., Nucl. Inst. & Meth 189 (1981) 453

Avignone, F.T., Moltz, D.M., Toth, K.S., Kern, B.D., and Noma, H., IEEE Trans. Nucl. Sci. NS-30, #2 (1983) 1136.

Aysto, J., Arje, J., Koponen, V., Taskinen, P., Hyvonen, H., Hautojarvi, A., and Vierinen, K., Phys. Lett. 138B (1984) 369.

Azuelos, G., and Kitching, J.E., Atomic Data & Nuclear Data Table 17 (1976) 103.

Azuelos, G., and Kitching, J.E., Nucl. Phys. A285 (1977) 19.

Azuelos, G., Belleau, M., Crawford, J.E., and Kitching, J.E., Nucl. Inst. & Meth. 142 (1977) 491.

Backe, H., Richter, L., Willwater, R., Kankeleit, E., Kuphal, E., Nakayama, Y., and Martin, B., Z. Physik A285 (1978) 159.

Backstrom, G., Backlin, A., Holmberg, N.E., and Bergkvist, K.E., Nucl. Inst. & Meth. 16 (1962) 199.

Bailey, C.A., Advanced Cryogenics, C.A. Bailey, ed., Plenum Press, New York (1971) 133.

Balcerek, K., and Rafalowicz, J., Proceedings of the Sixth International Cryogenic Engineering Conference, K. Mendelssohn, ed., IPC Science & Technology Press, Guildford, U.K. (1976) 255.

Bannerman, R.C., Lewis, G.M., and Curran, S. C., Phil. Mag 42 (1951) 1097.

Barron, R.F., Vacuum Technology at Low Temperatures, S.A. Stern, ed.,

American Institute of Chemical Engineers, Symposium Series, Vol 68, Number 125 (1972) 40.

Bartholomew, G.A., and Lee-Whiting, G.E., Nucl, Inst. & Meth 162 (1979) 239.

Bartlett, A.A., Ristinen, R.A., and Bird, R.P., Nucl. Inst. & Meth. 17 (1962) 188.

Beck, E., Nucl. Inst. & Meth. 76 (1969) 77.

Becquerel, H., Compt. Rend. Acad. Sci. 122 (1896) 420.

Beekhuis, H., and de Waard, H., Nucl. Phys. 74 (1965) 459.

Behrens, H., Kobelt, M., Thies, W.G., and Appel, H., Z. Physik 252 (1972) 349.

Behrens, H., Kobelt, M., Szybisz, L., and Thies, W.G., Nucl. Phys. A245 (1975) 515.

Behrens, H., and Szybisz, L., Shapes of Beta Spectra, Zentralstelle fur Atomkernenergie Documentation (ZAED), FRG, report 6-1 (1976).

Behrens, H. and Buhring, W., Electron Radial Wave Functions and Nuclear Beta Decay, Clarendon Press, Oxford (1982).

Behrens, H., and Christmas, P., Nucl. Phys. A399 (1983) 131.

Berg, H., Keyser, U., Munnich, F., Hawerkamp, K., Schrader, H., and Pfeiffer, B., Z. Physik A288 (1978) 59.

Berger, M.J., and Seltzer, S.M., Second Symposium on Protection against Radiations in Space, A. Reetz, ed., National Aeronautics and Space Administration, Washington, D.C., NASA SP-71 (1965) 437.

Berger, M.J., and Seltzer, S.M., Protection against Space Radiation, A. Reetz, Jr. and K. O'Brien, eds., National Aeronautics and Space Administration, Washington, D.C., NASA SP-169 (ANS-SD-5) (1968) 285.

Berger, M.J., Seltzer, S.M., Chappell, S.E., Humphreys, J.C., and Motz, J.W., Nucl. Inst. & Meth. 69 (1969) 181.

Bergstrom, I., Brown, F., Davies, J.A., Geiger, J.S., Graham, R.L., Kelly, R., Nucl. Inst. & Meth. 21 (1963) 249.

Bergstrom, I., Nucl. Inst. & Meth. 43 (1966a) 116.

Bergstrom, I., Nucl. Inst. & Meth. 43 (1966b) 129.

Berlovich, E.Ye, See CERN (1970) 497.

Bertolini, G., Cappelani, F., and Rota, A., Nucl. Inst. & Meth. 9 (1960) 107.

Bertolini, G., Capellani, F., Fantechi, R., and Restelli, G., Nucl. Inst. &

Meth. 27 (1964) 281.

Bertolini, G., and Rota, A., Semiconductor Detectors, G. Bertolini and A. Coche, eds., North Holland, Amsterdam (1968) 341.

Bethe, H.A., and Ashkin, J. Experimental Nuclear Physics, E. Segre, ed., John Wiley & Sons, New York, Vol 1 (1953) 166.

Birks, J.B., The Theory and Practice of Scintillation Counting, The Macmillan Company, New York (1964).

Bisi, A., Germagnoli, E., and Zappa, L., Nuovo Cimento 3 (1956) 1007.

Black, I.A., Fowle, A.A., and Glaser, P.E., Advances in Cryogenic Engineering 5 (1960) 181.

Black, I.A., and Glaser, P.E., Advances in Cryogenic Engineering 6 (1961) 32.

Blin-Stoyle, R.J., Fundamental Interactions and the Nucleus, North-Holland Amsterdam (1973).

Blomquist, J., Kerek, A., and Fogelberg, B., Z. Physik A314 (1983) 199.

Blonnigen, F., Wollnik, H., Rehfield, D., Geisse, C., Jung, G., Koglin, E., and Pfeiffer, B., Nucl. Inst. & Meth. 178 (1980) 357.

Bloom, S.D., Isobaric Spin in Nuclear Physics, J.D. Fox and D. Robson, eds., Academic Press, New York (1966) 123.

Boardman, J., Lynam, P., and Scurlock, R.G., Cryogenics 13 (1973) 520.

Bom, V.R., Nucl. Inst. & Meth. 207 (1983) 395.

Bom, V.R., Nucl. Inst. & Meth. 220 (1984) 479.

Booij, H.M.W., Van Hoek, E.A., and Blok, J., Nucl. Inst. & Meth. 72 (1969) 40.

Booij, H.M.W., Thesis, Free University, Amsterdam (1970).

Boothroyd, A.I., Markey, J., and Vogel, P., Phys. Rev. C29 (1984) 603.

Borovoy, A.A., Klimov, Yu. V., Kopeykin, V.I., and Shkolnik, K.D., J. Phys. G: Nucl. Phys 5 (1979) 723.

Bosch, H., Krmpotic, F., and Plastino, A., Nucl. Inst. & Meth. 23 (1963) 79.

Bosch, H.E., and Urstein, T., Nucl. Inst. & Meth. 24 (1963) 109.

Bosch, H.E., Davidson, J., Fariolli, M.A., and Silbergleit, V., Nucl. Inst. & Meth. 117 (1974) 213.

Bosch, H.E., Behar, M., Cambiaggio, M.C., Carcia Bermudez, G., and Szybisz, L., Can. J. of Phys. 51 (1973) 2260.

Boysen, J., and Brewer, W., Nucl. Inst. & Meth 141 (1977) 483.

Braden, C.H., Owen, G.E., Townsend, J., Cook, C.S., and Shull, F.B., Phys. Rev. 74 (1948) 1539.

Brechna, H., Superconducting Magnet Systems, Springer Verlag, New York (1973).

Brenner, D.S., Martel, M.K., Aprahamian, A., Chrien, R.E., Gill, R.L., Liou, H.I., Wohn, F.K., Rehfield, D.M., Dejbakhash, H., and Chung, C., Phys. Rev. C26 (1982) 2166.

Brewer, W.D., and Shirley, D.A., Nucl. Phys. A149 (1970) 392.

Browne, C.P., See AMCC 4 (1972) 15.

Brundrit, D.R., and Sen, S.K., Nucl. inst. & Meth. 34 (1965) 225.

Burginyon, G.A., and Greenberg, J.S., Nucl. Inst. & Meth. 41 (1966) 109.

Burgov, N.A., Davydov, A.V., and G.R. Kartashov, Nucl. Inst. & Meth. 12 (1961) 316.

Burson, S.B., Proceedings of the Conference on Slow-Neutron-Capture Gamma-Ray Spectroscopy, F.E. Throw, ed., ANL-7282 (1968) 279.

Calaprice, F.P., Alburger, D.E., Phys. Rev. C17 (1978) 730.

Cambi, A., Fazzini, T.F., Giannatiempo, A., and Maurenzig, P.R., Nucl. Inst. & Meth. 103 (1972) 331.

Camp, D.C., Langer, L.M., Phys. Rev. 129 (1963) 1782.

Camp, D.C., and Armantrout, G.A., Radioisotope Sample Measurement Techniques in Medicine and Biology, International Atomic Energy Agency, Vienna (1965) 647.

Caren, R.P., Applications of Cryogenic Engineering, R.W. Vance and H. Weinstock, eds., Tinnon-Brown, Inc., Los Angeles (1969) 45.

Carlson, B.C., and Notis, E.M., "Algorithms for Incomplete Elleptical Integrals", ACM TOMS 7(3) (1981) 398.

Catura, R.C., Nucl. Inst. & Meth. 32 (1965) 152.

CERN, International Conference on the Properties of Nuclei Far From the Region of Beta-Stability, Leysin, Switzerland (1970), CERN, Geneva, CERN 70-30 (1970).

CERN, Third International Conference on Nuclei Far from Stability, Cargese, Corsica (France) (1976), CERN, Geneva, CERN 76-13 (1976).

CERN, Fourth International Conference on Nuclei Far from Stability, Helsingor (Denmark) (1981), CERN, Geneva, CERN 81-09 (1981).

Charoenkwan, P., Nucl. Inst. & Meth. 34 (1965) 93.

Chrien, R.E., ed., Proceedings of the Isotope Separator On Line Workshop,

Brookhaven National Laboratory, BNL 50847 (1977).

Christensen, C.J., Nielsen, A., Bahnsen, A., Brown, W.K., and Rustad, B.M., Phys. Lett. 26B(1967) 11

Christmas, P., and Cross, P., Journal of Physics E: Scientific Instruments 6 (1973) 533.

Christmas, P., and Cross, P., Metrologia 14 (1978) 147.

Clark, J.A., and Thorogood, R.M., Cryogenic Fundamentals, G.G. Haselden, ed., Academic Press, New York (1971) 92.

Clifford, E.T.H., Thesis, University of Toronto (1981).

Coche, A., and Siffert, P., Semiconductor Detectors, G. Bertolini, and A. Coche, eds., North-Holland, Amsterdam (1968) 103.

Collings, E.W., and Hart, S.C., Cryogenics 19 (1979) 521.

Colyer, B., Proceedings of the Second International Conference on Magnet Technology, Oxford, H. Hadley, ed., Rutherford Laboratory, Chliton, U.K. (1967) 624.

Conte, R.R., Blot, R., and Mignen, J., Proceedings of the Third International Cryogenic Engineering Conference, Iliffe Science and Technology Publications Limited, Guildford, U.K. (1970) 127.

Coston, R.M., Advances in Cryogenic Engineering 11 (1966) 56.

Cramer, J.G., Farmer, B.J., and Class, C.M., Nucl. Inst. & Meth 16 (1962) 289.

CRC-49, Handbook of Chemistry and Physics, 49th edition, The Chemical Rubber Company (1968-1969).

C.S.C.C., Product List and Technical Data Booklet, Canada Superconductor and Cryogenics Company Limited, St. Lambert, Quebec, (no date).

Curran, S.C., and Wilson, H.W., Alpha-, Beta- and Gamma-Ray Spectroscopy, K. Siegbahn, ed., North-Holland, Amsterdam (1965) 303.

Dakubu, T., and Gilboy, W.B., Nucle. Inst. & Meth 150 (1978) 479.

Daniel, H., Rev. Mod. Phys. 40 (1968) 659.

Daniel, H., Jahn, P., Kuntze, M., and Martin, B., Nucl. Inst. & Meth. 82 (1970) 29.

D'Auria, J.M., and Preiss, I.L., Nucl. Phys. 84 (1966) 37.

D'Auria, J.M., Gruter, J.W., Westgaard, L., Nyman, G., Peuser, P., Roeckl, E., Otto, H., and The ISOLDE Collaboration, see CERN (1976) 100.

Davey, G., Advanced Cryogenics, C.A. Bailey, ed., Plenum Press, New York (1971) 339.

Davids, C.N., Goosman, D.R., Alburger, D.E., Gallmann, A., Guillaume, G., Wilkinson, D.H., and Lanford, W.A., Phys. Rev. C9 (1974) 216.

Davids, C.N., Gallardi, C.A., Murphy, M.J., and Norman, E.B., Phys. Rev. C19 (1979) 1463.

Dearnaley, G. and Northrop, D.C., Semiconductor Counters for Nuclear Radiations, E. & F. N. Spon Limited, London (1963).

De Beer, A., Blok, H.P., and Blok, J., Nucl. Inst. & Meth. 78 (1970) 19.

Decker, R., Wunsch, K.D., Wollnik, H., Koglin, E., Siegert, G., and Jung, Z. Physik A294 (1980) 35.

Decker, R., Wunsch, K.D., Wollnik, H., Jung, G., Munzel, J., Siegert, G., and Koglin, E., Z. Physik A301 (1981) 165.

Decker, R., Wunsch, K.D., Wollnik, H., Jung, G., Koglin, E., and Siegert, G., Nucl. Inst. & Meth. 192 (1982) 261.

Der Mateosian, E., and Smith, A., Phys. Rev. 88 (1952) 1186.

Della Negra, S., Jacquet, D., and Le Beyec, Y., Z. Physik A308 (1982) 243.

DeLyser, H., Ziemba, F.P., and Van Antwerp, W.R., IEEE Trans. Nucl Sci., NS-12,#1 (1965) 265.

Detraz, C., Langevin, M., Goffri-Kouassi, M.C., Guillemaud, D., Epherre, M., Audi, G., Thibault, C., and Touchard, F., Nucl. Phys. A394 (1983) 378.

Deutsch, M., and Kofoed-Hansen, O., Experimental Nuclear Physics, E. Segre, ed., John Wiley & Sons, New York, Vol. 3 (1959) 426.

Deutsch, J.P., Macq, P.C., van Elmbt, L., Phys. Rev. C15 (1977) 1587.

Dew-Hughes, D., Metallurgy of Superconducting Materials, T. Luhman and D. Dew-Hughes, eds., Academic Press, New York, Treatise on Materials Science and Technology, Vol. 14 (1979) 137.

Dickey, P.A., Bussoletti, J.E., and Adelberger, E.G., Nucl Phys. A303 (1978) 442.

Di Cola, G., Rota, A., and Bertolini, G., IEEE Trans. on Nucl. Sci. NS-14, #1 (1967) 640.

Donadieu, L.J., and Rose, D.J., High Magnetic Fields, H. Kolm, B. Lax, F. Bitter, and R. Mills, eds., John Wiley & Sons, New York (1962) 358.

Douglas, D.G., Phys. Rev. 75 (1949) 1960.

Draper, J.E., McDonald, R.J., and Wyckoff, W.G., Nucl. Inst. & Meth. 151 (1978) 135.

Efferson, K.R., Rev. Sci. Inst. 38 (1967) 1776.

Egelkraut, K., Leutz, H., Z. Physik 160 (1960) 74.

Egelkraut, K., Leutz, H., Z. Physik 161 (1961) 13.

EG&G ORTEC, Instruments for Research and Applied Sciences Catalog, EG&G ORTEC Oak Ridge Tennessee (1981).

Ejiri, H., Shibata, T., Nagai, V., and Nakayama, S., Nucl. Inst. & Meth. 134 (1976) 107.

Elbek, B., Nucl. Inst. & Meth. 48 (1967) 353.

ENERTEC Schlumberger, Si(Li) Detectors for Conversion Electrons Catalog, ENERTEC Schlumberger, Lingolsheim, France (1983).

Epherre, M., Audi, G., Thibault, C., Klapisch, R., Huber, G., Touchard, F., and Wollnik, H., Phys. Rev. C19 (1979) 1504.

Epherre, M., Audi, G., Thibault, C., and Klapisch, R., see AMC06 (1980) 299.

Ercan, A., Katayama, I., Zupancic, M., Retz, A., Rindfleisch, U., Nagai, Y., and Klienheinz, P., Annual Report, Institute fur Kernphysik, KFA (1981) 130, 137.

Evans, R.D., The Atomic Nucleus, McGraw-Hill, New York (1955).

Ewan, G.T., and Tavendale, A.J., Can. J. Phys. 42 (1964) 2286.

Ewan, G.T., Progress in Nuclear Techniques and Instrumentation, F.J.M. Farley, ed., North-Holland, Amsterdam, Vol. 3 (1968) 67.

Ewan, G.T., Nucl. Inst. & Meth. 162 (1979) 75.

Fazzini, T., Giannatiempo, A., and Perego, A., Nucl. Inst. & Meth. 211 (1983) 125.

Fehrentz, D., and Daniel, H., Nucl. Inst. & Meth. 10 (1961) 185.

Feldman, L., and Wu, C.S., Phys. Rev. 76 (1949) 697.

Flothmann, D., Wiesner, W., Lohken, R., and Rebel, H., Z. Physik 225 (1969) 164.

Flothmann, D., Gils, H.J., Loken, R., and Wiesner, W., Nucl. Inst. & Meth. 102 (1972) 237.

Forsling, W., Herrlander, C.J., and Ryde, H., eds., Proceedings of the International Symposium on "Nuclide Far Off The Stability Line", Lysekil, Sweden (1966), Arikv. Fys. 36 (1967).

Frankel, R.B., Shirley, D.A., and Stone, N.J., Phys. Rev. 136 (1964) B577.

Freedman, M.S., Novey, T.B., Porter, F.T., and Wagner, Jr., F., Rev. Sci. Inst. 27 (1956) 716.

Freedman, M.S., Wagner, Jr., F., Porter, F.T., Terandy, J., and Day, P.P.,

Nucl. Inst. & Meth. 8 (1960) 255.

Freedman, M.S., Porter, F.T., and Wagner, Jr., F., Rev. Sci. Inst. 38 (1967a) 190.

Freedman, M.S., Wagner, Jr., F., and Day, P., J. Appl. Phys. 38 (1967b) 1856.

Fromm, W.D., Brinckmann, H.F., Donau, F., Heiser, C., May, F.R., Pashkevich, V.V., and Rotter, H., Nucl Phys. A243 (1975) 9.

Fujioka, M., Nucl. Phys. A153 (1970) 337.

Fulbright, H., Beta- and Gamma-Ray Spectroscopy, K. Siegbahn, ed., North Holland, Amsterdam (1955) 184.

Fuller, P.D., and McLagan, J.N., Applied Cryogenic Engineering, R.W. Vance and W.M. Duke, eds., John Wiley & Sons, New York (1962) 215.

Gardner, D.G., and Meinke, W.W. Intern. J. Appl. Radiation and Isotopes 3 (1958) 232.

Gardner, L.B., IRE Trans. Nucl. Sci. NS-7, #4 (1960) 36.

Gelletly, W., ed., The Study of Nuclei Far from Stability, Proceedings of the Daresbury Study Weekend, National Research Council, Daresbury laboratory, Daresbury, Warrington, U.K. DL/NUC/R20 (1980).

Genz, H., Richter, A., and Schmitz, B.M., Nucl. Phys. A267 (1976a) 13.

Genz, H., Reisberg, J., Richter, A., Schmitz, B.M., Schrieder, G., Werner, K., and Behrens, H., Nucl. Inst. & Meth. 134 (1976b) 309.

Gerald II, R., Hyman, L.G., Ladbury, R., Rezmer, R., and Fernandez, E., Preprint, Argonne National Laboratory, Argonne, IL, ANL-HEP-PR-81-49 (1981).

Gerholm, T.R., Hanbuch der Physik, S. Flugge, ed., Springer-Verlag, Berlin, Vol. 33 (1956) 609.

Gerholm, T.R., Nuclear Physics, L.C.L. Yuan, and C.S. Wu, eds., Academic Press, New York, Methods of Experimental Physics, Vol. 5 A (1961) 341.

Gerholm, T.R., and Lindskog, J., Arkiv Fys. 24 (1963) 171.

Getty, R.C., Clay, J.P., Kremzier, E.J., and Leonhard, K.E., Advances in Cryogenic Engineering 11 (1966) 35.

Gibson, W.M., Miller, G.L. & Donovan, P.F., Alpha-, Beta-, and Gamma-ray spectroscopy, K. Siegbahn, ed., North-Holland, Amsterdam (1965) 345.

Gill, R.L., Brookhaven National Laboratory, Private Communication (1984).

Gils, H.J., Flothmann, D., Lohken, R., and Wiesner, W., Nucl. Inst. & Meth.

105 (1972) 179.

Girard, T.A., and Avigrone III, F.T., Nucl. Inst. & Meth. 154 (1978) 199.

Gono, Y., Watson, R.L., Sugihara, T.T., and Kuebbing, R.A., Nucl. Inst. & Meth. 127 (1975) 391.

Goudsmit, P.F., Thesis, University of Amsterdam (1969).

Goulding, F.S., Nucl. Inst. & Meth. 43 (1966) 1.

Goulding, F.S., and Pehl, R.H., Nuclear Spectroscopy and Reactions, Part A., J. Cerny, ed., Academic Press, New York, Pure and Applied Physics, Vol. 40-A (1974) 289.

Graham, R.L., Ewan, G.T., and Geiger, J.S., Nuc. Inst. & Meth. 9 (1960) 245.

Graham, R.L., and Gieger, J.S., Can. J. Phys. 39 (1961) 1357.

Graham, R.L., and Gieger, J.S., Radioactivity in Nuclear Spectroscopy, J.H. Hamilton, and J.C. Manthuruthil, eds., Gordon & Breach, New York, Vol. 2 (1972) 1447.

Grover, F.W., Inductance Calculations, D.Van Nostrand Co., New York (1964).

Grosswendt, B., Nucl. Inst. & Meth. 116 (1974) 97.

Gruhn, C.R., Todd, R.R., Maggiore, C.J., Kelley, W.H., Doebler, R.E., and McHarris, Wm. C., Nucl. Inst. & Meth. 75 (1969) 109.

Guttormsen, M., Von Grumbkow, A., Agarwal, Y.K., Blume, K.P., Hardt, K., Hubel, H., Recht, J., Schuler, P., Kluge, H., Maier, K.H., Maj, A., and Roy, N., Nucl. Phys. A398 (1983) 119.

Hagemann, U., Keller, H.J., Protochristow, Ch., and Stary, F., Nucl. Phys. A329 (1979) 157.

Halbig, J.K., Wohn, F.K., and Talbert Jr., W.L., Rev. Sci. Inst. 45 (1974) 789.

Haller, E.E., and Goulding, F.S., Handbook on Semiconductors, C. Hilsum, ed., North-Holland, Amsterdam, Vol. 4 (1981) 799.

Haller, E.E., Hansen, W.L., Luke, P., McMurray, R., and Jarret, B., IEEE Trans. Nucl. Sci NS-29, #1 (1982) 745.

Haller, E.E., IEEE Trans. Nucl. Sci., NS-29, #3 (1982) 1109.

Hamilton, J.H., Internal Conversions Processes, J.H. Hamilton, ed., Academic Press, New York (1966) 6.

Hamilton, J.H., The Electromagnetic Interaction in Nuclear Spectrometry, W.D. Hamilton, ed., North-Holland, Amsterdam (1975) 441.

Hamilton, J.H., Spejewski, E.H., Bringham, C.R., and Zganjar, E.F., eds. Future Difections in Studies of Nuclei Far From Stability, Proceedings of the International Symposium on Future Directions in Studies of Nuclei Far from Stability, Nashville, Tennessee, September 10-13, 1979, North-Holland, Amsterdam (1980).

Hamilton, J.H., Heavy Ion Collisions, R. Bock, ed., North-Holland, Amsterdam, Vol. 3 (1982) 537.

Hammond, M.B., Jr., Advances in Cyrogenic Engineering 16 (1971) 143.

Hancox, R., and Catterall, J.A., Cryogenic Fundamentals, G.G. Haselden, ed., Academic Press New York (1971) 491.

Hansen, P.G., Adv. in Nucl. Phys. 7 (1973) 159.

Hansen, P.G., Ann. Rev. Nucl. Part. Sci. 29 (1979) 69.

Hansen, W.L., Nucl. Inst. & Meth. 94 (1971) 377.

Hardy, J.C., and Towner, I.S., Nucl. Phys. A254 (1975) 221.

Hardy, J.C., Carraz, L.C., Jonson, B., and Hansen, P.G., Phys. Lett. 71B (1977) 307.

Hardy, J.C., See AMCO 6 (1980) 515.

Hardy, J.C., MARIA Design Symposium Vol. 5, Relativistic Heavy Ion Winter School, February, 1982, Banff, Alberta, Medical Accelerator Research Institute in Alberta, Edmonton, Alberta, Canada (1982).

Hardy, J.C., Superallowed Beta-decay as a Probe of Weak Interactons, Atomic Energy of Canada limited, Chalk River, Ontario, Canada, AECL-8258 (1983).

Hayward, R.W., Advances in Electronics 5 (1953) 97.

Hedgran, A., Arkiv Fys. 5 (1962) 1.

Henry, E.A., Stoffl, W., and West, H.I., Annual Report, Nuclear Chemistry Division, Lawrence Livermore National Laboratory, G. Struble, ed., UCAR 10062-82/1 (1982) 26,

Hetherington, D.W., Alousi, A., and Moore, R.B., Physics in Canada 39 (1983) 59.

Hetherington, D.W., Thesis, McGill University (1984).

H/F, High resolution Silicon Lithium drifted detector Catalog, H/F Industries, Inc., Vista, California (1981).

Hnilicka, M.P., Advances in Cryogenic Engineering 5 (1960) p 199.

Hoare, F.E., Jackson, L.C., and Kurt, N., eds., Experimental Cryophysics, Butterworths, London (1961).

Hofmann, A., Proceedings of the Third International Cryogenic Engineering Conference, Iliffe Science & Technology Publication limited, Guildford, U.K. (1970) 485.

Hofmann, I., & Baier H., Acta Physica Austriaca 20 (1965) 53 [Trans. by Sinclair, D.A., National Research Council of Canada Technical Translation, 1326 (1968)].

Hollander, J.M., Nucl. Inst. & Meth 43 (1966) 65.

Holstein, B.R., Phys. Rev. C9 (1974) 1646.

Holstein, B.R., Phys. Rev. C29 (1984) 623.

Howe, D.A., Nucl. Inst. & Meth 64 (1968) 231.

Hoyle, C.D., Adelberger, E.G., Blair, J.S., Snover, K.A., Swanson, H.E., and Von Lintig, R.D., Phys. Rev. C27 (1983) 1244.

Hsue, S.T., Langer, L.M., Spejewski, E.H., and Tang, S.M., Nucl. Phys. 80 (1966a) 657.

Hsue, S.T., Langer, L.M., and Tang, S.M., Nucl. Phys. 86 (1966b) 47.

Hughes, R.G., Thesis, Utah State University (1980).

Hung, S.T.-C., Krane, K.S., and Shirley, D.A., Phys. Rev. C14 (1976) 1162.

Iafigliola, R., Dautet, H., Lee, J.K.P., and XU, S.W., Physics in Canada 39 (1983a) 59.

Iafigliola, R., Chatterjee, M., Dautet, H., and Lee, J.K.P., Can. J. Chem. 61 (1983b) 694.

Ishii, M., Nucl. Inst. & Meth. 127 (1975) 53.

Iwasa, Y., and Montgomery, D.B., Applied Superconductivity, V.L. Newhouse, ed., Academic Press, New York, Vol. 2 (1975) 387.

Jackson, J.D., Classical Electrodynamics, John Wiley & Sons, New York, Second Edition (1975).

Jacobs, E., Dorkenss-Vanpraet, L., Demuynck, J., and DeFrenne, D., Nucl. Inst. and Meth. 47 (1967) 55.

Jeuch, P., and Mampe, W., Nucl. Inst. & Meth. 140 (1977) 347.

Jonson, B., Nucl. Phys. A354 (1981a) 77.

Jonson, B., Nucl. Inst. & Meth. 186 (1981b) 35.

Johnston, M.G., Grant, I.S., Misaelides, P., Nolan, P.J. Peuser, P., Kirchner, R., Klepper, O., Roeckl, E., and Tidemand-Petersson, P. See CERN (1981) 469.

Kaina, W., Thesis, University of Heildelberg (1977).

Kaina, W., Soergel, V., Thies, H., and Trost, W., Phys. lett. 70B (1977)

411.

Kane, W.R., Neutron Capture Gamma Ray Spectroscopy R.E. Chrien, and W.R. Kane, eds., Plenum Press, New york (1979) 485.

Kantele, J., Marttila, O.J., and Pakkanen, A., Nucl., Inst. & Meth. 30 (1964) 259.

Kantele, J., and Passoja, A., Nucl. Inst. & Meth. 92 (1971) 247.

Kantele, J., Luontama, M., Passoja, A., and Julin, R., Nucl. Inst. & Meth. 130 (1975) 467.

Kantele, J., Julin, R., Luontama, M., and Passoja, A., Nucl. Inst. & Meth. 200 (1982) 253.

Kennett, T.J., and Keech, G.L., Nucl. Inst. & Meth. 24 (1963) 142.

Ketelle, B.H., Phys. Rev. 80 (1950) 758.

Ketelle, B.H., Thomas, H., and Brosi, A.R., Phys. Rev. 103 (1956) 190.

Keyser, U., Berg, H., Munnich, F., Hawerkamp, K., Schrader, H., Pfeiffer, B., and Monnand, E., Z. Physik A289 (1979) 407.

Keyser, U., Munnich, F., Pahlmann, B., and Pfeiffer, B., See CERN (1981) 116.

Kittel, C., Introduction to Solid State Physics, John Wiley & Sons, New York (1976).

Klank, B., and Ristinen, R.A., Radioactivity in Nuclear Spectroscopy, J.H. Hamilton, and J.C. Manthuruthil, eds., Gordon & Breach, New York, Vol. 2 (1972) 207.

Klapdor, H.V., Metzinger, J., Oda, T., Thielemann, F.K., and Hillebrandt, W., See CERN (1981) 341.

Klien, V.E., Crygenics 7 (1967) 3.

Klyuchnikov, A.A., Mitrokhovich, N.F., and Feoktistov, A.I., Izv. Aka. Nauk. SSSR. Ser. Fiz. 32 (1968) 1523 (in English).

Knoll, G.F., Radiation Detection & Measurement, John Wiley & Sons, New York (1979).

Knop, G., and Paul, W., Alpha-, Beta-, and Gamma-Ray Spectroscopy, K. Siegbahn, ed., North-Holland, Amsterdam, Vol. 1 (1965) 1.

Knott, T.F., Andrews, H.R., Cohen, E.J., Pipkin, F.M., and Santry, D.C., Phys. Rev. Lett. 25 (1970) 543.

Knowles, J.W., Mills, W.F., King, R.N., Malm. H.L., Pich, B.O., Yen, S., and Drake, T.E., Nucl. Inst. & Meth. 193 (1982) 485.

Kofoed-Hansen, O.M., and Christensen, C.J., Handbuch der Physik, S.

Flugge, ed., Springer-Verlag, Berlin, Vol. 41 (2) (1962).

Komma, M., Nucl. Inst. & Meth. 154 (1978) 271.

Konijn, J., Posthumus, W.L., Goudsmit, P.F.A., Schiebaan, C., Geerke, H.P., Maarleveld, J.L., Andringa, J.H.S., and Evers, G.J., Nucl. Inst. & Meth. 129 (1975) 167.

Konopinski, E.J., The Theory of Beta Radioactivity, Oxford University Press, New York (1966).

Kotajima, K., and Beringer, R., Rev. Sci. Inst. 41 (1970) 632.

Krmpotic, F., and Tadic, D., Phys. Rev. 178 (1969) 1804.

Kropschot, R.H., Schrodt, J.E., Fulk, M.M., and Hunter, B.J., Advances in Cryogenic Engineering 5 (1960) 189.

Kropschot, R.H., Cryogenics 1 (1961) 171.

Kropschot, R.H., Applied Cryogenic Engineering, R.W. Vance, and W.M. Duke, eds., John Wiley & Sons, New York (1962) 152.

Kruger, Th., Appel, H., Thies, W.G., and Behrens, H., Phys. Lett. 121B (1983) 303.

KST, Effective Installation and Use of NRC-2 booklet, King-Seeley Thermos Co., Winchester, Massachuesetts (no date).

Kuraoka, Y., Saito, Nogi, T., and Misawa, T., Cryogenics 19 (1979) 182.

Kutzner, K., Schmidt, F., and Wietzke, I., Cryogenics 13 (1973) 396.

Kuzminikh, V.A., and Vorobiev, S.A., Nucl, Inst. & Meth. 129 (1975) 561.

Langer, L.M., and Cook, C.S., Rev. Sci. Inst. 19 (1948) 257.

Langer, L.M., Rev. Sci. Inst. 20 (1949) 216.

Langer, L.M., Moffat, R.D., and Price, H.C., Phys. Rev. 76 (1949) 1725.

Langer, L.M., Motz, J.W., and Price Jr., H.C., Phys. Rev. 77 (1950) 798.

Langer, L.M., Spejewski, E.H., and Wortman, D.E., Phys Rev. 135 (1964) B581.

Lederer, C.M., and Shirley, V.S., eds., Table of Isotopes, 7th edition, John Wiley & Sons, New York (1978).

Lee, H.C., and Cheng, W.K., Topics in Nuclear Physics I, T.T.S. Kuo, and S.S.M. Wong, eds., Springer-Verlag, Berlin, Lecture Notes in Physics, Vol. 144 (1981) 458.

Lee, J.K.P, Topics in Nuclear Physics II, T.T.S. Kuo, and S.S.M. Wong, eds., Springer-Verlag, Berlin, Lecture Notes in Physics, Vol. 144 (1981) 1026.

Lee, Y.K., Mo, L.W., and Wu, C.S., Phys. Rev. Lett. 10 (1963) 253.

Leonhard, K.E., and Tatro, R.E., Proceedings of the Third International Cryogenic Engineering Conference Iliffe Science & Technology Publications Limited, Guildford, U.K. (1970) 490.

Leung, E.M.W., Fast, R.W., Hart, H.L., Heim, J.R., Advances in Cryogenic Engineering 25 (1980) 489.

Leutz, H., Z. Physik 164 (1961) 78.

Leutz, H., & Ziegler, K., Z. Physik 166 (1962) 582.

Lewin, W.H.G., Internal Conversion Processes, J.H. Hamilton, ed., Academic Pess, New York (1966).

Lewis, G.M., Phil. Mag. 43 (1952) 1070.

Linblad, Th, and Linden, C.G., Nucl. Inst. & Meth. 126 (1975) 397.

Lindskog, J., and Svensson, L.-G., Nucl. Inst. & Meth. 133 (1976) 99.

Lipkin, H.J., Beta Decay for Pedestrians, North-Holland, Amsterdam (1962).

Lizurej, H.I., See AMCO 6 (1980) 437.

Lohken, R., Rebel, H., and Schatz, G., Z. Physik A245 (1971) 425.

Long, H.M., Vacuum Technology at Low Temperatures, S.A. Stern, ed., American Institute of Chemical Engineers Symposium Series, Vol. 68, Number 125 (1972) 50.

Lountama, M., Kantele, J., Julin, R., Passoja, A., Poikolainen, T., and Pylvanainen, M., Nucl. Inst. & Meth 159 (1979) 339.

Lund, E., and Rudstam, G., Nucl. Inst. & Meth. 134 (1976) 173.

Lynam, P., Mustafa, A.M., Proctor, W., and Scurlock, R.G., Cryogenics 9 (1969) 242.

Lyubimov, V.A., Novikov, E.G., Nozik, V.A., Tretyakov, E.F. and Kosik, V.S. Phys. Lett. 94B (1980) 266.

Lyutyi, I.N., Gavrilyuk, V.I., Kupryashkin, V.T., Latyshev, G.D., Makovestkii, Yu. V., and Feoktistov, A.I., Izv. Akad. Nauk. SSSR (Ser. Fiz.) 34, #4 (1970) 736 (in English).

Malmfors, K.G., Arkiv Fys, 13 (1958) 237.

Malmfors, K.G., and Nilsson, A., Arkiv Fys. 13 (1958) 247.

Mampe, W., Schreckenbach, K., Jeuch, P., Maier, B.P.K., Braumandl, F., Larysz, J., and von Egidy, T., Nucl. Inst. & Meth. 154 (1978) 127.

Marlow, K.W., and Waggoner, M.A., Phys. Rev. 163 (1967) 1098.

Mate, Z., Mahunka, I., Morik, D., Novak, D., Tarkani, F., Fenyes, T., and Fyule, K., Instruments and Experimental Techniques, 21, #5, part 1 (1978) 1197.

Michaelis, W., Lange, D., and Wilhelmi, G., Neutron Capture Gamma-Ray Spectroscopy, IAEA, Vienna (1969) 75.

Mikhalchenko, R.S., Pershin, N.P., and Sidorenko, I.G., Proceedings of the Sixth International Cryogenic Engineering Conference, K. Mendelssohn, Ed., IPC Science & Technology Press, Guildford, U.K. (1976) 298.

Mitchell, A.C.G., Alpha-, Beta-, and Gamma-Ray Spectroscopy K. Siegbahn, ed., North-Holland, Amsterdam, Vol. 1 (1965) 467.

Mladjenovic, M., Nucl Inst. & Meth. 10 (1961) 1.

Mladjenovic, M., Advances in Electronics & Electron Physics, 30 (1971) 43.

Mladjenovic, M.S., Radioactivity in Nuclear Spectroscopy, J.H. Hamilton, and J.C. Manthuruthil, eds., Gordon & Breach New York, Vol, 2 (1972) 581.

Mladjenovic, M., Development of Magnetic Beta-ray Spectroscopy Springer-Verlag, Berlin, Lecture Notes in Physics Vol. 52 (1976).

Mladjenovic, M.S., Nucl. Inst. & Meth. 162 (1979) 193.

Molnar, W., Cryogenic Fundamentals, G.G. Haselden, ed., Academic Press, New York (1971) 199.

Moltz, D.M., Toth, K.S., Avignone III, F.T., Noma, H., Ritchie, B.G., and Kern, B.D., Phys. Lett. 113B (1982) 16.

Montgomery, D.B., Solenoid Magnet Design, Wiley-Interscience, New York (1969).

Moore, R.B., Hayakawa, S.I., and Rehfield, D.M., Nucl, Inst. & Meth. 133 (1976) 457.

Morita, W., Beta Decay and Muon Capture, W.A. Benjamin, Inc., London (1973).

Morozov, V.I., and Pelekhov, V.I., Izv. Akad. Nauk. SSSR (Ser. Fiz.) 36, #3 (1972) 571 (in English).

Morozov, V.I., Instruments and Experimental Techniques 16, #3, part 1 (1973) 703.

Munnich, F., Nuclear Spectroscopy of Fission Products, T. von Egidy, ed., The Institute of Physics, Bristol & London, conference Series Number 51 (1980) 122.

Murray, G., Graham, R.L., and Gieger, J.S., Nucl, Phys. 63 (1965) 353.

McKenzie, J.M., Nucl. Inst. & Meth. 162 (1979) 49.

McMillan, D.K., Thesis, Simon Fraser University (1970).

Nagai, Y., Ejiri, H., Shibata, T., Okada, K., Nakayama, S., Suzuki, H., and Sakai, H., Nucl. Inst. & Meth. 204 (1982) 101.

Nagarajan, T., Ravindranath, M., and Venkata Reddy, K., Nucl. Inst. & Meth. 67 (1969) 77.

Nagarajan, T., and Venkata Reddy, K., Nucl. Inst. & Meth 80 (1970) 217.

Nast, T.C., and Williams, W.S., Advances in Cryogenic Engineering 12 (1967) 229.

Neiler, J.H., and Bell, P.R., Alpha-, Beta-, and Gamma-Ray Spectroscopy, K. Siegbahn, ed., North-Holland, Amsterdam, Vol. 1 (1965) 245.

Nelms, A., NBS Circular #577, National Bureau of Standards, (1956).

Neumann, W., Cleemann, L., Eberth, J., Wiehl, N., and Zobel, V., Nucl. Inst. & Meth. 164 (1979) 539.

Nichols, R.T., McAdams, R.E., and Jensen, E.N., Phys. Rev. 122 (1961) 172.

Niendorf, L.R., and Choksi, L.R., Advances in Cryogenic Engineering 12 (1967) 286.

Nilsson, O. Karlsson, S.-E., Andersson, I., Nordling, C., and Siegbahn, K., Nucl. Inst. & Meth. 47 (1967) 13.

Nitschke, J.M., Nucl. Inst. & Meth. 206 (1983) 341.

Noma, H., Avignone III, F.T., Moltz, D.M., and Toth, K.S., Nucl. Inst. & Meth. 211 (1983) 391.

Nuclear Enterprises, Scintillators for the Physical Sciences, Nuclear Enterprises Limited, Reading, U.K., Brochure No. 126P (1980) 11.

Ohya, S., Mutsuro, N., and Furusawa, A., Nucl. Inst. & Meth. 196 (1982) 169.

O'Kelley, G.D.O., Nuclear Physics, L.C.L. Yuan, and C.S. Wu, eds., Academic Press, New York, Methods of Experimental Physics, Vol. 5 A (1961) 411.

Otto, H., Peuser, P., Nyman, G. and Roeckl, E., Nucl. Inst. & Meth. 166 (1979) 507.

Owen, G.E., and Primakoff, H., Phys. Rev. 74 (1948) 1406.

Owen, G.E., and Cook, C.S. Rev. Sci. Inst. 20 (1949) 768.

Owen, G.E., and Primakoff, H., Rev. Sci. Inst. 21 (1950) 447.

Pahlmann, B., Keyser, U., Munnich, F., and Pfeiffer, B., Z. Physik A308 (1982) 345.

Painvanas, J.A., Roberts, O.P., and Wang, D. I.-J., Advances in Cryogenic

Engineering 10 (1965) 197.

Pais, Rev. Mod. Phys. 49 (1977) 925.

Pardo, R.C., Davids, C.N., Murphy, M.J., Norman, E.B., and Parks, L.A., Phys. Rev. C15 (1977) 1811.

Paris, P., and Treherne, J., Revue de Physique Appliquee 4 (1969) 291.

Parker, W., and Slatis, H., Alpha-, Beta-, and Gamma-Ray Spectorscopy, K. Siegbahn, ed., North-Holland, Amsterdam, Vol. 1 (1965) 379.

Parkinson, D.H., and Mulhall, B.E., The Generation of High Magnetic Fields, Plenum Press, New York (1967).

Parks, L.A., Davids, C.N., and Pardo, R.C., Phys. Rev. C15 (1977) 730.

Paul, H., and Hofmann, I., Nucl. Inst. & Meth. 22 (1963) 141.

Paul, H., Nucl. Inst. & Meth. 31 (1964) 307.

Paul, H., Nucl. Inst. & Meth 37 (1965) 109.

Paul, H., Nuclear Data A2 (1966) 281.

Pehl, R.H., Goulding, F.S., Landis, D.A., and Lenzlinger, M., Nucl. Inst & Meth. 59 (1968) 45.

Pehl, R.H., and Cordi, R.C., IEEE Trans. Nucl. Sci., NS-22 #1 (1975) 177.

Pehl, R.H., Physics Today 30, #11 (1977) 50

Perlmutter, M., and Siegel, R., Journal of Heat Transfer, Transactions of The American Society of Mechanical Engineers, Series C 85 (1963) 55.

Persson, B., Nucl. Inst. & Meth 27 (1964) 1.

Persson, B.I., Plesser, I., and Sunier, J.W., Nucl. Phys. A167 (1971) 470.

Pettersson, B.G., Alpha-, Beta-, and Gamma-Ray Spectroscopy, K. Siegbahn, ed., North-Holland, Amsterdam, Vol. 2 (1965) 1569.

Picone, J.M., Fitch, J.F., Baker, J.W., Hoffmann, G.W., and Moore, C.F., Nucl. Inst. & Meth. 105 (1972) 377.

Plochocki, A., Belcarz, E., Slapa, M., Szymczak, M., and Zylicz, J., Nucl. Inst. & Meth. 92 (1971) 85.

Popeko, L.A., Petrov, G.A., Rudnev, Yu.P., and Kochubei, E.F., Instruments and Experimental Techniques 19 (1976) 334.

Porter, F.T., Wagner, F., Jr. and Freedman, M.S., Phys. Rev. 107 (1957) 135.

Price, J.W., and Lee, T.G., Advances in Cryogenic Engineering 12 (1967) 265.

Price, J.W., Advances in Cryogenic Engineering, 13 (1968) 662.

Price, W.J., Nuclear Radiation Detection, McGraw-Hill, New York (1964).

Raman, S., Walkiewicz, T.A., and Behrens, H., Atomic Data & Nuclear Data Tables 16 (1975) 451.

Raman, S., Houser, C.A., Walkiewicz, T.A., and Towner, I.S., Atomic Data & Nuclear Data Tables 21 (1978) 567.

Ravn, H.L., Phys. Rep. 54 (1979) 201.

Rehfield, D.M., Thesis, McGill University (1977).

Rehfield, D.M., and Moore, R.B., Nucl. Inst. & Meth. 157 (1978) 365.

Rehifeld, D.M., Moore, R.B., and Hetherington, D., Nucl. Inst. & Meth. 178 (1980) 565.

Reitz, J.R., and Milford, F.J., Foundations of Electromagnetic Theory, Addison-Welsely, Reading, Massachuesetts (1967).

Restelli, G., Semiconductor Detectors, G. Bertolini, and A. Coche, ed., North-Holland, Amsterdam (1968) 9.

Restelli, G., and Rota, A., Semiconductor Detectors, G. Bertolini, and A., Coche, ed., North-Holland, Amsterdam (1968) 75.

Rettinghaus, G., and Huber, W.k., Vacuum 24 (1974) 259.

Rhode, J.I., and Johnson, O.E., Rev. Sci. Inst. 33 (1962) 1410.

Ricci, R.A., Physica 23 (1957) 693.

Riede, P.M. and Wang, D.I.-J. Advances in Cryogenic Engineering 5 (1960) 209.

Robert, K.Q., Linn, J.R., and Durham, F.E., Nucl. Inst. & Meth. 79 (1970) 251.

Rogers, P.C., and Gordon, G.E., Nucl. Inst. & Meth. 37 (1965) 259.

Rose-Innes, A.C., Low Temperature Techniques, D. Van Nostrand Company Inc., New York (1964).

Rosenberg, H.M., Advanced Cryogenics, C.A. Bailey, ed., Plenum Press, New York (1971) 77.

Reynolds, J., and Persson, B., Nucl. Inst. & Meth 33 (1965) 77.

Ruccia, F.E., and Hinckley, R.B. Advances in Cryogenic Engineering 12 (1967) 300.

Ruccia, F.E., Hinckley, R.B., and Ried, R.C., Advances in Cryogenic Engineering 12 (1967) 218.

Rudstam, G., Aagaard, P., Aleklett, K., and Lund, E., See CERN (1981) 696.

Sastry, K.S.R., Nuclear Isospin, J.D. Anderson, S.D. Bloom, J. Cerny, and W.W. True, eds., Academic Press, New York (1969) 831.

Sattler, E., Hansen, H.H. Hofmans, K., Mouchel, D. Nerb, H., and Schipke, H., Nucl. Inst. & Meth 124 (1975) 131.

Schmidt, F.H., Rev. Sci. Inst. 23 (1952) 361.

Schmitz, B.M., Farzine, K., and von Butlar, H., Nucl. Inst. & Meth., 105 (1972) 427.

Schopper, F.H., Weak Interactions and Nuclear Beta Decay, North-Holland, Amsterdam (1966).

Schupferling, H.M., and Hoffmann, K.W., Z. Physik A266 (1974) 129.

Schupferling, H.M., Nucl. Inst. & Meth. 123 (1975) 67.

Schwarzchild, A., Rustad, B.M., and Wu, C.S. Phys. Rev. 103 (1956) 1976.

Scott, R.B., Cryogenic Engineering, D. Van Nostrand Company, Inc., New York (1959).

Scurlock, R.G., and Saull, B., Proceedings of the Sixth International Cryogenic Engineering Conference, K. Mendelssohn, ed., IPC Science & Technology Press, Guildford, U.K. (1976) 249.

Seltzer, S.M., and Berger, M.J., Nucl. Inst. & Meth. 119 (1974) 157.

Sen, P. and Patro, A.P. Nucl Inst. & Meth. 40 (1966) 1.

Shahien, M.K.A., M.Sc. Thesis, McGill University (1981).

Sheline, R.K., Physica 23 (1957) 923.

Shera, E.B., Bedesem, M.P., and Casper, K.J., Rev. Sci. Inst. 38 (1967) 1110.

Shiraishi, F., Takami, Y., Hosoe, M., Oshawa, Y., and Sato, H., Nuclear Radiation Detector Materials, E.E. Haller, H.W. Kraner, and W.A. Higinbotham, eds., Elesevier Science Publishing Company, Inc., New York, Materials Research Society Symposia Proceedings, Vol. 16 (1983) 175.

Siegbahn, K., and Edvarson, K., Nucl Phys. 1 (1956) 137.

Siegbahn, K., Nordling, C., Karlsson, S.-E., Hagstrom, S., Fahlman, A., and Andersson, I. Nucl. Inst. & Meth. 27 (1964) 173.

Siegbahn, K., Alpha-, Beta-, and Gamma-Ray Spectroscopy, K. Siegbahn, ed., North-Holland, Amsterdam, Vol. 1 (1965) 79.

Simpson, J.J., Phys. Rev. D23 (1981) 649.

Slatis, H., Nucl. Inst. & Meth. 2 (1958) 332.

Slavinkas, D.D., Kennett, T.J. and Prestwich, W.V., Nucl. Inst. & Meth. 37 (1965) 36.

Smith, P.F., and Lewin, J.D., Nucl. Inst. & Meth. 52 (1967) 293.

Smith, H.A., and Simms, P.C., Phys. Rev. C1 (1970) 1809.

Smythe, W.R., Static and Dynamic Electricity, McGraw-Hill, New York (1968).

Snyder, R.E., and Beard, G.B., Nucl. Inst. & Meth. 26 (1964) 31.

Spalek, A., Nucl. Inst. & Meth. 198 (1982) 399.

Spejewski, E.H., Nucl. Phys. 82 (1966) 481.

Stern, S.A., and DiPaolo, F.S., J. Vac. Sci. Tech. 4 (1967) 347.

Stippler, R., Munnich, F., Schrader, H., Bocquet, J.P., Asghar, M., Siergert, G., Decker, R., Pfeiffer, B., Wollnik, H., Monnand, E. and Schussler, F., Z. Physik A284 (1978a) 95.

Stippler, R., Munnich, F., Schrader, H., Hawerkamp, K., Decker, R., Pfeiffer, B., Wollnik, H., Monnand, E., and Schussler, F., Z. Physik A285 (1978b) 287.

Stoy, S.T., Advances in Cryogenic Engineering 5 (1960) 216.

Strachan, C., The Theory of Beta-Decay, Pergamon Press, Oxford (1969).

Strauss, M.G., and Larsen, R.N., Semiconductor Nuclear-Particle Detectors and Circuits, W.L. Brown, W.A. Higinbotham, G.L. Miller, and R.L. Chase, eds., National Academy of Sciences, Washington, D.C. Publication 1593, Nuclear Science Series Report Number 44, (1969) 258.

Szybisz, L., A. Physik A292 (1979) 49.

Szybisz, L., and Silbergleit, V.M., J. Phys. G: Nucl. Phys. 7 (1981a) L201.

Szybisz, L., and Silbergleit, V.M., Z. Physik, A299 (1981b) 91.

Tabata, T., Phys. Rev. 162 (1967) 336.

Tabata, T., and Ito, R., Nucl. Inst. & Meth. 127 (1975) 429.

Tabata, T., and Ito, R., Nucl. Inst. & Meth. 136 (1976) 533.

Tabata, T., Ito, R., and Okabe, S., Nucl. Inst. & Meth. 94 (1971) 509.

Tavendale, A.J., Ann. Rev. Nucl. Sci. 17 (1967) 73.

Taylor, C.E., and Post, R.F., High Magnetic Fields, H. Kolm, B. Lax, F. Bitter, and R. Mills, John Wiley & Sons, New York (1962) 101.

Thies, W.G., Appel, H., and Behrens, H., Phys. Lett, 73B (1978) 411.

Thomas, M., and Weitzman, W., Advances in Cryogenic Engineering 12 (1967) 239.

Thornton, F.D., Advanced Cryogenics, C.A. Bailey, ed., Plenum Press, New

York (1971) 493.

Titus, F., Nucl. Inst. & Meth. 89 (1970) 93.

Toriyama, T., Nishio, T., Kanbe, M., and Hisatake, K., Future Directions in Studies of Nuclei Far From Stability, J.H., Hamilton, E.H., Spejewski, C.R. Bingham, and E.F.Zganjar, eds., North-Holland, Amsterdam (1980) 97.

Trischuk, J.M., and Kankeleit, E. Nucl. Phys. A90 (1967) 33.

Trischuk, J., and Kankeleit, E., Nucl. Inst. & Meth. 66 (1968) 197.

Trzaska, W., Aysto, J., and Kantele, J., Nucl. Inst. & Meth. 212 (1983) 221.

Tsoulfanidis, N., Wehring, B.W., and Wyman, M.E., Nucl. Inst. & Meth. 73 (1969) 98.

Tsoulfanidis, N., Measurement and Detection of Radiation, McGraw-Hill, New York (1983).

Van Atta, C.M., Warshaw, S.D., Chen, J.J.L., and Taimuty, S.I., Rev. Sci. Inst. 21 (1950) 985.

Van Elmbt, L., Thesis, Universite Catholique de Louvain (1981).

Van Klinken, J., Pleiter, F., and Dijkstra, H.T., Nucl. Phys. A112 (1968) 372.

Van Klinken, J., and Wisshak, K., Nucl. Inst. & Meth. 98 (1972) 1.

Van Klinken, J., Feenstra, S.J., Wisshak, K., and Faust, H., Nucl. Inst. & Meth. 130 (1975) 427.

Van Klinken, J., Feenstra, S.J., and Dumont, G., Nucl. Inst. & Meth. 151 (1978) 433.

Van Lieshout, R., Internal Conversion Processes, J.H., Hamilton, ed., Academic Press, New York (1966) 569.

Van Neste, L., Coussement, R., and Deutsch, J.P., Isobaric Spin in Nuclear Physics, J.D. Fox and D. Robson, Academic Press, New York (1966) 677.

Van Neste, L., Coussement, and Deutsch, J.P., Nucl. Phys. A98 (1967) 585.

Van Nooijen, B., Internal Conversion Processes, J.H. Hamilton, ed., Academic Press, New York (1966) 35.

Varley, B.J., Kitching, J.E., Leo, W., Miskin, J., Moore, R.B., Wunsch, K.D., Decker, R., Wollnik, H., and Siegert, G., Nucl. Inst. & Meth. 190 (1981) 543.

Vilet, G.C., and Coston, R.M., Advances in Cryogenic Engineering, 13

(1968) 671.

Vogel, P., Nuclear Spectroscopy of Fission Products, T. von Egidy, ed., The Institute of Physics, Bristol & London, Conference Series Number 51 (1980) 168.

von Egidy, T., Neutron Capture Gamma-Ray Spectroscopy, IAEA, Vienna (1969) 127.

von Egidy, T., ed., Nuclear Spectroscopy of Fission Products, The Institute of Physics, Bristol & London, Conference Series Number 51 (1980).

Vydrik, A.A., Instr. & Expt. Tech. 19, #4 (1977) 1026.

Waldschmidt, M., and Ostermann, P., Nucl. Inst. & Meth. 89 (1970) 65.

Watson, R.L., Bowman, H.R., Thompson, G., and Rasmussen. J.O., Internal Conversion Processes, J.H. Hamilton, ed., Academic Press, New York (1966) 423.

Watson, R.L., Rasmussen, J.O., Bowman, H.R., and Thompson, S.G., Rev. Sci. Inst. 38 (1967) 905.

Wegstedt, L., Science Tools, 4 (1957) 20.

Wenninger, H., Stiewe, J., and Leutz, H., Nucl, Phys. A109 (1968) 561.

Westerberg, L., Edvardson, L.O., Maduerne, G. Ch., and Thun J.E., Nucl. Inst. & Meth. 128 (1975) 61.

Westgaard, L., Zylicz, J., and Nielsen, O.B., See AMCO4 (1972) 94.

Wexler, A., J. Appl. Phys. 22 (1951) 1463.

Wexler, A., Experimental Cryophysics, F.E. Hoare, L.C. Jackson, and N. Kurti, eds., Butterworth, London (1961) 138.

White, G.K., Experimental Techniques in Low Termpoerature Physics, Clarendon Press, Oxford (1968).

Wiesner, W., Flothmann, D., and Gils, H.J., Nucl. Inst. & Meth. 112 (1973) 449.

Wigley, D.A., Mechanical Properties of Materials at Low Temperatures, Plenum Press, New York (1971).

Wigley, D.A., and Halford, P., Cryogenic Fundamentals, G.G. Haselden, ed., Academic Press, New York (1971) 311.

Wilkinson, D.H., Interaction Studies in Nuclei, H. Jochim and B. Ziegler, eds., North-Holland, Amsterdam (1975) 147.

Willett, J.B., and Spejewski, E.H., Nucl. Inst. & Meth. 52 (1967) 77.

Williams, J.E.C., Guide to Superconductivity, D. Fishlock, ed., American Elsevier, Inc. New York (1969) 35.

Wohn, F.K., Clifford, J.R., Carlson, G.H., and Talbert Jr., W.L. Nucl. Inst. & Meth 101 (1972) 343.

Wohn F.K., and Talbert Jr., W.L., Phys. Rev. C18 (1978) 2328.

Wollnik, H., Nuclear Spectroscopy of Fission Products, T. von Egidy, ed., The Institute of Physics, Bristol & London, Conference Series Number 51 (1980) 113.

Wollnik, H., Blonnigen, F., Rehfield, D., Jung, G., Pfeiffer, B., and Koglin, E., See AMCO 6 (1980) 465.

Wood, M.F., Advanced Cryogenics, C.A. Bailey, ed., Plenum Press, New York (1971) 293.

Wortman, D.E., and Langer, L.M., Phys. Rev. 131 (1963) 325.

Wortman, D.E., and Cramer Jr., J.G., Nucl. Inst. & Meth. 26 (1964) 257.

Wouters, J.M., Thierens, H.M., Aysto, J., Cable, M.D., Haustein, P.E., Parry, R.F., and Cerny, J., Phys. Rev. C27 (1983) 1745.

Wu, C.S., and Albert, R.D. Phys. Rev. 75 (1949) 315.

Wu, C.S., Ambler, E., Hayward, R.W. Hoppes, D.D., and Hudson, R.F. Phys. Rev. 105 (1957) 1413.

Wu, C.S., and Geoffrion, C., Nuclear Spectroscopy Part A, F. Ajzenberg-Selove, ed., Academic Press, New York (1960) 91.

Wu, C.S., Alpha-, Beta-, and Gamma-Ray Spectroscopy, K. Siegbahn, ed., North-Holland, Amsterdam, Vol. 2 (1965) 1384.

Wu. C.S., and Moszkowski, S.A., Beta Decay, Interscience Publishers, New York (1966).

Wu, C.S., Ben Lee Memorial International Conference on Parity Conservation, Weak Neutral Currents and Gauge Theories, Oct. 20-22, 1977 FNAL.

Wunsch, K.D., and Wollnik, H., Proceedings of the Isotope Separator On-line Workshop, R.E. Chrien, ed., Brookhaven National Laboratory, BNL 50847 (1977) 247.

Wunsch, K.D., Decker, R., Wollnik, H., Munzel, J., Siegert, G., Jung, G., and Koglin, E., Z. Physik A288 (1978) 105.

Yoshida, Y., Tsuji, K., Marubayashi, K., and Matsumoto, Y., Nucl. Inst. & Meth. 154 (1978) 261.

Zemann, H., Semrad, D., and Paul, H., Nucl. Phys. A175 (1971) 385.

APPENDIX A

GLOSSARY

(For a more detailed list of terms used to describe the performance of spectrometers see Wu & Geoffrion 1960; Mladjenovic 1971, 1972, 1976, 1979).

Solid Angle of Acceptance

The solid angle of acceptance, expressed in percentage of 4π describes what fraction of isotropically emitted monoenergetic electrons are accepted by the spectrometer.

Transmission

The transmission represents the percentage of emitted monoenergetic electrons reaching the plane of the detector. In the case where no electrons are lost between the entrance baffle and the detector plane, the transmission is equal to the solid angle of acceptance.

Effective Transmission

In cases where the detector surface area is smaller than the image formed by the spectrometer, the effective transmission is the percentage of all monoenergetic electrons leaving the source which are counted in the detector.

Luminosity

The luminosity of a spectrometer can be defined as the product of the surface area of the source and the transmission of the spectrometer.

Effective Luminosity

Similarly, the effective luminosity is simply defined as the product of the effective transmission and the source area.

Resolution

The resolution of a spectrometer is a measure of the apparent width of a monoenergetic electron line as measured by the spectrometer. It is usally

expressed as the full width at half maximum of the electron line.

It should be noted that for most magnetic beta spectrometer designs, the size of the spectrometer does not affect its transmission if the resolution is kept constant. However, the size of the spectrometer determines the surface area of the sources that can be used and therefore the luminosity of the spectrometer (Wu & Geoffrion 1960 p. 94).

APPENDIX B

THE TRIPLE COINCIDENCE METHOD

In this technique, the energy deposition β spectrometer is surrounded by two γ ray detectors operated in coincidence with each other and with the β spectrometer. The technique is usually used to suppress the effects of annihilation radiation pile-up in the β spectrometer by using the two γ ray detectors to gate on the two 511 keV photons emitted after the annihilation (D'Auria & Preiss 1966; Beck 1969; De Beer et al. 1970; Avignone et al. 1981). This method is also useful in eliminating the effects of positron backscattering from the β spectrometer (Sen & Patro 1966) and in suppressing most of the adverse effects of the detection of non coincident γ rays in the β detector.

The triple coincidence technique has been used extensively in conjunction with 4π and internal-source positron spectrometers for the suppression of annihilation radiation summing (Rhode & Johnson 1962 and references therein; Klyuchnikov et al. 1968; Wenninger et al. 1968; Gils et al. 1972). In certain cases when 4π β spectrometers are used, instead of operating the two annihilation radiation detectors in coincidence with each other, the signals from the two γ detectors are summed up and used to gate the counts in the β detector. A coincidence is triggered only if the total energy detected in the γ detectors is equal to the sum of the energies of the two 511 keV photons. Such an arrangement can also be used (in 4π β spectrometers only) to eliminate β - γ coincident summing in the β spectrometer by using the γ detectors to gate on the sum of the energies of the annihilation photons and the coincident γ ray (Wenninger et al. 1968; Gils et al. 1972).

The triple coincidence method is obviously useful only in the case of positron emission and is not applicable for β^- decays. Moreover it suffers from several drawbacks that restrict its usefulness.

1. Low Efficiency

The limited efficiency of this method results from the triple coincidence condition and the fact that the γ ray detectors always have an efficiency of less than one.

The efficiency of the triple coincidence method is further reduced if a third γ ray detector is operated in coincidence with the β spectrometer and the annihilation photon detectors. Such an arrangement, which is used to suppress the background caused by coincident γ ray summing, can reduce the efficiency of the triple coincidence spectrometer by up to a factor of 20 (Rhode & Johnson 1962; Klyuchnikov et al. 1968; De Beer et al. 1970).

2. Dependence of the Coincidence Efficiency on Pulse Height

A constant coincidence efficiency over the full range of β particle energies under study has to be ensured. The energy dependent coincidence efficiency can be caused by electronic effects such as the dependence of the triggering time on the heights or shapes of the pulses that are generated by the β detector (Rhode & Johnson 1962; Gils et al. 1972).

3. Chance Coincidences

Like all coincidence arrangements, the possibility of accidental coincidences in the triple coincidence circuit has to be carefully examined. Any dependencce of the true-to-chance coincidence counting rates on the energy (i.e. pulse heights) of the β particles detected in the β spectrometer would result in spectral shape distortions. Although a three fold coincidence condition is required in this technique (and sometimes even a four fold coincidence is imposed when a third γ ray detector is used to suppress coincident γ ray summing in the β detector), nevertheless, the rate of accidental coincidences can still be appreciable and has to be taken into account (De Beer et al. 1970; Gils et al. 1972).

4. Beta Spectrum Shape Distortions due to Backscattering

In cases where external sources are used, and when the solid angle for positron detection is less than or equal to 2π, distortions to the shape of the β spectrum can be caused by the backscattering of the positrons from the β spectrometer.

Since counts resulting from positrons that are not stopped in the β spectrometer are not retained, and because of the dependence of backscattering coefficient on energy, the efficiency of the triple coincidence spectrometer system will be energy dependent. This will obviously result in distortions to the shapes of β spectra measured with such a spectrometer.

Another distorting effect can be caused by positrons that are

backscattered from the β spectrometer and stopped outside it. Depending on the geometry of the set-up, there is a finite probability for the two annihilation photons to be detected by the two γ detectors and therefore to result in an event where the full energy of the positron was not deposited in the β spectrometer. The number of such events would depend on the backscattering coefficient and the angle at which backscattered positrons emerge from the detector. This effect can potentially cause serious distortions to the shape of the β spectrum if the two γ detectors are not shielded properly from the annihilation radiation of positrons stopped outside the β detector (De Beer et al. 1970).

5. Dependence of the Efficiency for the Detection of the Annihilation Radiation on the Energy of the Incident Positrons.

The efficiency for detecting the two oppositely directed annihilation quanta depends upon the location of the point of origin of these photons with respect to the two annihilation radiation detectors. Therefore, the efficiency of annihilation radiation detection is dependent on the range of the postirons in the β detector medium and hence on the energy of the incident positrons (Rhode & Johnson 1962).

The dependence of the efficiency of annihilation radiation detection on the annihilation site in the β detector results from two effects. The first is the change in the solid angle for detecting the two photons with changes in their point of origin, due to pure geometrical factors. The second effect is the dependence of the attentuation of the annihilation γ rays on the thickness of the β detector that they have to traverse before reaching the γ detectors, and therefore on the location of the annihilation site (Azuelos et al. 1977).

6. Beta Spectrum Shape Distortions due to Small Angle Compton Scattering of the Annihilation Photons

In order to increase the efficiency for detecting the annihilation photons, scintillation detectors (e.g. NaI(Tl)) are used as annihilation radiation detectors. The modest energy resolution of these spectrometers results in fairly wide energy window settings for the detection of the annihilation radiation. It is therefore possible for the annihilation quanta to undergo small-angle Compton scattering and lose some of their energy in the β spectrometer and still be counted in the annihilation γ detectors. The energy transferred to the β spectrometer during the

Compton scattering is added to the positron's energy resulting in spectral shape distortions (Rhode & Johnson 1962).

7. Distortions due to Positron Annihilation-in-Flight

There is a finite probability that some of the positrons incident on the β spectrometer will annihilate in-flight during their slowing down in the detector medium and before losing all of their kinetic energy in the β detector. Such an annihilation can result in the emission of one or two annihilation quanta. The photons emitted during in-flight annihilation events form a continuous energy spectrum extending from zero to a maximum energy equal to the total energy of the incident positron (kinetic energy + rest mass). The probability of in-flight annihilation increases with an increase in the energy of the incident positron and with an increase in the Z of the stopping material (Azuelos & Kitching 1976).

Depending of the width of the energy windows that are set on the γ ray detectors, only a fraction of the in-flight annihilation quanta result in proper coincidence counts. This in turn will cause variations in the efficiency of the spectrometer system over the range of β particle energies. Moreover, even for the in-flight annihilation photons that are detected within the proper energy windows, the energy deposited by the postiron in the β spectrometer will not be equal to the total kinetic energy of the positron and would therefore result in distortions to the shape of the β spectrum (Rhode & Johnsson 1962).

8. External Bremsstrahlung

As the positrons are stopped in the β spectrometer, they lose some of their kineticc energy through the emission of bremsstrahlung photons. This bremsstrahlung radiation forms a continuous energy spectrum extending up to the endpoint energy of the β spectrum (see Knoll 1979 fig. 1-6 p. 19,, fig. 10-5 p. 321). Since the emission of the bremsstrahlung photon is coincident with the β particle detection signal and with the annihilation photons, the detection of bremsstrahlung photons can trigger one or both annihilation radiation detectors if they fall within the energy windows set on the detectors. The emission and subsequent detection, in the annihilation γ detectors, of the bremsstrahlung photons can therefore interfere witn the proper operation of the triple coincidence selection circuit.

The intensity and the shape of the bremsstrahlung spectrum is

dependent on the energy of the incident positrons so that the probability for the detection of bremsstrahlung photons in the annihilation detectors is dependent on the positron energy. The triggering of the coincidence circuit, by bremsstrahlung photons, can therefore result in considerable distortions to the shape of the β spectrum.

Since the production of bremsstrahlung increases with the energy of the incident β particles and with the Z of the detector material, the distortions it causes are more important in high endpoint energy β decays and when high Z detectors (e.g. Ge or NaI) are used.

9. The Effects of Coincident γ Rays

In addition to the emission of a continuous spectrum of electromagnetic radiation (internal bremsstrahlung), the process of β decay usually populates some of the excited states of the daughter nucleus. The prompt decay of the excited states results in the emission of γ rays that are coincident with the β particle emission. Beyond the effects of β- γsumming resulting from the coincdient detection of a photons and a β particle in the β spectrometer, the emission of coincident γ rays can cause other problems in spectrometers where the triple coincidence method is used.

a) Compton Scattering

The process of Compton scattering of coincident γ rays in the β spectrometer can provide a third photon (in addition to the two 511 keV quanta) which can be detected in the annihilation radiation detectors. Therefore the presence of Compton scattered coincident γ rays can hinder the suppression of the annihilation radiation provided by the triple coincidence circuit.

b) Pair Production

One of the possible interactions of high energy γ rays (higher than 1.022 MeV) with the β detector is through the formation of an electron-positron pair in the detector material and the transfer of the γ ray energy to this pair. After the positron, formed in this process is stopped in the detector, it annihilates producing two annihilation quanta which can trigger the triple coincidence circuit.

Such events can interfere with the ideal operation of the triple coincidence annihilation radiation suppression system. For example they can cause a coincidence gate for events in which the β particle was not stopped in the β spectrometer but backscattered out of it.